

**Titre:** Analytical Modelling of full-time-scale heat transfer in ground heat exchangers  
Title:

**Auteur:** Carlos de Jesus Prieto Chavez  
Author:

**Date:** 2022

**Type:** Mémoire ou thèse / Dissertation or Thesis

**Référence:** Prieto Chavez, C. J. (2022). Analytical Modelling of full-time-scale heat transfer in ground heat exchangers [Thèse de doctorat, Polytechnique Montréal]. PolyPublie.  
Citation: <https://publications.polymtl.ca/10719/>

 **Document en libre accès dans PolyPublie**  
Open Access document in PolyPublie

**URL de PolyPublie:** <https://publications.polymtl.ca/10719/>  
PolyPublie URL:

**Directeurs de recherche:** Massimo Cimmino  
Advisors:

**Programme:** Génie mécanique  
Program:

**POLYTECHNIQUE MONTRÉAL**

affiliée à l'Université de Montréal

**Analytical modelling of full-time-scale heat transfer in ground heat exchangers**

**CARLOS DE JESUS PRIETO CHAVEZ**

Département de génie mécanique

Thèse présentée en vue de l'obtention du diplôme de *Philosophiæ Doctor*

Génie mécanique

Décembre 2022



**POLYTECHNIQUE MONTRÉAL**

affiliée à l'Université de Montréal

Cette thèse intitulée :

**Analytical modelling of full-time-scale heat transfer in ground heat exchangers**

présentée par **Carlos de Jesus PRIETO CHAVEZ**

en vue de l'obtention du diplôme de *Philosophiæ Doctor*

a été dûment acceptée par le jury d'examen constitué de :

**Michel BERNIER**, président

**Massimo CIMMINO**, membre et directeur de recherche

**Phillipe PASQUIER**, membre

**Alberto LAZZAROTTO**, membre externe

**DEDICATION**

*To the Almighty, Jesus Christ,  
and my awesome Dad, Carlitos,  
who is in a better place . . . waiting.*

## ACKNOWLEDGEMENTS

Undoubtedly this thesis could not have been carried out without the help, time and learning acquired under the superb supervision of Prof. Massimo Ciminno. Massimo, thank you for trusting my way of working and doing things. I recognize that our meetings, where I was supposed to show my progress in 15 minutes, often lasted more than an hour. I am grateful for your patience and for pushing me to be even more critical of my work and to solve one of the most exciting problems in this field of research. I will always be grateful in a non-finite way for the flexibility of work. Thank you very much for everything.

I also thank the members of the jury for agreeing to participate in this defense: Prof. Michel Bernier, Prof. Phillippe Pasquier and Dr. Alberto Lazzarotto.

Thanks to my professors during the courses at Polytechnique and even more for challenging me with quite interesting problems in some classes.

At the end of the tour, I had the great opportunity to be a researcher at Québec Artificial Intelligence Institute (MILA), working on interesting problems, where I met new personalities and acquired new knowledge.

I want to take this opportunity to thank my lab mates, who, despite having seen them very little, their opinions and kindness in helping will always be remembered: Alexandre, Aziz, Geoffrey, and Sepehr. To my friends and great people who were (and still are) in the most critical moments of this path, to you, I will always be indebted: Alvar, Irune, Julie (BW) and Rachelle.

Finally, my fabulous family. Brother Cesarin (with his wife, Jackie) and my mother Silvia, thank you for supporting me from afar, and although adverse situations were always present, you never stopped trusting me. To my nephews (Adarinis and Yasser), who are still kids, I hope they will someday want to read this document full of equations and know that their uncle did something strange and funny. Dad, I know you are no longer here to see this road finished, and you would like to see it. Don't worry, the only thing for sure is that I finished it, and it was all thanks to you and our Lord, Jesus Christ.

All this research was supported by the Natural Sciences and Engineering Research Council of Canada (NSERC).

## RÉSUMÉ

Lors de la conception, de la simulation et du contrôle des systèmes de pompes à chaleur géothermiques (GCHP), il est nécessaire de comprendre l'interaction entre le sol et le bâtiment pour répondre aux besoins thermiques. Le transfert de chaleur dans le sol, dû aux échangeurs de chaleur géothermiques (GHE) doit être étudié précisément, à l'aide de modèles mathématiques, afin de comprendre la réponse thermique entre le bâtiment et le fluide circulant dans les GHE. Ces modèles doivent prendre en compte l'interaction avec le sol à travers le coulis (les effets à court terme), l'échange thermique entre plusieurs GHE, y compris les effets axiaux pour de longues périodes de fonctionnement (les effets à long terme), et l'effet combiné des deux durant toute la durée de vie du GHE (les effets à court et à long terme). En outre, dans certaines circonstances, il est important de considérer l'impact des eaux souterraines qui se déplacent autour du GHE et leur effet sur la réponse thermique à l'intérieur du GHE.

Pour étudier l'interaction des effets thermiques dans un champ de GHE, un modèle transitoire semi-analytique en 3D est développé pour permettre l'étude des effets à court et à long terme. Pour élaborer ce modèle, une solution analytique en 2D permettant l'analyse du transfert thermique transitoire, y compris une distribution arbitraire de  $N$  tuyaux dans le GHE, appelée expansion multipole transitoire, est développée. Cette solution est basée sur la superposition des solutions de deux problèmes élémentaires : a) le problème transitoire homogène et b) le problème non homogène en régime permanent. Une expansion multipole basée sur des solutions exactes est proposée pour chaque problème élémentaire afin de résoudre le problème transitoire initial non-homogène. Ce modèle est ensuite validé en comparant les valeurs propres du problème transitoire homogène avec des valeurs trouvées dans la littérature. Le modèle en régime permanent non-homogène est validé avec un modèle multipole en régime permanent trouvé dans la littérature. Par ailleurs, le problème initial de transfert de chaleur transitoire non-homogène est validé par rapport à un modèle par éléments finis (FEA).

Pour transformer le modèle de 2D en 3D, une nouvelle méthode permettant d'étudier les interactions thermiques entre les GHEs et les effets axiaux, appelée la méthode du puits équivalent, a été développée. Cette méthode est basée sur le regroupement des puits qui ont une température moyenne de paroi et des taux d'extraction de chaleur similaires. Elle fait appel à un algorithme de regroupement hiérarchique qui sélectionne les puits similaires suivant le calcul de la différence maximale entre deux puits. Cette nouvelle technique est

validée en considérant d'autres méthodes trouvées dans la littérature. La méthode est utilisée pour le calcul des  $g$ -functions pour un large éventail de champs, allant de configurations régulières à des configurations aléatoires de grands champs géothermiques. La méthode aboutit à l'élaboration d'un outil de calcul efficace qui permet de trouver les facteurs de réponse thermique en quelques secondes.

L'extension du modèle mathématique en 3D est obtenue en couplant l'expansion multipole transitoire et la méthode du puits équivalent. Ce couplage a été réalisé en pénalisant l'expansion multipole transitoire pour y inclure l'effet des interactions thermiques entre les GHEs. Les effets axiaux ont été pris en compte en procédant à une discrétisation par différences finies du modèle d'advection du fluide caloporteur dans les tuyaux. Dans un premier temps, le modèle de calcul des effets à court terme a été validée en comparant les prédictions de température du fluide et de température moyenne de la paroi du puits avec celles présentées dans des données de mesures en bac à sable trouvées dans la littérature. Pour valider les effets à court et long terme, une simulation pluriannuelle de 10 ans avec un pas de temps de 1 h suivie d'une simulation de 7 jours avec un pas de temps de 1 min a été réalisée. Cela a permis de calculer les températures de fluide et la température moyenne de paroi des puits pour chaque puits équivalent. La validation est réalisée à l'aide d'un modèle de haute-fidélité basé sur une analyse par éléments finis. La nouvelle méthode, peu couteuse en temps de calcul, permet d'étudier les effets à court et long terme des grands champs géothermiques durant toute la durée de vie du système GCHP.

Enfin, pour étudier les effets de l'eau souterraine dans le GHE, une extension de l'expansion multipole transitoire qui prend en compte l'écoulement de l'eau souterraine, est présentée. L'eau souterraine se déplace autour du GHE selon un champ potentiel incompressible et non-rotationnel et avec un champ de vitesse éloignée constant. Le modèle permet d'étudier la distribution de la température à l'intérieur et à la périphérie du GHE en considérant une distribution arbitraire de  $N$  tuyaux dans le coulis. Grâce à un changement de variable, le modèle de diffusion-advection est réduit à un modèle de diffusion-réaction qui permet d'appliquer la même structure mathématique que l'expansion multipolaire transitoire en utilisant une approximation du terme de réaction pour résoudre le problème initial. Le modèle est validé en comparant la température moyenne de la paroi du puit avec un modèle FEA pour deux cas pour lesquels la distribution des tuyaux dans le coulis est différente. Cette distribution des tuyaux dans le coulis montre que la considération classique de la symétrie des résistances thermiques n'est pas toujours valable lorsque l'écoulement des eaux souterraines est considéré. Ainsi, elle devrait être prises en compte dans des modèles tels que les méthodes de résistance-capacité thermique (TRC).

## ABSTRACT

In each of the design, simulation, and control phases of ground-coupled heat pump (GCHP) systems, it is necessary to understand the interaction between the ground and the building to meet the energy demands. The heat transfer in the soil due to ground heat exchangers (GHEs) needs to be studied through accurate mathematical models to understand the thermal response between the building and the fluid flowing through the GHEs. These models should include interaction with the ground via the grout (i.e. short-term effects), the thermal exchange between several GHEs, including the axial effects for long periods of operation (i.e. long-term effects), and the effect that both have on the whole life cycle (i.e. short-to-long-term effects). In addition, in some circumstances, the effects of groundwater moving around the GHE are important, and their effect on the thermal response within the GHE should be studied.

To study the thermal effects in an interacting field of GHEs, a semi-analytical 3D transient model is developed to study short-to-long-term effects. For this model to be created, an analytical solution in 2D, called transient multipole expansion, is presented to allow the analysis of transient heat transfer, including an arbitrary distribution of  $N$  pipes within the GHE. This solution is based on the superposition of solutions from two sub-problems: a) homogeneous transient problem and b) non-homogeneous steady-state problem. A multipole expansion based on exact solutions is proposed in each sub-problem to solve the initial non-homogeneous transient problem. The validation of this model is done by comparing the eigenvalues from the transient homogeneous problem with those found in the literature. Finally, the non-homogeneous steady-state model is validated with the steady-state multipole model found in the literature. In addition, the initial transient non-homogeneous heat transfer problem is validated against a finite element analysis (FEA) model.

To extend the model from 2D to 3D, a new method, called the equivalent borehole method, is presented to study the thermal interactions between GHEs and the axial effects. This method is based on grouping boreholes with similar average borehole wall temperature and heat extraction rates by implementing a hierarchical clustering algorithm that selects these boreholes by considering the maximum dissimilarity between steady-state borehole wall temperatures of any two boreholes. This new technique is validated against state-of-the-art methods found in the literature for the  $g$ -function calculation for a wide range of fields, from regular arrays to random distributions of large geothermal fields. The method results in a computationally efficient tool that allows the calculation of the thermal response factors in

a matter of seconds.

The extension of the mathematical model to 3D is presented by coupling the transient multipole expansion and the equivalent borehole method. This coupling was done by penalizing the transient multipole expansion to consider the thermal interactions between the GHEs. Axial effects were included by a finite difference discretization of the pipes' advection model of the heat-carrier fluid. Initially, the validation of the proposed model for short-term effects was performed by comparing the fluid temperature predictions and average borehole wall temperature with those presented in experimental data for a sandbox test from the literature. A multi-annual simulation of 10 years with a 1 h time step followed by 7 days with a 1 min time step is proposed to validate the short-to-long-term effects by estimating the fluid temperatures and average borehole wall for each equivalent borehole. This validation is done using a high-fidelity model based on FEA. The method corresponds to a computationally efficient method that allows studying short-to-long-term effects of large geothermal fields throughout the life cycle of a GCHP system.

Finally, to study the effects of groundwater around the GHEs, an extension of the transient multipole expansion is presented to include groundwater flow moving around a GHE with an incompressible and irrotational potential field with constant far-field velocity. The model allows studying the temperature distribution inside and at the periphery of the GHE, considering an arbitrary distribution of  $N$  pipes in the grout. With a special change of variable, the diffusion-advection model is reduced to a diffusion-reaction model, allowing for the application of the same mathematical structure from the transient multipole expansion using an approximation of the reaction term to solve the initial problem. The model is validated by comparing the average borehole wall temperature with an FEA model for two cases in which the distribution of pipes in the grout is different. This distribution of pipes in the grout shows that the classical consideration of the symmetry of thermal resistances is not always valid when groundwater flow is considered and should be studied when including them in models such as thermal resistance-capacitance (TRC) methods.

## TABLE OF CONTENTS

DEDICATION . . . . .	iii
ACKNOWLEDGEMENTS . . . . .	iv
RÉSUMÉ . . . . .	v
ABSTRACT . . . . .	vii
TABLE OF CONTENTS . . . . .	ix
LIST OF TABLES . . . . .	xii
LIST OF FIGURES . . . . .	xiii
LIST OF SYMBOLS AND ACRONYMS . . . . .	xvi
LIST OF APPENDICES . . . . .	xx
CHAPTER 1 INTRODUCTION . . . . .	1
CHAPTER 2 LITERATURE REVIEW . . . . .	3
2.1 Interior of the ground heat exchangers . . . . .	3
2.1.1 Steady-state models . . . . .	3
2.1.2 Transient models . . . . .	5
2.1.3 Discussion . . . . .	16
2.2 Exterior of the ground heat exchangers . . . . .	17
2.2.1 Analytical models . . . . .	17
2.2.2 Numerical models . . . . .	19
2.2.3 Discussion . . . . .	20
2.3 Groundwater flow . . . . .	20
2.3.1 Discussion . . . . .	23
CHAPTER 3 OBJECTIVES AND THESIS STRUCTURE . . . . .	25
3.1 Objectives . . . . .	25
3.2 Thesis outline . . . . .	25
CHAPTER 4 ARTICLE 1: TRANSIENT MULTIPOLE EXPANSION FOR HEAT	



TRANSFER IN GROUND HEAT EXCHANGERS . . . . .	27
4.1 Abstract . . . . .	27
4.2 Introduction . . . . .	27
4.3 Mathematical model . . . . .	31
4.3.1 Transient heat equation with homogeneous boundary conditions . . .	35
4.3.2 Steady-state heat equation with nonhomogeneous boundary conditions	39
4.3.3 Time-dependent fluid temperatures . . . . .	42
4.4 Validation . . . . .	44
4.4.1 Eigenvalues of the Helmholtz equation . . . . .	44
4.4.2 Steady-state temperature field . . . . .	47
4.4.3 Transient multipole expansion . . . . .	49
4.5 Conclusions . . . . .	55
4.6 Funding . . . . .	56
CHAPTER 5 ARTICLE 2: THERMAL INTERACTIONS IN LARGE IRREGULAR FIELDS OF GEOTHERMAL BOREHOLES: THE METHOD OF EQUIVALENT BOREHOLES . . . . .	57
5.1 Abstract . . . . .	57
5.2 Introduction . . . . .	57
5.3 Methodology . . . . .	61
5.3.1 Thermal interaction between boreholes . . . . .	61
5.3.2 Thermal interaction between groups of boreholes . . . . .	63
5.3.3 Equivalent boreholes . . . . .	64
5.3.4 $g$ -function calculation . . . . .	67
5.4 Results . . . . .	68
5.4.1 Rectangular borefield of 20 boreholes . . . . .	69
5.4.2 Regular borefield configurations . . . . .	72
5.4.3 Irregular borefield configurations . . . . .	74
5.5 Conclusions . . . . .	77
5.6 Funding . . . . .	79
CHAPTER 6 ARTICLE 3: SEMI-ANALYTICAL METHOD FOR 3D TRANSIENT HEAT TRANSFER IN THERMALLY INTERACTING FIELDS OF GROUND HEAT EXCHANGERS . . . . .	80
6.1 Abstract . . . . .	80
6.2 Introduction . . . . .	80
6.3 Mathematical model . . . . .	84

6.3.1	2D transient heat transfer with time-dependent fluid temperatures . .	85
6.3.2	Thermal interactions between ground heat exchangers . . . . .	91
6.3.3	Advection inside the pipes . . . . .	95
6.3.4	Finite element modeling . . . . .	97
6.4	Validation . . . . .	99
6.4.1	Sandbox test . . . . .	99
6.4.2	Multi-annual simulation of a geothermal field . . . . .	103
6.5	Conclusions . . . . .	112
6.6	Appendix A: Load aggregation . . . . .	114
6.7	Appendix B: Additional expressions for the transient multipole method . . .	115
6.8	Funding . . . . .	117
CHAPTER 7 ARTICLE 4: TRANSIENT HEAT TRANSFER IN GROUND HEAT EXCHANGERS UNDER GROUNDWATER FLOW . . . . .		118
7.1	Abstract . . . . .	118
7.2	Introduction . . . . .	118
7.3	Mathematical Model . . . . .	119
7.3.1	Diffusion-advection model . . . . .	120
7.3.2	Groundwater transient multipole expansion . . . . .	121
7.4	Results . . . . .	124
7.5	Conclusions . . . . .	128
7.6	Acknowledgment . . . . .	128
CHAPTER 8 GENERAL DISCUSSION . . . . .		129
CHAPTER 9 CONCLUSION AND RECOMMENDATIONS FOR FUTURE WORK		133
9.1	Thesis limitations and future research . . . . .	133
REFERENCES . . . . .		136
APPENDICES . . . . .		153

## LIST OF TABLES

Table 4.1	Comparison of the eigenvalues from the proposed method and Chen et al. . . . .	47
Table 5.1	Borehole and ground parameters . . . . .	69
Table 5.2	Dimensions of the irregular borefield domains . . . . .	75
Table 5.3	Scalability of the proposed method . . . . .	77
Table 6.1	Sandbox test parameters. . . . .	100
Table 6.2	Borefield parameters. . . . .	104
Table 6.3	Errors of fluid temperatures during the 10th year. . . . .	107
Table 6.4	Errors on borehole wall temperatures during the 10th year. . . . .	108
Table 6.5	Errors of fluid temperatures during the 7-day period. . . . .	110
Table 6.6	Errors of borehole wall temperatures during the 7-day period. . . . .	111
Table 7.1	GHE Parameters . . . . .	125

## LIST OF FIGURES

Figure 2.1	a) Cross section of GHE and b) Delta circuit . . . . .	4
Figure 2.2	Configuration of ICMCS . . . . .	7
Figure 2.3	Plane discretization of CaRM . . . . .	9
Figure 2.4	Axial discretization of CaRM . . . . .	10
Figure 2.5	Improvement of CaRM . . . . .	10
Figure 2.6	TRC models . . . . .	11
Figure 2.7	3D TRC model . . . . .	11
Figure 2.8	Modified-TRC model . . . . .	12
Figure 2.9	Modified-TRC model . . . . .	12
Figure 2.10	Simplified-TRC model . . . . .	13
Figure 2.11	Simplified-TRC model . . . . .	13
Figure 2.12	EWS improvement . . . . .	14
Figure 2.13	B2G model . . . . .	14
Figure 2.14	BFTM model . . . . .	15
Figure 2.15	MDF model . . . . .	16
Figure 4.1	Ground heat exchanger domain geometry . . . . .	32
Figure 4.2	Translation of coordinates . . . . .	33
Figure 4.3	One pipe geometry (Left). Eigenvalues extracted by SVD (Right) . .	45
Figure 4.4	Two pipes geometry (Left). Eigenvalues extracted by SVD (Right) . .	45
Figure 4.5	Eigenmodes of the multipole expansion for one pipe . . . . .	46
Figure 4.6	Eigenmodes of the multipole expansion for two pipes . . . . .	47
Figure 4.7	Two asymmetrically positioned pipes geometry . . . . .	48
Figure 4.8	Validation against the multipole method of Claesson and Hellström .	49
Figure 4.9	One pipe geometry (Left). Eigenvalues extracted by SVD (Right) . .	50
Figure 4.10	Two pipes geometry (Left). Eigenvalues extracted by SVD (Right) . .	50
Figure 4.11	Borehole wall temperature and pipe heat transfer rate (one pipe geometry) . . . . .	51
Figure 4.12	Borehole wall temperature and pipe heat transfer rate (two pipes geometry) . . . . .	52
Figure 4.13	FEA simulation (left) and temperature profile at $y = 0$ (right) for the one pipe geometry: (a) $t = 1000$ s, (b) $t = 10000$ s, and (c) $t = 100000$ s	53
Figure 4.14	FEA simulation (left) and temperature profile at $y = 0$ (right) for the two pipes geometry: (a) $t = 1000$ s, (b) $t = 10000$ s, and (c) $t = 100000$ s	54

Figure 4.15	Inlet and outlet fluid temperature variations . . . . .	55
Figure 5.1	Field of 2 vertical boreholes of equal dimensions . . . . .	61
Figure 5.2	Dendrogram Example . . . . .	67
Figure 5.3	Hierarchical agglomerative clustering method for a $5 \times 4$ borefield . . .	70
Figure 5.4	$g$ -function comparison for a $5 \times 4$ borefield . . . . .	71
Figure 5.5	Heat extraction rates of a $5 \times 4$ borefield . . . . .	71
Figure 5.6	Regular borefield configurations . . . . .	72
Figure 5.7	Mean absolute percentage error on the $g$ -functions . . . . .	73
Figure 5.8	Calculation time for the evaluation of $g$ -functions of regular borefields	73
Figure 5.9	Shapes of the irregular borefield domains . . . . .	74
Figure 5.10	<i>MAPE</i> on the $g$ -function and number of groups for the irregular borefields	75
Figure 5.11	Sample results for configuration F . . . . .	76
Figure 5.12	$g$ -function for different random borefield configurations . . . . .	77
Figure 6.1	Field of 2 vertical boreholes of equal dimensions. . . . .	84
Figure 6.2	Computational domain of a GHE. . . . .	86
Figure 6.3	$(n_s)$ segments discretization of boreholes $i$ and $j$ . . . . .	91
Figure 6.4	Finite element discretization for model validation. (a) Mesh for Beier's experiment. (b) Mesh for a borefield with 24 GHE. . . . .	98
Figure 6.5	Beier et al. experiment: (a) ground load and (b) mass flow rate. . . .	101
Figure 6.6	Comparison of the proposed model with (a) the experimental data of Beier et al. and (b) the FEA model. . . . .	101
Figure 6.7	Fluid temperature profiles along pipes at 4 different times. . . . .	103
Figure 6.8	Equivalent boreholes for a field of 24 GHEs. . . . .	104
Figure 6.9	Multi-annual simulation over 10 years with the proposed method: (a) ground loads, (b) inlet and outlet fluid temperatures and (c) average borehole wall temperature at each equivalent borehole. . . . .	106
Figure 6.10	Comparison of predicted inlet and outlet fluid temperatures during the 10th year: (a) proposed method, (b) FEA model, (c) error of the inlet temperature and (d) error of the outlet temperature. . . . .	107
Figure 6.11	Comparison of predicted borehole wall temperatures for each equivalent group ( <i>I</i> , <i>II</i> , <i>III</i> ) during the 10th year: (a–c) proposed method, (d–f) FEA model and (g–i) error between models. . . . .	108

Figure 6.12	Comparison of predicted inlet and outlet fluid temperatures and borehole wall temperatures for each equivalent group ( <i>I, II, III</i> ) during the 7-day period: (a,b) proposed method, (c,d) FEA model, (e) errors of the inlet and outlet fluid temperatures, and (f) error of the borehole wall temperatures. . . . .	110
Figure 6.13	Fluid and borehole wall temperature profiles for each equivalent borehole at 7029 min: (a) fluid temperature profiles for the FEA (dotted line) and the proposed method (solid line) for each equivalent borehole, and (b) equivalent borehole wall temperature profiles for the FEA method (dotted line) and the proposed method (continuous line). . .	111
Figure 7.1	Domain geometry around a GHE . . . . .	120
Figure 7.2	Average borehole wall temperature comparison between FEA (continuous line) and present method (discontinuous line) for 4 different far-field velocities: a) Case I and b) Case II . . . . .	126
Figure 7.3	Internal thermal resistances for case I with different far-field velocities: a) $u_{\infty} = 0 \text{ m/s}$ , b) $u_{\infty} = 10^{-6} \text{ m/s}$ , c) $u_{\infty} = 10^{-5} \text{ m/s}$ and d) $u_{\infty} = 10^{-4} \text{ m/s}$ . . . . .	127
Figure 7.4	Internal thermal resistances for case II with different far-field velocities: a) $u_{\infty} = 0 \text{ m/s}$ , b) $u_{\infty} = 10^{-6} \text{ m/s}$ , c) $u_{\infty} = 10^{-5} \text{ m/s}$ and d) $u_{\infty} = 10^{-4} \text{ m/s}$ . . . . .	127

## LIST OF SYMBOLS AND ACRONYMS

### Acronyms

ASHRAE	American Society of Heating, Refrigerating and Air-Conditioning Engineers
BEC	Buried Electric Cable
BFTM	Borehole Fluid Thermal Mass
B2G	Borehole-to-Ground
CaRM	Capacitance Resistance Model
CHS	Cylindrical Heat Source
COP	Coefficient of Performance
CVFEM	Control-Volume Finite Element Method
FDM	Finite Difference Method
FEM	Finite Element Method
FLS	Finite Line Source
FVM	Finite Volume Method
GCHP	Ground-coupled Heat Pump
GHE	Ground Heat Exchanger
ICMCS	Infinite Composite Media Cylindrical Source
ICMLS	Infinite Composite Media Line Source
ILS	Infinite Line Source
MAPE	Mean Absolute Percentage Error
MDF	Multiple Degree of Freedom
MCHS	Moving Cylindrical Heat Source
MFLS	Moving Finite Line Source
MILS	Moving Infinite Line Source
MISOS	Multiple Input Single Output Simulation
OMEC	One-Material Equivalent Cylinder
RMSE	Root Mean Squared Error
SVD	Singular Value Decomposition
TRC	Thermal Resistance and Capacitance

### Symbols

$\alpha$	Thermal diffusivity ( $m^2/s$ )
----------	---------------------------------

$B$	Borehole spacing ( $m$ )
$\beta$	Dimensionless fluid to outer pipe wall thermal resistance
$C$	Fourier-Bessel coefficients
$c_{pf}$	Specific heat capacity at constant pressure ( $J/(kgK)$ )
$D$	Borehole buried depth ( $m$ )
$E$	Fluid-independent integrals in the multipole expansion
$E, R$	Thermal resistance ( $mK/W$ )
$\epsilon$	Porosity
erf	Error function
erfint	Integral of the error function
$g$	$g$ -function
$\mathcal{G}$	Number of equivalent boreholes groups
$\mathbb{G}$	Borehole group
$\gamma, \delta, \alpha, \beta, g$	Coefficients matching the boundaries
$h$	segment-to-segment thermal response factor
$H^1$	Hankel function of the first kind
$\bar{\mathbf{H}}$	Matrix of segment-to-segment response factor
$\theta$	Dimensionless temperature
$\bar{\Theta}$	Vector of dimensionless borehole wall temperature
$I$	Integral function
$J$	Bessel function of the first kind
$k$	Thermal conductivity ( $W/(mK)$ )
$K$	Modified Bessel function of the second kind
$\mathcal{K}$	Cluster precision increment
$l, e$	Pipe-to-pipe center distance ( $m$ )
$L$	Borehole length ( $m$ )
$\mathcal{L}$	Complete linkage criteria
$\bar{\mathbf{L}}$	Vector of length ratios
$\lambda$	Eigenvalue
$\dot{m}$	Mass flow rate ( $kg/s$ )
$\mathcal{M}$	Distance metric between two boreholes
$M, h$	Number of terms in the transient multipole expansion
$N$	Number of pipes
$n_s, n_q$	Number of segments in the FLS model
Nu	Nusselt number
$\nabla^2$	Laplace operator



$\nabla$	Nabla operator
$O$	Geometrical center $((m, rad))$
$\Omega$	Computational domain
$\partial\Omega$	Computational boundary
$\psi$	Auxiliary function
$\bar{\Phi}$	Vector of dimensionless heat extraction rates
$\dot{Q}$	Heat extraction rate ( $W$ )
$q', Q'$	Heat extraction rate per borehole length ( $W/m$ )
$R_0, r_b$	Borehole radius ( $m$ )
$r_k$	Pipe radius
$\rho$	Radial coordinate ( $m$ )
$\rho_f$	Fluid density ( $kg/m^3$ )
$Re$	Reynolds number
$s$	Integration variable
$t_h$	Pipe thickness
$t$	Time ( $s$ )
$\Delta t$	Time step ( $s$ )
$T$	Temperature profile ( $^{\circ}C$ )
$T^0$	Undisturbed ground temperature ( $^{\circ}C$ )
$\bar{T}$	Average temperature at specific boundary ( $^{\circ}C$ )
$T_b$	Average borehole wall temperature profile ( $^{\circ}C$ )
$T_f$	Fluid temperature ( $^{\circ}C$ )
$\tau(t)$	Temporal separation function
$u$	Groundwater velocity ( $m/s$ )
$\phi$	Tangential coordinate ( $rad$ )
$w$	Geometrical parameters
$\mathbf{x}$	Arbitrary point $((m, rad))$
$X$	Eigenfunction expansion
$z$	Axial coordinate

### Indices and exponents

$b$	Grout or borehole wall
$d, i$	Computational domain index
$\Delta$	Delta circuit
$eff$	Effective property
$f$	Fluid

$i, j$	Borehole index
$\mathcal{I}, \mathcal{J}$	Equivalent borehole group
$m$	Multipole expansion index
$n$	Current time step
$p$	Time step index
$p, k$	Pipes position index
$s$	Soil
$s$	Layer in the 3D transient multipole expansion
$u, v$	Segment in the FLS model
$out, in$	Outlet and inlet fluid temperature

## LIST OF APPENDICES

Appendix A	Time-dependent fluid temperatures by means of Duhamel's theorem .	153
Appendix B	Quasi-orthogonal condition for the groundwater transient multipole expansion . . . . .	156
Appendix C	Additional formulas for the groundwater transient multipole expansion	159

## CHAPTER 1 INTRODUCTION

Currently, the largest share of energy generation is from fossil fuels; however, this type of resource is non-renewable and generates large CO<sub>2</sub> emissions [1, 2]. Renewable energy trends include wind, biomass, solar, hydro, and geothermal [3]. Geothermal energy production consists of the capture of heat from the ground. Geothermal energy can be used for heating or cooling systems of buildings by ground-coupled heat pumps (GCHP) in addition to generating electricity [4].

A GCHP is a system that allows one to extract heat from (or reject heat to) the underground and take advantage of it for heating (or cooling) of buildings. This type of system can be divided into two categories: a closed loop system that is based on the direct coupling of a ground heat exchanger (GHE) that allows the rejection or extraction of heat, and open loop systems that directly uses circulating water in the ground [5]. A GHE consists of a drilled hole in the ground with collector pipes inserted into it and a filling material called grout. The notable advantage of GCHPs over traditional air-source heat pump systems is that GCHPs have a higher coefficient of performance (COP). This is because the soil presents a relatively constant temperature year long, and the soil temperature is higher than the air temperature in winter and lower in summer [6, 7].

Mathematical heat transfer models are used in all phases of GCHP system planning, design and operation. These mathematical models allow us to predict temperature changes in the fluid and the ground due to fluctuations in the heat rejection/extraction from the GHE. In site characterization applications, physical parameters (soil thermal conductivity, borehole thermal resistance, etc.) can be inferred by fitting a mathematical model to measurements from a thermal response test [8]. In the design phase of the GHE, a mathematical model can be used to estimate the size of GHE to satisfy the operation parameters of the equipment, for example, lower and upper fluid temperature limits for the heat pump operation. Heat pump and GHE heat transfer mathematical models can be coupled to predict the system's energy consumption. Also, these models could successfully pose an optimization strategy for the system design and development of model-based control strategies.

Using a time scale analysis proposed by Bejan [9], it is possible to separate the thermal behaviour of the GHE in different time scales to allow appropriate temperature predictions. This analysis, also shown in Li and Lai [10], shows that this time separation can be done as follows:

- Time analysis of the order of hours (often called short-term): The effect of the thermal

capacity and the internal geometry of the GHE is important and must be studied. Also, the fluid transit in the pipes is usually of the order of several minutes.

- Time analysis of the order of months (often called mid-term): Interactions between adjacent boreholes should be studied.
- Time analysis of the order of years/decades (often called long-term): Borehole length effects are important, also called end effects of GHE.

As we can see, temperature predictions in GHEs require the knowledge of each time scale, and for such, mathematical models are necessary to quantify the effects. Simulation models (i.e. mathematical models) of GHEs are obtained by coupling a model of the interior of the GHEs with a model of the exterior of the GHEs.

Models of the interior of GHEs solve the heat transfer between the fluid flowing through the pipes and the GHE wall. Exact methods for steady-state conduction inside the borehole are available. Still, only approximate methods (focusing on computationally efficient methods suitable for routine simulations) are available for transient conduction inside the borehole. Transient models are needed to analyze the short-time dynamics of GHEs, which are important because they impact the operation of heat pumps [11]. The thermal capacitance of GHE materials slows down temperature changes in and around the GHE following the extraction or injection of heat. When not considered, temperature changes may be overestimated, leading to an underestimation of the GCHP efficiency or an oversizing of the GHE.

Models of the exterior of the boreholes are obtained by superposition of analytical solutions or by numerical methods (such as FEM, FDM, or FVM). These models can predict the thermal response of multiple GHEs considering thermal interactions between GHEs and thermal processes involving the end effects of GHEs (i.e. effects of length in the thermal response). Thermal interactions significantly impact the thermal response of GHEs, as heat extraction or injection at a GHE eventually affects the temperature of neighbouring GHEs.

Groundwater flow has been shown to influence the thermal response of GHEs. It modifies the thermal response due to the advection effects in the soil [12, 13]. The scientific literature focuses on the impact of groundwater flow on the heat transfer process outside GHEs, using available models for the interior of the boreholes. These models were developed assuming pure conduction and are not necessarily valid when dealing with groundwater flow.

This dissertation addresses the topic of thermal modelling of GHEs. The project aims at filling the need for efficient and accurate methods for the short-term response of GHEs and apply them in the context of long-term 3D simulations. The impact of groundwater flow on thermal processes inside the borehole will be modelled and assessed.

## CHAPTER 2 LITERATURE REVIEW

The literature review is organized into three sections : (i) steady-state and transient modelling approaches for the interior of the boreholes, (ii) analytical and numerical modelling approaches to heat conduction in the soil surrounding GHEs, and (iii) modelling approaches to account for groundwater flow in the simulation of GHEs.

### 2.1 Interior of the ground heat exchangers

The thermal behaviour of GHEs is described in two scenarios: i) steady-state and ii) transient state. Steady-state corresponds to operations in which the temperature gradients have stabilized inside the GHE, i.e. the total heat transfer rate through the pipes is equal to the heat transfer rate through the borehole wall. Usually, this effect occurs in the first few hours of operation for the interior of the GHE. The transient state is the steady-state counterpart, meaning thermal capacity is considered for short-term periods corresponding from a couple minutes of operation until the steady-state is reached. The main purpose of studying these models is to establish relationships for evaluating heat transfer rates between pairs of pipes and between each pipe and the borehole wall.

#### 2.1.1 Steady-state models

One concept that needs an introduction for describing the heat transfer process in a GHE is the so-called thermal resistances. Thermal resistances are defined through analogy with classical electrical circuits. A representation of a two-pipe GHE geometry (i.e. a single U-tube) and its thermal resistance circuit is shown in Figure 2.1.  $T_{f_1}$ ,  $T_{f_2}$  and  $T_b$  are the fluid temperatures in each pipe and average borehole wall temperature, respectively.  $R_1^\Delta$  and  $R_2^\Delta$  are the delta thermal resistances between fluid-pipe and borehole wall, and  $R_{12}^\Delta$  is the resistance between pipes.

Bose et al. [14] studied the first equivalent pipe model using conformal mapping techniques. The equivalent pipe assumption transforms the locations of the internal pipes of the GHE into a simpler one with only one pipe, allowing for the development of closed-form solutions to the heat transfer problem in the GHE. This model proposes the analysis of a non-axisymmetric pipe with the change of coordinates to pose the problem as an axisymmetric pipe. Although the method results in an analytical solution for heat conduction, it does not consider the spacing effect between pipes on the thermal short-circuiting inside de GHE.

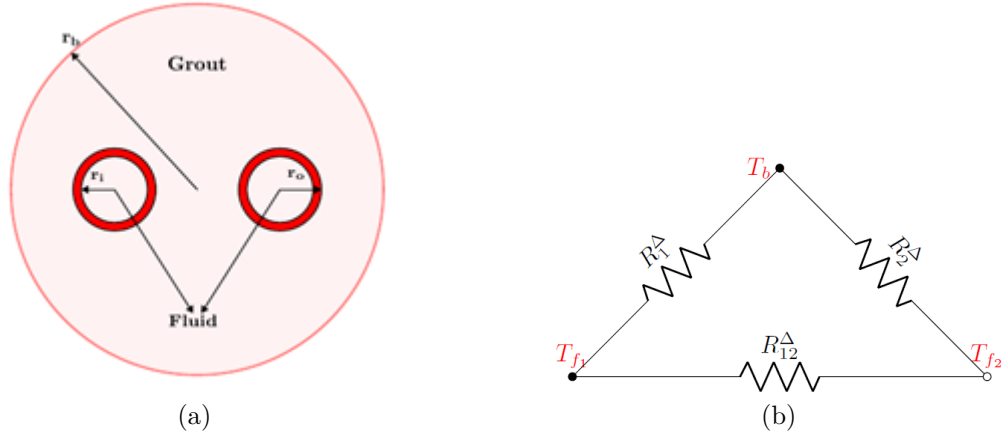


Figure 2.1 a) Cross section of GHE and b) Delta circuit

Gu and O’Neal [15], using the ideas of Bose et al. [14], solved the model in steady-state by assuming constant thermal conductivity without considering conformal mapping properties transition. Instead of having the equivalent pipe as equality of areas [16], they propose a modification using the spacing between pipes. To calculate the thermal interactions between pipes, each leg is considered concentric, and then spatial superposition is used to evaluate the temperatures at each pipe.

Bennet et al. [17] introduced the multipole method to evaluate the delta-circuit thermal resistances. This method solves the steady-state heat conduction problem in a horizontal cross-section of a GHE with any number of pipes within the GHE and different thermal conductivities for the soil and grout. Multipoles are created at the center of each boundary (i.e. pipes, borehole wall and infinite-exterior domain). It is imposed as boundary conditions the temperatures of the fluid in each pipe and the soil temperature at some distance from the borehole. This assumption allows to successfully evaluate thermal resistances using the superposition of temperatures at each pipe. Further development is done by Claesson and Hellström [18], in which the formulas for calculating thermal resistances and methodology are simplified by imposing heat fluxes at the pipes instead of temperatures and by imposing the average borehole wall temperature instead of a far-field temperature. This method is the state-of-the-art for the calculation of steady-state thermal resistances. The method approaches the exact solution as the multipole solution’s order increases.

Hu et al. [19] developed a multipole-based model to study heat transfer within the borehole by attaching a cylindrical heat source for the ground. The method considers the temperature variation in each pipe using an energy balance and the thermal resistance analogy. Temperature is modelled as Fourier series with unknown coefficients determined with matching boundaries. The heat transfer problem is steady-state within the borehole and transient for

ground by G-Factors created by the cylindrical heat source solution [20]. The main contribution of this work is that the multipole is created using the half-term of Fourier expansion, which reduces the complexity of matching coefficients.

Zeng et al. [21] proposed a quasi-3D model. In their work, they present from local form the solution of heat transfer using the line source approximation for the evaluation of thermal resistances [22]. An energy balance was used to analyze the axial temperature changes, considering the heat transfer in each of the pipes and the interaction between them. They were able to present closed formulas for fluid temperatures assuming an average borehole wall temperature for single and double U-tube based on the mathematical development of Helström [22]. Eslami-Nejad and Bernier [23] develop a model to study the steady-state heat transfer and simulate different arrangements of the pipes for a double U-pipe with two independent circuits. Belzile et al. [24] also study double U-pipe configurations with two independent circuits; however, they consider pipe locations as not necessarily symmetric. Cimmino [25] extends the methodology for  $N$  arbitrarily positioned pipes, coupling the effects with an analytical model of the ground heat transfer base on the finite line source solution.

### 2.1.2 Transient models

Thermal capacity in the grout causes the transient state or the so-called short-term by slowing down the heat propagation rate inside the GHE. A variety of models have been developed to establish a way to simulate and predict these effects. Here will be presented different approaches to solve this problem.

### Equivalent pipe models

Modelling transient state results in a non-easy task; thus, some authors have established geometrical assumptions to approximate the thermal behaviour. Such a consideration is an equivalent pipe model. Equivalent pipe models rely on the simplification of the real geometry of the borehole consisting of multiple pipes into an equivalent geometry with only one pipe. Usually, authors evaluate the size of the equivalent pipe by imposing equality of areas between pipes and the equivalent, as shown in Claesson and Dunand [16]. Although the model results in a simple one, this does not consider the real effect of the grout's thermal capacity because the pipes' location affects how quickly heat travels between the pipes and the borehole wall.

Gu and O'Neal [26] resolved the model considering only one infinite cylinder in the transient state using eigenexpansion. In their work, the problem is transformed into a dimensionless model. The calculation of eigenvalues is necessary to complete the solution of the problem.



The heat flow in the axisymmetric pipe is considered constant.

Shonder and Beck [27] studied the one-dimensional transient model (i.e. the equivalent pipe assumption) based on equality of areas, separating the pipe, grout and soil into an independent model. Thermal capacity is included, but the effects on the thermal resistances are not considered due to the one pipe assumption. At an effective radius, it is imposed an average heat flux considering the heat flux on each pipe (i.e. mean value theorem). Using the least squares method, they were able to interpret a thermal response test and estimate the thermal properties of the GHE.

Young [28], following the work of Carslaw and Jaeger [20], was able to simulate short-term effects. This model uses the equivalence between a buried electric cable (BEC) and the U-tube by geometric area ratio (i.e. equality of areas); with the fluid considered as the core of the cable, the grout as the sheath of the cable, and the borehole thermal resistance as the insulation of the cable. A grout allocation factor (GAF) is introduced to include the effects of grout and soil thermal capacities.

Xu and Spitler [29] developed a one-dimensional model using the finite volume method (FVM). Their model considered the fluid as an annular volume within the pipe with an equivalent thermal capacity. A heat flux is applied as a boundary condition on the inner surface of the fluid annulus. The convection between the fluid and the pipe is represented by a fictitious layer between the fluid and the inner pipe wall.

Lamarche and Beauchamp [30] solved the heat transfer in a transient state for an equivalent pipe. They solved two cases: i) heat flux at the equivalent pipe and ii) convection in the equivalent pipe. Laplace transform was used to transform the grout and soil heat transfer equation into time-independent models. Analytical solutions were obtained for both cases, which are helpful for computation.

Bandyopadhyay et al. [31] proposed an analytical solution of the transient model of GHE heat transfer using one pipe assumption and considering grout thermal properties equal to the ground. An equivalent pipe radius is obtained by equaling areas between two pipes in the borehole and the equivalent pipe area, and constant heat flux is considered in the borehole. The problem is solved in the Laplace domain, and the Stehfest algorithm [32] is used to reconstruct the Laplace domain solution to the temporal domain.

Javed and Claesson [33] proposed an analytical solution in the time domain using the inverse transform of the Laplace domain assuming equivalent pipe based on Bandyopadhyay et al. [31] ideas. Their model considers the constant heat flux injected into the borehole. In addition, they proposed a numerical solution to the transient state where they managed a change of

coordinates to simplify the flow of heat by coupling finite differences to validate the analytical model.

Beier [34] assumed an equivalent pipe and divided the GHE into two half pipe sections with an equivalent geometry, each one with independent fluid temperatures (Figure 2.2). The wall temperature of pipes is shared, so it is possible to couple the heat balance at each pipe. The method is called infinite composite-medium cylindrical source (ICMCS). The model includes transient effects and fluid, grout and soil thermal capacities, and axial heat transfer is neglected.

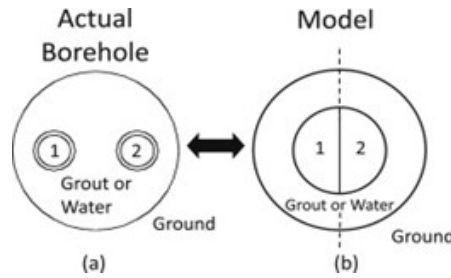


Figure 2.2 Configuration of ICMCS (Reused with permission from Beier [34])

Monteyne et al. [35], based on the work of Javed and Claesson [33], proposed a frequency domain solution. In this work, the authors assumed that the heat and fluid temperature could be modelled as a transfer function using the multiplicity theorem of transfer functions. Heat transfer functions do not depend on the reconstruction by classical methods such as the Stehfest algorithm or related. Furthermore, they only depend on the number of measurements. The model is quite useful for in-situ experiments since it is data-driven and would match the real heat transfer in the GHE.

Lamarche [36], based on the work of Javed and Claesson [33], was able to propose a closed solution to the proposed model in the time domain. Full inversion was used to complete the solution. This equivalent pipe model includes the fluid, grout, and soil thermal capacity. Heat transfer on the pipe is modelled by the infinite cylindrical source of Carslaw and Jaeger [20], and they were able to propose an equivalent pipe considering the modification of fluid and pipe thermal capacity. This equivalent pipe transformation differs from the past authors by considering an equivalent pipe thermal conductivity, fluid capacity and grout thermal capacity, while the other authors neglect this transformation. This consideration is necessary to maintain the heat transfer distribution inside the GHE as similar to a single U-tube.

Kuzmic et al. [37] studied and implemented a model using FVM for transient heat transfer in cylindrical coordinates called "homespun 2D" taking equivalent pipe as consideration of the pipes inside the borehole. This equivalent pipe is chosen in the same manner as Lamarche [36].

Uniform heat flux is imposed in the pipe considering the demand of the building and zero heat flux at the exterior boundary. The equivalent pipe is modelled as a finite-dimension cylinder. This model is used for hybrid-GCHP simulations.

Brussieux and Bernier [38] presented a work based on the finite volume method (FVM) technique for transient resolution. Based on the ideas of Xu and Spitler [29], the authors proposed the geometric model as an equivalent pipe, consisting of an FVM inside the borehole and infinite cylindrical source of Carslaw and Jaeger [20]. The model was used to define universal  $g^*$ -functions for short-term effects, which describe the response of the borehole wall temperature to a unit step heat injection in a single borehole or borefield.

Yu et al. [39], based on work from Bose et al. [14], proposed an equivalent pipe model to simulate the short-term response of the single U-tube GHE. The model encompasses a one-dimensional model for the ground heat transfer with uniform properties (i.e. thermal diffusivity, thermal conductivity and thermal capacity). The heat transfer model was solved using a finite difference method. They modified the Fourier and Biot number definition by considering it as a function of time step and radial step, allowing them to evaluate the short-term effects. Fluid temperatures are then calculated by heat balance considering the heat induced in the equivalent pipe by an energy balance on the fluid.

Naldi and Zanchini [40] proposed a new equivalent pipe model called a one-material equivalent cylinder (OMEC) to study transient heat transfer. In the model, they used a finite element (FEM) technique with a 2D model, including thermal capacity as the sum of fluid, pipe and grout capacity. The radius of the equivalent pipe is calculated by an iterative process considering a cylindrical heat source in the borehole. After iterations, the authors established a correlation for the radius of the equivalent pipe.

## **Thermal resistance and capacitance models**

Thermal resistance and capacitance (TRC) models rely on the analogy between the electrical and thermal processes. TRC models are obtained by modifying thermal resistance networks (as presented in section 2.1.1) to introduce thermal capacitance nodes representing the fluid, the grout, and sometimes the ground. The number of capacitance nodes, their location, and the distribution of the total capacitance between the nodes varies among the models in the surveyed literature. The following methods analyze the heat transfer inside the GHE and consider symmetrically positioned pipes within the GHE (as opposed to arbitrarily positioned pipes).

De Carli et al. [41] developed a Capacitance Resistance Model (CaRM), which studies heat

transfer in the transient state. The interaction between GHEs is also considered by discretizing the borefield into subsections and imposing an adiabatic boundary at some distance between them. They divide the GHE model into three regions: fluid, grout and soil (Figure 2.3) .

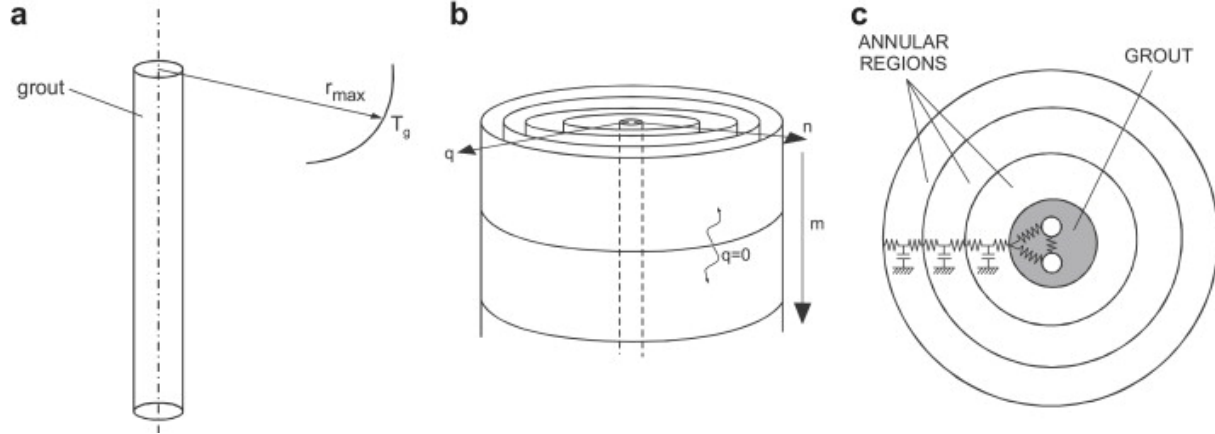


Figure 2.3 Plane discretization of CaRM (Reused with permission from De Carli et al. [41])

The inside of the GHE is modelled as a thermal resistance network while the soil is discretized into annular cells represented by thermal resistances and capacitances. The calculation domain is split axially into layers, and the heat transfer is analyzed radially in each layer (Figure 2.4). Since the inside of the GHE does not include thermal capacitance nodes, the short-term effects due to grout thermal capacitance are not considered inside the GHE.

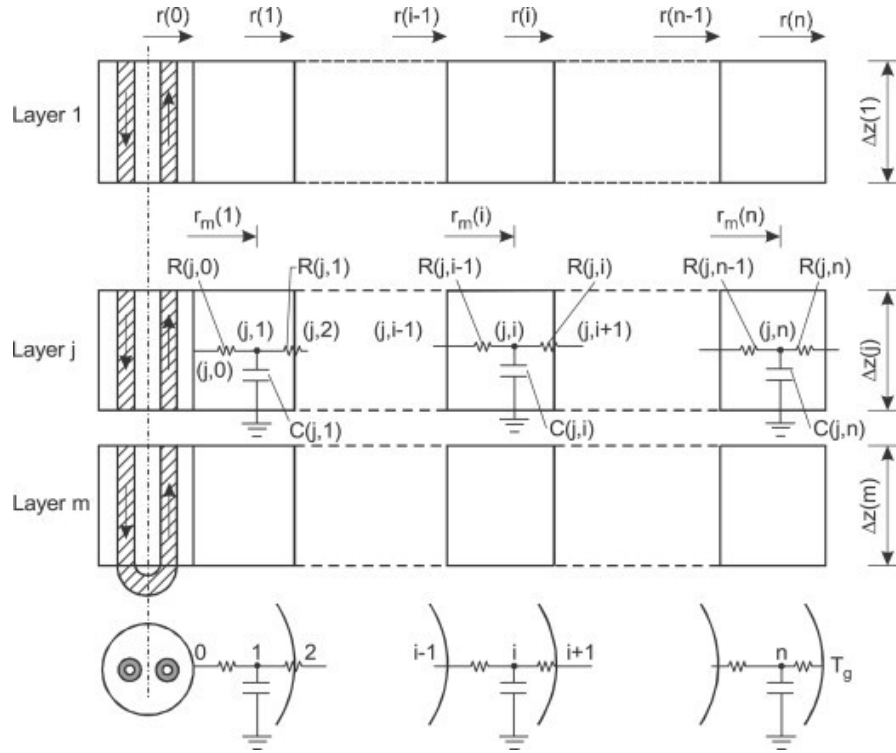


Figure 2.4 Axial discretization of CaRM (Reused with permission from De Carli et al. [41])

Zarrella et al. [42] developed an improvement of CaRM by including the thermal capacity of the grout (Figure 2.5) for double U-tube GHEs. The model separates the borehole as core (circle containing pipes) and shell (annular section outside pipes), and the thermal capacitance of each zone is allocated to a thermal capacity node in the thermal resistance network.

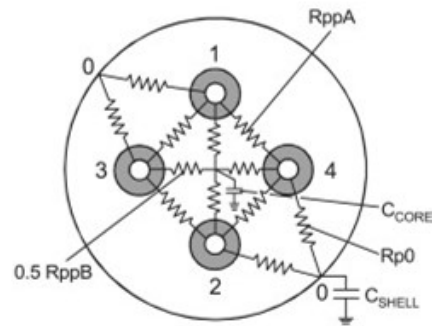


Figure 2.5 Improvement of CaRM (Reused with permission from Zarrella et al. [42])

Bauer et al. [43] introduced a thermal resistance-capacitance model (TRCM) model. The capacitance nodes represent the thermal capacity of each zone of the discretized GHE (e.g. half section of a single U-tube GHE). They studied three possible GHE configurations in

their work: single U-tube, double U-tube and coaxial tube (Figure 2.6). The model considers the thermal capacities of fluid, grout and soil. In each configuration, heat transfer occurs between fluid nodes, ground nodes, and the borehole wall node.

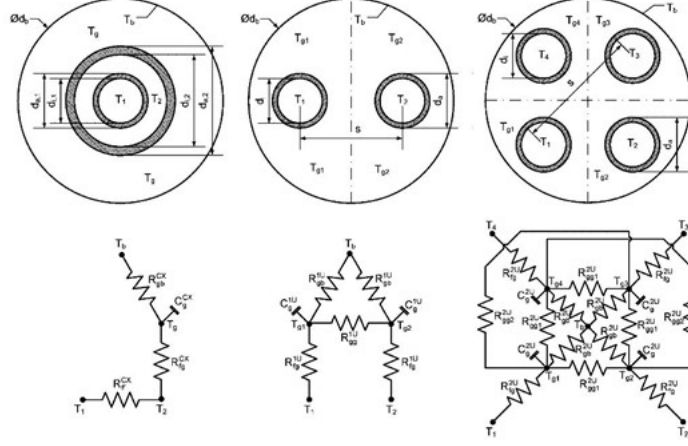


Figure 2.6 TRC models (Reused with permission from Bauer et al. [43])

Improving the method for taking into account fluid flowing inside the pipes, Bauer et al. [44] introduced a 3D TRC model by coupling the local model with the finite differences method (FDM), including the interactions of each pipe in the GHE (Figure 2.7). At each layer, the borehole and soil are discretized in the same manner as in their previous work. The extension to 3D is done by a heat balance on the fluid at each pipe, dividing it into subsections.

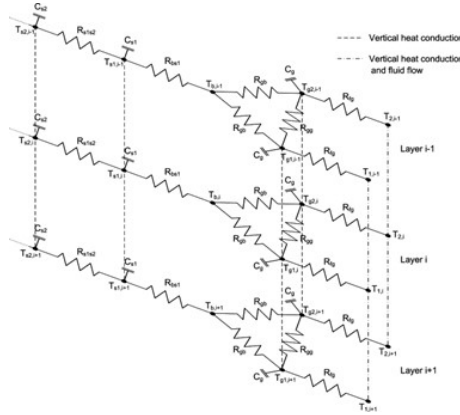


Figure 2.7 3D TRC model (Reused with permission from Bauer et al. [44])

Pasquier and Marcotte [45] improved the TRCM model by adding more capacitances and resistances to refine the discretization of the GHE (Figure 2.8). This improvement results in a more accurate method than the previous; however, the main drawback is that the computational time increases substantially as the number of nodes increases.

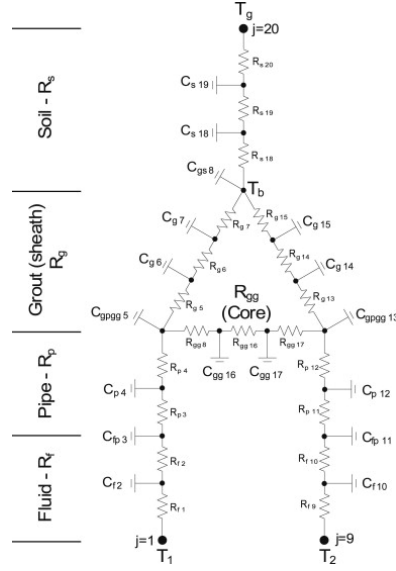


Figure 2.8 Modified-TRC model (Reused with permission from Pasquier and Marcotte [45])

Since the TRCM method from Pasquier and Marcotte [45] is not able to study the thermal interactions between pipes along the length of GHE, Pasquier and Marcotte [46] presented a modification of the 3D TRC extending their previous ideas (Figure 2.9) and used it for constructing response functions by means of a spectral method and the solution of the TRCM. They showed an efficient way to calculate the temperature response using these coupled techniques.

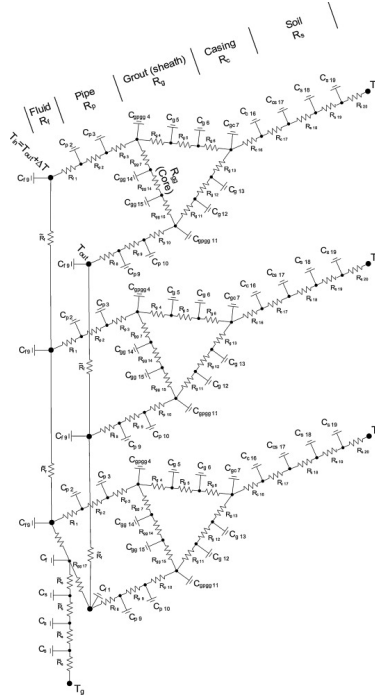


Figure 2.9 Modified-TRC model (Reused with permission from Pasquier and Marcotte [46])

Minaei and Maerefat [47] simplified the TRCM model because the complexity of accounting for more nodes involves high computational expenditure and assesses the numerical stability of TRCM due to the possibility of thermal resistances with negative values. They proposed a discretization of the grout using only 4 nodes and solve the problem in the Laplace domain by coupling the CHS model for the ground (Figure 2.10).

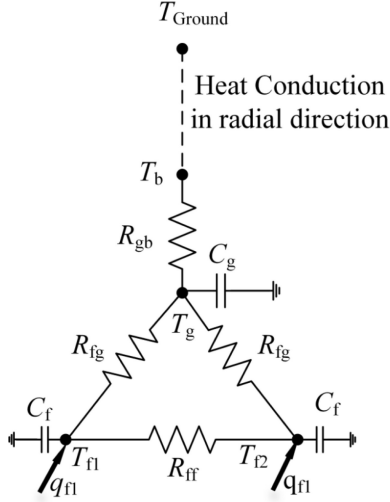


Figure 2.10 Simplified-TRC model (Reused with permission from Minaei and Maerefat [47])

Subsequently, Minaei and Maerefat [48] exhibited a simplified model of TRC by coupling the 2D TRC shown in Minaei and Maerefat [47] for the fluid-borehole and nodes discretization for the soil (Figure 2.11).

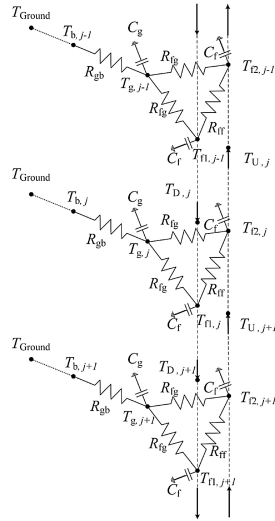


Figure 2.11 Simplified-TRC model (Reused with permission from Minaei and Maerefat [48])

The first commercial implementation of FEM for GHEs in the transient state was due to



Wetter and Huber [49], which is implemented in TRNSYS software in Type 451 called EWS. The model is relatively simple since only radial conduction is considered. For radial direction, equidistant elements are proposed, considering the soil for this discretization. The model is solved using the Crank-Nicholson scheme at the radial coordinate. For vertical or axial direction, uniform discretization is defined based on a finite given partition.

Oppelt et al. [50] created a new multiple input single output simulation (MISOS) model to improve the EWS model. The discretization of the new model is more complicated since the grout is divided into three zones: core, half annulus of outlet pipes and half annulus of inlet pipes (Figure 2.12). The model allows evaluating the transient response of fluid temperature using an energy balance in each element of the grout. The model relies on the geometrical discretization of the domain, which the authors consider symmetrically positioned pipes only. 3D heat conduction in GHE is neglected.

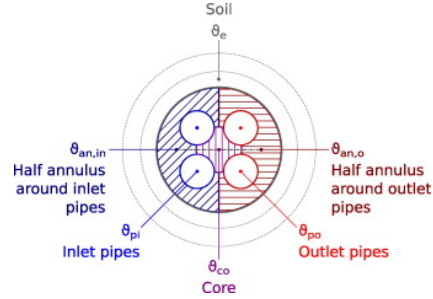


Figure 2.12 EWS improvement (Reused with permission from Oppelt et al. [50])

Ruiz-Calvo et al. [51] developed the borehole-to-ground (B2G) model to include the short-term thermal response based on the work from Bauer et al. (2011). The model is discretized axially to evaluate the temperature variation of the fluid, and radial heat transfer is calculated with the resistance analogy. They represent the grout as two nodes with capacitances and one node for the soil (Figure 2.13). The model includes the thermal capacities of fluid, grout and ground.

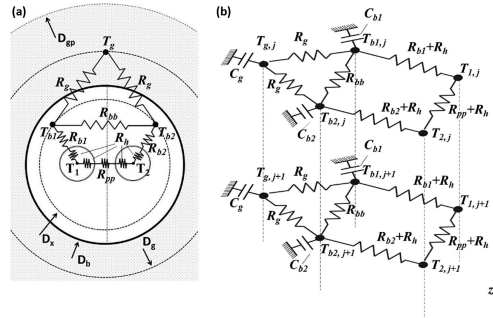


Figure 2.13 B2G model (Reused with permission from Ruiz-Calvo et al. [51])

## Other models

Yavuzturk and Spitler [52] developed a 2D (radial-angular) model using the finite volume method (FVM) called Borehole Fluid Thermal Mass (BFTM) model. In their work, pipes are discretized as pie sectors (Figure 2.14). The authors generated g-functions for short-time periods. Although the model approximates the exact pipe locations and thermal capacity of GHE, the effects of axial heat transfer are neglected.

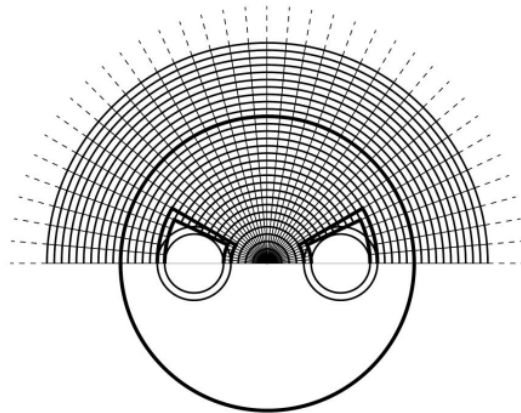


Figure 2.14 BFTM model

Li and Lai [53] proposed a method called infinite composite-medium line source (ICMLS) based on previous solutions for composite circular cylinders given by Jaeger [54]. In this model, each pipe is assumed as an infinite line source in the grout. The thermal capacity of the fluid is not considered. Each line source releases heat non strictly at the same rate, thus evaluating the temperature at each pipe wall. Using this assumption and the method for calculating borehole wall temperature shown in Li and Lai [55], they were able to calculate the fluid temperature. Yang and Li [56] proposed a modification to the ICMLS model by coupling a finite volume method (FVM) considering the thermal capacities of the fluid, pipes, grout and soil. While line sources can represent the individual positions of the pipes within the GHE, the real geometry of the GHE is only approximated as the pipes are cylindrical in reality. Axial heat transfer is not considered.

BniLam and Al-Khoury [57] introduced a spectral model. This approach takes the change of time domain to frequency using Fourier transform, and for the axial model of heat transfer is made, the use of eigenexpansion. The method also considers the heat friction gain due to fluid flow in a pipe. The method requires the discretization of the domain following the principles of FVM to simplify the requirement regarding the eigenexpansion and effecting the eigenvalues of this expansion.

Multiple degrees of freedom (MDF) for the FEM technique is adopted in the work of Woloszyn

and Gola [58,59]. A clear difference with the FEM models adopted by other authors is the grout separation in 3 regions, as the temperature variations in each pipe are considered (Figure 2.15). 3D heat conduction is considered, but due to the geometrical discretization of grout regions, the models are limited to symmetrically positioned pipes.

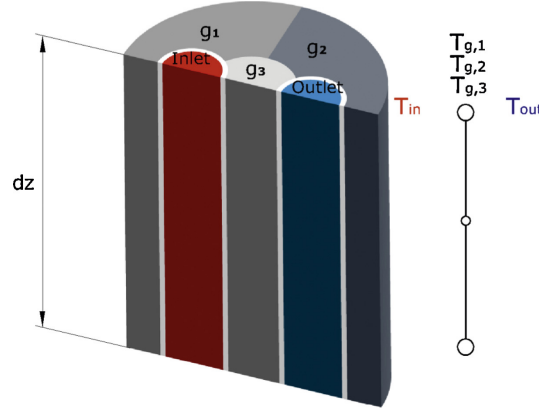


Figure 2.15 MDF model (Reused with permission from Woloszyn and Gola [58])

Rivero and Hermanns [60] have proposed an exact analytical solution to study the transient heat transfer inside a GHE for arbitrarily positioned pipes. The model is solved in the spectral domain employing matching asymptotic expansions. Although the model results in an exact solution for the transient heat transfer phenomena, the main objective is calculating the thermal resistances. It is computationally expensive since the model works in the spectral domain, and in routine simulations, the time domain is usually preferred.

### 2.1.3 Discussion

As seen, by definition, steady-state models cannot simulate short-term effects (operating times less than 10 hours); therefore, the sudden fluctuations in a typical GCHP cannot be accurately studied. Because of this, it is necessary to include both short-term effects in the modelling for the correct prediction of GCHP performance.

The models presented for the transient effects of heat transfer inside the GHE show that it is possible to model the short-term effects both in an approximate way (i.e. equivalent pipes, TRCM, FVM-FEM) and in an exact way in the frequency domain [60]. In the case of the approximate methods, the interior of the GHE is discretized so that the geometrical area is preserved (i.e. equivalent pipe) or the heat balance between pipes and grout with the connecting borehole wall is maintained (i.e. TRC methods). This is done by simulating only pipes symmetrically positioned in the grout with an analogy of thermal resistances and capacitances (i.e. TRCM). However, these solutions do not correspond to what happens

inside the GHE. For instance, the heat transfer around the pipes is not well described, leading to a possible overestimation (or underestimation) of the thermal response in the interior of the GHE. There are methods such as FEM and FVM, which are computationally expensive and discretizes the interior using a mesh-based technique. They are however computationally demanding, and rarely used in GHE simulations.

On the other hand, the exact solution in the spectral domain allows us to estimate the thermal resistances at the interior of the GHE for arbitrarily positioned pipes in the grout. Although it is an exact solution (or approaching exact), this method could not be easily adapted for routine simulations for control or performance of a GCHP. This is due to the fact that this solution works on the frequency domain rather than the time domain. Thus, the literature shows that there are currently no exact time-domain analytical solutions to the transient state heat transfer in a GHE.

## 2.2 Exterior of the ground heat exchangers

The exterior domain is the ground where the GHEs are placed. Both analytical and numerical models have been studied. The ground is mostly modelled as a semi-infinite domain with a uniform initial temperature (i.e. the undisturbed ground temperature); thus, radial heat transfer is considered. Analytical (or semi-analytical) and numerical models are presented in this section.

### 2.2.1 Analytical models

The first mathematical model studied is due to Kelvin in 1882 [61], called point source theory, and was later used for GHEs by Ingersoll and Plass [62] to define the so-called infinite line source (ILS). The model calculates the temperature changes at a distance  $r$  from an infinite line. Another classical model studied is the so-called cylindrical heat source (CHS) studied by Carslaw and Jaeger [20] and applied to GHEs by Ingersoll et al. [63]. This model studies heat conduction in a hollow cylinder of radius  $r_b$ , with infinite length. It obtains the temperature response of an infinite line positioned at  $r \geq r_b$ , when the heat flow from the GHE to the soil is imposed. Some authors have used and modified this CHS model to calculate fluid temperatures of the GHE [64–66].

Eskilson [67] introduced the finite line source (FLS), in which the GHE is modelled as a finite dimension line buried in the ground. The concept of g-function is also introduced, which is defined as a non-dimensional temperature response factor that relates the borehole wall temperature and the injecting or extracting heat transfer rate from the ground caused by the

thermal diffusion process in the ground. Subsequently, Zeng et al. [68] calculated the thermal response of a GHE when the borehole is buried below the earth's surface. Lamarche and Beauchamp [69] developed a new solution for the FLS model for the same case, simplifying the computation of integrals of the model. Bandos et al. [70] proposed new analytical models to compute the ground temperature field produced by the FLS and considered the asymptotic behaviour of the thermal response due to surface temperature oscillations. Claesson and Javed [71] were able to compute the temperature variation of GHE for a depth greater or equal to zero and improve the FLS model. These methods rely on isoflux lines that consider spatial and temporal superposition of heat rates in the borehole or borefields. Cimmino et al. [72], based on Eskilson's method, consider equal borehole wall temperatures along all GHEs in the borefield. Both temporal and spatial superposition is used to calculate the thermal response. They show that  $g$ -functions could not be calculated with the classical FLS solution. Cimmino and Bernier [73] extend the model to consider a uniform temperature along the boreholes. The GHEs are discretized into segments, and segment-to-segment response factors are defined and superimposed in temporal and spatial domains to obtain borehole wall temperatures in the borefield. This new methodology allows the construction of thermal response factors of borefields, including the heat extraction variation over time along the length of the boreholes. Abdelaziz et al. [74] extended the FLS to include anisotropic soil along the length of the borehole, including different thermal properties as a layered solution. Lazzarotto [75] proposed a methodology to evaluate the  $g$ -functions of borefields with inclined boreholes using a simplification of the FLS solution for inclined boreholes of Lamarche [76].

As shown in Cimmino [77], the internal thermal resistances significantly impact the heat transfer process of GHEs. Cimmino's work relies on the impact study of thermal resistances and fluid flow rate in the thermal response of GHE. When the thermal resistances change, both the temperature and heat transfer rate distributions along the boreholes change, which modifies the long-term response of the bore field. An accurate prediction of the long-term temperature changes thus requires considering the heat transfer process inside the boreholes.

Zhang et al. [78] proposed a quasi-3D model for simulating heat transfer in a transient state. The models use the delta circuit of resistance for the horizontal heat transfer process (i.e. steady-state) and the heat balance on each pipe for expressing fluid temperatures as a function of thermal resistances at some depth of the borehole. The soil is modelled by the superposition of ILS, FLS and ICMLS models at the borehole wall, defining a "new G-factor". They proposed an equivalent borehole thermal resistance for the transient state. Fluid temperatures are calculated by a fundamental heat balance solution on each pipe.

Zhang et al. [79] improved the FLS solution by adding more complex initial and boundary

conditions. In their method, surface temperature variations are represented as a superposition of sinusoidal waves, and the initial temperature includes the geothermal gradient. The method requires many integral evaluations.

### 2.2.2 Numerical models

Claesson and Hellström developed the Duct Ground Heat Storage (DST) model [22, 80, 81]. The DST model is useful for modelling energy storage for thermal systems with borehole connected in series. The model simulates 2D heat transfer. It assumes a large number of heat exchangers evenly distributed in a cylindrical ground volume to simulate heat transfer in a cylindrical mesh. This is done using spatial superposition. DST consists of two parts: local and global solutions. The local solution is the thermal process surrounding a single GHE and soil. The global process involves the relationship between steady state and short-term for the complete volume storage. It was subsequently implemented in the TRNSYS software [82]. Although this model is state-of-the-art for simulating energy storage, it does not consider the fluid temperature variations for short-term periods inside the borehole.

Diersch et al. [83, 84] introduced a transient model using FEM by coupling the TRC solution. They present simulations for single, double U-tube and coaxial arrangements. This technique represents each pipe as a line element. The proposed model considers the porous media model for solving soil heat transfer. The method is highly dependent on the discretization domain in two parts: i) the TRC model and ii) the mesh. This technique results in a highly accurate performance if there is a good discretization of the domain. However, from an engineering point of view, this class of methods could not be a designing tool due to their time expenditure, which is highly computationally demanding.

Monzó et al. [85] developed a numerical method based on FEM to describe the thermal response (i.e.  $g$ -functions) in the soil. The model relies on the imposition of isothermal lines in the borehole wall with a highly conductive material inside the GHE. This technique can also model a temperature gradient by modifying the thermal conductivity of the borehole. Although the model allows for manipulation of different boundary conditions in the borehole, the accuracy is mesh dependent. The configuration of pipes inside the GHE is not considered.

Belzile et al. [24] proposed a 2D diffusion solver to model a geothermal field. Each GHE is simulated with its analytical solution from steady-state thermal resistances in its solution. They used control volumes to simulate the interaction between GHE. The solution uses a shape factor for simulating the heat flow between the ground and GHE as an inner circle with an exterior boundary as a square. This method does not consider the thermal capacity of the grout, and hence short-term effects are neglected.

### 2.2.3 Discussion

The study of both the thermal interactions in a GHE field and the axial effects in long periods of operation of a GCHP is studied analytically and numerically, as shown. The analytical models, as well as their solutions, present a robust and flexible alternative for the study of these operations. However, they present an important limitation in their implementation. Since the models presented are based on the FLS solution, their solution complexity increases with the square of the number of GHE (or the square of the total number of segments for the segmented FLS solution). This limitation does not efficiently analyze large thermal interaction fields for their implementation in the design, performance and control of a GCHP system.

In contrast to analytical solutions, numerical models allow the analysis of different boundary conditions in one and several GHEs positioned in the soil, such as methods based on discretizing the continuous medium into grids or control volumes. The ability to change and mix boundary conditions and to include different arrangements of GHEs, as opposed to existing analytical solutions, allows the heat transfer phenomenon to be studied with better detail and approximation. However, this advantage is also an important limitation. As the model includes more detail and the number of GHEs increases, so does its computational requirement, making these detailed models unfeasible in typical geothermal system control and performance applications. As seen, the new numerical and analytical models must be robust and flexible so that the new solutions can scale them to new novel geothermal field applications. For instance, including short-term effects in the interior of the ground heat exchangers.

## 2.3 Groundwater flow

Modelling groundwater effects around the GHE is a complex process, and advection effects must be studied against conduction to know which (or both) effects are more important. Many authors have proposed models for studying these effects in GHEs, both numerical and analytical.

Chiasson et al. [12] made a study to assess the effects of groundwater flow on the heat transfer process for a GHE. They solved a finite element model to describe the groundwater flow effects in the GHE coupled with a heat transfer model. Peclet number was the parameter that they used to assess the effects. They have found that heat transfer by groundwater flow is only important when ground with high hydraulic conductivity is present. Following the previous conclusions, they performed an in-situ thermal response test by simulating the conditions in

a single GHE under different flow conditions.

Claesson and Hellström [86] proposed a method for considering the advection phenomena in a 2D domain in a transient state based on work from [67]. This work provides an extension of the classical g-function by introducing a groundwater g-function. This definition allows the authors to consider the total g-function as the difference between classical and groundwater g-function, thus allowing them to evaluate the borehole wall temperature.

Sutton et al. [87] studied the thermal response of GHEs under groundwater flow using the solution from Carslaw and Jaeger [20] in an infinite soil domain. This work defines two ground thermal resistances: conductive and convective. These resistances are used to evaluate the thermal response of the borehole and thus evaluate an average fluid temperature.

Diao et al. [88] presented a study for heat transfer in GHE under groundwater effects called moving infinite line source (MILS). The model encompasses an ILS model for the borehole, the properties of the ground remain constant through the simulation, and the ground's initial temperature is considered undisturbed. The model is two-dimensional, and the advection effects are considered in steady state, meaning the velocity field for groundwater effects is proposed as an equivalent velocity.

Chiasson and O'Connell [89], based on the work of Diao et al. [88] and Claesson and Hellström [86], were able to propose an analytical solution for heat transfer under the influence of groundwater flow. Groundwater flow and MILS are coupled by the advection-mass mathematical model, a transport equation. In the model, the fluid temperature is calculated as a function of constant heat flux in the borehole with a specified borehole thermal resistance and a temperature variation of borehole wall employing the coupled analytical solution.

Al-Khoury et al. [90] implemented a model using FEM for steady state for a single U-tube configuration. The GHE is represented as two one-dimensional lines along the borehole depth to simulate 3D heat transfer and the groundwater flow effect. Interactions between pipes are also considered. Subsequently, Al-Khoury and Bonnier [91] extended the model to a transient state, considering multiple pipes and incorporating groundwater flow. This method is highly accurate; however, it is not practically applicable for a borefield because of the high computational requirements.

Fan et al. [92] studied the performance of a GHE field under groundwater flow in a transient state. The soil was modelled as homogeneous and isotropic porous media in which thermo-mechanical dispersion is neglected. Every GHE is considered as an equivalent pipe and thus the real geometry of the boreholes is neglected. Unidirectional groundwater movement is considered. This study results in an impact analysis of groundwater flow in different seasons



(i.e. summer, winter) and correlate how different is the outlet fluid temperature of GHE with and without this effect. They have found that the discharge ratio (cold energy discharge from the soil and cold energy discharge to the soil) is higher when the groundwater flow is not present.

Nabi and Al-Khoury [93, 94] present a second-order finite volume method (FVM) model for transient heat transfer in 3D. The model uses two different mathematical models, one to represent the soil and the other for the GHE. The impact of groundwater flow (steady-state), heat-carrier fluid and GHE interaction are explicitly considered. Heat flow is proposed as a function within the equation system and not as a boundary condition (i.e. Duhamel principle).

Molina-Giraldo et al. [95] proposed a new method called moving finite line source (MFLS) based on the work of Diao et al. [88]. In their work, they extend the ideas by considering variation along the depth of the borehole. They obtained an analytical solution for the three-dimensional case using the relationship between FLS and the images method.

Wagner et al. [96] studied the applicability of the moving finite line source (MFLS) for a thermal response test under groundwater flow in a double U-tube GHE. In their work, groundwater velocity is considered constant for comparing the MFLS, and a FEM based on Diersch et al. [83, 84]. They found that the borehole wall temperature calculated using the MFLS is lower than FEM when constant heat is injected into the ground. As a conclusion of this work, the authors propose a correction procedure in calculating groundwater velocity to consider the advection effects between GHE and ground.

Tye-Gingras and Gosselin [97] studied the ground response under groundwater flow in a transient state. They created a “generic” ground response function (G-function). The method relies on coupling two analytical solutions, CHS and MFLS, and superimposing them to consider the effects of groundwater flow. This method is applied to single or multiple boreholes.

Rivera et al. [98] extended the ideas from the moving line source. In their work, Green functions are used to impose complex initial and boundary conditions. Analytical solutions were obtained for the thermal response of the ground.

Dai et al. [99] proposed a FEM to simulate short-term effects inside and outside the borehole under groundwater flow in the soil. The method couples a porous media mathematical heat transfer model in the soil, and U-tube and grout are modelled as a turbulent model and heat conduction, respectively.

Erol and François [100] created a new method based on multilayer soil domain and anisotropic media with groundwater flow. The solution requires the computation of the Green function

by assuming a point (pole) with a uniform infinite amount of heat and coupling with MFLS. The extension of this method for a multilayer media was done by spatial superposition of a point on each layer and studying the impact on the other layers. The method of layers is quite useful when the velocity is not constant along the depth of borehole.

Cimmino and Baliga [101] studied the thermal process in geothermal borefields. In their work, they use a coupled method: i) control-volume finite element method (CVFEM) to solve the complete heat transfer process in the soil under groundwater flow and ii) semi-analytical model to calculate fluid temperatures inside boreholes assuming quasi-steady state phenomenon. It is assumed that the heat transfer process inside is steady-state, which neglects the thermal capacity of the borehole.

Cai et al. [102] have developed a technique to simulate full-time heat transfer under groundwater flow. Based on work from Eskilson [67]; Diao et al. [88]; Molina-Giraldo et al. [95]; Beier [34], the authors established a complete setup to conduct short-, mid- and long-term simulations. As Fourier number is a function of time, the authors use it as a parameter to activate which model (i.e. MILS, MFLS, ICMCS) is responsible for the ground response.

Al-Khoury et al. [103] have created a model for the moving cylindrical heat source (MCHS) based on a spectral solution. The model encompasses groundwater moving with constant velocity and stagnating at the periphery of the GHE. The method can consider two boundary conditions at the borehole wall: a) arbitrary heat flux and b) arbitrary borehole wall temperature. The technique results in an excellent model to solve the exterior phenomena in the GHE; however, the groundwater does not stagnate at the whole borehole wall. Also, the short-term effects are neglected.

Luo et al. [104] proposed a solution for the groundwater water flow moving unidirectionally in the soil using an extension of the model proposed by Cimmino and Baliga [101], which rely on the groundwater segmented FLS. Their solution was able to adapt to include geothermal gradients and layered solutions corresponding to different thermal properties. Although the model is accurate regarding thermal response between soil and GHE, the short-term effects inside the GHE are neglected.

### 2.3.1 Discussion

The literature showed that the effects at the periphery of GHE are studied analytically and numerically. The analytical models, like those shown for pure heat conduction in the previous section, are quite flexible; however, simplifying the physical conditions of what happens around (and inside) the GHE does not allow a detailed study (e.g. whether or not

a typical configuration plays an important role in the overall thermal performance of the GHE). For example, based on an extension of the classical FLS and CHS solutions, these models consider that the groundwater flow passes through (or stagnates) in the borehole wall, which does not happen in reality due to the porous media. Because of this, the effects of this phenomenon from an analytical perspective have not been studied and assessed.

Numerical models, in turn, allow studying more realistic conditions, such as anisotropy of the porous media, different GHEs in the soil, groundwater moving around the GHEs, etc. However, the same limitation presented by the numerical models of the previous section is inherited: the more complex the model is, the more computational requirements are demanded, and therefore, its application in engineering solutions is not suggested.

Therefore, the need for an analytical model and its solution allows for studying effects when considering groundwater flow moving around the GHE. This is due to its flexibility both to include effects inside the GHE and to analyze both short- and long-term effects in the operation of GCHP systems.

## CHAPTER 3 OBJECTIVES AND THESIS STRUCTURE

### 3.1 Objectives

The general objective is to develop efficient and accurate methods for the short-term response of GHEs, with or without groundwater flow, and apply them in the context of long-term 3D simulations. This general objective is accomplished by fulfilling three specific objectives listed below:

- Solve the 2D transient heat transfer in a ground heat exchanger, considering the real geometry of the ground heat exchangers;
- Extend the 2D model to 3D, considering fluid flow through the pipes and thermal interactions between ground heat exchangers;
- Assess the effects of groundwater advection on the thermal resistances and on the transient thermal response of ground heat exchangers.

### 3.2 Thesis outline

The content of this thesis consists of nine chapters. Chapter 1 presents this thesis' introduction and motivation for this research work. Chapter 2 shows the literature review of heat transfer models describing the behaviour of GHE. The review in question is separated into models describing the inside and the outside of the GHEs, showing both numerical and analytical solutions existing in both transient and steady states. In addition, the study of groundwater flow is considered within the ground models. Chapter 3 shows the objectives and the structure of this dissertation.

In Chapter 4, the first article published in the journal *Science and Technology for the Built Environment* is shown. This paper presents an analytical and exact solution called transient multipole expansion to study heat transfer, considering the short-term effects with pipes arbitrarily positioned inside the GHE. The first scheme for estimating fluid temperatures is shown and complemented in Appendix A. The model is validated against results presented in the literature and an FEA model. This chapter addresses the first specific objective of this thesis.

Chapter 5 corresponds to the second article published in the *Journal of Building Performance Simulation*. This chapter analyzes the thermal interaction in the fields of GHEs. The study

allows us to estimate the thermal response of large geothermal fields considering groups of boreholes having similar borehole wall temperatures and heat extraction rates, thus proposing a new method called equivalent borehole using a hierarchical clustering approach. The evaluation of the accuracy of the method is made in comparison with existing models in the literature.

Chapter 6 shows the third article published in the open access journal, *Thermo*. In this chapter, we use the previous chapters to extend the idea of the heat conduction phenomenon from 2D to 3D. This extension estimates the fluid temperatures by coupling the exact solution defined by transient multipole expansion and the equivalent borehole method that allows the study of thermal interactions and axial effects in a field of GHEs. Also included are the advection effects on the pipes inside the GHE. The validation is performed using experimental data found in the literature and a high-fidelity FEA model. This chapter and the previous one fulfill the second specific objective of this thesis.

Chapter 7 presents the fourth and final paper accepted for presentation at the conference *International Ground Source Heat Pump Association (IGSHPA) Research Track 2022*. This chapter presents an extension of the transient multipole expansion that includes groundwater moving around the GHE and pipes arbitrarily positioned in the interior. The effect of groundwater movement is studied by calculating the average borehole wall temperature and estimating the thermal resistances defined inside the GHE. Appendices B and C complement the mathematical foundation presented in this article. This chapter addresses the third specific objective of this research work.

Finally, Chapter 8 presents a general discussion of this thesis, highlighting the contributions of each chapter. Chapter 9 shows the conclusions and recommendations for future work of the research presented in this thesis.

## CHAPTER 4 ARTICLE 1: TRANSIENT MULTIPOLE EXPANSION FOR HEAT TRANSFER IN GROUND HEAT EXCHANGERS

**Authors:** Carlos Prieto and Massimo Cimmino

**Article published in the journal:** *Science and Technology for the Built Environment*, Volume 27, Issue 3, pages 253–270.

**Date of publication:** 14 December 2020

### 4.1 Abstract

A transient multipole method for short-term simulations of ground heat exchangers (GHEs) is presented. The two-dimensional unsteady heat equation over a GHE cross-section is separated into two problems: (i) a transient heat equation with homogeneous boundary conditions, and (ii) a steady-state heat equation with non-homogeneous boundary conditions. An eigenfunction expansion is proposed for the solution of the transient heat equation, where the treatment of boundary conditions is considered by a multipole expansion of the eigenfunctions. A singular value decomposition is applied to extract the eigenvalues of the problem. The solution of the steady-state heat equation is obtained from a multipole expansion. The proposed method is validated against reference results for the evaluation of the eigenvalues and for the steady-state temperature field. The complete transient solution is validated against finite element analysis simulations. The proposed method is meshless, and its accuracy is only dependent on the evaluation of eigenvalues and on the number of terms in each of the multipole expansions.

### 4.2 Introduction

Ground-coupled heat pump (GCHP) systems consist in one or multiple heat pumps that supply heating and cooling to a building by extracting or rejecting heat to one or multiple boreholes, i.e. the bore field or ground heat exchanger (GHE). A GHE is composed of a drilled hole into which one or several U-tubes are inserted (or alternatively, coaxial pipes) to circulate the heat carrier fluid, and then backfilled with grouting material. The design of GCHP systems aims at evaluating the required GHE length to maintain the temperature of the secondary fluid circulating in the GHE within an acceptable range to ensure safe and efficient operation of the system. The fluid and ground temperatures evolve during the operation of the system following the extraction and rejection of heat to the ground

through the GHE. The short-term response of the GHE at time-scales of minutes to a few hours, corresponding to the time-scales of on/off and daily operation of the system, has been shown to have a significant impact on the required GHE length and on the energy use of the GCHP [11]. The short-term response of the GHE is driven by the transit of the fluid through the U-tube and the thermal capacity of borehole materials (i.e. the fluid, pipe and grout), and thus their inclusion into simulation models is required for accurate temperature predictions at short time-scales.

The classical approach to the heat transfer modelling of the interior of a borehole is through the thermal resistance analogy, where thermal interaction between pairs of pipes and between individual pipes and the ground are represented by a network of thermal resistances. The multipole method, introduced by Bennet et al. [17] and further developed by Claesson and Bennet [105] and Claesson and Hellström [18], provides an analytical solution to the two-dimensional steady-state heat conduction in a borehole cross-section and enables the evaluation of the thermal resistances of a borehole. The multipole method consists in the construction of the exact solution to the heat equation by superimposing solutions translated at each pole (i.e. at each pipe) to apply the boundary conditions of the heat transfer problem. While analytical steady-state methods, such as the multipole method, provide exact solutions to the heat transfer inside the borehole, they are not able to accurately simulate the short-term response of the borehole, before quasi-steady-state conditions (or constant heat-flux conditions) are attained within the borehole.

Authors have proposed solutions to the transient heat transfer in a GHE by introducing the equivalent pipe assumption, which consists in representing all pipes by a single equivalent pipe with appropriately chosen dimensions and thermal properties to create a one-dimensional geometry with similar thermal characteristics to the real two-dimensional geometry. The simplified one-dimensional geometry has facilitated the development of analytical and numerical solutions to the transient heat transfer of GHEs.

Authors have proposed solutions to the transient heat transfer in a GHE by introducing the equivalent pipe assumption, which consists in representing all pipes by a single equivalent pipe with appropriately chosen dimensions and thermal properties to create a one-dimensional geometry with similar thermal characteristics to the real two-dimensional geometry. The simplified one-dimensional geometry has facilitated the development of analytical and numerical solutions to the transient heat transfer of GHEs. Bose et al. [14] applied a conformal mapping technique to obtain an equivalent pipe model of a borehole. The method was used by Gu and O'Neal [15] to solve the steady-state heat conduction equation and calculate fluid temperatures under the assumption of constant thermal conductivity coefficients. Shonder

and Beck [27] applied a finite difference scheme to solve the transient heat transfer in the equivalent geometry. The authors used their numerical model to analyze field monitored data and estimate the thermal properties of the GHE and the soil using a parameter estimation technique. Young [28] adapted the Buried Electrical Cable solution of Carslaw and Jaeger [20] to the simulation of boreholes, with the thermal capacitances of the grout and the fluid inside the equivalent pipes allocated to the sheath and core regions of the buried electric cable, respectively. Lamarche and Beauchamp [30] developed an analytical solution to the transient heat transfer in the equivalent geometry with an imposed heat flux at the equivalent pipe. Bandyopadhyay et al. [31] proposed an analytical solution in the Laplace domain where the thermal capacity of the fluid is introduced as a virtual solid with a lumped capacitance. In their work, Laplace domain solutions were obtained for the equivalent pipe GHE. A time domain solution is then obtained by means of the Gaver–Stehfest algorithm for inversion of the Laplace domain solution [32]. Time-domain solutions were later proposed by Javed and Claesson [33] and by Lamarche [36]. The dimensions and thermal characteristics of the single equivalent pipe geometry are chosen to preserve the total thermal resistance and the total lumped capacitance of the GHE. The short-term response of the GHE is thus only approximated due to the centrally located pipe which does not present the same distribution of heat transfer than multiple off-centered pipes. The dimensions and thermal characteristics of the single equivalent pipe geometry are chosen to preserve the total thermal resistance and the total lumped capacitance of the GHE. The short-term response of the GHE is thus only approximated due to the centrally located pipe which does not present the same distribution of heat transfer than multiple off-centered pipes.

Transient heat transfer in geothermal boreholes with a simplified equivalent pipe geometry was also solved numerically. Xu and Spitler [29] developed a finite volume model of a GHE, where the thermal capacity of the fluid is included in an annular region within the pipe in the equivalent geometry. Brussieux and Bernier [38] presented a hybrid variant of this approach, modelling the ground as a semi-infinite media using the Cylindrical Heat Source (CHS) solution of Carslaw and Jaeger [20]. The authors introduced dimensionless parameters to define universal short time-step  $g^*$ -functions which take into account the short-time behavior of GHEs. Short time-step  $g$ -functions were introduced by Yavuzturk [52] who proposed a two-dimensional finite volume method in cylindrical coordinates to evaluate the thermal response of GHEs, taking into account the effects of the thermal capacities of the grout and pipe materials. Short time-step  $g$ -functions (and  $g^*$ -functions) provide an extension of Eskin's  $g$ -functions [67] to short time-step simulations and enable the design of GHEs with attention to short-time effects.

Li and Lai [53] proposed to model the short-term response of a GHE using the infinite



composite-medium line source (ICMLS) analytical solution, in which each pipe is represented as a line source in the grout of the GHE. The model accounts for the split of heat transfer rate between the pipes, since each pipe is modelled and may have different external wall temperatures. The model was validated by Yang and Li [56] using a finite volume method (FVM). The limitation of this method is that the pipes are simplified as lines (rather than cylinders), and thus the distribution of temperatures and heat transfer rate on the perimeter of the pipes is not taken into account.

Another class of simulation models aimed at the simulation of the short-time response of GHEs is composed of so-called thermal resistance and capacitance (TRC) models. Rather than attempting to solve the transient heat equation, this class of models introduces thermal capacitance nodes to the network of thermal resistances inferred from the multipole method or its approximations. Zarrella et al. [42] extended the capacity resistance model (CaRM) of De Carli et al. [41] to introduce thermal capacity nodes at the core and at the sheath of the borehole. Bauer et al. [43,44] developed a TRC model where thermal capacity nodes are introduced to represent the thermal capacity of half the GHE (for a single U-tube borehole). Pasquier and Marcotte [45] proposed an extension of the TRC model where each of the fluid, pipe and grout are represented as a series of thermal resistances and capacitances. The distribution of fluid temperatures along the GHE can then be obtained by coupling a series of TRC models each representing a segment of the GHE [46]. Minaei and Maerefat [47] observed that negative values of thermal resistances can be obtained in TRC models. While negative values have no effect on the accuracy of steady-state temperatures, they can cause a non-physical thermal response at short-time scales. The authors proposed a modified thermal resistance network to eliminate the negative thermal resistances. Like equivalent pipe geometries, TRC models preserve the total thermal resistance and the total lumped capacitance of the GHE. Thermal capacitances are split into core and exterior zones of the GHE, and thus the short-term response is expected to be more accurate but is still an estimate of the exact short-term response. The distribution of thermal capacitance nodes are based on arbitrary geometrical divisions of the GHE cross-sectional area and none of the surveyed methods are applicable to non-symmetric pipe configurations.

As per the surveyed literature, current analytical methods to solve the transient heat conduction equation in a cross-section of a GHE are limited to simplified one-dimensional geometries in cylindrical coordinates. The short-term response of the real geometry requires the solution of a partial differential equation (i.e. the heat equation) in a multiply-connected two-dimensional domain (i.e. a domain with multiple boundaries). Solutions to this type of problem have been obtained in other fields of application of heat transfer analysis. Commonly applied techniques are finite integral transforms (often applied to single layer materials), Green

functions, orthogonal expansions, and Laplace transforms [20]. In Cartesian coordinates, examples of applications of these techniques are Salt [106] and Mikhailov and Özisik [107] (orthogonal expansion technique in slabs) as well as Haji-Sheikh and Beck [108] (Green function). In cylindrical coordinates, example works are Abdul Azeez and Vakakis [109] (integral transform) and Miloevic and Raynaud [110] (orthogonal expansion in cylinders).

Numerical methods, such as finite difference, finite volume, finite element and boundary element methods, are often used to solve partial differential equations in multiple dimensions. The accuracy of these methods strongly depends on the quality of the mesh, and the generation of the mesh is complicated in cases where the geometry of the problem is highly variable—for instance, the number and position of pipes in a GHE. These methods also become time-intensive when applied to higher dimensions. There has been a growing interest in meshless methods over the past decade for heat transfer applications [111]. A popular class of meshless methods are Trefftz methods [112], which consist in approximating a regular solution to a partial differential equation problem in variational form. This technique is extended to use analytical solutions of the governing equations (e.g. Fourier-Bessel series) [113]. These methods are meshless. They can thus be implemented without the complexity of domain meshing and only require matching the boundaries over specific portions in a domain.

This paper presents a new method to solve the transient heat conduction problem in  $\mathbb{R}^2$  for a circular multiply-connected domain representing a cross-section of a GHE with multiple pipes. The separation of variables is applied to separate the problem into two equations, a Helmholtz partial differential equation for space and an ordinary differential equation for time. The complete solution is obtained by the superposition of a solution of the steady-state problem with inhomogeneous boundary conditions and a solution of a transient problem with homogeneous boundary conditions (i.e. a Sturm-Liouville problem). The transient problem is solved by applying a multipole expansion technique [114, 115], using an eigenfunction expansion of the solution. The solution considers constant fluid temperatures within each pipe. A scheme to update the coefficients of the multipole expansion is proposed to consider time-dependent fluid temperatures. The proposed method is validated by comparison with the results of Chen et al. [116, 117] for the evaluation of the eigenvalues of the expansion, with the results of Claesson and Hellström [18] for the solution of the steady-state problem, and to finite element analysis (FEA) simulations for the complete transient solution.

### 4.3 Mathematical model

A mathematical model for 2D transient heat conduction in geothermal boreholes is presented. The model assumes homogeneous, isotropic and constant physical properties for the grout

and the ground, with uniform temperature at time  $t = 0$ . The thermal capacity of the fluid flowing through the pipes and that of the pipe material are neglected. Axial heat transfer, through advection of the fluid flowing through the pipes and conduction in the vertical direction, is neglected and thus only pure conduction on the horizontal plane in the grout and ground is considered. The fluid to outer pipe wall thermal resistances, combining the film thermal resistances and the conduction thermal resistance through the pipe walls, is constant for each pipe.

Figure 4.1 shows the horizontal cross-section of a geothermal borehole with  $N = 2$  pipes (i.e. a single U-tube) as well as the computational domain of the mathematical model. The borehole, centered at  $O_0$ , has a radius  $R_0$  and each pipe  $i$ , centered at  $O_i$ , has an external radius  $R_i$ . The computational domain  $\Omega (= \Omega_1 \cup \Omega_2)$  comprises the grout sub-domain  $\Omega_1$  and the ground sub-domain  $\Omega_2$ , with  $\partial\Omega_0$  the interface between the grout and the ground (i.e. the borehole wall). The interior boundaries  $\partial\Omega_i$  correspond with the external wall of each pipe  $i$ . The domain extends to a radial distance  $R_e$  from the borehole center, corresponding with the external boundary  $\partial\Omega_e$ .  $R_e$  is considered infinite, and thus the ground domain  $\Omega_2$  is unbounded.

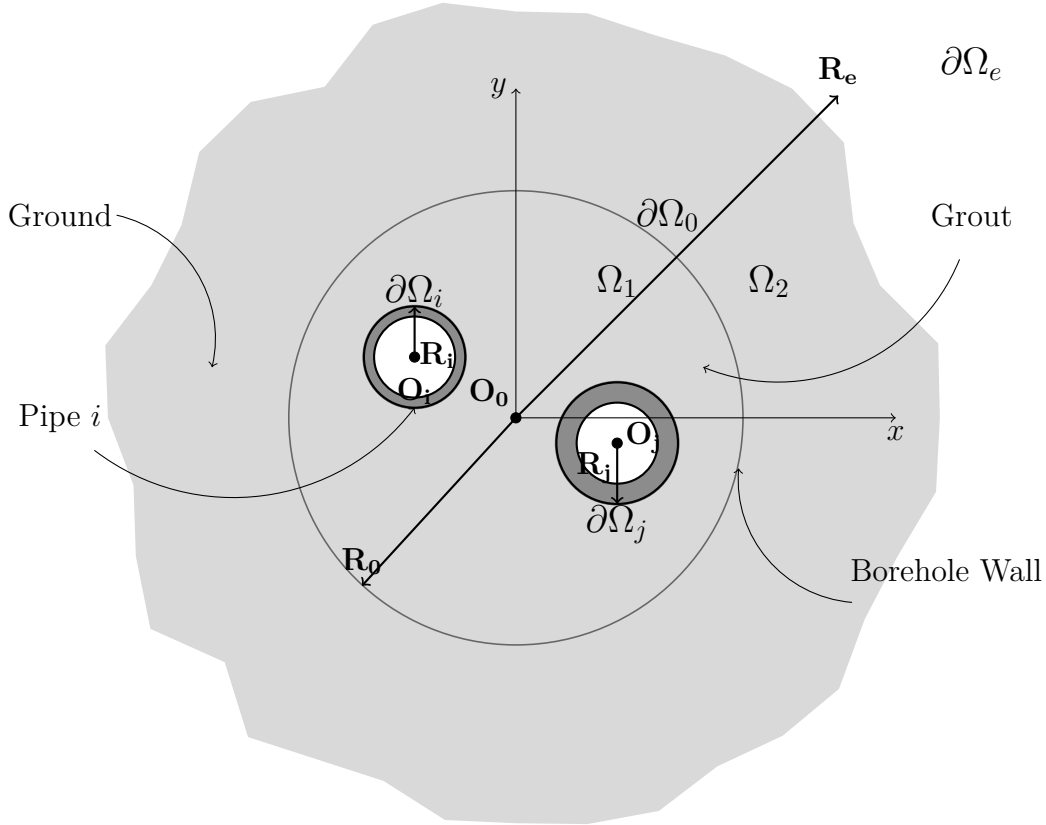


Figure 4.1 Ground heat exchanger domain geometry

A point  $\mathbf{x} = (\rho, \phi)$  in cylindrical coordinates could be centered at any pole  $O_k$ , with  $\mathbf{x}_k = (\rho_k, \phi_k)$ , as shown on Figure 4.2. Throughout the paper, the non-index coordinates  $\mathbf{x} = (\rho, \phi)$  are used when it is not needed to express the coordinates at any particular pole.

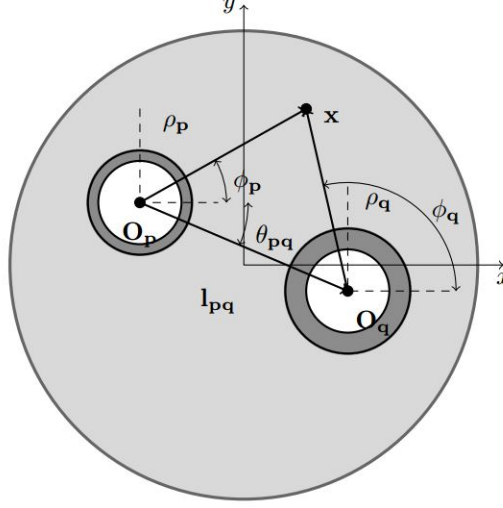


Figure 4.2 Translation of coordinates

The governing equation for heat transfer for calculating the temperature  $T_i = T_i(\mathbf{x}, t)$  is given by the transient heat conduction equation:

$$\frac{1}{\alpha_i} \frac{\partial T_i}{\partial t} = \nabla^2 T_i \text{ in } \Omega_i, i = 1, 2 \quad (4.1)$$

where  $T_1$  is the temperature in the grout domain  $\Omega_1$ ,  $T_2$  is the temperature in the ground domain  $\Omega_2$ , and  $\alpha_i$  is the thermal diffusivity at each domain  $\Omega_i$ .

The fluid temperature  $T_{f_k}$  at each pipe  $k$  is prescribed. As such, the boundary condition at the external wall of each pipe is:

$$-\beta_k R_k \frac{\partial T_1}{\partial \rho_k} \Big|_{R_k} + T_1 = T_{f_k} \text{ on } \partial\Omega_k, k = 1, \dots, N \quad (4.2)$$

where  $\beta_k = 2\pi k_b E_k$  is the dimensionless fluid to outer pipe wall thermal resistance of pipe  $k$ ; with  $k_b$  the grout thermal conductivity and  $E_k$  the fluid to outer pipe wall thermal resistance of pipe  $k$ .

Continuity is imposed at the borehole wall ( $\partial\Omega_0$ ):

$$-k_b \frac{\partial T_1}{\partial \rho_0} \Big|_{R_0} = -k_s \frac{\partial T_2}{\partial \rho_0} \Big|_{R_0} \text{ on } \partial\Omega_0 \quad (4.3)$$

and

$$T_1|_{R_0} = T_2|_{R_0} \text{ on } \partial\Omega_0 \quad (4.4)$$

where  $k_s$  is the thermal conductivity of the ground.

The temperature at the exterior domain boundary  $\partial\Omega_e$  (at  $R_e \rightarrow \infty$ ) is equal to the undisturbed ground temperature:

$$T_2(R_e, \phi, t)|_{R_e \rightarrow \infty} = T^0 \text{ on } \partial\Omega_e \quad (4.5)$$

At time  $t = 0$ , the initial grout and ground temperature are uniform and equal to the undisturbed ground temperature:

$$T_i(\rho, \phi, 0) = T^0 \text{ in } \Omega_i, i = 1, 2 \quad (4.6)$$

The set of boundary conditions (Equations (4.2)-(4.6)) is non-homogeneous. To obtain a solution to the temperature, the problem (Equation (4.1)) is separated into a transient problem with homogeneous boundary conditions (i.e. a Sturm-Liouville problem) and a steady-state problem with non-homogeneous boundary conditions. The complete solution becomes  $T_i = T_{i_h} + T_{i_{ss}}$ , where  $T_{i_h} = T_{i_h}(\rho, \phi, t)$  is the solution to the homogeneous transient boundary conditions and  $T_{i_{ss}} = T_{i_{ss}}(\rho, \phi)$  is the steady state solution of Equation (4.1).

The governing equation as well as boundary and initial conditions of the transient problem with homogeneous boundary conditions are given by:

$$\frac{1}{\alpha_i} \frac{\partial T_{i_h}}{\partial t} = \nabla^2 T_{i_h} \text{ in } \Omega_i, i = 1, 2 \quad (4.7a)$$

$$-\beta_k R_k \frac{\partial T_{1_h}}{\partial \rho_k} \Big|_{R_k} + T_{1_h} = 0 \text{ on } \partial\Omega_k, k = 1, \dots, N \quad (4.7b)$$

$$-k_b \frac{\partial T_{1_h}}{\partial \rho_0} \Big|_{R_0} = -k_s \frac{\partial T_{2_h}}{\partial \rho_0} \Big|_{R_0} \text{ on } \partial\Omega_0 \quad (4.7c)$$

$$T_{1_h}|_{R_0} = T_{2_h}|_{R_0} \text{ on } \partial\Omega_0 \quad (4.7d)$$

$$T_{2_h}(R_e, \phi, t)|_{R_e \rightarrow \infty} = 0 \text{ on } \partial\Omega_e \quad (4.7e)$$

$$T_{i_h}(\rho, \phi, 0) = T^0 - T_{i_{ss}} \text{ in } \Omega_i, i = 1, 2 \quad (4.7f)$$

The governing equation as well as boundary and initial conditions of the steady-state problem

with non-homogeneous boundary conditions are given by:

$$\nabla^2 T_{i_{ss}} = 0 \text{ in } \Omega_i, i = 1, 2 \quad (4.8a)$$

$$-\beta_k R_k \frac{\partial T_{1_{ss}}}{\partial \rho_k} \Big|_{R_k} + T_{1_{ss}} = T_{f_k} \text{ on } \partial\Omega_k, k = 1, \dots, N \quad (4.8b)$$

$$-k_b \frac{\partial T_{1_{ss}}}{\partial \rho_0} \Big|_{R_0} = -k_s \frac{\partial T_{2_{ss}}}{\partial \rho_0} \Big|_{R_0} \text{ on } \partial\Omega_0 \quad (4.8c)$$

$$T_{1_{ss}}|_{R_0} = T_{2_{ss}}|_{R_0} \text{ on } \partial\Omega_0 \quad (4.8d)$$

$$T_{2_{ss}}(R_e, \phi)|_{R_e \rightarrow \infty} = T^0 \text{ on } \partial\Omega_e \quad (4.8e)$$

The solutions to both problems are presented in the next sections. Note that even though the solution to the transient problem (Equation (4.7)) is presented first, its initial condition (Equation (4.7f)) is dependent upon the solution to the steady state problem (Equation (4.8)).

#### 4.3.1 Transient heat equation with homogeneous boundary conditions

The transient problem with homogeneous boundary conditions (Equation (4.7)) is solved by means of spatial-time decomposition using separation of variables. Assuming the solution is  $T_{i_h} = X_i(\rho, \phi)\tau_i(t)$ , then the problem becomes:

$$\frac{\nabla^2 X_i}{X_i} = \frac{\dot{\tau}_i}{\alpha_i \tau_i} = -\lambda_i^2 \quad (4.9)$$

where  $\lambda$  is the eigenvalue associated with the homogeneous boundary problem partial differential equation (PDE). Note that  $\lambda > 0$  and that  $\lambda$  is not unique [107, 109].

The solution for  $\tau_i$  is straightforward:

$$\tau_i(t) = e^{-\lambda_i^2 \alpha_i t} \quad (4.10)$$

The problem for  $X_i$  defined in Equation (4.9) takes the form of the Helmholtz equation. The Helmholtz equation is encountered in many fields, for example in the study of wave propagation in continuous media [118], scattering with non-obstacles [119], or electrical propagation in integrated circuits [115]. The complete Helmholtz homogeneous boundary problem is well defined and has a unique solution.

The governing equation as well as boundary conditions for  $X_i$  are given by:

$$\nabla^2 X_i + \lambda_i^2 X_i = 0 \text{ in } \Omega_i, i = 1, 2 \quad (4.11a)$$

$$-\beta_k R_k \frac{\partial X_1}{\partial \rho_k} \Big|_{R_k} + X_1 = 0 \text{ on } \partial\Omega_k, k = 1, \dots, N \quad (4.11b)$$

$$-k_b \frac{\partial X_1}{\partial \rho_0} \Big|_{R_0} = -k_s \frac{\partial X_2}{\partial \rho_0} \Big|_{R_0} \text{ on } \partial\Omega_0 \quad (4.11c)$$

$$X_1|_{R_0} = X_2|_{R_0} \text{ on } \partial\Omega_0 \quad (4.11d)$$

$$X_2(R_e, \phi)|_{R_e \rightarrow \infty} = 0 \text{ on } \partial\Omega_e \quad (4.11e)$$

The continuity condition (Equations (4.11c)-(4.11d)) results in the eigenvalue connection between the grout and ground domains ( $\Omega_1$  and  $\Omega_2$ ), with  $\lambda_2 = \lambda_1 \sqrt{\alpha_1/\alpha_2}$  [106, 120]. Equation (4.11) was solved to obtain its solution at any point  $\mathbf{x} = (\rho, \phi)$  in  $\Omega$  by Chen et al. [121, 122] in the context of acoustic analysis of multiply-connected membranes. Here, the solution is presented for transient homogeneous heat transfer with mixed boundary conditions.

A complete eigenfunction expansion for the solution in a circular multiply-connected domain  $\Omega$  is proposed as follows:

$$X_i(\rho, \phi) = \sum_{m=-M}^M \gamma_m \psi(\rho, \phi) \quad (4.12)$$

where  $\psi(\mathbf{x})$  is the Trefftz basis at pole  $O$  and  $\gamma_m$  are the coefficient matching the boundaries. The number of terms in the expansion is formally infinite, but is reduced to  $2M+1$  to obtain a finite sum.

For the circular multiply-connected domain  $\Omega$ , the following Trefftz basis for a point  $\mathbf{x}_p = (\rho_p, \phi_p)$  related to a pole  $O_p$ , is defined for a circular boundary  $\partial\Omega_p$  with radius  $R_p$  (Figure 4.2):

$$\psi(\rho_p, \phi_p) = \begin{cases} J_m(\lambda \rho_p) e^{im\phi_p} & \text{if } \rho_p < R_p \\ H_m^{(1)}(\lambda \rho_p) e^{im\phi_p} & \text{if } \rho_p > R_p \end{cases} \quad (4.13)$$

where  $J$  and  $H^{(1)}$  are the Bessel and Hankel functions of the first kind, respectively.

To obtain the solution of Equation (4.11) for any  $N$  number of pipes,  $\psi$  needs to be expressed at any pole  $O_j$  in the domain  $\Omega_1$ . For the translation of coordinates shown in Figure 4.2, the

Graf-Gegenbauer addition theorem [123] yields:

$$J_m(\lambda\rho_p)e^{im\phi_p} = \sum_{n=-\infty}^{\infty} J_{m-n}(\lambda l_{pq})e^{i(m-n)\theta_{pq}} J_n(\lambda\rho_q)e^{in\phi_q} \quad (4.14a)$$

$$H_m^{(1)}(\lambda\rho_p)e^{im\phi_p} = \begin{cases} \sum_{n=-\infty}^{\infty} J_{m-n}(\lambda l_{pq})e^{i(m-n)\theta_{pq}} H_n^{(1)}(\lambda\rho_q)e^{in\phi_q} & \text{if } l_{pq} < \rho_q \\ \sum_{n=-\infty}^{\infty} H_{m-n}^{(1)}(\lambda l_{pq})e^{i(m-n)\theta_{pq}} J_n(\lambda\rho_q)e^{in\phi_q} & \text{if } l_{pq} > \rho_q \end{cases} \quad (4.14b)$$

Superimposing the contributions of all poles ( $O_j$ ) and considering only  $2M + 1$  terms in Equation (4.14), Equation (4.13) in  $\Omega_1$  becomes:

$$X_1(\mathbf{x}) = \sum_{m=-M}^M \gamma_m^0 J_m(\lambda_1\rho_0)e^{im\phi_0} + \sum_{j=1}^N \sum_{m=-M}^M \gamma_m^j H_m^{(1)}(\lambda_1\rho_j)e^{im\phi_j} \quad (4.15)$$

The solution in  $\Omega_2$  follows the same procedure but with only 1 internal pipe at  $\partial\Omega_0$ :

$$X_2(\mathbf{x}) = \sum_{m=-M}^M \delta_m^0 H_m^{(1)}(\lambda_2\rho_0)e^{im\phi_0} \quad (4.16)$$

As  $\Omega_2$  is unbounded, Equation (4.16) vanishes if  $R_e \rightarrow \infty$ , as shown by the asymptotic expansion expressed in Abramowitz and Stegun [124]. Equation (4.11e) is thus satisfied. Therefore, the Trefftz basis for  $\Omega_2$  defined in Equation (4.13) is considered exterior domain and thus only the Hankel function is required.

The boundary conditions in Equation (4.11) require the evaluation of  $X_1$  and  $X_2$  and their derivatives at all boundaries ( $\partial\Omega_j$ ) in  $\Omega_1$  and  $\Omega_2$ , respectively. At the borehole wall ( $\partial\Omega_0$ ):

$$X_1(R_0, \phi_0) = \sum_{m=-M}^M \gamma_m^0 J_m(\lambda_1 R_0) e^{im\phi_0} + \sum_{j=1}^N \sum_{m=-M}^M \gamma_m^j \sum_{n=-M}^M J_{m-n}(\lambda_1 l_{j0}) e^{i(m-n)\theta_{j0}} H_n^{(1)}(\lambda_1 R_0) e^{in\phi_0} \quad (4.17a)$$

$$X_2(R_0, \phi_0) = \sum_{m=-M}^M \delta_m^0 H_m^{(1)}(\lambda_2 R_0) e^{im\phi_0} \quad (4.17b)$$

$$\left. \frac{\partial X_1}{\partial \rho_0} \right|_{R_0} = \lambda_1 \sum_{m=-M}^M \gamma_m^0 J'_m(\lambda_1 R_0) e^{im\phi_0} + \lambda_1 \sum_{j=1}^N \sum_{m=-M}^M \gamma_m^j \sum_{n=-M}^M J_{m-n}(\lambda_1 l_{j0}) e^{i(m-n)\theta_{j0}} H_n'^{(1)}(\lambda_1 R_0) e^{in\phi_0} \quad (4.17c)$$

$$\left. \frac{\partial X_2}{\partial \rho_0} \right|_{R_0} = \lambda_2 \sum_{m=-M}^M \delta_m^0 H_m'^{(1)}(\lambda_2 R_0) e^{im\phi_0} \quad (4.17d)$$



At the external wall of each pipe ( $\partial\Omega_l$ ):

$$\begin{aligned}
X_1(R_l, \phi_l) = & \sum_{m=-M}^M \gamma_m^0 \sum_{n=-M}^M J_{m-n}(\lambda_1 l_{0l}) e^{i(m-n)\theta_{0l}} J_n(\lambda_1 R_l) e^{in\phi_l} \\
& + \sum_{m=-M}^M \gamma_m^l H_m^{(1)}(\lambda_1 R_l) e^{im\phi_l} \\
& + \sum_{j=1, j \neq l}^N \sum_{m=-M}^M \gamma_m^j \sum_{n=-M}^M g_{mn}
\end{aligned} \tag{4.18a}$$

$$\begin{aligned}
\left. \frac{\partial X_1}{\partial \rho_l} \right|_{R_l} = & \lambda_1 \sum_{m=-M}^M \gamma_m^0 \sum_{n=-M}^M J_{m-n}(\lambda_1 l_{0l}) e^{i(m-n)\theta_{0l}} J'_n(\lambda_1 R_l) e^{in\phi_l} \\
& + \lambda_1 \sum_{m=-M}^M \gamma_m^l H'_m^{(1)}(\lambda_1 R_l) e^{im\phi_l} \\
& + \lambda_1 \sum_{j=1, j \neq l}^N \sum_{m=-M}^M \gamma_m^j \sum_{n=-M}^M g'_{mn}
\end{aligned} \tag{4.18b}$$

where

$$g_{mn} = \begin{cases} J_{m-n}(\lambda_1 l_{jl}) e^{i(m-n)\theta_{jl}} H_n^{(1)}(\lambda_1 R_l) e^{in\phi_l} & \text{if } l_{jl} < R_l \\ H_{m-n}^{(1)}(\lambda_1 l_{jl}) e^{i(m-n)\theta_{jl}} J_n(\lambda_1 R_l) e^{in\phi_l} & \text{if } l_{jl} > R_l \end{cases} \tag{4.19a}$$

$$g'_{mn} = \begin{cases} J_{m-n}(\lambda_1 l_{jl}) e^{i(m-n)\theta_{jl}} H'_n^{(1)}(\lambda_1 R_l) e^{in\phi_l} & \text{if } l_{jl} < R_l \\ H_{m-n}^{(1)}(\lambda_1 l_{jl}) e^{i(m-n)\theta_{jl}} J'_n(\lambda_1 R_l) e^{in\phi_l} & \text{if } l_{jl} > R_l \end{cases} \tag{4.19b}$$

The substitution of Equations (4.17)-(4.19) into (4.11) yields a linear system  $\mathbf{\Phi}\gamma = \mathbf{0}$ , where the square matrix  $\mathbf{\Phi}$  is a function of  $\lambda$ . Singular Value Decomposition (SVD) is used in order to extract the value  $\lambda$  of the square matrix  $\mathbf{\Phi}$  by collecting the minimum singular value of the decomposition and finding the drop of this singular value. The multiplicity of  $\lambda$  is obtained, seeking how many singular values are equal to the minimum. The dimension of the matrix is  $\dim \mathbf{\Phi} = [(2M+1)(N+2) \times (2M+1)(N+2)]$ . The solution  $\gamma$  is obtained at each eigenvalue  $\lambda$  by multiplying the eigenvector associated and  $\mathbf{\Phi}$ .

Recalling Equation 4.7, the homogeneous solution is then calculated as a Fourier-Bessel expansion:

$$T_{i_h}(\rho, \phi, t) = \sum_{j=1}^{\infty} C_j X_i(\rho, \phi; \lambda_i^j) e^{-(\lambda_i^j)^2 \alpha_i t} \tag{4.20}$$

where  $X_i$  is a quasi-orthogonal eigenfunction [120] and  $\lambda_i^j$  is the  $j$ -th eigenvalue for the expansion in  $\Omega_i$ .

The calculation of coefficients  $C_j$  requires imposing the initial condition and applying orthogonal conditions:

$$C_j = \frac{\frac{k_b}{\alpha_1} \int_{\Omega_1} (T^0 - T_{1ss}) \bar{X}_1 d\Omega_1 + \frac{k_s}{\alpha_2} \int_{\Omega_2} (T^0 - T_{2ss}) \bar{X}_2 d\Omega_2}{\frac{k_b}{\alpha_1} \int_{\Omega_1} X_1 \bar{X}_1 d\Omega_1 + \frac{k_s}{\alpha_2} \int_{\Omega_2} X_2 \bar{X}_2 d\Omega_2} \quad (4.21)$$

where  $\bar{X}_i$  is the conjugate of  $X_i$ . It is important to point out that  $\gamma$ ,  $\delta$  and  $C_j$  are complex-valued, and thus Equation (4.20) implies that only the real part of the temperature is considered. However, as long as Equation (4.7) has real-valued initial and boundary conditions, the solution will have real temperature values.

### 4.3.2 Steady-state heat equation with nonhomogeneous boundary conditions

A T-complete basis is required to obtain the solution to Equation (4.8). Such a basis was proposed by Liu [125] for the Laplace equation in a doubly-connected domain. In the present case, for  $N + 1$  poles, the temperature in  $\Omega_1$  is given by:

$$T_{1ss} = \alpha_0 + \sum_{m=1}^h \left[ \alpha_m \left( \frac{\rho_0}{R_{max}} \right)^m \cos(m\phi_0) + \beta_m \left( \frac{\rho_0}{R_{max}} \right)^m \sin(m\phi_0) \right] + \sum_{j=1}^N \left\{ \gamma_0^j \ln \rho_j + \sum_{m=1}^h \left[ \gamma_m^j \left( \frac{\rho_j}{R_{min}} \right)^{-m} \cos(m\phi_j) + \delta_m^j \left( \frac{\rho_j}{R_{min}} \right)^{-m} \sin(m\phi_j) \right] \right\} \quad (4.22)$$

and the temperature in  $\Omega_2$  (with only one pole shared by  $\partial\Omega_0$  and  $\partial\Omega_e$ ) is given by:

$$T_{2ss} = \alpha'_0 + \sum_{m=1}^h \left[ \alpha'_m \left( \frac{\rho_0}{R_e} \right)^m \cos(m\phi_0) + \beta'_m \left( \frac{\rho_0}{R_e} \right)^m \sin(m\phi_0) \right] + \gamma'_0 \ln \rho_0 + \sum_{m=1}^h \left[ \gamma'_m \left( \frac{\rho_0}{R_{min}} \right)^{-m} \cos(m\phi_0) + \delta'_m \left( \frac{\rho_0}{R_{min}} \right)^{-m} \sin(m\phi_0) \right] \quad (4.23)$$

where  $R_{min} = \min_{i \in \{1, \dots, N\}} R_i$  is the minimum external radius of the pipes,  $R_{max} \geq R_0$  is an arbitrary radius and is set equal to  $R_0$ , and  $h$  is the number of terms in the complete expansion (Equations (4.22)-(4.23)). Note that  $\gamma_m^j$  are different from the preceding expansion in Equation (4.15).

By definition Equations (4.22)-(4.23) have infinite terms but it is reduced here to the  $h$  first terms of the expansion. To have a unique solution, the coefficients that match boundaries,  $\alpha_0, \alpha_m, \dots, \delta'_m$ , have to be unique and finite. For  $R_e \rightarrow \infty$ , Equation (4.23) results in arbitrary values for  $\alpha'_m, \beta'_m$ , and they are thus considered equal to 0. Also,  $\gamma'_0$  has to be equal to 0 for  $T_{2ss}$  to remain finite. Therefore, the solution of this problem results in the coefficient  $\alpha'_0 =$

$T_{2ss}(R_e, \phi)|_{R_e \rightarrow \infty} = T^0$ . The presented method for steady-state allows to successfully allocate the boundary conditions for the unbounded domain  $\Omega_2$  and thus compute the coefficients in the T-basis.

For the translation of coordinates shown in Figure 4.2, an addition theorem was proposed by Bird and Steele [126] for the Laplace equation in a multiply-connected domain:

$$\rho_p^m \cos(m\phi_p) = \sum_{n=0}^m \binom{m}{n} (-1)^n \rho_p^{m-n} l_{pq}^n \cos(m\theta_{pq} + n(\phi_q - \theta_{pq})) \quad (4.24a)$$

$$\rho_p^m \sin(m\phi_p) = \sum_{n=0}^m \binom{m}{n} (-1)^n \rho_p^{m-n} l_{pq}^n \sin(m\theta_{pq} + n(\phi_q - \theta_{pq})) \quad (4.24b)$$

$$\rho_p^{-m} \cos(m\phi_p) = \begin{cases} \sum_{k=-1}^{\infty} \binom{m+k}{k+1} \frac{\rho_q^{k+1}}{l_{pq}^{k+m+1}} \cos[(k+1)\phi_q - (k+m+1)\theta_{pq}] & \text{if } l_{pq} > \rho_q \\ \sum_{k=-1}^{\infty} (-1)^m \binom{m+k}{k+1} \frac{l_{pq}^{k+1}}{\rho_p^{k+m+1}} \cos[(k+1)\theta_{pq} - (k+m+1)\phi_q] & \text{if } l_{pq} < \rho_q \end{cases} \quad (4.24c)$$

$$\rho_p^{-m} \sin(m\phi_p) = \begin{cases} \sum_{k=-1}^{\infty} \binom{m+k}{k+1} \frac{\rho_q^{k+1}}{l_{pq}^{k+m+1}} \sin[(k+1)\phi_q - (k+m+1)\theta_{pq}] & \text{if } l_{pq} > \rho_q \\ \sum_{k=-1}^{\infty} (-1)^m \binom{m+k}{k+1} \frac{l_{pq}^{k+1}}{\rho_p^{k+m+1}} \sin[(k+1)\theta_{pq} - (k+m+1)\phi_q] & \text{if } l_{pq} < \rho_q \end{cases} \quad (4.24d)$$

$$\ln \rho_p = \begin{cases} \ln(l_{pq}) - \sum_{m=1}^{\infty} \left(\frac{1}{m}\right) \left(\frac{\rho_p}{l_{pq}}\right)^m \cos[m(\theta_{pq} - \phi_q)] & \text{if } l_{pq} > \rho_q \\ \ln(\rho_q) - \sum_{m=1}^{\infty} \left(\frac{1}{m}\right) \left(\frac{l_{pq}}{\rho_p}\right)^m \cos[m(\theta_{pq} - \phi_q)] & \text{if } l_{pq} < \rho_q \end{cases} \quad (4.24e)$$

The boundary conditions in Equation (4.8) require the evaluation of  $T_{1ss}$  and  $T_{2ss}$  and their derivatives at all boundaries ( $\partial\Omega_j$ ) in  $\Omega_1$  and  $\Omega_2$ , respectively. At the borehole wall ( $\partial\Omega_0$ ):

$$\begin{aligned} T_{1ss} = & \alpha_0 + \sum_{m=1}^h \left[ \alpha_m \left(\frac{R_0}{R_{max}}\right)^m \cos(m\phi_0) + \beta_m \left(\frac{R_0}{R_{max}}\right)^m \sin(m\phi_0) \right] \\ & + \sum_{j=1}^N \left\{ \gamma_0^j \left( \ln R_0 - \sum_{m=1}^{\infty} \left(\frac{1}{m}\right) \left(\frac{l_{j0}}{R_0}\right)^m \cos[m(\theta_{j0} - \phi_0)] \right) \right. \\ & + \sum_{m=1}^h \sum_{k=-1}^h \left[ \gamma_m^j (-1)^m \binom{m+k}{k+1} R_{min}^m \frac{l_{j0}^{k+1}}{R_0^{k+m+1}} \cos[(k+1)\theta_{j0} - (k+m+1)\phi_0] \right. \\ & \left. \left. + \delta_m^j (-1)^m \binom{m+k}{k+1} R_{min}^m \frac{l_{j0}^{k+1}}{R_0^{k+m+1}} \sin[(k+1)\theta_{j0} - (k+m+1)\phi_0] \right] \right\} \end{aligned} \quad (4.25a)$$

$$T_{2ss} = T^0 + \sum_{m=1}^h \left[ \gamma'_m \left(\frac{R_0}{R_{min}}\right)^{-m} \cos(m\phi_0) + \delta'_m \left(\frac{R_0}{R_{min}}\right)^{-m} \sin(m\phi_0) \right] \quad (4.25b)$$

$$\begin{aligned}
\left. \frac{\partial T_{1ss}}{\partial \rho_0} \right|_{R_0} &= \sum_{m=1}^h m \left[ \alpha_m \left( \frac{1}{R_{max}} \right)^m R_0^{m-1} \cos(m\phi_0) + \beta_m \left( \frac{1}{R_{max}} \right)^m R_0^{m-1} \sin(m\phi_0) \right] \\
&+ \sum_{j=1}^N \left\{ \gamma_0^j \left( \frac{1}{R_0} + \sum_{m=1}^{\infty} \left( \frac{1}{R_0} \right)^{m+1} l_{j0}^m \cos[m(\theta_{j0} - \phi_0)] \right) \right. \\
&- \sum_{m=1}^h \sum_{k=-1}^h \left[ \gamma_m^j (-1)^m (k+m+1) \binom{m+k}{k+1} R_{min}^m \frac{l_{j0}^{k+1}}{R_0^{k+m+2}} \cos[(k+1)\theta_{j0} - (k+m+1)\phi_0] \right. \\
&\left. \left. + \delta_m^j (-1)^m (k+m+1) \binom{m+k}{k+1} R_{min}^m \frac{l_{j0}^{k+1}}{R_0^{k+m+2}} \sin[(k+1)\theta_{j0} - (k+m+1)\phi_0] \right] \right\} \\
&\quad (4.25c)
\end{aligned}$$

$$\left. \frac{\partial T_{2ss}}{\partial \rho_0} \right|_{R_0} = - \sum_{m=1}^h m \left[ \alpha'_m \left( \frac{1}{R_{min}} \right)^{-m} R_0^{-m-1} \cos(m\phi_0) + \beta'_m \left( \frac{1}{R_{min}} \right)^{-m} R_0^{-m-1} \sin(m\phi_0) \right] \quad (4.25d)$$

At the external wall of each pipe ( $\partial\Omega_l$ ):

$$\begin{aligned}
T_{1ss} &= \alpha_0 + \sum_{m=1}^h \frac{1}{R_{max}^m} \left[ \alpha_m \sum_{k=0}^m \binom{m}{k} (-1)^k R_l^{m-k} l_{0l}^k \cos[m\theta_{0l} + k(\phi_l - \theta_{0l})] \right. \\
&+ \beta_m \sum_{k=0}^m \binom{m}{k} (-1)^k R_l^{m-k} l_{0l}^k \sin[m\theta_{0l} + k(\phi_l - \theta_{0l})] \left. \right] \\
&+ \gamma_0^l \ln R_l + \sum_{m=1}^h \left[ \gamma_m^l \left( \frac{R_l}{R_{min}} \right)^{-m} \cos(m\phi_l) + \delta_m^l \left( \frac{R_l}{R_{min}} \right)^{-m} \sin(m\phi_l) \right] \\
&+ \sum_{j=1, j \neq l}^N \left( \gamma_0^j g_j + \sum_{m=1}^h (\gamma_m^j g_{jk}^1 + \delta_m^j g_{jk}^2) \right) \quad (4.26a)
\end{aligned}$$

$$\begin{aligned}
\left. \frac{\partial T_{1ss}}{\partial \rho_l} \right|_{R_l} &= \sum_{m=1}^h \frac{1}{R_{max}^m} \left[ \alpha_m \sum_{k=0}^m (m-k) \binom{m}{k} (-1)^k R_l^{m-k-1} l_{0l}^k \cos[m\theta_{0l} + k(\phi_l - \theta_{0l})] \right. \\
&+ \beta_m \sum_{k=0}^m (m-k) \binom{m}{k} (-1)^k R_l^{m-k-1} l_{0l}^k \sin[m\theta_{0l} + k(\phi_l - \theta_{0l})] \left. \right] \\
&+ \gamma_0^l \frac{1}{R_l} - \sum_{m=1}^h m \left[ \gamma_m^l \left( \frac{1}{R_{min}} \right)^{-m} R_l^{-m-1} \cos(m\phi_l) + \delta_m^l \left( \frac{1}{R_{min}} \right)^{-m} R_l^{-m-1} \sin(m\phi_l) \right] \\
&+ \sum_{j=1, j \neq l}^N \left( \gamma_0^j g'_j + \sum_{m=1}^h (\gamma_m^j g'_{jk}{}^1 + \delta_m^j g'_{jk}{}^2) \right) \quad (4.26b)
\end{aligned}$$

where

$$g_j = \begin{cases} \ln(l_{jl}) - \sum_{m=1}^h \left(\frac{1}{m}\right) \left(\frac{R_l}{l_{jl}}\right)^m \cos[m(\theta_{jl} - \phi_l)] & \text{if } l_{jl} > R_l \\ \ln(R_l) - \sum_{m=1}^h \left(\frac{1}{m}\right) \left(\frac{l_{jl}}{R_l}\right)^m \cos[m(\theta_{jl} - \phi_l)] & \text{if } l_{jl} < R_l \end{cases} \quad (4.27a)$$

$$g_{jk}^1 = \begin{cases} \sum_{k=-1}^h \binom{m+k}{k+1} R_{min}^m \frac{R_l^{k+1}}{l_{jl}^{k+m+1}} \cos[(k+1)\phi_l - (k+m+1)\theta_{jl}] & \text{if } l_{jl} > R_l \\ \sum_{k=-1}^h (-1)^m \binom{m+k}{k+1} R_{min}^m \frac{l_{jl}^{k+1}}{R_l^{k+m+1}} \cos[(k+1)\theta_{jl} - (k+m+1)\phi_l] & \text{if } l_{jl} < R_l \end{cases} \quad (4.27b)$$

$$g_{jk}^2 = \begin{cases} \sum_{k=-1}^h \binom{m+k}{k+1} R_{min}^m \frac{R_l^{k+1}}{l_{jl}^{k+m+1}} \sin[(k+1)\phi_l - (k+m+1)\theta_{jl}] & \text{if } l_{jl} > R_l \\ \sum_{k=-1}^h (-1)^m \binom{m+k}{k+1} R_{min}^m \frac{l_{jl}^{k+1}}{R_l^{k+m+1}} \sin[(k+1)\theta_{jl} - (k+m+1)\phi_l] & \text{if } l_{jl} < R_l \end{cases} \quad (4.27c)$$

$$g'_j = \begin{cases} -\sum_{m=1}^h \left(\frac{1}{l_{jl}}\right)^m R_l^{m-1} \cos[m(\theta_{jl} - \phi_l)] & \text{if } l_{jl} > R_l \\ \frac{1}{R_l} + \sum_{m=1}^h \left(\frac{1}{R_l}\right)^{m+1} l_{jl}^m \cos[m(\theta_{jl} - \phi_l)] & \text{if } l_{jl} < R_l \end{cases} \quad (4.27d)$$

$$g_{jk}^{'1} = \begin{cases} \sum_{k=-1}^h (k+1) \binom{m+k}{k+1} R_{min}^m \frac{R_l^k}{l_{jl}^{k+m+1}} \cos[(k+1)\phi_l - (k+m+1)\theta_{jl}] & \text{if } l_{jl} > R_l \\ -\sum_{k=-1}^h (-1)^m (k+m+1) \binom{m+k}{k+1} R_{min}^m \frac{1}{R_l^{k+m+2}} l_{jl}^{k+1} \cos[(k+1)\theta_{jl} - (k+m+1)\phi_l] & \text{if } l_{jl} < R_l \end{cases} \quad (4.27e)$$

$$g_{jk}^{'2} = \begin{cases} \sum_{k=-1}^h (k+1) \binom{m+k}{k+1} R_{min}^m \frac{R_l^k}{l_{jl}^{k+m+1}} \sin[(k+1)\phi_l - (k+m+1)\theta_{jl}] & \text{if } l_{jl} > R_l \\ -\sum_{k=-1}^h (-1)^m (k+m+1) \binom{m+k}{k+1} R_{min}^m \frac{1}{R_l^{k+m+2}} l_{jl}^{k+1} \sin[(k+1)\theta_{jl} - (k+m+1)\phi_l] & \text{if } l_{jl} < R_l \end{cases} \quad (4.27f)$$

A linear system of equations, in the form  $\Phi\gamma = \mathbf{F}$ , is obtained by the substitution of Equations (4.25)-(4.27) into Equation (4.8). The right-hand side vector  $\mathbf{F}$  is a function of the fluid temperatures into the pipes. The matrix  $\Phi$ , of dimension  $\dim \Phi = [(2h+1)(N+2) \times (2h+1)(N+2)]$ , is ill-conditioned and requires preconditioning before the system can be solved for  $\gamma$ :

$$\Phi^T \Phi \gamma = \Phi^T \mathbf{F} \quad (4.28)$$

### 4.3.3 Time-dependent fluid temperatures

The method presented in Sections 4.3.1 and 4.3.2 can be adapted to consider time-dependent fluid temperatures. Step-wise variations of fluid temperatures at each pipe  $k$  are considered at each time step  $n$ , i.e. over  $t^{(n-1)} < t \leq t^n$  (where  $t^n = t^{(n-1)} + \Delta t$ ). In this updating scheme, the initial temperatures in Equations (4.7f) and (4.21) are replaced by the temperature at

the end of the latest time step:

$$T_1^{(n-1)} = \sum_{m=1}^{\infty} C_m^{(n-1)} X_1(\rho, \phi; \lambda_1^m) e^{-(\lambda_1^m)^2 \alpha_1 \Delta t} + T_{1_{ss}}^{(n-1)} \quad (4.29a)$$

$$T_2^{(n-1)} = \sum_{m=1}^{\infty} C_m^{(n-1)} X_2(\rho, \phi; \lambda_2^m) e^{-(\lambda_2^m)^2 \alpha_2 \Delta t} + T_{2_{ss}}^{(n-1)} \quad (4.29b)$$

The Fourier-Bessel coefficients in Equation (4.21) become:

$$C_j^n = \frac{\frac{k_b}{\alpha_1} I_{1j}^{(n-1)} + \frac{k_s}{\alpha_2} I_{2j}^{(n-1)}}{\frac{k_b}{\alpha_1} \int_{\Omega_1} X_1(\rho, \phi; \lambda_1^j) \bar{X}_1(\rho, \phi; \lambda_1^j) d\Omega_1 + \frac{k_s}{\alpha_2} \int_{\Omega_2} X_2(\rho, \phi; \lambda_2^j) \bar{X}_2(\rho, \phi; \lambda_2^j) d\Omega_2} \quad (4.30)$$

where

$$\begin{aligned} I_{1j}^{(n-1)} &= \int_{\Omega_1} (T_1^{(n-1)} - T_{1_{ss}}^n) \bar{X}_1(\rho, \phi; \lambda_1^j) d\Omega_1 \\ &= \int_{\Omega_1} (C_j^{(n-1)} X_1(\rho, \phi; \lambda_1^j) e^{-(\lambda_1^j)^2 \alpha_1 \Delta t} + T_{1_{ss}}^{(n-1)} - T_{1_{ss}}^n) \bar{X}_1(\rho, \phi; \lambda_1^j) d\Omega_1 \\ I_{2j}^{(n-1)} &= \int_{\Omega_2} (T_2^{(n-1)} - T_{2_{ss}}^n) \bar{X}_2(\rho, \phi; \lambda_2^j) d\Omega_2 \\ &= \int_{\Omega_2} (C_j^{(n-1)} X_2(\rho, \phi; \lambda_2^j) e^{-(\lambda_2^j)^2 \alpha_2 \Delta t} + T_{2_{ss}}^{(n-1)} - T_{2_{ss}}^n) \bar{X}_2(\rho, \phi; \lambda_2^j) d\Omega_2 \end{aligned} \quad (4.31)$$

where  $T_{i_{ss}}^n$  is the solution of the steady-state problem considering the fluid temperatures at the  $n$ -th time step, and  $T_1^0 = T_2^0 = T^0$ .

Equations (4.30) and (4.31) allow the calculation of the temperature field when fluid temperatures are variable over time and known. In a simulation of a GHE, fluid temperatures are typically unknown. It is however possible to build a system of equation to consider other known values. As an example, assuming the total heat transfer rate,  $\dot{q}^n (= \dot{q}'^n H)$ , into a GHE containing two pipes is known and that  $T_{f_1}^n$  and  $T_{f_2}^n$  are equal to the inlet and outlet fluid temperatures:

$$\dot{q}'_k = \frac{1}{E_k} (T_{f_k}^n - \bar{T}_1^n|_{R_k}) \quad (4.32a)$$

$$\dot{q}'^n = \sum_{k=1}^N \dot{q}'_k \quad (4.32b)$$

$$\dot{q}'^n H = \dot{m}^n c_p (T_{f_1}^n - T_{f_2}^n) \quad (4.32c)$$

where  $\dot{q}'_k$  is the heat transfer rate per unit length from pipe  $k$ ,  $T_{f_k}^n$  is the fluid temperature in pipe  $k$ ,  $\bar{T}_1^n|_{R_k}$  is the average temperature at the outer wall at pipe  $k$ ,  $\dot{m}^n$  is the fluid mass flow rate into the pipes,  $c_p$  is the fluid specific heat capacity, and  $H$  is the GHE length.

The coefficient updating scheme can also be adapted to consider the fluid temperature variations along the pipes by discretizing the GHE into segments and taking into account the advection of the fluid into the pipes, as commonly done in resistance-capacitance models [41–43, 46]. This will be addressed in future work.

#### 4.4 Validation

The proposed method is implemented into Python, using numpy’s implementation of the SVD algorithm [127] and scipy’s implementation of Bessel and Hankel functions [128] which includes the asymptotic expansions for large values of the argument. Integrals are evaluated by a quadrature domain technique [129].

The accuracy of the proposed method is dependent upon the number of terms considered in the Fourier-Bessel expansion for  $T_{i_h}$  (Equation (4.20)), the number of terms  $M$  in the multipole expansion for  $X_i$  (Equations (4.15)-(4.16)), and the number of terms  $h$  in the multipole expansion for  $T_{i_{ss}}$  (Equations (4.22)-(4.23)). The number of terms considered in the Fourier-Bessel expansion was fixed at 100 eigenvalues. The solution for  $X_i$  is still dependent on the eigenvalues of the Helmholtz equation (Equation (4.11)) and thus their correct evaluation needs to be validated. The validation of the proposed approach is conducted in three steps. First, the eigenvalues are computed for the geometries presented by Chen et al. [116, 117]. Second, the steady-state temperature field calculated with the proposed method is compared with the one calculated using the multipole method, as presented by Claesson and Hellström [18]. Finally, the solution of the transient heat conduction is validated against Finite Element Analysis (FEA) simulations for constant and time-dependent fluid temperatures.

##### 4.4.1 Eigenvalues of the Helmholtz equation

The calculation of eigenvalues is validated by comparing the results from the presented method to the results of Chen et al. [116, 117] for two geometries, calculated from a Boundary Element Method (BEM). The first geometry consists in a single pipe of radius  $R_1 = 0.5 \text{ m}$  centered into a circular domain of outer radius  $R_0 = 2 \text{ m}$ , as shown on Figure 4.3. The second geometry consists in two pipes of radius  $R_1 = R_2 = 0.3 \text{ m}$  symmetrically positioned at a distance  $e = 0.5 \text{ m}$  from the center of a circular domain of outer radius  $R_0 = 1 \text{ m}$ , as shown on Figure 4.4. For both geometries, Dirichlet boundary conditions ( $X = 0$ ) are imposed at all domain boundaries ( $\partial\Omega_1$ ,  $\partial\Omega_2$  and  $\partial\Omega_0$ ). At this stage,  $M = 5$  terms are used in the multipole expansion for  $X$ . The proposed method was modified to accommodate Dirichlet boundary conditions on the grout domain  $\Omega_1$  (thereby excluding the soil domain

$\Omega_2$ ), which differ from the convection (Equation (4.11b)) and continuity (Equations (4.11c)-(4.11d)) boundary conditions presented herein. This change is necessary for comparison with the results of Chen et al. [116,117].

The eigenvalues are extracted using SVD by locating the minimums, corresponding to the eigenvalues  $\lambda$ , of the minimum singular value of  $\Phi$ . The extracted eigenvalues are visualized alongside the geometries in Figures 4.3 and 4.4. The four former eigenmodes (i.e. the function  $X$ ), corresponding to the first four non-repeated eigenvalues, are shown in Figures 4.5 and 4.6. Table 4.1 compares the eigenvalues obtained with the proposed method with the eigenvalues obtained by Chen et al. [116,117] using BEM. As shown, the computed eigenvalues are in close agreement with the reference.

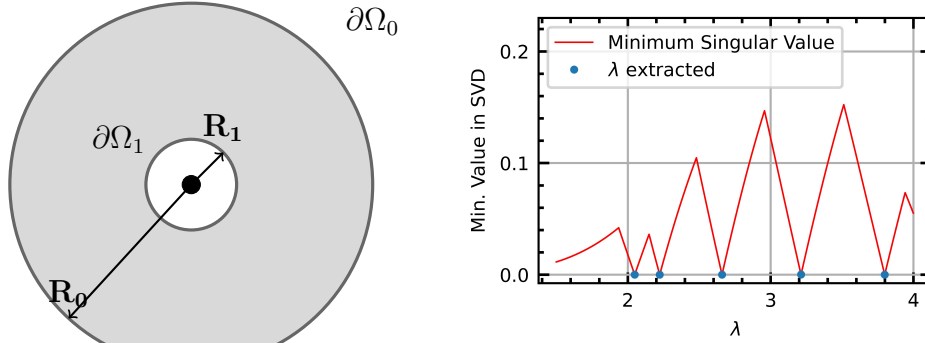


Figure 4.3 One pipe geometry (Left). Eigenvalues extracted by SVD (Right)

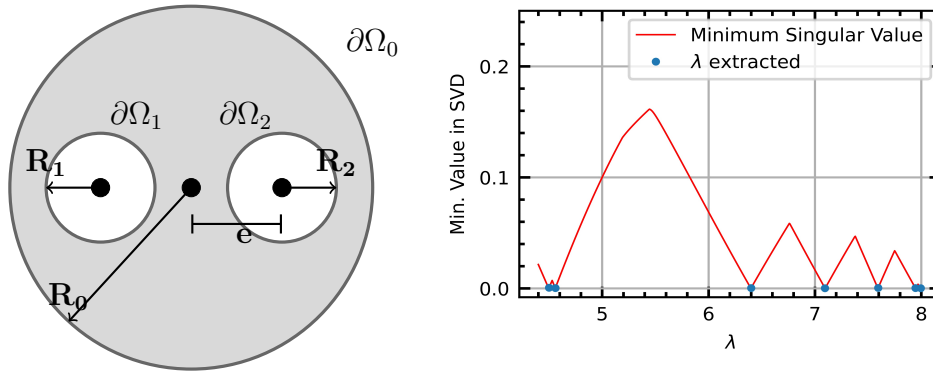


Figure 4.4 Two pipes geometry (Left). Eigenvalues extracted by SVD (Right)



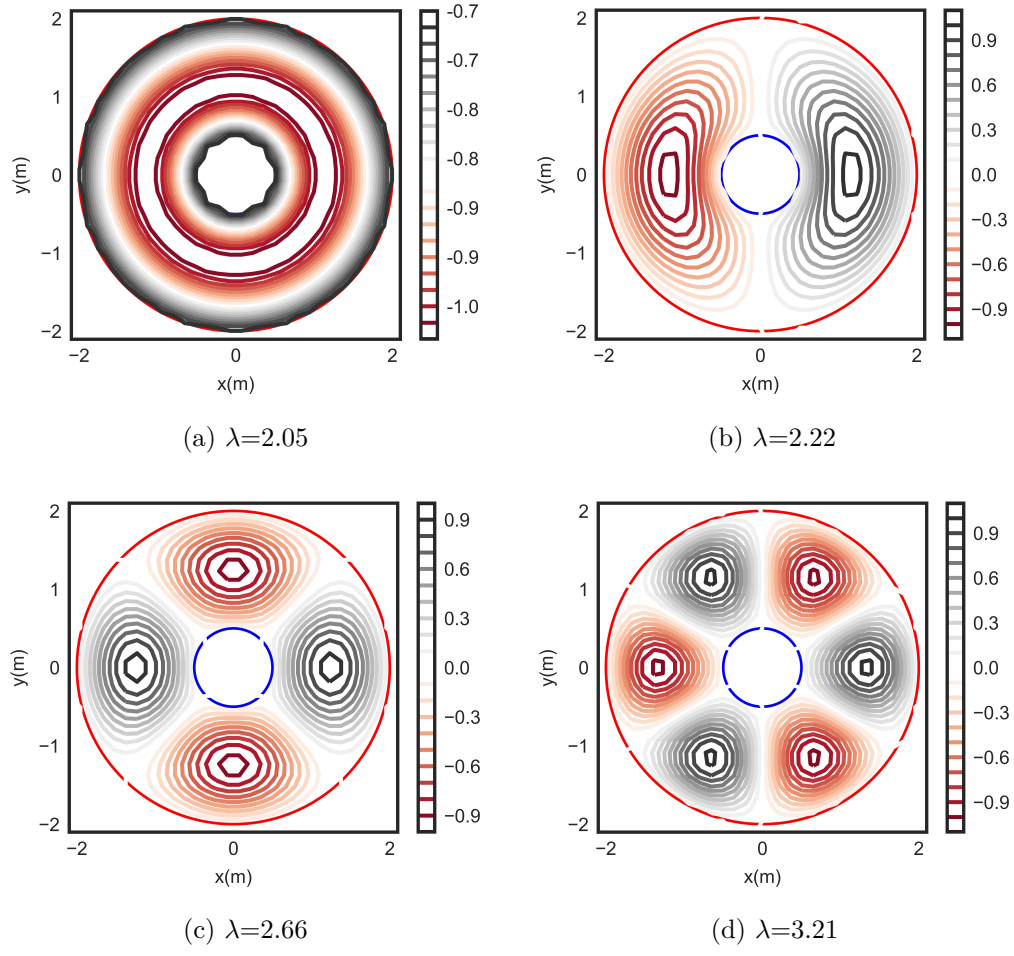


Figure 4.5 Eigenmodes of the multipole expansion for one pipe

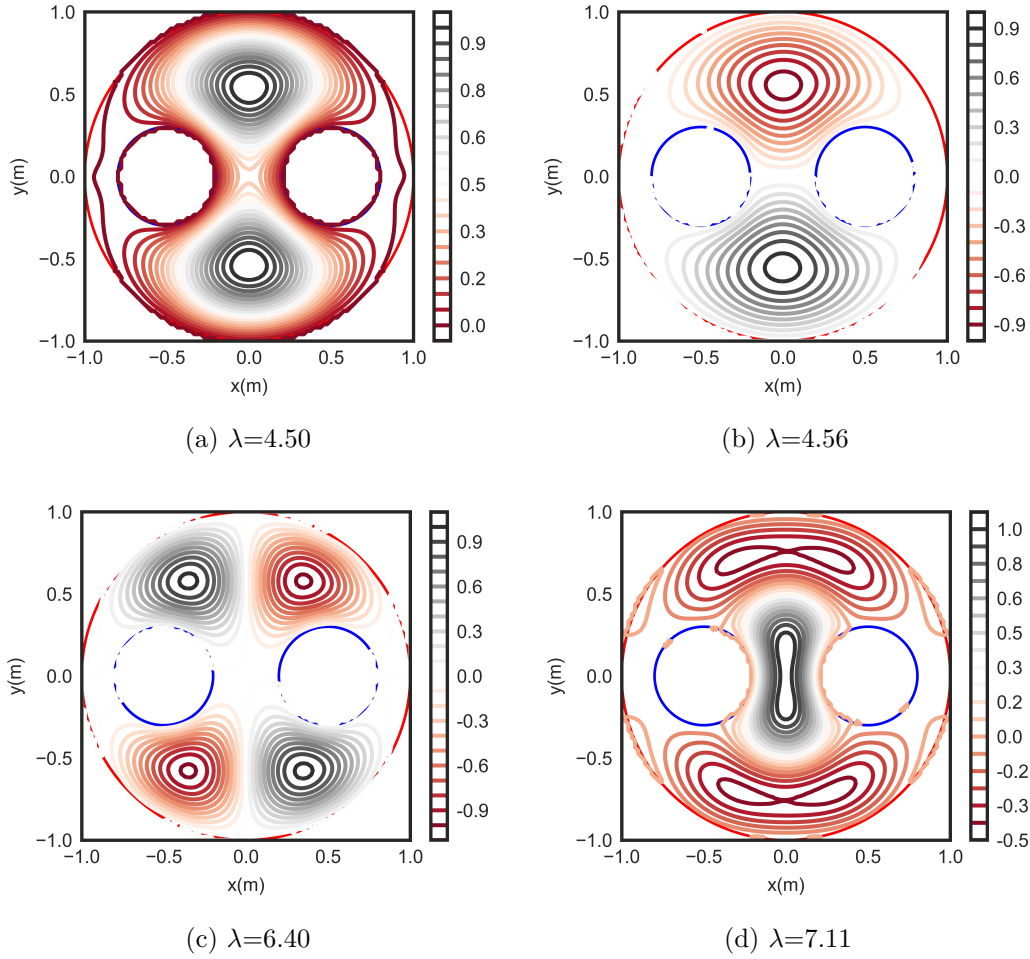


Figure 4.6 Eigenmodes of the multipole expansion for two pipes

Table 4.1 Comparison of the eigenvalues from the proposed method and Chen et al. [116,117]

Single pipe (Figure 4.3)		Two pipes (Figure 4.4)	
BEM in Chen et al. [116]	Multipole Expansion	BEM in Chen et al. [117]	Multipole Expansion
$\lambda_1 = 2.06$	$\lambda_1 = 2.05$	$\lambda_1 = 4.50$	$\lambda_1 = 4.50$
$\lambda_2 = 2.23$	$\lambda_2 = 2.22$	$\lambda_2 = 4.50$	$\lambda_2 = 4.56$
$\lambda_3 = 2.67$	$\lambda_3 = 2.66$	$\lambda_3 = 6.37$	$\lambda_3 = 6.40$
$\lambda_4 = 3.22$	$\lambda_4 = 3.21$	$\lambda_4 = 7.16$	$\lambda_4 = 7.11$

#### 4.4.2 Steady-state temperature field

The steady-state temperature field is validated by comparing the solution of the steady-state heat equation with non-homogeneous boundary conditions presented in Section 4.3.2 to the multipole method of Claesson and Hellström [18] for two asymmetrically positioned pipes, as shown on Figure 4.7. The dimensions and physical properties associated with the geometry

are:

$$\begin{aligned} k_b &= 1.5 \text{ W}/(m \cdot K), k_s = 2.5 \text{ W}/(m \cdot K), R_0 = 0.07 \text{ m} \\ O_1 &= (-0.03 \text{ m}, 0.02 \text{ m}), O_2 = (0.03 \text{ m}, 0 \text{ m}), R_1 = 0.02 \text{ m} \\ R_2 &= 0.02 \text{ m}, \beta_1 = \beta_2 = 1.2, T_{f1} = T_{f2} = 1 \text{ K} \end{aligned} \quad (4.33)$$

The values of  $T_{f1} = T_{f2} = 1 \text{ K}$  correspond to a unit ( $1 \text{ K}$ ) temperature difference between the fluid and borehole wall temperatures, as considered in Claesson and Hellström [18]. The boundary conditions presented by Claesson and Hellström [18] are slightly different from the ones considered in Equation (4.8). In Claesson and Hellström [18], the average borehole wall temperature is imposed on  $\partial\Omega_0$ :

$$\bar{T}_{2ss} \Big|_{R_0} = \frac{1}{2\pi} \int_{-\pi}^{\pi} T_{2ss}(R_0, \phi) d\phi = \alpha'_0 + \gamma'_0 \ln R_0 = 0 \quad (4.34)$$

where  $\bar{T}_{2ss} \Big|_{R_k}$  is the perimeter average temperature at a radius  $R_k$  and  $\bar{T}_{2ss} \Big|_{R_0}$  corresponds to the borehole wall temperature.

With this boundary condition, Equation (4.23) for the temperature in  $\Omega_2$  is modified as follows:

$$T_{2ss} = \bar{T}_{2ss} \Big|_{R_0} + \gamma'_0 \ln \frac{\rho_0}{R_0} + \sum_{m=1}^h \left[ \gamma'_m \left( \frac{\rho_0}{R_{\min}} \right)^{-m} \cos(m\phi_0) + \delta'_m \left( \frac{\rho_0}{R_{\min}} \right)^{-m} \sin(m\phi_0) \right] \quad (4.35)$$

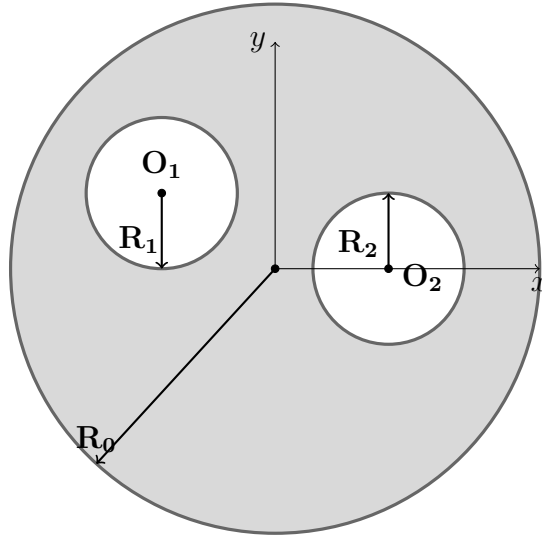


Figure 4.7 Two asymmetrically positioned pipes geometry

The method presented in Section 4.3.2 is still consistent as a solution to the Laplace equations (Equations (4.8) and (4.34)) and can thus be applied with the new boundary condition. Figure 4.8 shows the steady-state temperature field (left) and a comparison of the temperature profile at  $y = 0$  between the proposed method and Claesson and Hellström [18].  $h = 15$  terms are used in the multipole expansions for  $T_{i_{ss}}$ .

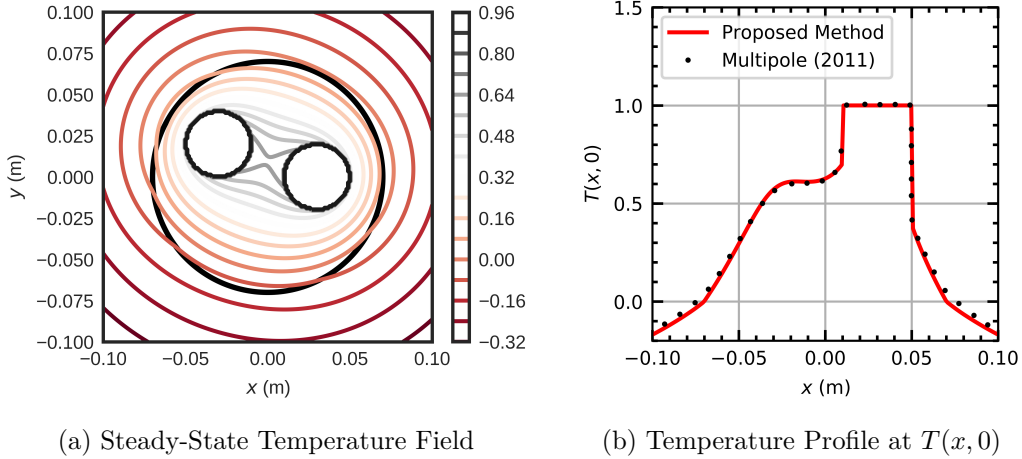


Figure 4.8 Validation against the multipole method of Claesson and Hellström

#### 4.4.3 Transient multipole expansion

The complete proposed transient multipole expansion method is validated against FEA simulations for two geometries, a single centered pipe (shown on Figure 4.9) and two symmetrically positioned pipes (shown on Figure 4.10). FEA simulations are posed with meshes of 10228 nodes and 20216 triangular elements for the single pipe geometry, and 11572 nodes and 22850 triangular elements for the two pipes geometry with an external boundary of  $R_e = 100 \text{ m}$ . For both simulations, 2nd order Lagrange polynomials are used to solve the weak formulation. Backward Euler difference for time derivative is used with a time step  $\Delta t = 100 \text{ s}$ .

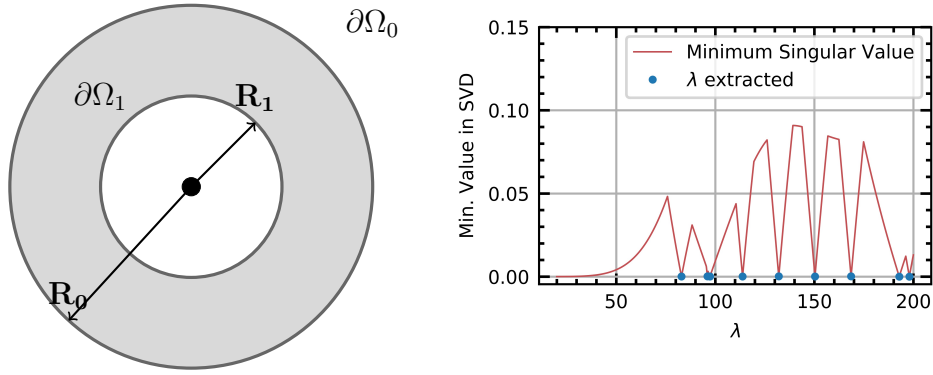


Figure 4.9 One pipe geometry (Left). Eigenvalues extracted by SVD (Right)

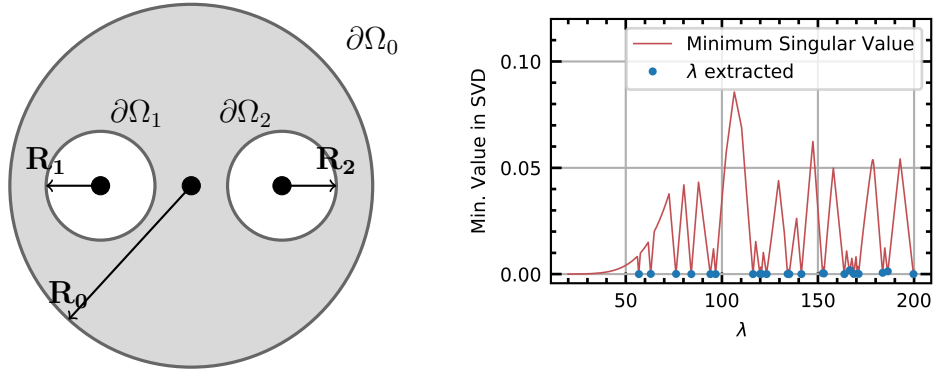


Figure 4.10 Two pipes geometry (Left). Eigenvalues extracted by SVD (Right)

The dimensions and physical properties of the single pipe geometry are:

$$\begin{aligned}
 k_b &= 0.73 \text{ W}/(\text{m} \cdot \text{K}), k_s = 2.82 \text{ W}/(\text{m} \cdot \text{K}), \alpha_1 = 1.921 \times 10^{-7} \text{ m}^2/\text{s}, \\
 \alpha_2 &= 1.410 \times 10^{-6} \text{ m}^2/\text{s}, R_1 = 0.035 \text{ m}, R_0 = 0.063 \text{ m}, \\
 \beta_1 &= 0.1985, T^0 = 293.15 \text{ K}, T_{f1} = 295.15 \text{ K}
 \end{aligned} \tag{4.36}$$

The dimensions and physical properties of the two pipes geometry are:

$$\begin{aligned}
 k_b &= 0.73 \text{ W}/(\text{m} \cdot \text{K}), k_s = 2.82 \text{ W}/(\text{m} \cdot \text{K}), \alpha_1 = 1.921 \times 10^{-7} \text{ m}^2/\text{s}, \alpha_2 = 1.410 \times 10^{-6} \text{ m}^2/\text{s} \\
 O_1 &= (-0.03 \text{ m}, 0), O_2 = (0.03 \text{ m}, 0), R_0 = 0.063 \text{ m}, R_1 = 0.0167 \text{ m} \\
 T^0 &= 293.15 \text{ K}, \beta_1 = \beta_2 = 0.4022, T_{f1} = T_{f2} = 295.15 \text{ K}
 \end{aligned} \tag{4.37}$$

Figure 4.11 presents the total heat transfer rate at the pipe and the average borehole wall

temperature for the single pipe geometry and their dependence on the number of terms in the multipole expansions ( $M$  and  $h$ ). Figure 4.12 presents the same for the two pipes geometry. As shown in both figures, proper values for the parameters  $M$  and  $h$  are required to ensure convergence of the temperatures and heat transfer rates. For the single pipe geometry,  $M = 5$  and  $h = 15$  are sufficient to attain convergence, while  $M = 7$  and  $h = 15$  are needed in the two pipes geometry. The parameter  $M$  influences the early transient phase of the temperature and heat transfer rates, and  $h$  has a stronger impact on the later stages of the simulation. While the heat transfer rates show good agreement with the FEA simulation, borehole wall temperatures present some differences at early times.

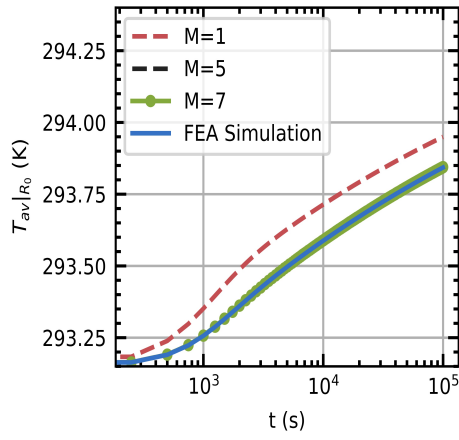
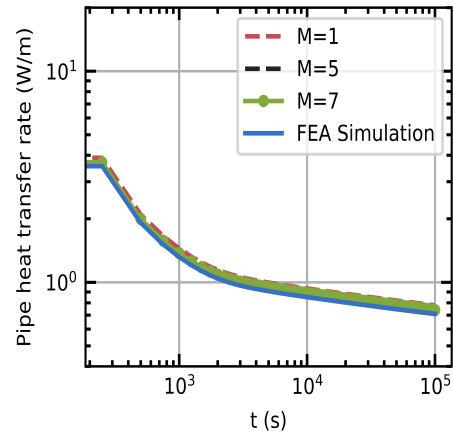
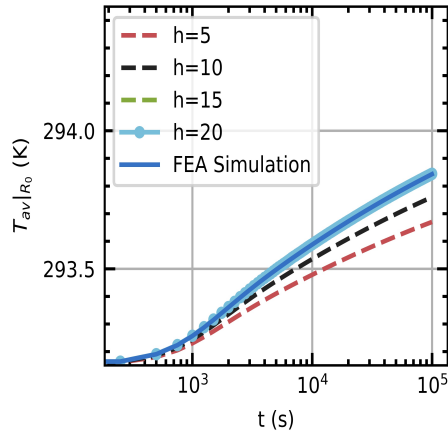
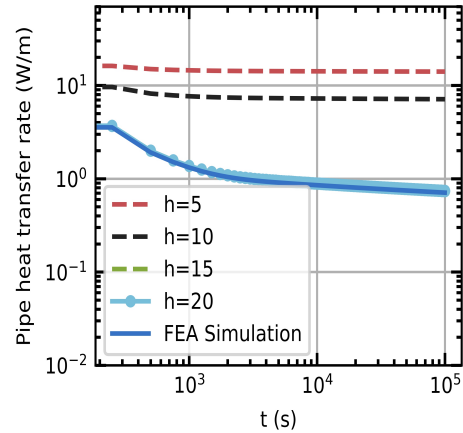
(a) Avg. Borehole Wall Temp. ( $h = 15$ )(b) Heat Flow Rate ( $h = 15$ )(c) Avg. Borehole Wall Temp. ( $M = 5$ )(d) Heat Flow Rate ( $M = 5$ )

Figure 4.11 Borehole wall temperature and pipe heat transfer rate (one pipe geometry)

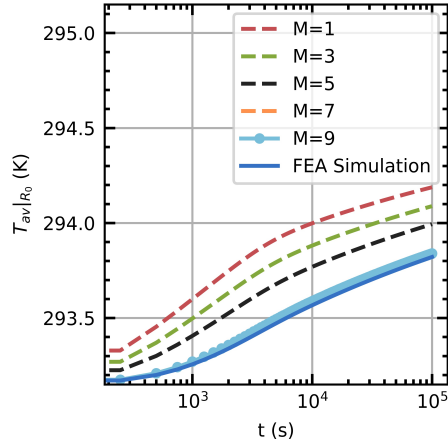
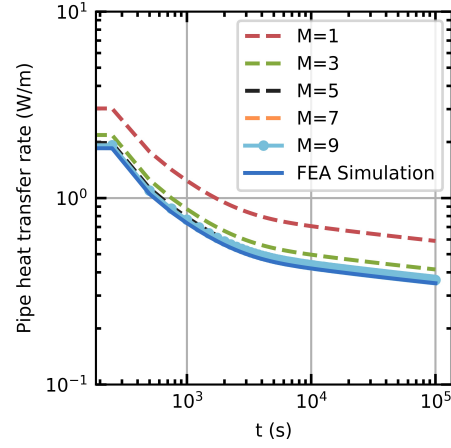
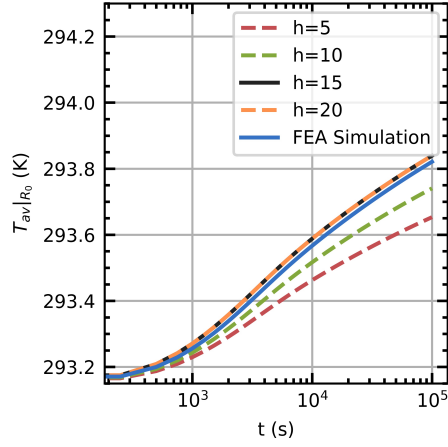
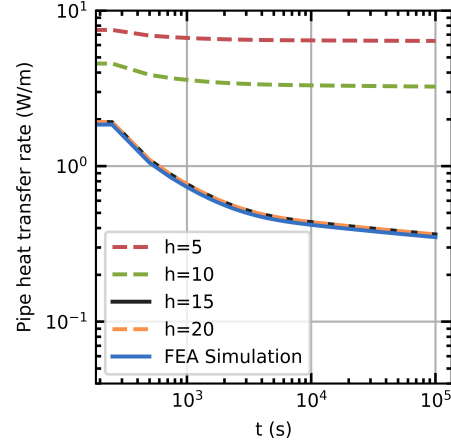
(a) Avg. Borehole Wall Temp. ( $h = 15$ )(b) Heat Flow Rate ( $h = 15$ )(c) Avg. Borehole Wall Temp. ( $M = 7$ )(d) Heat Flow Rate ( $M = 7$ )

Figure 4.12 Borehole wall temperature and pipe heat transfer rate (two pipes geometry)

Figures 4.13 and 4.14 show the temperature fields calculated from the FEA simulation and the temperature profiles at  $y = 0$  calculated from the FEA simulation and the proposed method. The temperature fields and temperatures profile are shown at times  $t = 1000$ ,  $10000$  and  $100000$  seconds for both of the single pipe and the two pipes geometries. The same temperature differences are observed as were seen in Figures 4.11 and 4.12 for the average borehole wall temperatures.

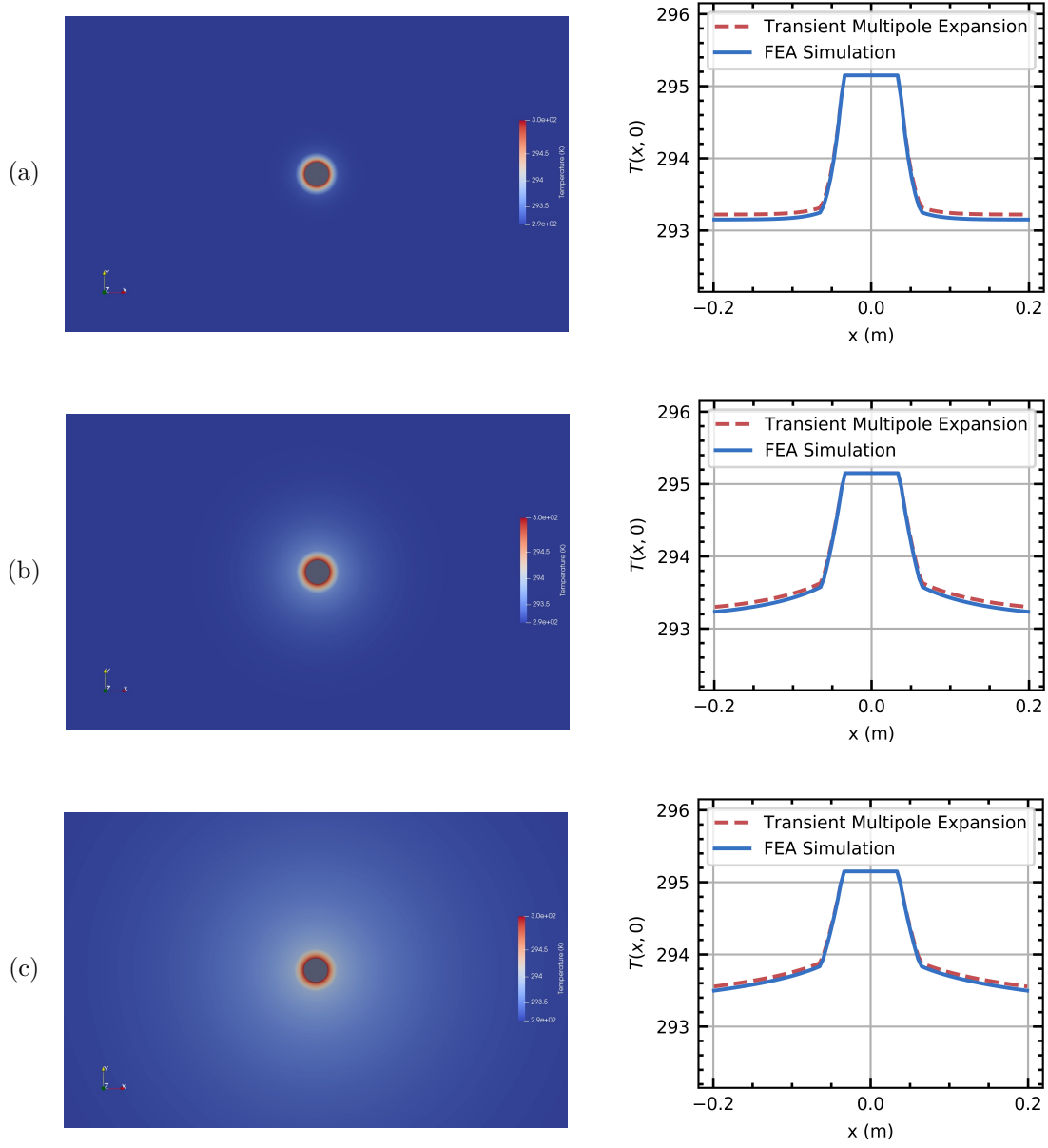


Figure 4.13 FEA simulation (left) and temperature profile at  $y = 0$  (right) for the one pipe geometry: (a)  $t = 1000$  s, (b)  $t = 10000$  s, and (c)  $t = 100000$  s



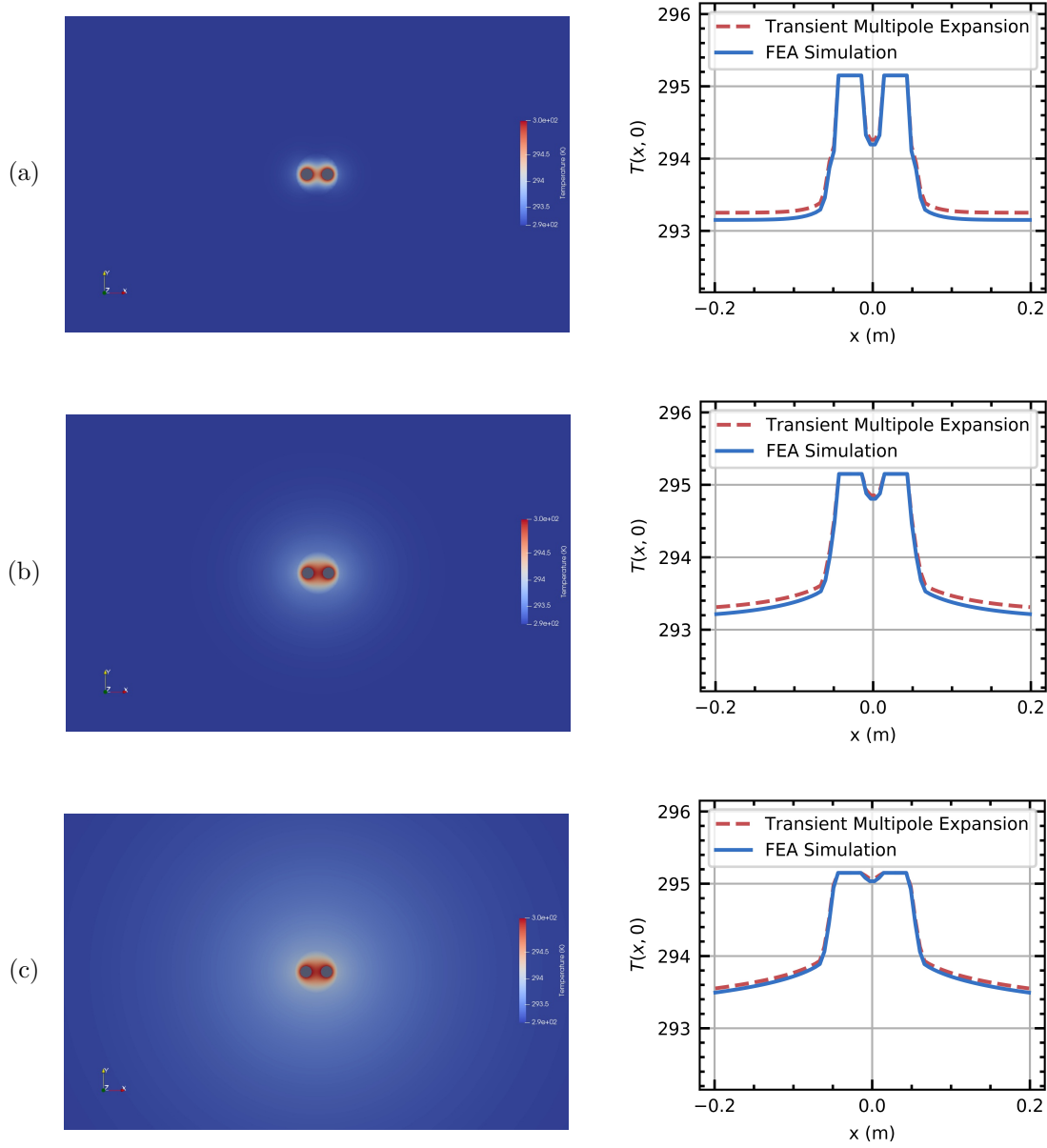


Figure 4.14 FEA simulation (left) and temperature profile at  $y = 0$  (right) for the two pipes geometry: (a)  $t = 1000$  s, (b)  $t = 10000$  s, and (c)  $t = 100000$  s

Finally, the coefficient updating scheme presented in Section 4.3.3 is used to calculate the fluid temperature variations in the two pipes geometry of Equation (4.37) (Figure 4.15). A constant total heat transfer rate per unit length  $\dot{q}' = 58 \text{ W/m}$  and a constant temperature difference between the pipes  $\Delta T = T_{f1} - T_{f2} = 1.3 \text{ K}$  (representative of a constant fluid mass flow rate) are applied with an initial temperature  $T^0 = 293.15 \text{ K}$ . The simulation time step is  $\Delta t = 20 \text{ s}$  and the maximum simulation time is  $t = 3100 \text{ min}$ , totaling 9300 time steps. FEA calculations take 220 seconds to complete and the presented method takes 80 seconds

to complete, including 61 seconds to evaluate the eigenvalues and integrals and 19 seconds to simulate the heat transfer process over all 9300 time steps.

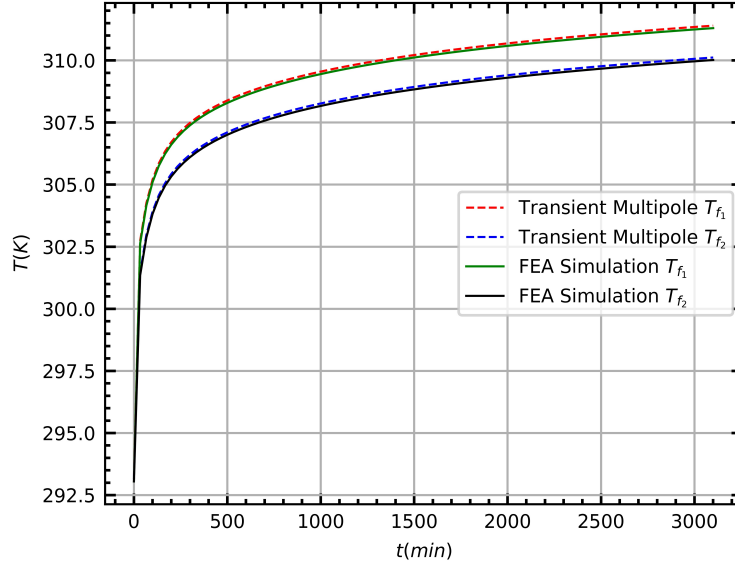


Figure 4.15 Inlet and outlet fluid temperature variations

## 4.5 Conclusions

This paper introduces a new transient multipole method to solve the short-term heat transfer in ground heat exchangers. The method does not require any simplification of the borehole geometry or discretization of the borehole thermal capacitance and can accommodate any number of arbitrarily positioned pipes within the borehole, as opposed to equivalent pipe methods and resistance-capacitance methods found in the literature. The method shows good agreement with reference FEA simulations when considering the 100 former eigenvalues of the expansion, identified from singular value decomposition. The method is then only dependent on the number of terms in the expansions,  $h$  and  $M$ , without any requirement for mesh generation of the calculation domain. For the considered cases  $h = 15$  is sufficient for the steady-state expansion, and  $M = 5$  and  $M = 7$  are sufficient for the transient expansion in the one pipe and two pipes geometries, respectively. While boundary conditions of imposed fluid temperatures and undisturbed ground temperature as far field are considered in the paper with a unbounded domain, the proposed method can be applied to other types of boundary conditions, as shown in Sections 4.4.1 and 4.4.2 for validation against the literature. A coefficient updating scheme is adopted to consider time-dependent fluid temperature. Fluid temperatures can be calculated by updating Fourier-Bessel coefficients and change the

boundary conditions at each time step. Further investigation is required to consider the fluid temperature variation along pipes, coupling the proposed method to an advection-convective model of the fluid inside the pipes. The number of considered eigenvalues and the coefficient updating scheme will then be analyzed for their impact on the accuracy and computational efficiency of GCHP simulations.

#### **4.6 Funding**

This study is funded by the Natural Sciences and Engineering Research Council of Canada (NSERC) [grant number: RGPIN-2018-04471].

## CHAPTER 5    ARTICLE 2: THERMAL INTERACTIONS IN LARGE IRREGULAR FIELDS OF GEOTHERMAL BOREHOLES: THE METHOD OF EQUIVALENT BOREHOLES

**Authors:** Carlos Prieto and Massimo Cimmino

**Article published in the journal:** *Journal of Building Performance Simulation*, Volume 14, Issue 4, pages 446-460

**Date of publication:** 25 August 2021

### 5.1 Abstract

A new method is presented to evaluate thermal interactions between vertical geothermal boreholes. The finite line source (FLS) solution is extended to consider thermal interactions between groups of boreholes. Groups of boreholes that share similar temperatures and heat extraction rates are identified using hierarchical agglomerative clustering, and each group is represented in the model as a single equivalent borehole. Each equivalent borehole is split into segments, and temporal and spatial superposition of the FLS solution are employed to calculate the total temperature change along the length of the equivalent boreholes. The new method is shown to provide an accurate calculation of the  $g$ -function, with a mean absolute percentage error below 0.612 % on the  $g$ -functions of regular borefields of up to 144 boreholes using only 3 to 5 equivalent boreholes. Calculation times are significantly reduced: the  $g$ -function of a borefield of 1024 randomly positioned boreholes is calculated in 3.65 seconds.

### 5.2 Introduction

Ground-coupled heat pump (GCHP) systems use the ground as a heat source (or sink) to supply heating (or cooling) to buildings. GCHP systems are composed of one or multiple heat pumps coupled to a set of geothermal boreholes (i.e. a borefield) that allow the exchange of thermal energy with the ground. A geothermal borehole consists in a drilled hole, typically of a diameter ranging from 100 mm to 150 mm and of a length ranging from 15 m to 180 m [130]. One or several U-tubes (or alternatively coaxial pipes) are inserted into the borehole and the borehole is subsequently back-filled with grouting material. In some cases, no grouting material is used and the borehole is filled with groundwater. The heat carrier fluid from the heat pump(s) is circulated through the boreholes to exchange heat with the

surrounding ground and then fed back to the heat pump(s). Heat extraction and rejection in the borefield cause fluid and ground temperature variations which may compound over the GCHP system's life cycle and impact on its performance and operability.

Mathematical models of heat transfer are used in all phases of GCHP system planning, design and operation. These mathematical models allow to predict temperature changes in the fluid and the ground due to fluctuations in the heat extraction and rejection into the borefield. In site characterization applications, physical parameters (e.g. soil thermal conductivity, borehole thermal resistance) can be inferred by fitting mathematical models to measurements from a thermal response test [131]. In the design phase of the system, mathematical models can be used to estimate the required borehole size to satisfy the operation parameters of the equipment, for example lower and upper fluid temperature limits for the operation of the heat pump [132]. Heat pump and borefield heat transfer mathematical models can be coupled to predict the energy consumption of the system. Also, these models could allow successfully posing an optimization strategy for the system design and the development of model-based control strategies [133]. Accurate predictions of fluid and ground temperatures require the modeling of both of the long-term and short-term heat transfer effects in geothermal boreholes [10]. Long-term heat transfer effects are characterized by the three-dimensional heat transfer in the soil and the thermal interactions between boreholes. Short-term heat transfer effects are characterized by the transit of the fluid through the boreholes and the thermal capacitance of the borehole materials.

Long-term temperature predictions in geothermal borefields can be obtained by temporal superposition of thermal response factors, or  $g$ -functions.  $g$ -Functions are unit step-response functions of the effective borehole wall temperature change due to a unit heat extraction rate from the borefield. They can be superimposed in time to achieve simulations of geothermal systems [134]. Eskilson [67] calculated the  $g$ -functions of geothermal borefields from the spatial superposition of temperature fields around individual boreholes. The individual temperature fields were calculated using a finite difference method. The inside and outside of the boreholes, delimited by the borehole wall, were uncoupled by considering a uniform borehole wall temperature along the length of the boreholes and equal for all boreholes. In recent work,  $g$ -functions are calculated by superimposing suitable analytical heat source solutions to model various physical phenomena, for example the finite line source (FLS) solution to model purely conductive heat transfer in isotropic and homogeneous ground [67], the moving finite line source to model the effects of groundwater advection [95], and the multilayer finite line source to model layered ground physical properties [74]. For pure conduction, the FLS solution was spatially superposed by Zeng et al. [68] to calculate thermal response factors of geothermal borefields. Lamarche and Beauchamp [69] and later Claesson and Javed [71]

obtained simplified expressions for the FLS solution involving a single integral, down from a computationally expensive double integral.

The simple spatial superposition of the FLS solution fails to accurately evaluate  $g$ -functions, due to the different boundary conditions at the borehole wall : the FLS solution considers a uniform heat extraction rate and Eskilson's  $g$ -functions consider a uniform borehole wall temperature. Cimmino et al. [72] and Cimmino and Bernier [73] were able to evaluate the  $g$ -functions for a uniform temperature boundary condition by first considering the time variation of the heat extraction rates of individual boreholes, and then by considering the distribution of heat extraction rates along boreholes using a segmented FLS solution. This method was also applied to inclined boreholes by Lazzarotto [75]. Cimmino [77] coupled the segmented FLS solution to a thermal circuit representation of the inside of geothermal boreholes and showed that the distribution of temperatures and heat extraction rates along boreholes are needed for accurate predictions of temperature variations. The spatial and temporal superposition of the FLS solution can also be used to assemble so-called network-based models of geothermal systems that account for the hydraulic configuration of the geothermal borefield, where the full distribution of borehole wall temperatures are evaluated every time step of simulations [135–137].

A drawback of analytical models for thermal interactions between boreholes, such as the FLS solution, is the computational effort required to evaluate the solution (due to the integral) and to solve the system of equations. The number of evaluations of the FLS solution scales with the square of the number of line source segments (i.e. the number of segment pairs). Cimmino [138] considered similarities between pairs of line sources to reduce the number of evaluations of the FLS solution. Dussault et al. [139] approximated the integrand of the FLS solution using Chebyshev polynomials, thereby reducing the time taken for numerical integration. Nguyen and Pasquier [140] make use of interpolations of a priori calculated FLS values at different distances, thereby reducing the time in the calculation of the borefield thermal response. These last two techniques, however, do not consider the distribution of heat extraction rates over the length of the boreholes. In all cases, the size of the system of equations is unaffected. The size of the system of equations is particularly damaging in network-based methods where it needs to be solved at each time step of the simulation. Lamarche [141] proposed a new FLS solution for piecewise linear distributions of heat extraction rates along the boreholes that achieves the same accuracy as the piecewise constant solution using fewer borehole segments and thereby reducing the size of the system of equations.

Short-term effects, caused by the transit of the fluid through the boreholes and the thermal capacitance of the borehole materials, dampen the variations of fluid and ground tempera-

tures during the first few hours of heat extraction and injection. The lower bound of validity of long-term models that neglect short-term effects is estimated to be  $t_b = 5r_b^2/\alpha_s$ , with  $r_b$  the borehole radius and  $\alpha_s$  the ground thermal diffusivity [67]. Neglecting short-term effects leads to an overestimation of the fluid and ground temperature changes, and possibly to an underestimation of the heat pump efficiency in simulations and an overestimation of the required borehole length in design [11,142]. There are several modeling approaches that include short-term effects, some of them are: equivalent pipe models [15,29,30,33,38], thermal resistance and capacitance methods (TRCMs) [42,43,46,47] and other models based on numerical methods [52,56,57]. Recently, transient multipole solutions have been developed in the time domain [143] and spectral domain [60] for 2D transient heat conduction. These solutions, that in their mathematical formalism approach exact solutions, have yet to be extended to include end-effects (i.e. axial heat transfer) in the boreholes and include fluid capacity in inside the pipes. There are works in which some of the mentioned methods are used to simulate both short- and long-term effects, such as Laferrière et al. [144]; Li et al. [145] and Claesson and Javed [71]. In these applications, the short- and long-term models are loosely coupled : only one borehole is used in the short-term model to represent the entire borefield, and the distribution of temperatures and heat extraction rates along the length of the borehole from the short-term model is not taken into account for long-term predictions. This approach is justifiable since modeling hundreds boreholes individually, both in the short- and long-term, would make the computational requirements for simulation impractical. As a result, the impact of short-term effects on the long-term temperature changes is unknown. New computationally-efficient and scalable (with regards to the number of boreholes) approaches to model long-term heat transfer in geothermal borefields are thereby needed to achieve detailed axially-discretized models of geothermal borefields that can be used in multi-annual simulations of GCHP systems.

This paper introduces a new *equivalent borehole* concept to model thermal interactions in geothermal borefields and to reduce the size of the system of equations in thermal models, and enable the efficient modelling of thermal interactions in large geothermal borefields comprised of hundreds of boreholes. A hierarchical agglomerative clustering is applied to identify groups of boreholes that share similar temperatures and heat extraction rates, and the FLS solution is adapted to evaluate thermal interactions between groups of boreholes each represented by a single equivalent borehole. The new approach is validated by calculating the  $g$ -function of borefields against a reference method from the literature [138,146].

### 5.3 Methodology

#### 5.3.1 Thermal interaction between boreholes

Figure 5.1 shows a field of  $N_b = 2$  vertical boreholes of equal dimensions. All boreholes have the same length  $L$  and radius  $r_b$ , and are buried at the same distance  $D$  from the ground surface. Each borehole  $i$  is located at coordinates  $(x_i, y_i)$ . The ground has a uniform and isotropic thermal conductivity  $k_s$  and thermal diffusivity  $\alpha_s$ , and is initially at a uniform temperature  $T(x, y, z, t = 0) = T_0$  (i.e. the undisturbed ground temperature).

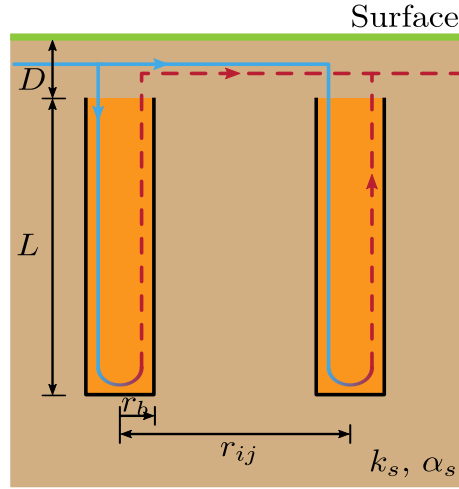


Figure 5.1 Field of 2 vertical boreholes of equal dimensions

Following the methodology of Cimmino and Bernier [73], each borehole is divided into  $n_q$  segments, and each borehole segment is modeled as a line segment located along its axis with a uniform heat extraction rate. The temperature drop at the wall of a segment  $u$  of a borehole  $i$  at time  $t_k$  can then be evaluated from the spatial and temporal superposition of the analytical FLS solution :

$$\Delta T_{b,i,u,k} = T_0 - T_{b,i,u,k} = \frac{1}{2\pi k_s} \sum_{j=1}^{N_b} \sum_{v=1}^{n_q} \sum_{p=1}^k Q'_{j,v,p} (h_{ij,uv}(t_k - t_{p-1}) - h_{ij,uv}(t_k - t_p)) \quad (5.1)$$

where  $\Delta T_{b,i,u,k}$  is the temperature drop at the wall of segment  $u$  of borehole  $i$  at time  $t_k$ ,  $T_0$  is the initial ground temperature,  $T_{b,i,u,k}$  is the temperature at the wall of segment  $u$  of borehole  $i$  at time  $t_k$ ,  $Q'_{j,v,p}$  is the heat extraction rate per unit length of segment  $v$  of borehole  $j$  from time  $t_{p-1}$  to  $t_p$ , and  $h_{ij,uv}$  is the segment-to-segment thermal response factor for the borehole wall temperature change over segment  $u$  of borehole  $i$  caused by heat extraction



from segment  $v$  of borehole  $j$ . The segment-to-segment response factor is given by the FLS solution:

$$h_{ij,uv}(t) = \frac{1}{2L_u} \int_{\frac{1}{\sqrt{4\alpha_s t}}}^{\infty} \frac{1}{s^2} \exp(-r_{ij}^2 s^2) I_{FLS}(s) ds \quad (5.2a)$$

$$\begin{aligned} I_{FLS}(s) = & \operatorname{erfint}((D_u - D_v + L_u)s) - \operatorname{erfint}((D_u - D_v)s) \\ & + \operatorname{erfint}((D_u - D_v - L_v)s) - \operatorname{erfint}((D_u - D_v + L_u - L_v)s) \\ & + \operatorname{erfint}((D_u + D_v + L_u)s) - \operatorname{erfint}((D_u + D_v)s) \\ & + \operatorname{erfint}((D_u + D_v + L_v)s) - \operatorname{erfint}((D_u + D_v + L_u + L_v)s) \end{aligned} \quad (5.2b)$$

$$\operatorname{erfint}(x) = \int_0^x \operatorname{erf}(x') dx' = x \operatorname{erf}(x) - \frac{1}{\sqrt{\pi}} (1 - \exp(-x^2)) \quad (5.2c)$$

where  $r_{ij}$  is the radial distance between boreholes  $i$  and  $j$  (with  $r_{ii} = r_b$ ),  $\operatorname{erf}(x)$  is the error function and  $\operatorname{erfint}(x)$  is the integral of the error function.

In non-dimensional form:

$$\theta_{b,i,u,k} = \sum_{j=1}^{N_b} \sum_{v=1}^{n_q} \sum_{p=1}^k \phi'_{j,v,p} (h_{ij,uv}(\tau_k - \tau_{p-1}) - h_{ij,uv}(\tau_k - \tau_p)) \quad (5.3)$$

where  $\theta_{b,i,u,k} = \frac{T_0 - T_{b,i,u,k}}{Q'^*/2\pi k_s}$  is the dimensionless temperature at the wall of segment  $u$  of borehole  $i$  at a dimensionless time  $\tau_k = \frac{9\alpha_s t_k}{L^2} = \frac{t_k}{t_s}$  with  $t_s$  the borefield characteristic time,  $\phi'_{j,v,p} = \frac{Q'_{j,v,p}}{Q'^*}$  is the normalized heat extraction rate per unit length of segment  $v$  of borehole  $j$  from time  $\tau_{p-1}$  to  $\tau_p$ , and  $Q'^*$  is an arbitrary heat extraction rate per unit length.

Equation (5.3) can be simplified by introducing matrix notation:

$$\Theta_{b,k} = \sum_{p=1}^k (\mathbf{H}(\tau_k - \tau_{p-1}) - \mathbf{H}(\tau_k - \tau_p)) \mathbf{\Phi}'_p \quad (5.4)$$

$$= \sum_{p=1}^{k-1} (\mathbf{H}(\tau_k - \tau_{p-1}) - \mathbf{H}(\tau_k - \tau_p)) \mathbf{\Phi}'_p + \mathbf{H}(\tau_k - \tau_{k-1}) \mathbf{\Phi}'_k \quad (5.5)$$

$$= \Theta_{b,k}^0 + \mathbf{H}(\tau_k - \tau_{k-1}) \mathbf{\Phi}'_k \quad (5.6)$$

where  $\Theta_{b,k} = [\theta_{b,1,1,k}, \theta_{b,1,2,k}, \dots, \theta_{b,N_b,n_q,k}]^T$  is a vector of dimensionless borehole wall temperatures along all segments of all boreholes at time  $\tau_k$  and  $\mathbf{\Phi}'_k = [\phi'_{1,1,k}, \phi'_{1,2,k}, \dots, \phi'_{N_b,n_q,k}]^T$  is a vector of dimensionless heat extraction rates per unit length along all segments of all

boreholes at time  $t_k$ .  $\mathbf{H}$  is a  $N_b n_q \times N_b n_q$  matrix of segment-to-segment response factors:

$$\mathbf{H}(\tau_k) = \begin{bmatrix} h_{11,11}(\tau_k) & h_{11,12}(\tau_k) & \cdots & h_{1N_b,1n_q}(\tau_k) \\ h_{11,21}(\tau_k) & h_{11,22}(\tau_k) & \cdots & h_{1N_b,2n_q}(\tau_k) \\ \vdots & \vdots & \ddots & \vdots \\ h_{N_b1,n_q1}(\tau_k) & h_{N_b1,n_q2}(\tau_k) & \cdots & h_{N_bN_b,n_qn_q}(\tau_k) \end{bmatrix} \quad (5.7)$$

### 5.3.2 Thermal interaction between groups of boreholes

The size of the system of equations presented in Equation (5.4) increases with the square of the total number of segments in the borefield ( $N_b^2 n_q^2$ ). The calculation time for the simulation of borefields using network-based methods (e.g. [135–137]) or for the evaluation of  $g$ -functions (e.g. [138, 139]) thereby increases substantially when the number of boreholes increases. This makes the simulation of geothermal borefields increasingly impractical as the number of boreholes increase. One method for decreasing the size of the system of equations is to consider symmetries in the borefield layout, as done by Cimmino et al. [72]. This method is however only applicable to regular borefield geometries where symmetrical groups of boreholes, which share the same borehole wall temperatures and heat extraction rates, can be easily identified. This section extends the concept of borehole groups to consider groups of non-symmetrically positioned boreholes. Boreholes in the same group are assumed to have similar borehole wall temperature profiles and heat extraction rate profiles, such that all boreholes in a group can be replaced with a single *equivalent* borehole representative of that group.

There exists a fundamental group composed with all the boreholes in the borefield defined as  $\mathbb{G} = \{1, 2, 3, \dots, i, \dots, j, \dots, N_b\}$ , which is a non-empty finite set where every element in the group corresponds to a borehole index. Since  $\mathbb{G}$  is non-empty and finite, it is possible to decompose this group as a set of  $\mathcal{G}(\leq N_b)$  non-empty groups such that  $\mathbb{G} = \bigcup_{\mathcal{I}=1}^{\mathcal{G}} \mathbb{G}_{\mathcal{I}}$  (i.e. all boreholes are in a group),  $\mathbb{G}_{\mathcal{I}} \cap \mathbb{G}_{\mathcal{J}} = \emptyset$  for  $\mathcal{I} \neq \mathcal{J}$  (i.e. a borehole is an element of only one group), and consequently  $\bigcap_{\mathcal{I}=1}^{\mathcal{G}} \mathbb{G}_{\mathcal{I}} = \emptyset$ . The cardinality of the borefield group is  $\#\mathbb{G} = \sum_{\mathcal{I}=1}^{\mathcal{G}} \#\mathbb{G}_{\mathcal{I}} = \sum_{\mathcal{I}=1}^{\mathcal{G}} N_{b,\mathcal{I}} = N_b$ , where  $N_{b,\mathcal{I}}(\geq 1)$  corresponds to the number of boreholes belonging to group  $\mathbb{G}_{\mathcal{I}}$ . The formation of borehole groups is described in section 5.3.3.

The dimensionless borehole wall temperature at the wall of equivalent borehole segments is calculated from the spatial and temporal superposition of the FLS solution:

$$\bar{\theta}_{b,\mathcal{I},u,k} = \sum_{n=1}^{\mathcal{G}} \sum_{v=1}^{n_q} \sum_{p=1}^k \bar{\phi}'_{\mathcal{J},v,p} \left( \bar{h}_{\mathcal{I}\mathcal{J},uv}(\tau_k - \tau_{p-1}) - \bar{h}_{\mathcal{I}\mathcal{J},uv}(\tau_k - \tau_p) \right) \quad (5.8)$$

where  $\bar{\theta}_{b,\mathcal{I},u,k}$  is the dimensionless temperature at the wall of segment  $u$  of equivalent borehole

$\mathcal{I}$  at time  $\tau_k$ ,  $\bar{\phi}'_{\mathcal{J},v,p}$  is the normalized heat extraction rate per unit length of segment  $v$  of equivalent borehole  $\mathcal{J}$  from time  $\tau_{p-1}$  to  $\tau_p$ , and  $\bar{h}_{\mathcal{I}\mathcal{J},uv}$  is the equivalent segment-to-segment response factor for the borehole wall temperature change over segment  $u$  of equivalent borehole  $\mathcal{I}$  caused by heat extraction from segment  $v$  of equivalent borehole  $\mathcal{J}$ .

The equivalent segment-to-segment response factor is given by the average segment-to-segment response factors for the borehole wall temperature change along segments  $u$  of all boreholes in group  $\mathbb{G}_{\mathcal{I}}$  due to the heat extraction at all segments  $v$  of all boreholes in group  $\mathbb{G}_{\mathcal{J}}$ :

$$\bar{h}_{\mathcal{I}\mathcal{J},uv}(t) = \frac{1}{2L_u} \frac{1}{N_{b,\mathcal{I}}} \int_{\frac{1}{\sqrt{4\alpha_s t}}}^{\infty} \sum_{i \in \mathbb{G}_{\mathcal{I}}} \sum_{j \in \mathbb{G}_{\mathcal{J}}} \frac{1}{s^2} \exp(-r_{ij}^2 s^2) I_{FLS}(s) ds \quad (5.9)$$

$$\bar{h}_{\mathcal{J}\mathcal{I},vu}(t) = \frac{N_{b,\mathcal{I}}}{N_{b,\mathcal{J}}} \frac{L_u}{L_v} \bar{h}_{\mathcal{I}\mathcal{J},uv}(t) \quad (5.10)$$

In matrix notation:

$$\bar{\Theta}_{b,k} = \sum_{p=1}^k \left( \bar{\mathbf{H}}(\tau_k - \tau_{p-1}) - \bar{\mathbf{H}}(\tau_k - \tau_p) \right) \bar{\Phi}'_p \quad (5.11)$$

$$= \sum_{p=1}^{k-1} \left( \bar{\mathbf{H}}(\tau_k - \tau_{p-1}) - \bar{\mathbf{H}}(\tau_k - \tau_p) \right) \bar{\Phi}'_p + \bar{\mathbf{H}}(\tau_k - \tau_{k-1}) \bar{\Phi}'_k \quad (5.12)$$

$$= \bar{\Theta}_{b,k}^0 + \bar{\mathbf{H}}(\tau_k - \tau_{k-1}) \bar{\Phi}'_k \quad (5.13)$$

where  $\bar{\Theta}_{b,k} = [\bar{\theta}_{b,1,1,k}, \bar{\theta}_{b,1,2,k}, \dots, \bar{\theta}_{b,\mathcal{G},n_q,k}]^T$  is a vector of dimensionless borehole wall temperatures along all segments of all equivalent boreholes at time  $\tau_k$  and  $\bar{\Phi}'_k = [\bar{\phi}'_{1,1,k}, \bar{\phi}'_{1,2,k}, \dots, \bar{\phi}'_{\mathcal{G},n_q,k}]^T$  is a vector of dimensionless heat extraction rates per unit length along all segments of all boreholes at time  $\tau_k$ .  $\bar{\mathbf{H}}$  is a  $\mathcal{G}n_q \times \mathcal{G}n_q$  matrix of equivalent segment-to-segment response factors:

$$\bar{\mathbf{H}}(\tau_k) = \begin{bmatrix} \bar{h}_{11,11}(\tau_k) & \bar{h}_{11,12}(\tau_k) & \cdots & \bar{h}_{1\mathcal{G},1n_q}(\tau_k) \\ \bar{h}_{11,21}(\tau_k) & \bar{h}_{11,22}(\tau_k) & \cdots & \bar{h}_{1\mathcal{G},2n_q}(\tau_k) \\ \vdots & \vdots & \ddots & \vdots \\ \bar{h}_{\mathcal{G}1,n_q1}(\tau_k) & \bar{h}_{\mathcal{G}1,n_q2}(\tau_k) & \cdots & \bar{h}_{\mathcal{G}\mathcal{G},n_qn_q}(\tau_k) \end{bmatrix} \quad (5.14)$$

Comparing Equations (5.3) and (5.8), it can be seen that the size of the system of equations using equivalent boreholes is reduced by a factor  $N_b^2/\mathcal{G}^2$ .

### 5.3.3 Equivalent boreholes

This section introduces a systematic way to compute the finite set of groups for the borefield group  $\mathbb{G} = \bigcup_{\mathcal{I}=1}^{\mathcal{G}} \mathbb{G}_{\mathcal{I}}$ . A hierarchical clustering approach is introduced to define the groups.

Then, an optimal number of groups is defined based on the maximum dissimilarity between the identified groups.

### Hierarchical agglomerative clustering

A hierarchical agglomerative clustering method is applied to form groups of boreholes that share similar borehole wall temperatures. Agglomerative clustering methods present advantages compared to other clustering methods (e.g.  $k$ -means,  $k$ -medoids), as they do not require the number of groups to be known prior to clustering. In hierarchical agglomerative clustering, each element (i.e. borehole) is initialized as their own cluster (i.e. group). At each iteration of the algorithm, the two closest clusters are merged according to a *linkage* criterion evaluated from a *distance metric* based on the distance between elements of the two clusters. The product of the hierarchical agglomerative clustering can be visualized on a dendrogram tree from which the clusters can be identified for a known number of clusters or based on a criterion to identify the optimal number of groups (as will be presented in section 5.3.3).

Recalling from section 5.3.2 that boreholes in the same group should have similar borehole wall temperatures and heat transfer rate, the absolute temperature difference between boreholes is used as the distance metric. A complete linkage is proposed, meaning the distance between two groups of boreholes is given by the maximum absolute temperature difference between boreholes of the two groups:

$$\mathcal{L}(\mathcal{I}, \mathcal{J}) = \max_{i \in \mathbb{G}_{\mathcal{I}}, j \in \mathbb{G}_{\mathcal{J}}} \mathcal{M}(i, j) \quad (5.15)$$

$$\mathcal{M}(i, j) = |\theta_i - \theta_j| \quad (5.16)$$

where  $\mathcal{L}(\mathcal{I}, \mathcal{J})$  is the complete linkage criterion between groups  $\mathcal{I}$  and  $\mathcal{J}$  (i.e. the distance between the groups),  $\mathcal{M}(i, j)$  is the distance metric between two boreholes, and  $\theta_i$  is the dimensionless temperature at the wall of borehole  $i$ .

Dimensionless borehole wall temperatures are calculated considering a unit normalized heat extraction rate equal for all boreholes (i.e.  $\phi' = 1$ ). For the purpose of the hierarchical agglomerative clustering, the single segment steady-state finite line source (FLS) is used to evaluate the dimensionless borehole wall temperatures, rather than the FLS solution used in sections 5.3.1 and 5.3.2. It was found that the single segment steady-state FLS solution provides sufficient accuracy for clustering with the advantage of being much less computationally intensive to evaluate than Equation (5.2) since there exists a formulation free of integrals. The average dimensionless temperature change at the location of a borehole  $i$  due to a unit normalized heat extraction rate per unit length at a borehole  $j$  is given by:

$$w_l = \{D_i - D_j + L_i, D_i - D_j, D_i - D_j - L_j, D_i - D_j + L_i - L_j, \\ D_i + D_j + L_i, D_i + D_j, D_i + D_j + L_j, D_i + D_j + L_i + L_j\} \quad (5.17a)$$

$$\theta_{ij} = \frac{1}{2L_i} \sum_{l=1}^8 (-1)^{l+1} \left\{ w_l \ln \left[ \left( w_l + \sqrt{w_l^2 + r_{ij}^2} \right) / r_{ij} \right] - \sqrt{w_l^2 + r_{ij}^2} \right\} \quad (5.17b)$$

where  $\theta_{ij}$  is the steady-state dimensionless temperature change at the location of a borehole  $i$ , located at a distance  $r_{ij}$  from a borehole  $j$  (with  $r_{ii} = r_b$ ), caused by a unit normalized heat extraction rate per unit length.

The dimensionless borehole wall temperature change is given by the spatial superposition of the temperature changes caused by all boreholes:

$$\theta_i = \sum_{j=1}^{N_b} \theta_{ij} \quad (5.18)$$

### Optimal number of groups

The result of the hierarchical agglomerative clustering can be visualized on a dendrogram. Figure 5.2 shows an example dendrogram generated from the clustering of a field of 16 boreholes. The dendrogram shows the complete clustering process, starting with all boreholes in separate groups until all groups are merged into a single group. The leaf nodes at the bottom of the dendrogram represent the initial groups. At each iteration, the two closest groups (according to Equations (5.15) and (5.16)) are merged. The created group is represented as an internal node, with branches connecting the node to the two merged groups, and its height represents the distance between the two groups. The root node, at the top of the dendrogram, contains all boreholes.

A minimum number of groups, expressed as  $\mathcal{G}_{\min}$ , can be identified from a cut-off threshold on the dendrogram. A simple technique to identify the minimum number of groups is to cut the dendrogram at the half-height with an horizontal line at the longest distance between two consecutive nodes on the tree, as shown on Figure 5.2. The number of branches crossed by the cut-off line corresponds to the minimum number of groups. In the example,  $\mathcal{G}_{\min} = 2$ . The optimal number of groups is greater than the minimum. However, it is not possible to identify the optimal number of groups on rigorous formalism (not based on nonlinear programming) but particular techniques have been studied [147–149]. Therefore, the number

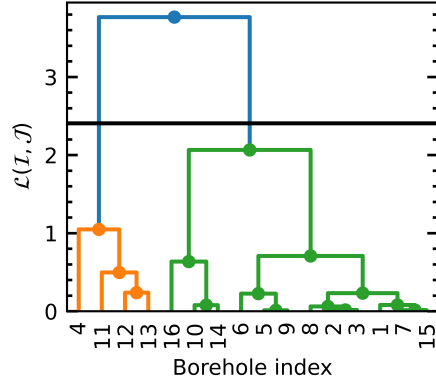


Figure 5.2 Dendrogram Example

of groups can be chosen by increasing the minimum number of groups:

$$\mathcal{G} = \mathcal{G}_{\min} + \mathcal{K} \quad (5.19)$$

where  $\mathcal{K}$  is a precision increment from which the number of groups can be increased from the minimum. It will be shown later that the proposed method achieves acceptable accuracy for  $\mathcal{K} = 1$ .

#### 5.3.4 $g$ -function calculation

The proposed method is validated by calculating the  $g$ -function. The  $g$ -function represents the effective borehole wall temperature variation in a field of thermally interacting boreholes for a constant total heat extraction rate. Temporal superposition can later be applied to the  $g$ -function to simulate borefields with varying heat extraction rates. As shown by Cimmino and Bernier [73], the accurate evaluation of the  $g$ -function requires detailed modeling of the borefield where the variation of heat extraction rates along the boreholes is considered.

In the proposed method, each group of boreholes is modeled using a single equivalent borehole and the variation of the heat extraction rate along its length is applied to all boreholes of the same group, thereby limiting the degrees of freedom of the borefield. If the equivalent boreholes are indeed representative of their respective groups and the number of groups is sufficient, the proposed method should produce the same  $g$ -function as if all boreholes are modeled individually. The proposed method will thus be validated by evaluating the  $g$ -function and comparing the variation of heat extraction rates in the borefield.

For a field of boreholes connected in parallel, the  $g$ -function is typically evaluated by imposing a uniform borehole wall temperature equal for all boreholes [67], based on the assumptions

that the fluid temperature variation inside boreholes is small and that fluid and borehole wall temperatures are sufficiently close. At each time step, a system of equations is built and solved to identify the required borehole wall temperature to achieve the desired constant total heat extraction rate:

$$\begin{bmatrix} \bar{\mathbf{H}}(\tau_k - \tau_{k-1}) & \mathbf{1} \\ \bar{\mathbf{L}} & 0 \end{bmatrix} \begin{bmatrix} \bar{\Phi}'_k \\ \bar{\theta}_{b,k} \end{bmatrix} = \begin{bmatrix} -\bar{\Theta}_{b,k}^0 \\ 1 \end{bmatrix} \quad (5.20a)$$

$$\bar{\mathbf{L}} = \begin{bmatrix} \frac{N_{b,1}}{N_b n_q} & \frac{N_{b,1}}{N_b n_q} & \dots & \frac{N_{b,2}}{N_b n_q} & \frac{N_{b,2}}{N_b n_q} & \dots & \frac{N_{b,g}}{N_b n_q} & \frac{N_{b,g}}{N_b n_q} \end{bmatrix} \quad (5.20b)$$

where  $\bar{\theta}_{b,k}$  is the uniform dimensionless borehole wall temperature at time  $\tau_k$ , corresponding to the  $g$ -function, and  $\bar{\mathbf{L}}$  is a vector of length ratios that imposes a constant total unit normalized heat extraction rate per unit length. A similar system of equations can be built from the relations in section 5.3.1 to evaluate the  $g$ -function considering each borehole individually. The method is not limited to the calculation of  $g$ -functions using a uniform temperature boundary condition. The same hierarchical agglomerative clustering approach can be considered to evaluate  $g$ -functions using an equal inlet fluid temperature boundary condition by extending Equation (5.20) to include the interaction between the fluid and the borehole walls [77]. Boreholes of unequal lengths can also be considered by applying the clustering approach to each subset of boreholes of equal lengths in the borefield.

## 5.4 Results

The proposed method is implemented in Python, using the `SciPy` library [128] for the implementation of the hierarchical agglomerative clustering, the evaluation of integrals and the evaluation of special functions (e.g. the error function), and the `NumPy` library [127] to handle matrix and vector manipulations. The reference  $g$ -functions, evaluated with all boreholes modeled individually as presented in section 5.3.1, are calculated using the `pygfunction` (version 2.0.0) library [146] which implements the similarities method of Cimmino [138] to accelerate calculations. The `pygfunction` library was extended to accommodate the proposed method.

The proposed method is first applied to the calculation of the  $g$ -function of a field of 20 boreholes in a rectangular configuration and compared to the reference method with regards to the  $g$ -function values and the predicted heat extraction rates. Then, the accuracy and computational time of the proposed method is assessed on various regular borefield configurations with up to 144 boreholes. Finally, the robustness and scalability of the method, in terms of accuracy and calculation time, is tested on borefields of randomly positioned bore-

holes with up to 1024 boreholes. Simulation parameters are presented in Table 5.1, where the borehole spacing  $B$  only applies to regular borefield configurations.

Table 5.1 Borehole and ground parameters

Parameter	Value
Borehole buried depth	$D = 4 \text{ m}$
Borehole length	$L = 150 \text{ m}$
Borehole spacing	$B = 7.5 \text{ m}$
Borehole radius	$r_b = 0.075 \text{ m}$
Ground thermal diffusivity	$\alpha_s = 1.0 \times 10^{-6} \text{ m}^2/\text{s}$

In all cases, the number of equivalent boreholes is chosen according to the criterion of section 5.3.3 with  $\mathcal{K} = 1$ , the number of segments per borehole is  $n_q = 12$  as per the recommendation of Cimmino and Bernier [73], and the  $g$ -functions are calculated at  $N_t = 25$  time values in geometrically expanding time-steps in the range  $-10 \leq \ln(t/t_s) \leq 5$ . All calculations were done on a personal computer with 16 GB of RAM and a 6-core processor (12 threads) running at normal speed of 2.60 GHz and maximum speed of 4.80 GHz.

The accuracy of the proposed method is quantified using the mean absolute percentage error:

$$MAPE = \frac{100}{N_t} \sum_{k=1}^{N_t} \left| \frac{g_{\text{reference}}(\tau_k) - g(\tau_k)}{g_{\text{reference}}(\tau_k)} \right| \quad (5.21)$$

where  $MAPE$  is the mean absolute percentage error and  $g_{\text{reference}}$  is the  $g$ -function evaluated using the reference method.

#### 5.4.1 Rectangular borefield of 20 boreholes

Figure 5.3 shows the results of the hierarchical agglomerative clustering method applied to a borefield of 20 boreholes in a  $N_x \times N_y = 5 \times 4$  rectangular configuration. Figure 5.3a shows the borefield layout, with markers representing the positions of the boreholes and different marker colors representing the identified borehole groups. Figure 5.3b shows the dendrogram resulting from the clustering method. It can be seen that the minimum number of groups is  $\mathcal{G}_{\min} = 2$  since the cut-off line, at half-height of maximum  $\mathcal{L}(\mathcal{I}, \mathcal{J})$  between two consecutive nodes, crosses two branches of the dendrogram, and therefore the number of groups is  $\mathcal{G} = 3$  for a precision increment  $\mathcal{K} = 1$ . For simplicity, groups will be referred to using roman numerals (e.g. group *III* refers to  $\mathbb{G}_3$ ). In this example, group *I* contains 6 boreholes, group *II* contains 10 boreholes, and group *III* contains the remaining 4 boreholes. It should be noted that, due to symmetries in the borefield layout, the borefield could be



modeled with no error (compared to the reference) using only 6 groups. Figure 5.3a shows that the clustering approach successfully places symmetrically positioned boreholes in the same group.

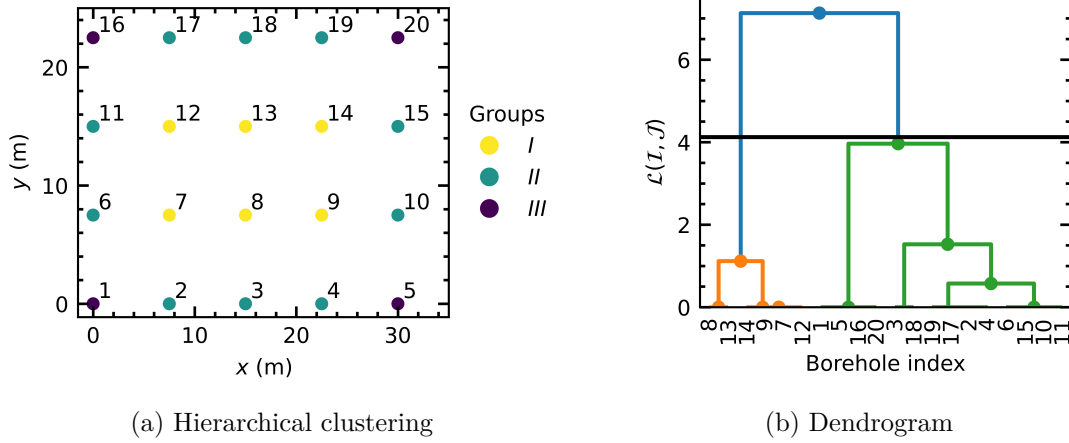
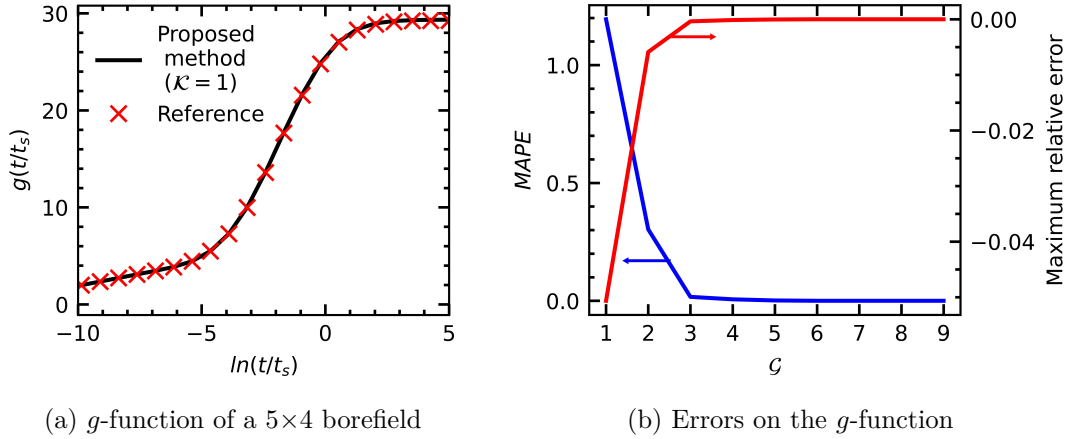


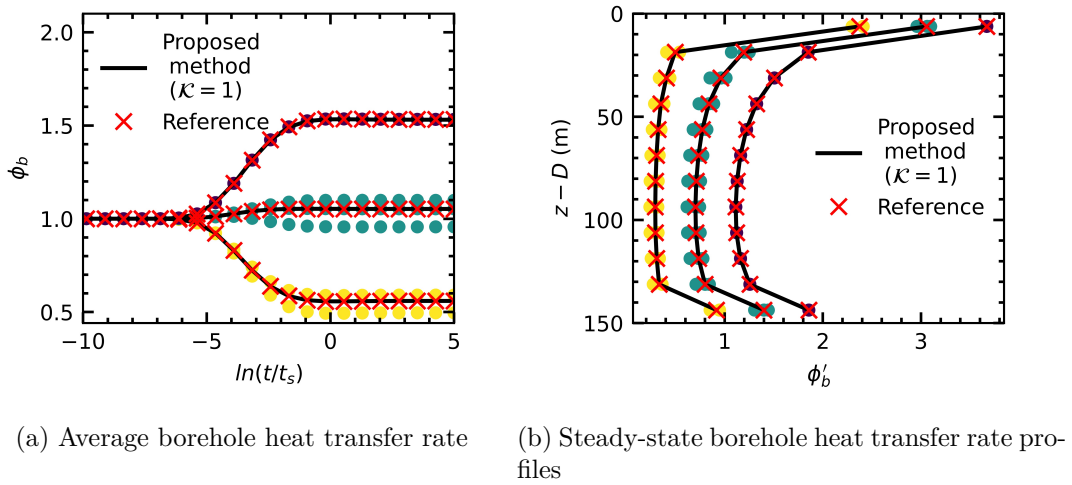
Figure 5.3 Hierarchical agglomerative clustering method for a  $5 \times 4$  borefield

Figure 5.4a compares the  $g$ -function of the  $5 \times 4$  borefield evaluated using the proposed method to the reference method of Cimmino [138] for a  $\mathcal{K} = 1$ . Figure 5.4b shows the  $MAPE$  and the maximum relative error as a function of the number of groups  $\mathcal{G}$  used for the calculation of the  $g$ -function (with  $\mathcal{G}_{\min} + 1 = 3$ ). It is shown that the errors are maximum when only one group is considered, with a  $MAPE$  (left y-axis) of 1.2% and a maximum relative error (right y-axis) of -0.05. A negative sign on the maximum relative error means that the  $g$ -function calculated by the proposed method overestimates the value given by the reference method. As expected, the errors reach 0 when  $\mathcal{G} = 6$ . According to these results, a precision increment  $\mathcal{K} = 1$  is sufficient to estimate the  $g$ -function. For a precision increment  $\mathcal{K} = 1$  ( $\mathcal{G} = 3$ ), the  $MAPE$  is equal to 0.017 % and the maximum relative error is equal to  $-3.75 \times 10^{-4}$  and is found at the last time step  $\ln(t/t_s) = 5$ . It is thus found that thermal interactions in a  $5 \times 4$  borefield totaling 20 boreholes can be accurately represented by 3 equivalent boreholes.

The heat extraction rates of the equivalent boreholes are compared to the heat transfer rates of the individual boreholes calculated using the reference method to verify that equivalent boreholes are representative of their respective group. Figure 5.5a presents the time-variation of the average over-the-length heat extraction rate profile and Figure 5.5b presents the vertical steady-state heat extraction rate profile along for the same  $5 \times 4$  borefield evaluated at  $\ln(t/t_s) = 5$ . Colored markers correspond to the heat transfer rates calculated by the reference method and their colors correspond to the groups identified in Figure 5.3a. Solid black lines correspond to the heat transfer rates of the equivalent boreholes calculated using the proposed

Figure 5.4  $g$ -function comparison for a  $5 \times 4$  borefield

method while the red crosses correspond to the average of the heat transfer rates calculated by the reference method for each group. It is shown that core boreholes in group *I* experiment lower heat transfer rates than perimeter boreholes in group *III*. The good agreement between the heat transfer rates of equivalent boreholes and the group averages shows that the proposed hierarchical agglomerative clustering method is able to identify equivalent boreholes which are representative of their group. The maximum relative error on the average over-the-length heat extraction rates of equivalent boreholes is less than  $-7 \times 10^{-4}$  for all groups when compared to the group average evaluated using the reference method. The maximum relative error on the steady-state heat extraction rate profiles is  $-5 \times 10^{-4}$  for group *III*.

Figure 5.5 Heat extraction rates of a  $5 \times 4$  borefield

### 5.4.2 Regular borefield configurations

The accuracy and calculation time of the method is assessed for various regular borefield configurations with up to 144 boreholes. Figure 5.6 presents schematic representations of rectangular, L-, Box- and U-shaped borefields. For each of the configurations, the method is applied to borefields in all possible combinations of  $2 \times 1$  up to  $12 \times 12$  boreholes on the horizontal and vertical directions, respectively. For these simulations, the number of groups varies between 2 and 4 for  $\mathcal{K} = 1$  and between 2 and 5 for  $\mathcal{K} = 2$ . A number of groups  $\mathcal{G} = 2$  is only found in the case of the  $2 \times 1$  configurations. Figure 5.7 compares the *MAPE* for  $\mathcal{K} = 1$  and  $\mathcal{K} = 2$  for regular borefield configurations from  $2 \times 1$  up to  $12 \times 12$  boreholes. *MAPE* values lower than  $10^{-4}$  are shown on a linear scale. Markers are colored according to the number of equivalent boreholes used for the calculation of the *g*-function. The largest *MAPE* is equal to 0.612 % and found for the  $12 \times 9$  rectangular borefield totaling 108 boreholes for  $\mathcal{K} = 1$  ( $\mathcal{G} = 4$ ), and is equal to 0.490% for a  $12 \times 7$  rectangular borefield totaling 84 boreholes with  $\mathcal{K} = 2$  ( $\mathcal{G} = 5$ ). For the largest borefield, totaling 144 boreholes in a  $12 \times 12$  rectangular configuration, the *MAPE* is equal to 0.493 and 0.254 % with 3 ( $\mathcal{K} = 1$ ) and 4 groups ( $\mathcal{K} = 2$ ), respectively. It is thus observed that the precision increment  $\mathcal{K}$  has a positive but not significant impact on the *MAPE* when increasing its value by one. A value of  $\mathcal{K} = 1$  is found to provide sufficient accuracy across all regular configurations. The borefield configuration was not found to have any significant impact on the *MAPE*. It should be noted that the *MAPE* reaches zero when the number of groups is equal to the number of boreholes in the borefield, or earlier if there are any symmetries in the borefield layout.

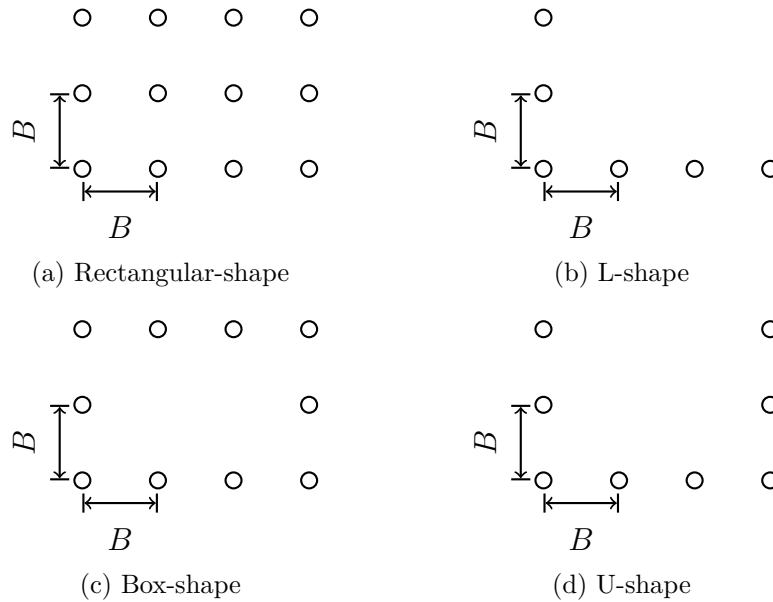


Figure 5.6 Regular borefield configurations

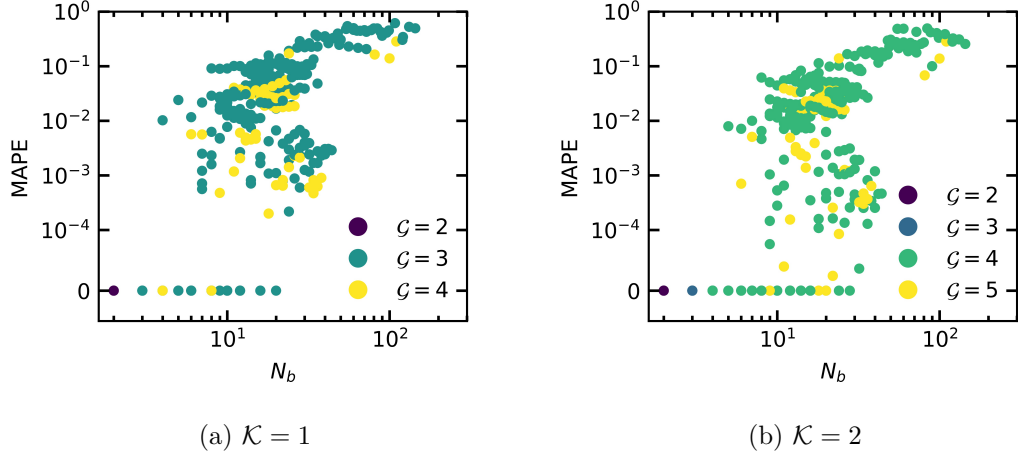


Figure 5.7 Mean absolute percentage error on the  $g$ -functions

The method presents substantial improvements in calculation time due to the decrease in the number of modeled boreholes for large borefields. Figure 5.8 presents the calculation times of the reference method (using `pygfunction`) and the proposed method. As can be seen, the calculation time starts increasing rapidly in the reference method once the number of boreholes reaches approximately 100 boreholes. Comparatively, the calculation time in the proposed method increases very slowly with the number of boreholes. As an example, for the  $12 \times 12$  rectangular borefield with 144 boreholes, the calculation time is 7.4 sec and 0.9 sec for the reference method and the proposed method, respectively.

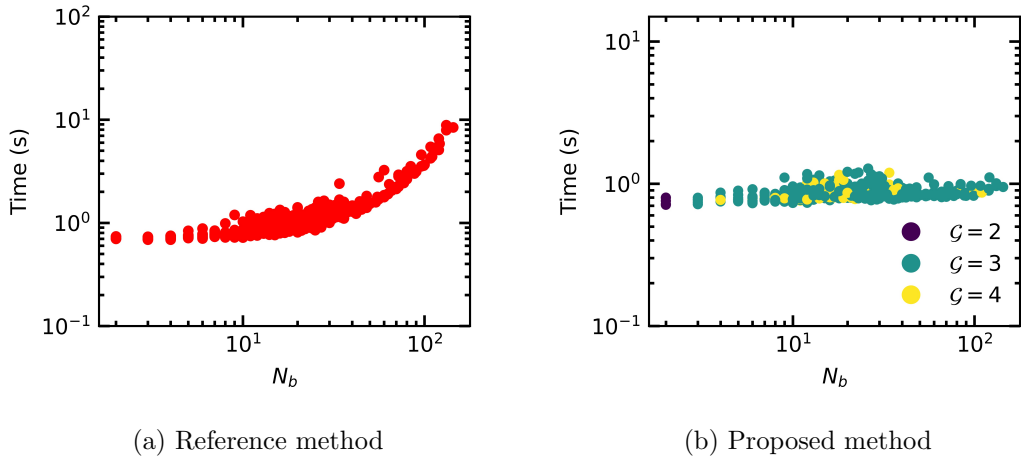


Figure 5.8 Calculation time for the evaluation of  $g$ -functions of regular borefields

### 5.4.3 Irregular borefield configurations

The proposed methodology is not limited to regular configurations such as those presented in the previous section but also to non-conventional configurations. The applicability of the method to irregular configurations is tested in this section by evaluating the  $g$ -functions of 100 randomly positioned boreholes in different borefield shapes. Two series of cases are presented: (i) four configurations with boreholes randomly positioned in a rectangular domain with different form factors (ii) four configurations with the same overall rectangular domain but with a geometric constraint in the center of it (e.g. a building). The scalability of the method to very large borefields is then tested in section 5.4.3.

#### Mean absolute percentage error

The accuracy of the proposed method is now evaluated by calculating  $g$ -functions of borefields of randomly positioned boreholes. 100 boreholes are randomly positioned in rectangular and hollow-rectangular domains as shown on figure 5.9. In all cases, the overall domain area is  $40,000 \text{ m}^2$  and the minimum spacing between boreholes is 7.5 m. Configurations A, B, C and D have varying shape factors  $L_y/L_x$  of 1, 2, 4 and 8, respectively. Configurations E, F, G and H have the same overall dimensions as configuration A but boreholes cannot be placed in a rectangular area at the center of the field (which could represent a building in practical cases). The physical dimensions of the borefield domains are presented in table 5.2.

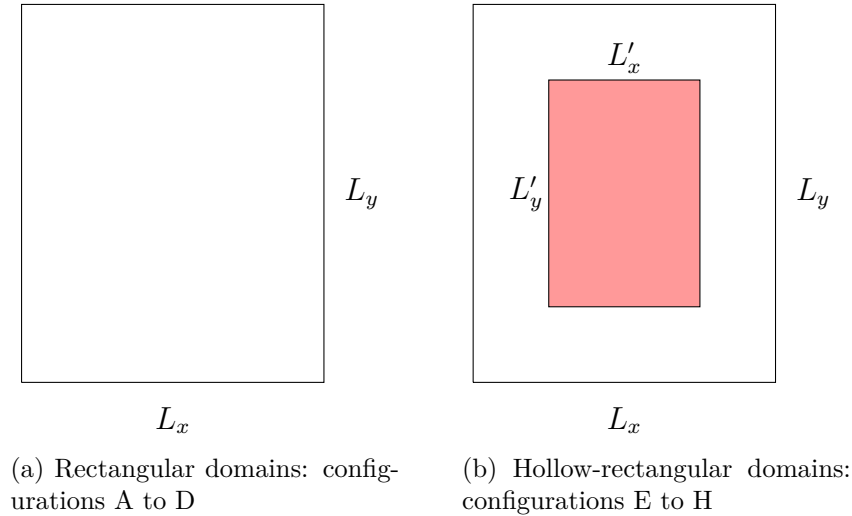


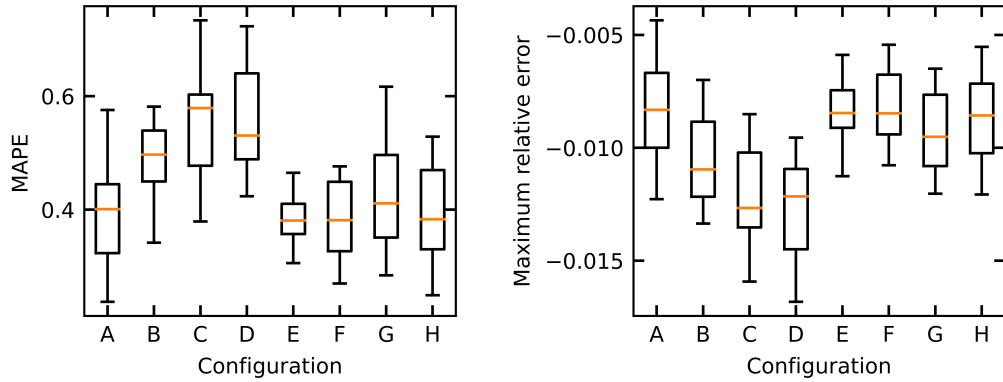
Figure 5.9 Shapes of the irregular borefield domains

Figure 5.10 shows the  $MAPE$  and maximum relative error for 20 random borefields in each of the 8 configurations. The number of groups identified from the clustering method varies

Table 5.2 Dimensions of the irregular borefield domains

Parameter	Configuration							
	A	B	C	D	E	F	G	H
$L_x$ [m]	200	141	100	71	200	200	200	200
$L_y$ [m]	200	238	400	566	200	200	200	200
$L'_x$ [m]	-	-	-	-	160	128	102	82
$L'_y$ [m]	-	-	-	-	160	128	102	82

from  $\mathcal{G} = 3$  and  $\mathcal{G} = 5$  depending on the positions of the boreholes in the randomly generated borefields. The proposed method maintains a *MAPE* below 0.72 % in all cases, and below 0.62% when considering the *MAPE* under the third quartile. The maximum relative error (in magnitude) is -0.0168 and found in configuration D at  $\ln(t/t_s) = 5$ . Again, the negative sign means the proposed method overpredicts the reference value. An overestimation of the  $g$ -function is consistent with results obtained when decreasing the axial discretization of boreholes, i.e. using fewer segments per borehole to evaluate the  $g$ -function [73]. As the number of segments decreases, the temperature at the borehole walls moves away from an equal and uniform temperature and the  $g$ -function is overpredicted. In the same way, when using fewer equivalent boreholes, the borehole wall temperatures of the boreholes (as opposed to the *equivalent* boreholes) move away from an equal and uniform value and the  $g$ -function should likewise be overpredicted.



(a)  $g$ -function *MAPE* on random field configurations (b)  $g$ -function maximum relative error on random field configurations

Figure 5.10 *MAPE* on the  $g$ -function and number of groups for the irregular borefields

Sample results for a borefield of 100 boreholes on a hollow-rectangular domain in configuration F are shown on Figure 5.11. The  $g$ -function, calculated using only 3 equivalent boreholes and shown on Figure 5.11b, is evaluated with a *MAPE* = 0.334 % and with a maximum rel-

ative error of -0.006 (at  $\ln(t/t_s) = 5$ ). The numbers of boreholes per group are 54, 33 and 13 (*I*, *II* and *III*), respectively. Despite the large number of boreholes and the irregular configuration, Figures 5.11c and 5.11d show that the heat extractions rates of equivalent boreholes are in good agreement with the average heat extraction rates calculated with the reference method. The maximum relative error on the heat extraction rate profiles at  $\ln(t/t_s) = 5$  is -0.002 for group *I*.

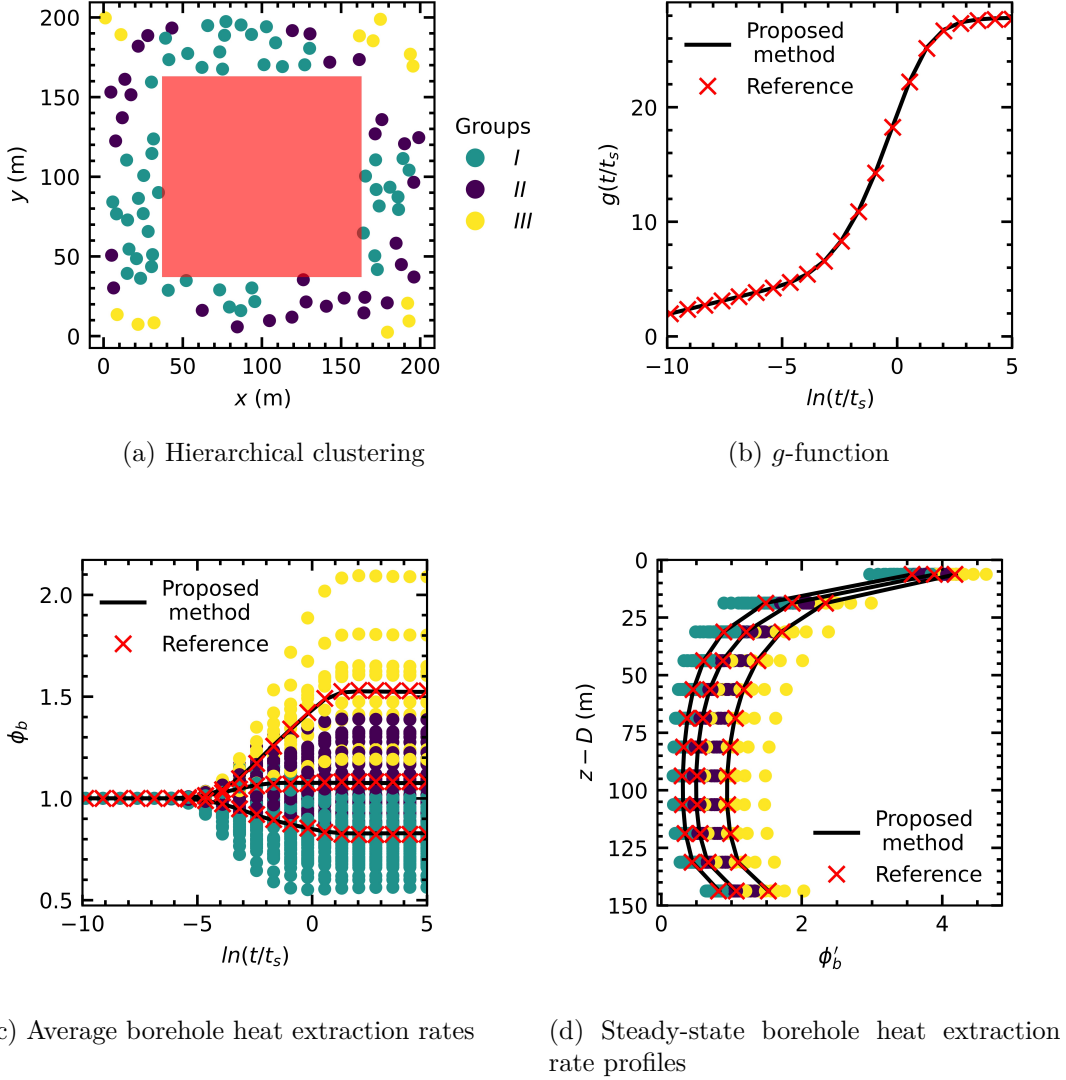


Figure 5.11 Sample results for configuration F

### Scalability of the proposed method

Figure 5.12 shows the  $g$ -function computation based on the proposed and reference methods for different random borefields with numbers of boreholes in increments of powers of 2,

starting from 8 up to 1024 in a limited region with dimensions  $L_x \times L_y = 500 \times 500 \text{ m}^2$ . Table 5.3 presents the *MAPE*, the maximum relative error and the calculation time for each of the cases. The results show good agreement with the reference method. In general, the maximum relative error is found at  $\ln(t/t_s) = 5$ . The calculation time was significantly reduced for large borefields. For instance, the calculation time of the reference method for 1024 boreholes is 5125 sec. For the calculation of the  $g$ -function of the field of 1024 boreholes, `pygfunction` had to be configured to use single precision (float32) instead of double precision (float64) so that the available memory was sufficient to do the computation.

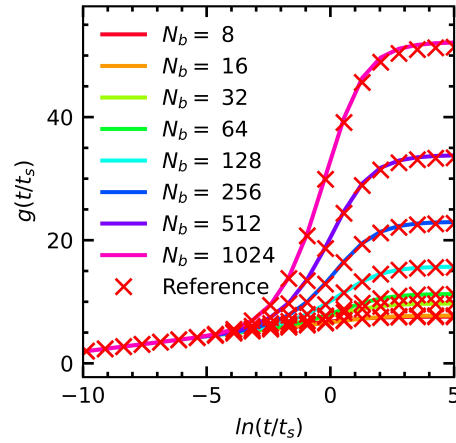


Figure 5.12  $g$ -function for different random borefield configurations

Table 5.3 Scalability of the proposed method

$N_b$	8	16	32	64	128	256	512	1024
<i>MAPE</i> (%)	0.002	0.007	0.092	0.115	0.224	0.405	0.540	0.690
Maximum relative error	$6.95 \times 10^{-5}$	$2.69 \times 10^{-4}$	-0.003	-0.003	-0.005	-0.009	-0.011	-0.015
Calculation time [s]	0.79	0.84	0.86	0.87	0.93	1.24	1.86	3.65

## 5.5 Conclusions

A new method is proposed to evaluate thermal interactions between geothermal boreholes. The finite line source (FLS) solution is extended to consider thermal interactions between groups of boreholes rather than between individual boreholes. It is shown that a small number of representative groups of boreholes, each modeled using a single equivalent borehole, can accurately represent the heat transfer process in a bore field. Hierarchical agglomerative clustering allows the identification of representative groups using a simplified heat transfer model, based on the steady-state finite line source (FLS) solution. A cut-off line is drawn on



the borefield dendrogram to estimate the minimum number of groups and incremented by a precision increment ( $\mathcal{K} = 1$ ).

The accuracy of the proposed method is assessed by calculating  $g$ -functions of geothermal borefields and comparing the results to the reference method [138] implemented in `pygfunction` [146]. A comparison of regular borefield configurations with up to 144 boreholes shows that the proposed method achieves a mean absolute percentage error ( $MAPE$ ) of less than 0.612 % using 4 or fewer equivalent boreholes. A marginal increase of the precision increment (i.e. from  $\mathcal{K} = 1$  to  $\mathcal{K} = 2$ ) is shown not to have a significant impact on the clustering method and the accuracy of the heat transfer model, however the error approaches 0 as the number of equivalent boreholes increases. The proposed method also presents important savings in calculation time : for a rectangular borefield of  $12 \times 12$  boreholes, the calculation time is decreased from 7.4 sec to 0.9 sec.

The proposed method maintains accuracy even when considering irregular borefield configurations. Comparisons of  $g$ -functions of borefields of 100 randomly positioned boreholes shows a third-quartile  $MAPE$  below 0.62% and a third-quartile maximum relative error below -0.015 in the worst configuration studied (configuration D). For a borefield of 1024 randomly positioned boreholes, the new method presents a  $MAPE$  of 0.69 %, a maximum relative error of -0.015 and a calculation time of 3.65 sec. In comparison, the reference method has a calculation time of 5125 sec. The method thereby demonstrates efficient scaling properties and makes it possible to model thermal interactions in very large borefields comprising hundreds of boreholes, which was previously impractical due to the large computational requirements.

Using suitable analytical solutions, the new method could also be extended to consider more complex borefield geometries (e.g. inclined boreholes [75]), groundwater flow [88, 95], or layered ground physical properties [74]. Fields of mixed series and parallel connections between boreholes [150] could be considered but require a new distance metric to substitute Equation (5.16) and extend the equivalent *borehole* concept to an equivalent *loop* (or *branch*) concept. The presented method is only applicable to parallel-connected boreholes but is not only limited to the calculation of  $g$ -functions using a uniform borehole wall temperature condition. The same clustering approach can be applied to the calculation of  $g$ -functions using an equal inlet fluid temperature boundary condition [77]. Most importantly, it has been shown that thermal interactions between geothermal boreholes can be represented using a small number of equivalent boreholes. This approach can thereby be applied to network-based methods [135–137] for parallel-connected boreholes and coupled to accurate short-term borehole models [60, 143] to obtain detailed axially discretized borefield models that are valid at all time scales.

## 5.6 Funding

This study is funded by the Natural Sciences and Engineering Research Council of Canada (NSERC) [grant number: RGPIN-2018-04471].

## CHAPTER 6    ARTICLE 3: SEMI-ANALYTICAL METHOD FOR 3D TRANSIENT HEAT TRANSFER IN THERMALLY INTERACTING FIELDS OF GROUND HEAT EXCHANGERS

**Authors:** Carlos Prieto and Massimo Cimmino

**Article published in the journal:** *Thermo*, Volume 2, Issue 3, pages 171-199

**Date of publication:** 8 July 2022

### 6.1 Abstract

The study of heat transfer in ground heat exchangers (GHEs) considering the fluid advection inside the pipes; the heat transfer between the fluid and the ground through the grout material; and the thermal interaction between GHEs is a challenging task. The present paper presents a new semi-analytical method that takes into account the aforementioned effects to consider both the short- to long-term effects of GHEs. The heat transfer between the fluid and grout was studied by a transient multipole expansion considering time-dependent fluid temperatures and an advection model for the pipes obtained from an energy balance on the heat carrier fluid. Thermal interactions were analyzed using an equivalent borehole method while penalizing the transient multipole expansion to include thermal interaction effects. Validation of the short-term predictions was performed by comparing the proposed model to experimental data found in the literature and to an FEA model. The proposed model was then compared with a FEA model in long-term simulations of a geothermal field comprised of 24 GHEs for multi-annual simulation. The method resulted in substantial reduction in computational time while preserving good accuracy when compared with the FEA model.

### 6.2 Introduction

One of the renewable energy sources that has been growing steadily worldwide in the last decade is geothermal energy [151]. Ground coupled heat pump (GCHP) systems are among the most efficient geothermal systems used for heating and cooling buildings [152]. GCHP systems consist of one (or several) heat pump that supplies heating or cooling to a building through the ground via ground heat exchangers (GHEs). GHEs are a core part of the GCHP system and consist of boreholes containing one or several U-tubes through which a heat-carrier fluid flows, and it is backfilled with grout material. In each of the GCHP design, control and operation phases, it is necessary to understand the heat transfer process between

not only one but several GHEs. For instance, meeting the energy demands of a building requires that the GHEs are adequately sized so that returning fluid temperatures remain within the operating bounds of the GCHP system. Fluid temperature variations can be predicted from a model of the heat transfer between the fluid and the soil given ground thermal loads, accounting for possible thermal interactions between GHEs located in close proximity. Thus, improvements in the accuracy of heat transfer models lead to improvements in the accuracy of the design of GHEs.

Heat transfer phenomena are studied on different time scales, from short-term to long-term effects. Short-term effects are due to the flow of the fluid inside the U-tube coupled with the heat conduction between the pipes and the grout. At this time scale that ranges from minutes to a few hours, the thermal capacity of the grout decreases the rate of heat propagation between the fluid and the soil, and not taking this phenomenon into account can lead to an overestimation of the fluid temperatures [11]. The short-term effects end when quasi-steady conditions are reached inside the GHE, i.e., when temperature gradients are constant under a constant ground load. Long-term effects, spanning days to hundreds of years, include thermal interactions between boreholes and axial heat transfer effects due to interaction with the surface and the ground below the GHEs. It is necessary to consider both the short- and long-term effects to properly design a field of GHEs and ensure proper operation of a GCHP system throughout its life cycle [142].

Long-term heat transfer outside GHEs is studied both analytically and numerically. The well-known classical analytical solutions correspond to the infinite line source (ILS) [62] and the cylindrical heat source (CHS) [20]. Analytical solutions can be superimposed in time and space to consider variable ground loads and thermal interactions between GHEs. An important limitation of these classical solutions is that they cannot represent axial effects. Eskilson [67] solved the radial and axial heat transfer problem using a finite difference method. GHEs were represented as hollow cylinders with uniform and equal—but time-varying—temperatures. The model was used to produce dimensionless unit-step response functions, called  $g$ -functions, that give the relation between the borehole wall temperature and the heat extraction rates. Like analytical solutions,  $g$ -functions can be superimposed on time to consider variable ground loads. The  $g$ -function is defined by:

$$T_b(t) = T^0 - \frac{Q}{2\pi k_s L N_b} g(t) \quad (6.1)$$

where  $T_b$  is the borehole wall temperature,  $T^0$  is the undisturbed ground temperature,  $k_s$  is the thermal conductivity,  $Q$  is the total heat extraction rate into the borefield,  $L$  is the borehole length and  $N_b$  is the number of boreholes.

Eskilson [67] proposed the analytical finite line source (FLS) to estimate the  $g$ -function of a single borehole. The FLS was later superimposed on space to evaluate  $g$ -functions of fields of GHEs [18,68,69]. For larger fields, the FLS can lead to important errors in the  $g$ -functions due to a mismatch of the boundary conditions at the borehole wall between the FLS (uniform and equal heat extraction rates) and the  $g$ -functions (uniform and equal temperatures). These errors can be eliminated by discretizing the GHEs to consider the variation in heat extraction rates along the lengths of GHEs and their variations in time to reproduce the uniform temperature condition of Eskilson [72,73]. In reality, neither the heat extraction rates nor the borehole wall temperatures are uniform along the lengths of the boreholes, since heat transfer is driven by the temperature difference between the fluid and the borehole wall. A more proper boundary condition is that of an imposed inlet fluid temperature, considering the internal thermal resistances of the boreholes and the piping connections between them [25,77,150]. The  $g$ -functions—and thus the returning fluid temperatures—are dependent on the borehole thermal resistances and the fluid mass flow rate. Spatial and temporal superposition of the FLS solution are also used for network-based models that study, at every time step, the complete distribution of the borehole wall temperatures considering the hydraulic connections between GHEs [135–137]. The computational requirements of analytical models increase as the complexity of the boundary condition increases. In the case of the imposed inlet fluid temperature, a system of equations must be built and solved to evaluate heat extraction rate profiles and borehole wall temperature profiles along all GHEs in the field. Prieto and Cimmino [153] proposed a method to limit the sizes of the systems of equations by forming groups of similarly behaving boreholes and modeling each of these groups using a single equivalent borehole. This results in an efficient and robust method that allows the study of geothermal fields composed of thousands of GHEs.

Knowing that internal configurations have a direct impact on the thermal interactions among boreholes and the long-term responses of GHEs, some researchers have coupled short-term models with long-term models to conduct simulations. Yavuzturk and Spitler [52] were the first to introduce an extension of the  $g$ -function considering short time steps while including thermal capacity inside the GHE but disregarding the thermal capacity in the fluid. Later, Xu and Spitler [29], based on the work from Yavuzturk and Spitler [52], developed a one-dimensional model using a finite volume method, where the fluid is considered as an annular volume within the pipe, along with an equivalent thermal capacity. Brussieux and Bernier [38] coupled a finite volume method for the interior of a GHE with the CHS solution for the exterior of a GHE, resulting in the definition of  $g^*$ -functions for short-term effects. Claesson and Javed [18] coupled an equivalent geometry model for the interior of the GHE [33] and used the FLS solution to study thermal interactions between the GHEs. Li et al. [145] used the

analytical infinite composite-medium line source (ICMLS) [53] to model the insides of GHEs and the  $g$ -functions to account for thermal interactions among GHEs. In all aforementioned cases, despite the coupling of the short- to long-term solutions, the methods do not consider the advection inside the pipes and consider that all the GHEs have the same borehole wall temperature, which is not the case, as demonstrated by Cimmino [77] and Monzó et al. [85]. Pasquier and Marcotte [46] developed a response model based on a thermal resistance and capacitances (TRC) method to generate the thermal response factor of a GHE and estimate the fluid temperatures. Laferrière et al. [144] considered the axially-discretized thermal resistances and capacitances (TRC) model of Bauer et al. [43] coupled to an advection model and to  $g$ -functions, using a single uniform temperature at the wall of a GHE that represents the entire bore field. Recently, Alaie et al. [154] developed a solution based on the TRC method proposed by Minaei and Maerefat [47] and the segment-to-segment response factors proposed by Cimmino and Bernier [73] to consider both short- to long-term responses. As opposed to the earlier methods, their method does not consider that borehole wall temperatures are the same for all GHEs and thus achieves better representations of the distribution of heat extraction rates and temperatures within the field of GHEs. Additionally, there exist mesh-dependent approaches, such as those of Al-Khoury and Bonnier [91] and Diersch et al. [83,84], which are able to impose many boundary conditions and use many arrangements of GHEs; however, these methods are computationally demanding when considering multiple boreholes and including short- to long-term effects.

Axially-discretized methods become computationally demanding when very large fields of GHEs are considered. Thus, there is a need for accurate and computationally-efficient models that consider short-term effects, including advection in the pipes, and are able to simulate not only a single GHE but thousands. Coupled short- and long-term models can also benefit from recent advancements in short-term models, such as the transient multipole methods. Rivero and Hermanns [60] proposed a solution by means of matched asymptotic expansion to evaluate the thermal resistances in a spectral domain. Prieto and Cimmino [143] developed a transient multipole expansion to describe the variations in fluid, pipe and borehole wall temperatures in the time domain. In both approaches, the fluid thermal capacity and the advection of the fluid through the pipes are not taken into account.

This paper introduces a new methodology to study the transient heat transfer for both the interiors and exteriors of GHEs, considering fluid flow inside the pipes, fluid-to-soil heat conduction via grout, thermal interactions among GHEs and axial effects. The equivalent borehole method of Prieto and Cimmino [153] is used to model the exteriors of the GHEs, including thermal interactions between GHEs. The transient multipole method of Prieto and Cimmino [143] is used to model the interiors of the GHEs, including temperature penalization

to account for thermal interactions. A finite difference model of fluid advection inside the pipes is used to consider the axial distributions of fluid temperatures and heat extraction rates. The model was first compared against the sandbox test of Beier et al. [155] to validate the accuracy of the short-term response, and then against a multi-annual simulation of a thermally interacting field of 24 boreholes using a finite element analysis (FEA) solver based on Diersch et al. [83, 84] to show that the method is able to include both short-term effects and thermal interactions between boreholes for larger periods of time.

### 6.3 Mathematical model

Figure 6.1 shows a borefield composed of  $N_b = 2$  vertical GHEs,  $i$  and  $j$ , of the same dimensions and separated by a horizontal distance  $r_{ij}$ . All GHEs are connected in parallel and are fed a heat carrier fluid at the same inlet temperature and mass flow rate. Each GHE is composed of a single U-tube (although the presented model can be extended to any U-tube configuration). The geometrical parameters are the same for each GHE and include: the borehole length  $L$ , the buried depth  $D$ , the borehole radius  $r_b$ , the pipe outer radius  $r_p$  with wall thickness  $t_h$  and the U-tube shank spacing  $e$ . The thermal properties are considered homogeneous, isotropic and constant.  $k_b$  and  $k_s$  are the thermal conductivities ( $k$ ) of the grout ( $b$ ) and soil ( $s$ ), respectively.  $\alpha_b$  and  $\alpha_s$  are the thermal diffusivities ( $\alpha$ ) of the grout and soil, respectively.

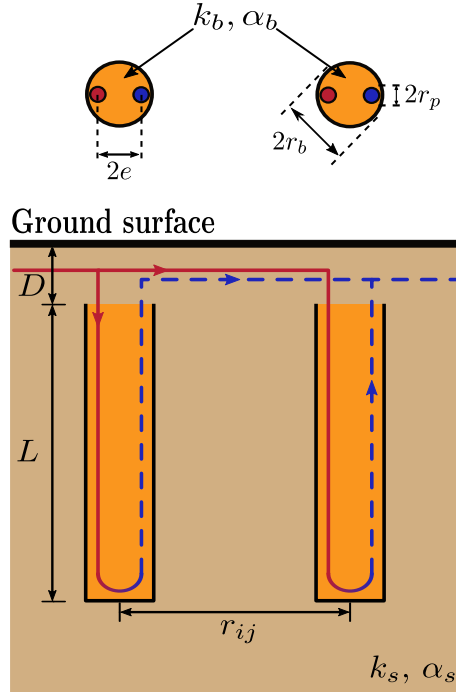


Figure 6.1 Field of 2 vertical boreholes of equal dimensions.

The horizontal conduction heat transfer inside the GHE is studied in a transient state using the transient multipole expansion method developed by Prieto and Cimmino [143]. This solution is extended to consider time-dependent fluid temperatures inside the U-tube by means of a coefficient updating scheme. The radial and axial heat conduction in the soil around GHEs, and the interactions between GHEs, are modeled with the FLS solution by considering thermal interactions between equivalent boreholes as proposed by Prieto and Cimmino [153]. The transient multipole method is coupled to the FLS solution to consider both of the short- and long-term effects around GHEs, and to a discretized finite difference model of the advection heat transfer process inside the U-tubes. The proposed model was compared to a finite element analysis (FEA) model, based on the methodology developed by Diersch et al. [83, 84], with specific modifications to ensure solution stability, as will be discussed in Section 6.3.4.

### 6.3.1 2D transient heat transfer with time-dependent fluid temperatures

#### Transient multipole expansion

The short-term transient heat transfer problem in the local vicinity of a GHE  $j$  is modeled in 2D for a horizontal cross-section of the GHE, considering conduction in the grout ( $\Omega_b$ ) and the soil ( $\Omega_s$ ). The heat transfer problem relies on the transformation of coordinates based on geometrical characteristics of the GHE; thus, a point  $\mathbf{x} = (\rho, \phi)$  in the 2D-polar space could be expressed at any center  $O_k$  with translated coordinates  $\mathbf{x}_k = (\rho_k, \phi_k)$ , as shown in Figure 6.2. The combination of the convection from the fluid to the pipe inner surfaces and the conduction across the pipes is represented as Robin boundary conditions at the pipe outer surfaces  $\partial\Omega_k$  (at a radius  $\rho_k = r_k$  from a pipe axis). The thermal capacitance of the pipes is neglected.



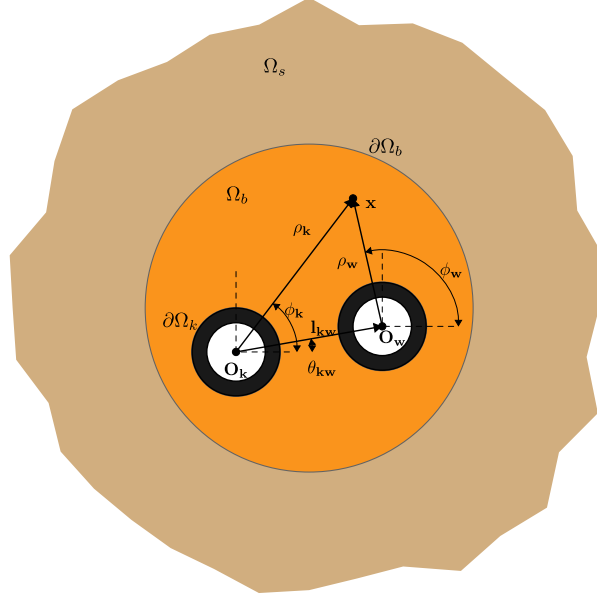


Figure 6.2 Computational domain of a GHE.

The temperature at a far-field boundary  $\partial\Omega_e$  (at  $r_e \rightarrow \infty$ ) is considered constant and equal to the undisturbed ground temperature  $T^0$ . For constant fluid temperatures  $T_{f_{k,j}}$  inside  $N$  arbitrary positioned pipes and a uniform initial temperature  $T^0$  in the grout and soil (i.e., in  $\Omega_b \cup \Omega_s$ ), the transient heat transfer problem in radial coordinates  $(\rho, \phi)$  is given by:

$$\frac{1}{\alpha_d} \frac{\partial T_{d,j}}{\partial t} = \nabla^2 T_{d,j} \text{ in } \Omega_b \cup \Omega_s \quad (6.2a)$$

$$-\beta_k T_k \frac{\partial T_{1,j}}{\partial \rho_k} \Big|_{r_k} + T_{1,j} = T_{f_{k,j}} \text{ on } \partial\Omega_k, \quad k = 1, \dots, N \quad (6.2b)$$

$$-k_b \frac{\partial T_{1,j}}{\partial \rho_0} \Big|_{r_b} = -k_s \frac{\partial T_{2,j}}{\partial \rho_0} \Big|_{r_b} \text{ on } \partial\Omega_b \quad (6.2c)$$

$$T_{1,j}|_{r_b} = T_{2,j}|_{r_b} \text{ on } \partial\Omega_b \quad (6.2d)$$

$$T_{2,j}(r_e, \phi, t)|_{r_e \rightarrow \infty} = T^0 \text{ on } \partial\Omega_e \quad (6.2e)$$

$$T_{d,j}(\rho, \phi, 0) = T^0 \text{ in } \Omega_b \cup \Omega_s \quad (6.2f)$$

where  $\alpha_d$  is equal to the thermal diffusivity in the grout or soil ( $\alpha_b$  and  $\alpha_s$ ) for indices  $d = 1, 2$ , respectively;  $\beta_k = 2\pi k_b R_k$  is the dimensionless fluid to outer pipe wall thermal resistance of pipe  $k$ ; and  $R_k$  is the fluid to outer pipe wall thermal resistance.  $T_{f_{k,j}}$  is the fluid temperature at pipe  $k$  in a GHE  $j$ .

Following the method of Prieto and Cimmino [143], the transient heat transfer problem with non-homogeneous boundary conditions for  $T_{d,j}$  is separated into two sub-problems:

a transient heat transfer problem with homogeneous boundary conditions for  $T_{d_h,j}$ , and a steady-state heat transfer problem with non-homogeneous conditions for  $T_{d_{ss},j}$ . The complete solution is then given by superposition, with  $T_{d,j} = T_{d_h,j} + T_{d_{ss},j}$ .

The homogeneous transient heat transfer problem is then:

$$\frac{1}{\alpha_d} \frac{\partial T_{d_h,j}}{\partial t} = \nabla^2 T_{d_h,j} \text{ in } \Omega_b \cup \Omega_s \quad (6.3a)$$

$$-\beta_k r_k \frac{\partial T_{1_h,j}}{\partial \rho_k} \bigg|_{r_k} + T_{1_h,j} = 0 \text{ on } \partial\Omega_k, \quad k = 1, \dots, N \quad (6.3b)$$

$$-k_b \frac{\partial T_{1_h,j}}{\partial \rho_0} \bigg|_{r_b} = -k_s \frac{\partial T_{2_h,j}}{\partial \rho_0} \bigg|_{r_b} \text{ on } \partial\Omega_b \quad (6.3c)$$

$$T_{1_h,j}|_{r_b} = T_{2_h,j}|_{r_b} \text{ on } \partial\Omega_b \quad (6.3d)$$

$$T_{2_h,j}(r_e, \phi, t)|_{r_e \rightarrow \infty} = 0 \text{ on } \partial\Omega_e \quad (6.3e)$$

$$T_{d_h,j}(\rho, \phi, 0) = T^0 - T_{d_{ss},j} \text{ in } \Omega_b \cup \Omega_s \quad (6.3f)$$

The non-homogeneous steady-state heat transfer problem is given by:

$$\nabla^2 T_{d_{ss},j} = 0 \text{ in } \Omega_b \cup \Omega_s \quad (6.4a)$$

$$-\beta_k r_k \frac{\partial T_{1_{ss},j}}{\partial \rho_k} \bigg|_{r_k} + T_{1_{ss},j} = T_{f_k,j} \text{ on } \partial\Omega_k, \quad k = 1, \dots, N \quad (6.4b)$$

$$-k_b \frac{\partial T_{1_{ss},j}}{\partial \rho_0} \bigg|_{r_b} = -k_s \frac{\partial T_{2_{ss},j}}{\partial \rho_0} \bigg|_{r_b} \text{ on } \partial\Omega_b \quad (6.4c)$$

$$T_{1_{ss},j}|_{r_b} = T_{2_{ss},j}|_{r_b} \text{ on } \partial\Omega_b \quad (6.4d)$$

$$T_{2_{ss},j}(r_e, \phi)|_{r_e \rightarrow \infty} = T^0 \text{ on } \partial\Omega_e \quad (6.4e)$$

The solution to the homogeneous transient heat transfer problem is obtained by means of separation of variables and expressed as a Fourier–Bessel expansion:

$$T_{d_h,j}(\mathbf{x}, t) = \sum_{w=1}^{\infty} C_{w,j} X_{d,j}(\mathbf{x}; \lambda_{d,j}^w) e^{-(\lambda_{d,j}^w)^2 \alpha_d t} \quad (6.5)$$

where  $\lambda_{d,j}^w$  is the  $w$ -eigenvalue associated with the separation of variables sub-problem for each domain  $d$  satisfying the continuity condition  $\lambda_{2,j} = \lambda_{1,j} \sqrt{\alpha_b/\alpha_s}$  for a GHE  $j$ .  $X_{d,j}(\mathbf{x}; \lambda_{d,j}^w)$  are the quasi-orthogonal eigenfunctions related to the eigenvalue  $\lambda_{d,j}^w$  for each domain  $d$  in GHE  $j$ .

For the grout domain ( $d = 1$ ), containing  $N$  arbitrarily positioned pipes, the quasi-orthogonal

eigenfunction is expressed as follows:

$$X_{1,j}(\mathbf{x}; \lambda_{1,j}^w) = \sum_{l=-M}^M \gamma_{l,j}^0 J_l(\lambda_{1,j}^w \rho_0) e^{il\phi_0} + \sum_{k=1}^N \sum_{l=-M}^M \gamma_{l,j}^k H_l^{(1)}(\lambda_{1,j}^w \rho_k) e^{il\phi_k} \quad (6.6)$$

and for the soil domain ( $d = 2$ ):

$$X_{2,j}(\mathbf{x}; \lambda_{2,j}^w) = \sum_{l=-M}^M \delta_{l,j}^0 H_l^{(1)}(\lambda_{2,j}^w \rho_0) e^{im\phi_0} \quad (6.7)$$

where  $J$  and  $H^{(1)}$  are Bessel and Hankel functions of the first kind;  $M$  is the number of terms of the multipole expansion; and  $\gamma_{l,j}^0$ ,  $\gamma_{l,j}^k$  and  $\delta_{l,j}^0$  are coefficients introduced to match the boundary conditions in Equations (6.3b)–(6.3e).  $C_{m,j}$  are the Fourier–Bessel coefficients satisfying the initial condition (Equation (6.3f)) and are given by:

$$C_{m,j} = \frac{\frac{k_b}{\alpha_b} \int_{\Omega_b} (T^0 - T_{1ss,j}) \bar{X}_1 d\Omega + \frac{k_s}{\alpha_s} \int_{\Omega_s} (T^0 - T_{2ss,j}) \bar{X}_2 d\Omega}{\frac{k_b}{\alpha_b} \int_{\Omega_b} X_{1,j} \bar{X}_{1,j} d\Omega + \frac{k_s}{\alpha_s} \int_{\Omega_s} X_{2,j} \bar{X}_{2,j} d\Omega} \quad (6.8)$$

The solution to the non-homogeneous steady-state heat transfer problem defined in Equations (6.4) is treated as a multipole expansion for a T-complete basis. For the grout domain ( $d = 1$ ), containing  $N$  arbitrarily positioned pipes, the solution is expressed as follows:

$$\begin{aligned} T_{1ss,j}(\mathbf{x}) = & \alpha_{0,j} + \sum_{m=1}^h \left[ \alpha_{m,j} \left( \frac{\rho_0}{r_{max}} \right)^m \cos(m\phi_0) + \beta_{m,j} \left( \frac{\rho_0}{r_{max}} \right)^m \sin(m\phi_0) \right] \\ & + \sum_{l=1}^N \left\{ \gamma_{0,j}^l \ln \rho_l + \sum_{m=1}^h \left[ \gamma_{m,j}^l \left( \frac{\rho_l}{r_{min}} \right)^{-m} \cos(m\phi_l) + \delta_{m,j}^l \left( \frac{\rho_l}{r_{min}} \right)^{-m} \sin(m\phi_l) \right] \right\} \end{aligned} \quad (6.9)$$

and for the soil domain ( $d = 2$ ):

$$\begin{aligned} T_{2ss,j}(\mathbf{x}) = & \alpha'_{0,j} + \sum_{m=1}^h \left[ \alpha'_{m,j} \left( \frac{\rho_0}{r_e} \right)^m \cos(m\phi_0) + \beta'_{m,j} \left( \frac{\rho_0}{r_e} \right)^m \sin(m\phi_0) \right] \\ & + \gamma'_{0,j} \ln \rho_0 + \sum_{m=1}^h \left[ \gamma'_{m,j} \left( \frac{\rho_0}{r_{min}} \right)^{-m} \cos(m\phi_0) + \delta'_{m,j} \left( \frac{\rho_0}{r_{min}} \right)^{-m} \sin(m\phi_0) \right] \end{aligned} \quad (6.10)$$

where  $r_{min} = \min_{i \in \{1, \dots, N\}} r_i$  is the minimum external radius of the pipes;  $r_{max} \geq r_b$  is an arbitrary radius and is equal to  $r_b$ ; and  $h$  is the number of terms in the complete expansion. Similarly to multipole expansion for the quasi-orthogonal eigenfunctions, terms  $\alpha_{m,j}$ ,  $\beta_{m,j}$ ,  $\gamma_{m,j}^l$ ,  $\gamma'_{m,j}$ ,  $\delta_{m,j}^l$  and  $\delta'_{m,j}$  are determined by matching the boundary conditions in Equations (6.4b)–(6.4e).

According to Prieto and Cimmino [143], the values of  $\alpha_{0,j} = T^0$  and  $\gamma'_{0,j}$ ,  $\alpha'_{m,j}$  and  $\beta_{m,j}$  are set to 0. Here, the authors note that, for the present method, keeping all terms expressed in Equation (6.10) stabilizes the integration in Equation (6.8), where terms  $\gamma'_{0,j}$  and  $\alpha'_{m,j}$ ,  $\beta_{m,j}$  are small when matching the far-field boundary with  $r_e = 100$  m. For more details concerning the evaluation of eigenvalues and coefficients to match the boundary conditions in both problems, readers are referred to Prieto and Cimmino [143].

### Time-dependent fluid temperatures

Prieto and Cimmino [143] introduced a coefficient updating scheme to consider the variations in fluid temperatures as step-wise variations at each time step  $n$  for every  $t^{(n-1)} < t \leq t^n$  (where  $t^n = t^{(n-1)} + \Delta t$ ). The initial temperatures in Equations (6.3f) and (6.8) are replaced by the temperature at the end of the latest time step as follows:

$$T_{1,j}^{(n-1)}(\mathbf{x}) = \sum_{w=1}^{\infty} C_{w,j}^{(n-1)} X_{1,j}(\mathbf{x}; \lambda_{1,j}^w) e^{-(\lambda_{1,j}^w)^2 \alpha_b \Delta t} + T_{1ss,j}^{(n-1)} \quad (6.11a)$$

$$T_{2,j}^{(n-1)}(\mathbf{x}) = \sum_{w=1}^{\infty} C_{w,j}^{(n-1)} X_{2,j}(\mathbf{x}; \lambda_{2,j}^w) e^{-(\lambda_{2,j}^w)^2 \alpha_s \Delta t} + T_{2ss,j}^{(n-1)} \quad (6.11b)$$

Therefore, the Fourier–Bessel coefficients are calculated using this scheme at each time step:

$$C_{m,j}^n = \frac{\frac{k_b}{\alpha_b} I_{1m,j}^{(n-1)} + \frac{k_s}{\alpha_s} I_{2m,j}^{(n-1)}}{\frac{k_b}{\alpha_b} \int_{\Omega_b} X_{1,j} \bar{X}_{1,j} d\Omega + \frac{k_s}{\alpha_s} \int_{\Omega_s} X_{2,j} \bar{X}_{2,j} d\Omega} \quad (6.12)$$

with

$$\begin{aligned} I_{1m,j}^{(n-1)} &= \int_{\Omega_b} (T_{1,j}^{(n-1)} - T_{1ss,j}^n) \bar{X}_{1,j}(\mathbf{x}; \lambda_{1,j}^m) d\Omega \\ &= \int_{\Omega_b} (C_{m,j}^{(n-1)} X_{1,j}(\mathbf{x}; \lambda_{1,j}^m) e^{-(\lambda_{1,j}^m)^2 \alpha_b \Delta t} + T_{1ss,j}^{(n-1)} - T_{1ss,j}^n) \bar{X}_{1,j}(\mathbf{x}; \lambda_{1,j}^m) d\Omega \\ I_{2m,j}^{(n-1)} &= \int_{\Omega_s} (T_{2,j}^{(n-1)} - T_{2ss,j}^n) \bar{X}_{2,j}(\mathbf{x}; \lambda_{2,j}^m) d\Omega \\ &= \int_{\Omega_s} (C_{m,j}^{(n-1)} X_{2,j}(\mathbf{x}; \lambda_{2,j}^m) e^{-(\lambda_{2,j}^m)^2 \alpha_s \Delta t} + T_{2ss,j}^{(n-1)} - T_{2ss,j}^n) \bar{X}_{2,j}(\mathbf{x}; \lambda_{2,j}^m) d\Omega \end{aligned} \quad (6.13)$$

where  $T_{dss,j}^n$  is the solution of the steady-state problem considering the fluid temperatures at the  $n$ -th time step, and  $T_1^0 = T_2^0 = T^0$  in a GHE  $j$ . Note that when Equations (6.11) are substituted into Equation (6.8), the sums in Equations (6.11) disappear, since the integrals with terms  $X_{d,j}(\mathbf{x}; \lambda_{d,j}^w) \bar{X}_{d,j}(\mathbf{x}; \lambda_{d,j}^m)$  are 0 if  $w \neq m$  due to the quasi-orthogonal condition in the whole domain  $\Omega_b \cup \Omega_s$ .

As written, Equation (6.12) is computationally intensive, since at every time step the integrals expressed in Equation (4.31) must be calculated. However, using the linearity in the steady-state problem described by Equation (6.4), it is possible to decompose the temperature field as a weighted sum of the fluid temperatures at each pipe. The temperature field can be expressed as  $N$  subproblems, and subtracting  $T^0$  from the global problem yields:

$$T_{d_{ss},j}^n = T^0 + \sum_{l=1}^N \psi_{dl,j} (T_{fl,j}^n - T^0) \quad (6.14)$$

where  $\psi_{dl,j}$  are the weighting functions in the domain  $d$  for a subproblem  $l$  in a GHE  $j$ :

$$\nabla^2 \psi_{dl,j} = 0 \text{ in } \Omega_b \cup \Omega_s \quad (6.15a)$$

$$-\beta_k r_k \left. \frac{\partial \psi_{1l,j}}{\partial \rho_k} \right|_{r_k} + \psi_{1l,j} = \delta_k^l \text{ on } \partial \Omega_k, \quad k = 1, \dots, N \quad (6.15b)$$

$$-k_b \left. \frac{\partial \psi_{1l,j}}{\partial \rho_0} \right|_{r_b} = -k_s \left. \frac{\partial \psi_{2l,j}}{\partial \rho_0} \right|_{r_b} \text{ on } \partial \Omega_b \quad (6.15c)$$

$$\psi_{1l,j}|_{r_b} = \psi_{2l,j}|_{r_b} \text{ on } \partial \Omega_b \quad (6.15d)$$

$$\psi_{2l,j}(r_e, \phi)|_{r_e \rightarrow \infty} = 0 \text{ on } \partial \Omega_e \quad (6.15e)$$

where  $\delta_k^l$  is the Kronecker delta function which takes the value 1 if  $l = k$  and 0 otherwise. Equations (6.14) and (6.15) constitute a decomposition on  $N$  subproblems representing a unitary pulse at each pipe for each  $\psi_{dl,j}$ ; therefore,  $\psi_{dl,j}$  is time independent. Solving  $\psi_{dl,j}$  follows the same multipole expansion structure shown in Section 6.3.1.

Substituting Equation (6.14) into Equations (4.31) yields:

$$\begin{aligned} I_{1m,j}^{(n-1)} &= C_{m,j}^{(n-1)} e^{-(\lambda_{1,j}^m)^2 \alpha_b \Delta t} \int_{\Omega_b} X_{1,j}(\mathbf{x}; \lambda_{1,j}^m) \bar{X}_{1,j}(\mathbf{x}; \lambda_{1,j}^m) d\Omega + \\ &\quad \sum_{l=1}^N (T_{fl,j}^{(n-1)} - T_{fl,j}^m) \int_{\Omega_b} \psi_{1l,j} \bar{X}_{1,j}(\mathbf{x}; \lambda_{1,j}^m) d\Omega \\ I_{2m,j}^{(n-1)} &= C_{m,j}^{(n-1)} e^{-(\lambda_{2,j}^m)^2 \alpha_s \Delta t} \int_{\Omega_s} X_{2,j}(\mathbf{x}; \lambda_{2,j}^m) \bar{X}_{2,j}(\mathbf{x}; \lambda_{2,j}^m) d\Omega + \\ &\quad \sum_{l=1}^N (T_{fl,j}^{(n-1)} - T_{fl,j}^m) \int_{\Omega_s} \psi_{2l,j} \bar{X}_{2,j}(\mathbf{x}; \lambda_{2,j}^m) d\Omega \end{aligned} \quad (6.16)$$

Substituting Equations (6.16) into Equation (6.12), rearranging and simplifying terms result in:

$$C_{m,j}^n = C_{m,j}^{(n-1)} e^{-(\lambda_{1,j}^m)^2 \alpha_b \Delta t} + \sum_{l=1}^N (T_{fl,j}^{(n-1)} - T_{fl,j}^m) E_{ml,j} \quad (6.17)$$

with

$$E_{ml,j} = \frac{\frac{k_b}{\alpha_b} \int_{\Omega_b} \psi_{1l,j} \bar{X}_{1,j}(\mathbf{x}; \lambda_{1,j}^m) d\Omega + \frac{k_s}{\alpha_s} \int_{\Omega_s} \psi_{2l,j} \bar{X}_{2,j}(\mathbf{x}; \lambda_{2,j}^m) d\Omega}{\frac{k_b}{\alpha_b} \int_{\Omega_b} X_{1,j}(\mathbf{x}; \lambda_{1,j}^m) \bar{X}_{1,j}(\mathbf{x}; \lambda_{1,j}^m) d\Omega + \frac{k_s}{\alpha_s} \int_{\Omega_s} X_{2,j}(\mathbf{x}; \lambda_{2,j}^m) \bar{X}_{2,j}(\mathbf{x}; \lambda_{2,j}^m) d\Omega} \quad (6.18)$$

The terms  $E_{ml,j}$  are independent of the fluid temperatures and thereby only need to be evaluated once at the initialization of a simulation.

### 6.3.2 Thermal interactions between ground heat exchangers

A temperature penalization approach is proposed to extend the transient multipole model to 3D, including axial heat transfer and thermal interactions between boreholes. Following the method of Cimmino and Bernier [73], each GHE is divided into  $n_s$  segments (totaling  $(n_s + 1)$  layers), and each segment is modeled as a line heat source with a uniform heat extraction rate positioned at the axis of the GHE segment. Figure 6.3 shows a uniform discretization for two boreholes  $i$  and  $j$  separated with a distance  $r_{ij}$ . Each segment  $u$  has a length  $L_u = L/n_s$ . The finite line source (FLS) solution can then be superimposed to evaluate a penalty on the temperatures predicted by the transient multipole method. Additionally, the equivalent borehole method of Prieto and Cimmino [153] is used to simplify the thermal interaction problem and obtain a computationally-efficient simulation model of the bore field by only requiring the simulation of a limited number  $\mathcal{G}$  of equivalent boreholes instead of the entire field of  $N_b$  boreholes.

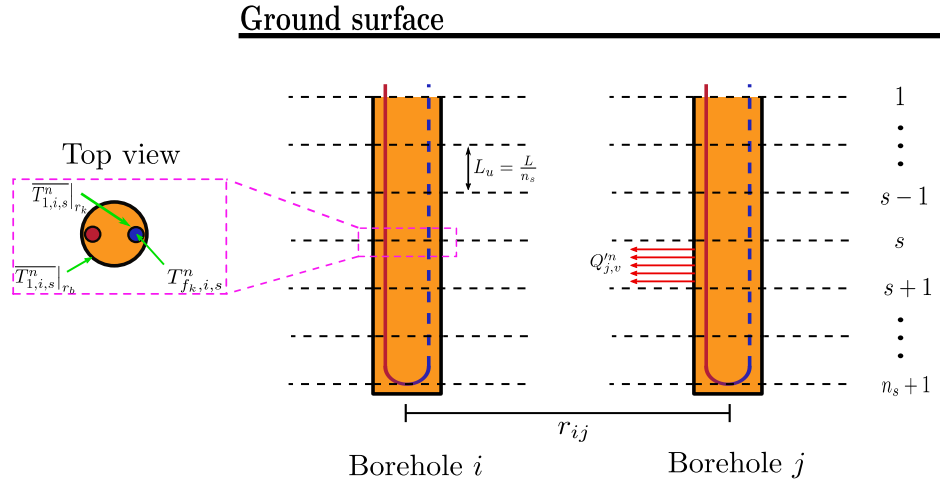


Figure 6.3  $(n_s)$  segments discretization of boreholes  $i$  and  $j$ .

### Spatial and temporal superposition of the finite line source solution

The temperature drop at the borehole wall of a segment  $u$  of a borehole  $i$  at time  $t^n$  can be evaluated from the spatial and temporal superposition of the analytical FLS solution:

$$\Delta T_{b,i,u}^n = T^0 - T_{b,i,u}^n = \frac{1}{2\pi k_s} \sum_{j=1}^{N_b} \sum_{v=1}^{n_s} \sum_{p=1}^n Q_{j,v}^p \left( h_{ij,uv}(t^n - t^{p-1}) - h_{ij,uv}(t^n - t^p) \right) \quad (6.19)$$

where  $\Delta T_{b,i,u}^n$  is the temperature drop at the wall of segment  $u$  of borehole  $i$  at time  $t^k$ ;  $T_{b,i,u}^n$  is the temperature at the wall of segment  $u$  of borehole  $i$  at time  $t^k$ ;  $Q_{j,v}^p$  is the heat extraction rate per unit length of segment  $v$  of borehole  $j$  from time  $t^{p-1}$  to  $t^p$ ; and  $h_{ij,uv}$  is the segment-to-segment thermal response factor for the borehole wall temperature change over segment  $u$  of borehole  $i$  caused by heat extraction from segment  $v$  of borehole  $j$ .

The segment-to-segment response factor is given by the FLS solution:

$$h_{ij,uv}(t) = \frac{1}{2L_u} \int_{\frac{1}{\sqrt{4\alpha_s t}}}^{\infty} \frac{1}{s^2} \exp\left(-r_{ij}^2 s^2\right) I_{FLS}(s) ds \quad (6.20a)$$

$$\begin{aligned} I_{FLS}(s) = & \operatorname{erfint}\left((D_u - D_v + L_u)s\right) - \operatorname{erfint}\left((D_u - D_v)s\right) \\ & + \operatorname{erfint}\left((D_u - D_v - L_v)s\right) - \operatorname{erfint}\left((D_u - D_v + L_u - L_v)s\right) \\ & + \operatorname{erfint}\left((D_u + D_v + L_u)s\right) - \operatorname{erfint}\left((D_u + D_v)s\right) \\ & + \operatorname{erfint}\left((D_u + D_v + L_v)s\right) - \operatorname{erfint}\left((D_u + D_v + L_u + L_v)s\right) \end{aligned} \quad (6.20b)$$

$$\operatorname{erfint}(x) = \int_0^x \operatorname{erf}(x') dx' = x \operatorname{erf}(x) - \frac{1}{\sqrt{\pi}} \left(1 - \exp(-x^2)\right) \quad (6.20c)$$

where  $r_{ij}$  is the radial distance between boreholes  $i$  and  $j$  (with  $r_{ii} = r_b$ ),  $\operatorname{erf}(x)$  is the error function and  $\operatorname{erfint}(x)$  is the integral of the error function.

Recently, Prieto and Cimmino [153] proposed a methodology to account for thermal interactions among boreholes as interactions between equivalent boreholes sharing similar borehole wall temperatures and heat extraction rates. The field is divided into  $\mathcal{G}$  equivalent boreholes using a hierarchical agglomerative algorithm. Each equivalent borehole  $\mathcal{I}$  represents a group  $\mathbb{G}_{\mathcal{I}}$  composed of  $N_{b,\mathcal{I}}$  boreholes. The temperature drop at the borehole wall of a segment  $u$  of an equivalent borehole  $\mathcal{I}$  at time  $t^n$  is then:

$$\Delta \bar{T}_{b,\mathcal{I},u}^n = \frac{1}{2\pi k_s} \sum_{\mathcal{J}=1}^{\mathcal{G}} \sum_{v=1}^{n_s} \sum_{p=1}^n Q_{\mathcal{J},v}^p \left( \bar{h}_{\mathcal{I}\mathcal{J},uv}(t^n - t^{p-1}) - \bar{h}_{\mathcal{I}\mathcal{J},uv}(t^n - t^p) \right) \quad (6.21)$$

where  $\Delta \bar{T}_{b,\mathcal{I},u}^n$  is the temperature drop at the wall of segment  $u$  of equivalent borehole  $\mathcal{I}$  at time  $t_k$ ;  $Q_{\mathcal{J},v}^p$  is the heat extraction rate per unit length of segment  $v$  of equivalent borehole  $\mathcal{J}$  from time  $t^{p-1}$  to  $t^p$ ; and  $\bar{h}_{\mathcal{I}\mathcal{J},uv}$  is the equivalent segment-to-segment response factor for the borehole wall temperature change over segment  $u$  of equivalent borehole  $\mathcal{I}$  caused by heat extraction from segment  $v$  of equivalent borehole  $\mathcal{J}$ .

The equivalent segment-to-segment response factor is given by the average segment-to-segment response factors for the borehole wall temperature change along segments  $u$  of all boreholes in group  $\mathbb{G}_{\mathcal{I}}$  due to the heat extraction at all segments  $v$  of all boreholes in group  $\mathbb{G}_{\mathcal{J}}$ :

$$\bar{h}_{\mathcal{I}\mathcal{J},uv}(t) = \frac{1}{2L_u} \frac{1}{N_{b,\mathcal{I}}} \int_{\frac{1}{\sqrt{4\alpha_s t}}}^{\infty} \sum_{i \in \mathbb{G}_{\mathcal{I}}} \sum_{j \in \mathbb{G}_{\mathcal{J}}} \frac{1}{s^2} \exp(-r_{ij}^2 s^2) I_{FLS}(s) ds \quad (6.22)$$

$$\bar{h}_{\mathcal{J}\mathcal{I},vu}(t) = \frac{N_{b,\mathcal{I}}}{N_{b,\mathcal{J}}} \frac{L_u}{L_v} \bar{h}_{\mathcal{I}\mathcal{J},uv}(t) \quad (6.23)$$

To reduce the computation time involved in the Equation (6.21), a load aggregation scheme is employed and presented in Section 6.6. This scheme is already implemented in the `pygfunction` library [146], which was used here both for the aggregation of loads (Equation (6.21)) and for the calculation of segment-to-segment response factors (Equation (6.22)).

### Penalization of the transient multipole solution

A penalization technique is proposed to couple the transient multipole method presented in Section 6.3.1 with the equivalent borehole method. The transient multipole method can be used to evaluate the borehole wall heat extraction rate on ground layers, and the equivalent borehole method can be used to evaluate the borehole wall temperature change over segments (see Figure 6.3). Thus, an interpolation scheme is introduced to evaluate the heat extraction rate over a segment  $u$  from the transient multipole solution of its two delimiting layers,  $s$  and  $s + 1$  (with  $u = s$ ):

$$Q_{\mathcal{I},u}^n = -\frac{k_b r_b}{2} \int_0^{2\pi} \left( \left. \frac{\partial T_{1,\mathcal{I},s}^n}{\partial \rho} \right|_{r_b} + \left. \frac{\partial T_{1,\mathcal{I},s+1}^n}{\partial \rho} \right|_{r_b} \right) d\phi \quad (6.24)$$

where  $Q_{\mathcal{I},u}^n$  is the heat extraction rate per unit borehole length of a segment  $u$  of equivalent borehole  $\mathcal{I}$ . Expressions for the temperature derivatives at the borehole wall are given in Section 6.7.

The borehole wall temperature drop at a layer  $s$  is obtained from the borehole wall temper-



ature drops at the two adjoining segments  $u - 1$  and  $u$  (with  $u = s$ ):

$$\Delta \tilde{T}_{b,\mathcal{I},s}^n = \frac{\Delta \bar{T}_{b,\mathcal{I},u-1}^n + \Delta \bar{T}_{b,\mathcal{I},u}^n}{2} ; s = 2, 3, \dots, n_s \quad (6.25)$$

where  $\Delta \tilde{T}_{b,\mathcal{I},s}^n$  is the borehole wall temperature drop at a layer  $s$  of an equivalent borehole  $\mathcal{I}$ . For the top ( $s = 1$ ) and bottom ( $s = n_s + 1$ ) layers:

$$\Delta \tilde{T}_{b,\mathcal{I},s=1}^n = 2\Delta \bar{T}_{b,\mathcal{I},1}^n - \Delta \tilde{T}_{b,\mathcal{I},s=2}^n \quad (6.26a)$$

$$\Delta \tilde{T}_{b,\mathcal{I},s=n_s+1}^n = 2\Delta \bar{T}_{b,\mathcal{I},n_s}^n - \Delta \tilde{T}_{b,\mathcal{I},s=n_s}^n \quad (6.26b)$$

The penalization is applied to the transient multipole expansion solution for each layer  $s$  by introducing the difference between the temperature drop at borehole wall for an equivalent borehole  $\mathcal{I}$  and the temperature drop at the same layer  $s$  by means of the transient multipole expansion,  $\Delta \bar{T}_{1,\mathcal{I},s}^{n-1} \Big|_{r_b} = T^0 - \bar{T}_{1,\mathcal{I},s}^{n-1} \Big|_{r_b}$  and Equation (6.17):

$$C_{j,\mathcal{I},s}^n = C_{j,\mathcal{I},s}^{(n-1)} e^{-(\lambda_{1,\mathcal{I},s}^j)^2 \alpha_b \Delta t} + \sum_{l=1}^N \left( T_{f_l,\mathcal{I},s}^{n-1} - T_{f_l,\mathcal{I},s}^n + \Delta \tilde{T}_{b,\mathcal{I},s}^n - \Delta \bar{T}_{1,\mathcal{I},s}^{n-1} \Big|_{r_b} \right) E_{jl,\mathcal{I},s} \quad (6.27)$$

where  $C_{j,\mathcal{I},s}^n$  is the  $j$ -th Fourier–Bessel coefficient at time step  $t^n$  for a layer  $s$  in an equivalent borehole  $\mathcal{I}$ , and  $\lambda_{1,\mathcal{I},s}^j$  are the eigenvalues related to a layer  $s$  in an equivalent borehole  $\mathcal{I}$ . Expressions for the average temperature at the borehole wall are given in Section 6.7.

The complete solution by means of transient multipole expansion for a particular layer  $s$  in an equivalent borehole  $\mathcal{I}$  at time step  $t^n$  in the grout and soil is then:

$$T_{1,\mathcal{I},s}^n = \sum_{j=1}^{\infty} C_{j,\mathcal{I},s}^n X_{1,\mathcal{I},s}(\mathbf{x}; \lambda_{1,\mathcal{I},s}^j) e^{-(\lambda_{1,\mathcal{I},s}^j)^2 \alpha_b \Delta t} + \sum_{l=1}^N (T_{f_l,\mathcal{I},s}^n - T^0) \psi_{1l,\mathcal{I},s} + T^0 \quad (6.28a)$$

$$T_{2,\mathcal{I},s}^n = \sum_{j=1}^{\infty} C_{j,\mathcal{I},s}^n X_{2,\mathcal{I},s}(\mathbf{x}; \lambda_{2,\mathcal{I},s}^j) e^{-(\lambda_{2,\mathcal{I},s}^j)^2 \alpha_s \Delta t} + \sum_{l=1}^N (T_{f_l,\mathcal{I},s}^n - T^0) \psi_{2l,\mathcal{I},s} + T^0 \quad (6.28b)$$

where  $\psi_{dl,\mathcal{I},s}$  are the weighting functions for a layer  $s$  in an equivalent borehole  $\mathcal{I}$  in domain  $d$  (i.e., grout and soil).

Although the complete solution in Equation (6.28) looks computationally intensive due to eigenvalues, eigenfunctions, integrals and weighting functions, in practical applications, all boreholes possess a uniform geometry along their length and across the field. These terms thus only need to be evaluated once at the initialization of the simulation, except for the Fourier–Bessel coefficients that depend on the layer and the time step. Another interesting thing in Equation (6.28) is that even though  $T^0$ ,  $k_s$  and  $\alpha_s$  are considered constant, the

undisturbed ground temperature could change at each equivalent borehole, enabling the inclusion of thermal gradients and layered solutions when the soil thermal properties are not isotropic.

### 6.3.3 Advection inside the pipes

The model described in Sections 6.3.1 and 6.3.2 allows the evaluation of ground temperatures based on known fluid temperature profiles  $T_{f_k, \mathcal{I}}(z, t)$  at each pipe  $k$  at every equivalent borehole  $\mathcal{I}$ . This model needs to be coupled to a model of advection inside the pipes to complete the simulation model and predict fluid and ground temperatures based on ground loads.

Assuming quasi-steady plug flow inside the pipes and neglecting heat conduction in the direction of flow (i.e., only considering heat convection between the fluid and the inner pipe wall), energy balances on a layer at downward-flowing pipe  $p$  and an upward-flowing pipe  $q$  are given by:

$$\pi \rho_f c_{p_f} r_k^2 \frac{\partial T_{f_p, \mathcal{I}}}{\partial t} + c_{p_f} \dot{m}_{\mathcal{I}}^n \frac{\partial T_{f_p, \mathcal{I}}}{\partial z} + \frac{1}{R_p} T_{f_p, \mathcal{I}} = \frac{1}{R_p} \overline{T_{1, \mathcal{I}}} \Big|_{r_p} \quad (6.29a)$$

$$\pi \rho_f c_{p_f} r_k^2 \frac{\partial T_{f_q, \mathcal{I}}}{\partial t} - c_{p_f} \dot{m}_{\mathcal{I}}^n \frac{\partial T_{f_q, \mathcal{I}}}{\partial z} + \frac{1}{R_q} T_{f_q, \mathcal{I}} = \frac{1}{R_q} \overline{T_{1, \mathcal{I}}} \Big|_{r_q} \quad (6.29b)$$

where  $z$  is the axial position along the pipe (positive in the downward direction);  $\rho_f$  and  $c_{p_f}$  are the fluid density and specific heat at constant pressure, respectively; and  $\dot{m}_{\mathcal{I}}^n$  is the average mass flow rate in a U-tube containing pipes  $p$  and  $q$  for an equivalent borehole  $\mathcal{I}$  at the particular time step  $t^n$ .

The fluid to outer pipe thermal resistance,  $R_p$ , is given by the sum of the film resistance at the inner pipe wall and the conduction resistance across the pipe wall:

$$R_p = \frac{1}{\text{Nu} \pi k_f} + \frac{\ln(\frac{r_p}{r_p - t_h})}{2 \pi k_p} \quad (6.30a)$$

$$\text{Nu} = \begin{cases} 3.66 & \text{if } \text{Re} < 2300 \\ 0.023 \text{Re}^{0.8} \text{Pr}^{0.35} & \text{if } \text{Re} \geq 2300 \end{cases} \quad (6.30b)$$

where Nu is the Nusselt number, Re is the Reynolds number, Pr is the Prandtl number and  $k_p$  is the pipe thermal conductivity.

An implicit finite difference scheme is used to solve the problem. The GHE is discretized into layers, according to Figure 6.3. The discretized energy balance on a control volume delimited

by two consecutive ground layers is given by:

$$-\frac{c_{p_f} \dot{m}_{\mathcal{I}}^n}{L_u} T_{p,\mathcal{I},s-1}^n + \left( \frac{\pi \rho_f c_{p_f} r_k^2}{\Delta t} + \frac{c_{p_f} \dot{m}_{\mathcal{I}}^n}{L_u} + \frac{1}{R_p} \right) T_{f_p,\mathcal{I},s}^n = \frac{1}{R_p} \overline{T_{1,\mathcal{I},s}^n} \Big|_{r_p} + \frac{\pi \rho_f c_{p_f} r_k^2}{\Delta t} T_{f_p,\mathcal{I},s}^{n-1} \quad (6.31a)$$

$$\frac{c_{p_f} \dot{m}_{\mathcal{I}}^n}{L_u} T_{q,\mathcal{I},s-1}^n + \left( \frac{\pi \rho_f c_{p_f} r_k^2}{\Delta t} - \frac{c_{p_f} \dot{m}_{\mathcal{I}}^n}{L_u} + \frac{1}{R_q} \right) T_{f_q,\mathcal{I},s}^n = \frac{1}{R_q} \overline{T_{1,\mathcal{I},s}^n} \Big|_{r_q} + \frac{\pi \rho_f c_{p_f} r_k^2}{\Delta t} T_{f_q,\mathcal{I},s}^{n-1} \quad (6.31b)$$

The number of unknowns for the fluid temperatures per equivalent borehole,  $T_{k,\mathcal{I},s}^n$ , at each time step  $t^n$  in Equation (6.31), is equal to  $N(n_s + 1)$ . A continuity condition is imposed at the bottom of the equivalent borehole:

$$T_{f_p,\mathcal{I},n_s+1}^n = T_{f_q,\mathcal{I},n_s+1}^n \quad (6.32)$$

where pipes  $p \neq q$  but belong to the same U-tube.

The system of equations is completed by imposing the ground loads  $\dot{Q}^n$ , for the complete borefield. In this case, boreholes are assumed to be connected in parallel:

$$\dot{Q}^n = \dot{m}_T^n c_{p_f} (T_{out}^n - T_{in}^n) \quad (6.33)$$

where  $T_{in}^n$  and  $T_{out}^n$  are the inlet and outlet temperatures at time step  $n$  in the borefield and  $\dot{m}_T^n = N_b \dot{m}_b^n$  is the total mass flow rate, with  $\dot{m}_b^n$  the mass flow rate per borehole.

As the borefield is parallel-connected, the inlet temperature is the same for each equivalent borehole  $\mathcal{I}$ :

$$T_{in}^n = T_{f_p,\mathcal{I},1}^n \quad (6.34)$$

The outlet temperature of the borefield,  $T_{out}^n$ , is obtained by mixing of the fluid at the outlet of all equivalent boreholes:

$$T_{out}^n = \frac{1}{N_b} \sum_{\mathcal{I}=1}^{\mathcal{G}} N_{b,\mathcal{I}} T_{f_q,\mathcal{I},1}^n \quad (6.35)$$

The problem is then complete, and it is possible to estimate the fluid temperatures at each equivalent borehole while imposing the heat extracted or rejected from the ground. An iterative scheme is used to solve the simulation model at each time step  $n$ :

1. Calculate fluid temperatures,  $T_{f_p,\mathcal{I},s}^n$ , using the pipe temperatures  $\overline{T_{1,\mathcal{I},s}^{n-1}} \Big|_{r_p}$  at the previous time step  $(n-1)$  as a first guess in Equation (6.31) with their boundary conditions

- and ground loads at time step  $n$ ;
2. Calculate the heat transfer rates and borehole wall temperatures using Equations (5.8), (6.24) and (6.26);
  3. Update the coefficients in Equation (6.27) using the fluid temperatures  $T_{f_p, \mathcal{I}, s}^n$ , heat transfer rates and average borehole wall temperatures calculated in steps (1) and (2);
  4. Recalculate  $\overline{T_{1, \mathcal{I}, s}^n} \Big|_{r_p}$  according to Equation (6.28) using the new coefficients obtained in step (3);
  5. Compute the new fluid temperatures as in step (1) with the new pipe temperature calculated in step (4);
  6. Repeat from (2) if the difference of  $T_{f_p, \mathcal{I}, s}^n$  between the previous and current iterations is greater than  $10^{-4}$  °C.

The method converges quickly, usually after two or three iterations. In this case, a linear system is solved with a guessed or updated value for  $\overline{T_{1, \mathcal{I}, s}^n} \Big|_{r_q}$ ; thus, the unknowns in the system of equations for estimating the fluid temperatures are equal to  $\mathcal{G}N(n_s + 1)$ . For the limiting case when the ground load is 0 W, the mass flow is set to 0 kg/s. Therefore, the solution of Equations (6.29) does not require solving a system of equations, since the term containing the derivative with respect to  $z$  is eliminated.

### 6.3.4 Finite element modeling

A reference finite element analysis (FEA) model was developed to validate the proposed method. Diersch et al. [83, 84] developed a complete FEA model that includes the transient effects inside and outside GHEs and thermal interactions between them. This is an extension of the model previously proposed by Al-Khoury and Bonnier [91]. The same mathematical formalism is used in the present paper with some modifications.

The method was created on double-continuum finite element (i.e., one continuum media for the soil and one for the GHEs) space based on Galerkin discretization with 6-node prismatic elements for the 3D model. Each GHE is simulated as a line element surrounded by six nodes that virtually represent the borehole wall, located at a distance greater than  $r_b$ , as presented in Diersch et al. [84]. Figure 6.4 shows the discretizations used for the two simulations used to validate the proposed semi-analytical methodology. First, the discretization shown in Figure 6.4a corresponds to a single borehole and was used for the comparison against

experimental data. Then, Figure 6.4b shows the discretization for a borefield composed of 24 GHEs that was used in multi-annual simulations.

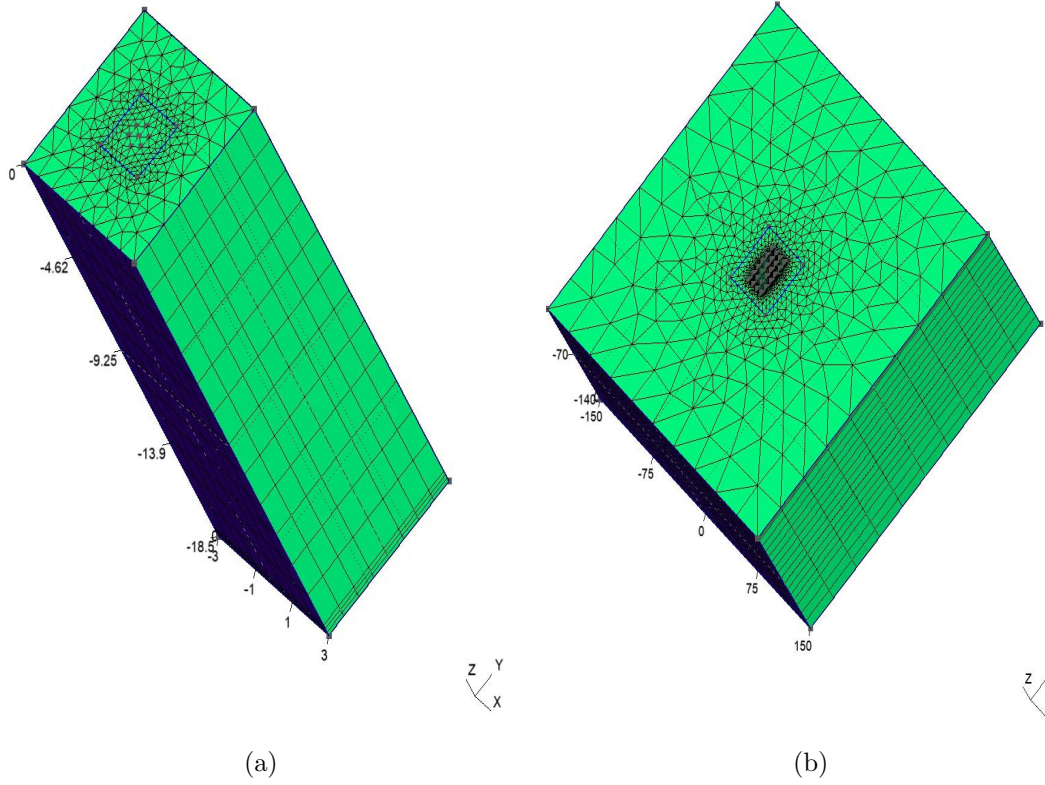


Figure 6.4 Finite element discretization for model validation. (a) Mesh for Beier's experiment. (b) Mesh for a borefield with 24 GHE.

For each line element, short-term effects were modeled using the TRC model developed by Bauer et al. [43, 44]. The correction noted by Bauer et al. [43] and presented in FEFLOW white papers (Section 1.5.5) [156] was used when negative internal thermal resistances were present. Depending on the number of U-tubes, each node over the line element presents two pairs of temperatures: two for the inlet temperature and the grout temperature where the inlet pipe is located, and two for the outlet temperature and the grout temperature where the outlet pipe is located. The TRC model is coupled to the FE-discretized equations considering a steady-state problem for a given borehole wall temperature, as solved by Eskilson and Claesson [157], to predict the fluid temperatures inside the pipes. This procedure is the same as that described by Diersch et al. [83].

A Picard iteration was employed to solve the system of equations and ensure the temperatures converge. Diersch et al. [84] suggest that the GHE domain should be separated from the whole domain and only later included in the soil domain by means of Schur complement operation.

However, in the present FEA model, the Picard iteration achieved convergence after one or two iterations without the need to separate domains. Additionally, due to the initialization of the model, a few iterations with a small time step (i.e.,  $\Delta t/10$  for a fixed time step  $\Delta t$ ) are required to stabilize the heat transport between the fluid and grout. After this stabilization, larger time steps ( $\Delta t$ ) can be used.

## 6.4 Validation

The proposed method and the reference FEA model were first validated by comparison to the experimental results of Beier et al. [155] for a single borehole. Then, the proposed method was validated against the FEA model for a multi-year simulation of a borefield comprised of 24 boreholes. Inlet and outlet fluid temperatures and borehole wall temperatures were compared in both cases. The accuracy of the method was evaluated by computing the root mean square error (RMSE) and temperature differences between models and an experiment.

For the proposed method, the discretization along the GHE was done using 12 segments based on the recommendation of Cimmino and Bernier [73]. Following the recommendations of Prieto and Cimmino [143], the order of the transient multipole expansion was set to  $M = 7$  and  $h = 15$ , corresponding to the homogeneous transient heat equation and non-homogeneous steady-state heat equation, respectively, and the first 100 eigenvalues were used for each simulation. All calculations were done on a personal computer with 16 GB of RAM and a 6-core processor (12 threads) running at normal speed of 2.60 GHz and maximum speed of 4.80 GHz.

### 6.4.1 Sandbox test

Beier et al. [155] designed a sandbox test widely used in the context of short-term response validation of a GHE. The experiment consists of an average heat injection of 1051 W while maintaining an average mass flow rate of 0.197 kg/s in an 18 m long single U-tube GHE for 3106 min (approximately 52 h). The dimensions and parameters used for the experiment are shown in Table 6.1. Since in the experiment the GHE included an aluminum housing that affects heat transfer to the soil, Pasquier and Marcotte [46] use a modified thermal conductivity of the grout that preserves the borehole thermal resistance reported in the experiment. Therefore, the thermal conductivity calculated by Pasquier and Marcotte [46] was used in the proposed method.

Table 6.1 Sandbox test parameters.

Parameter	Value
Borehole buried depth	$D = 0$ m
Borehole length	$L = 18$ m
Borehole radius	$r_b = 0.063$ m
U-tube pipe outer radius	$r_p = 0.0167$ m
U-tube pipe thickness	$t_h = 0.00303$ m
U-tube shank spacing	$e = 0.0265$ m
Ground thermal conductivity	$k_s = 2.82$ W/(mK)
Ground thermal diffusivity	$\alpha_s = 1.4 \times 10^{-6}$ m <sup>2</sup> /s
Grout thermal conductivity	$k_b = 0.9$ W/(mK)
Grout thermal diffusivity	$\alpha_b = 2.4 \times 10^{-7}$ m <sup>2</sup> /s
Fluid thermal conductivity	$k_f = 0.63$ W/(mK)
Fluid thermal capacity	$(\rho c_p)_f = 4.2 \times 10^6$ J/(m <sup>3</sup> K)
U-tube pipe thermal conductivity	$k_p = 0.39$ W/(mK)
Undisturbed ground temperature	$T^0 = 22$ °C
Number of segments	$n_s = 12$
Time step	$\Delta t = 60$ s

The time step used in the simulation corresponds to the resolution time reported in the experiment and was equal to 60 s. Regarding the FEA model, 7260 6-node prismatic elements were used, equivalent to 4144 nodes in total. A square domain was proposed to consider the soil part with 6 m per side to avoid that the boundary conditions affect the thermal response of the GHE. The length of the FEA along the GHE axis was equal to 18.5 m. The ground load and mass flow rate reported in Beier et al. [155] were variable in time. Instead of using the average of ground load and mass flow rate, time varying values were used. Figure 6.5 shows the ground load and mass flow rate over the duration of the experiment.

Figure 6.6 shows the inlet and outlet fluid temperatures and the average borehole wall temperatures calculated with the proposed method, (a) the sandbox test and (b) the FEA model, showing good agreement. Both the proposed method and the FEA model were shown to accurately predict temperatures when compared to the experimental results.

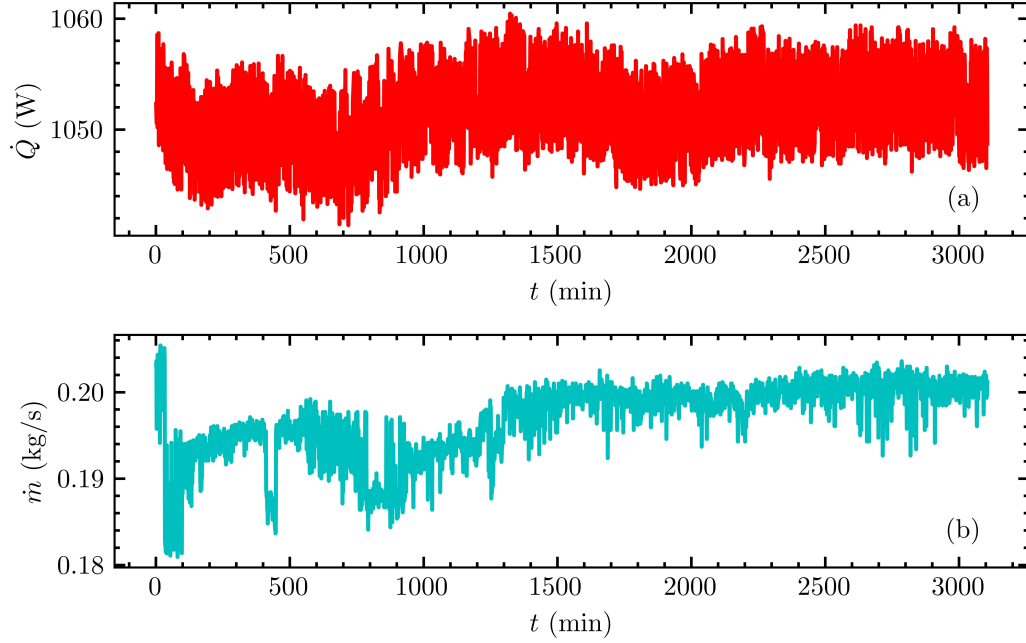


Figure 6.5 Beier et al. [155] experiment: (a) ground load and (b) mass flow rate.

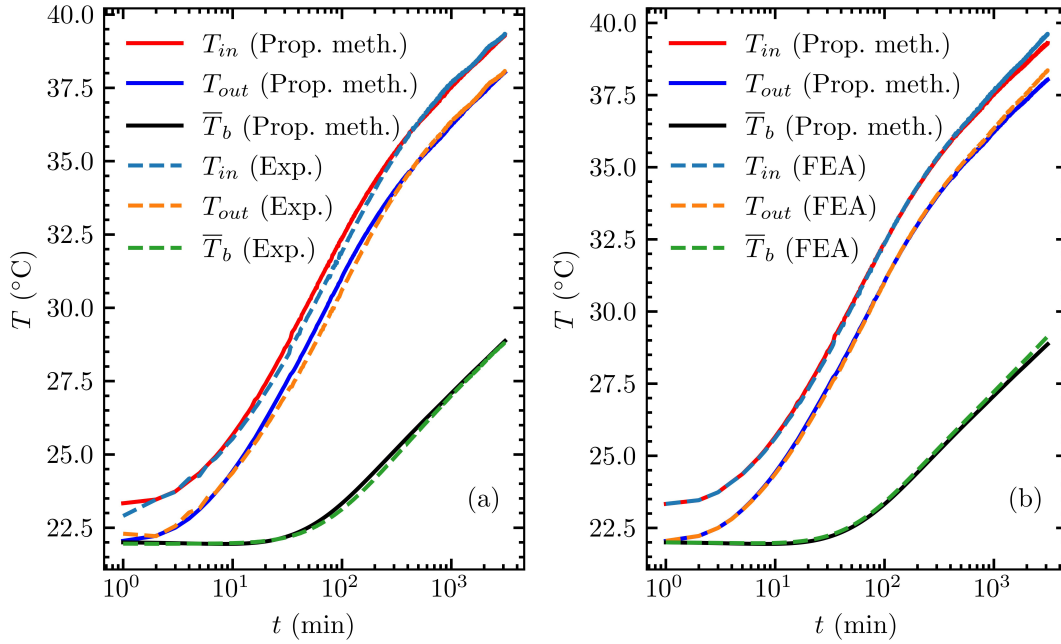


Figure 6.6 Comparison of the proposed model with (a) the experimental data of Beier et al. [155] and (b) the FEA model.

The comparison between the proposed model and the experimental data is shown in Figure 6.6a, resulting in RMSEs for inlet and outlet fluid temperatures and for the average



borehole temperature equal to 0.134, 0.131 and 0.105 °C, respectively. The maximum absolute errors for inlet and outlet fluid temperatures occurred at the 76th minute of the simulation and were 0.556 °C and 0.519 °C, respectively. In contrast, the maximum absolute error for the average borehole wall temperature occurred at the 196th minute and was equal to 0.253 °C. The fact that the errors did not occur at the same time for inlet and outlet fluid temperatures and the borehole wall is explained by the fact that the heat transfer process inside the borehole reached a quasi-steady state (or constant heat flux) at a time in the order of  $r_b^2/\alpha_s$ . Figure 6.6b shows the comparison between the FEA model and the proposed method computing inlet and outlet fluid temperature and average borehole wall temperature, similar to what was shown for comparison with the experimental data. For this case, the RMSEs for the inlet and outlet fluid temperatures and average borehole wall temperature were equal to 0.196, 0.196 and 0.183 °C, respectively. The maximum absolute errors for each temperature,  $T_{in}$ ,  $T_{out}$  and  $\bar{T}_b$ , occurred at the end of the simulations with values equal to 0.317, 0.317 and 0.270 °C.

Figure 6.7 shows a comparison of the fluid temperature profiles along the pipes between the proposed model and the FEA model at four different times, corresponding to 1, 10, 100 and 1000 min. Arrows indicate fluid flow direction. For the inlet pipe, the maximum absolute errors for 1, 10, 100 and 1000 min were equal to 0.003, 0.047, 0.013 and 0.125 °C. Similarly, for the outlet pipe, the maximum absolute errors were equal to 0.002, 0.048, 0.013 and 0.125 °C, corresponding to 1, 10, 100 and 1000 min of the simulation. The maximum absolute errors for inlet and outlet pipes were expected to be approximately equal, since the energy balance is preserved by the ground load in the discretization of the advection equation.

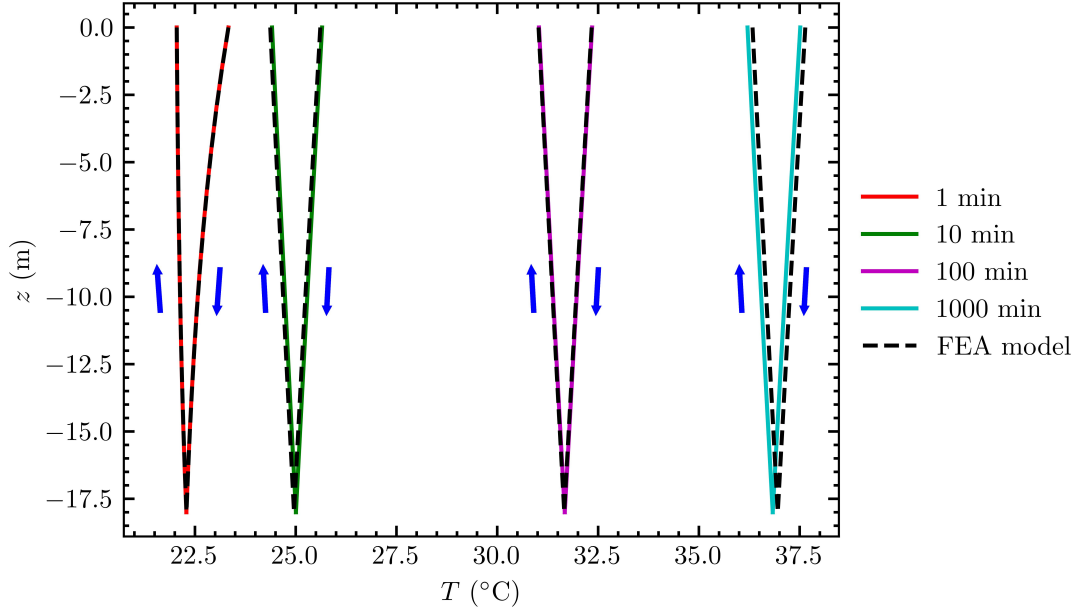


Figure 6.7 Fluid temperature profiles along pipes at 4 different times.

The calculation time for Beier's experiment by means of the proposed method was equal to 214 s, including 210 s for the initialization and 4 s for the solution of the system of equations and coefficient updating scheme.

#### 6.4.2 Multi-annual simulation of a geothermal field

Two simulations were used to evaluate the accuracy of the proposed method for long-term and short-term temperature predictions. A first multi-annual simulation was performed for a period of 10 years using a 1 h time step to evaluate the long-term accuracy of the method, followed by a period of 7 days using a time step of 1 min to evaluate the short-term accuracy of the method. The borefield was comprised of 24 boreholes in a rectangular configuration. Every GHE received the same inlet temperature and the same mass flow rate. The parameters used in the simulation are shown in Table 6.2.

Table 6.2 Borefield parameters.

Parameter	Value
Borehole buried depth	$D = 4$ m
Borehole length	$L = 100$ m
Borehole radius	$r_b = 0.075$ m
U-tube pipe outer radius	$r_p = 0.0211$ m
U-tube pipe thickness	$t_h = 0.00406$ m
U-tube shank spacing	$e = 0.05$ m
Ground thermal conductivity	$k_s = 2.4$ W/(mK)
Ground thermal diffusivity	$\alpha_s = 1.2 \times 10^{-6}$ m <sup>2</sup> /s
Grout thermal conductivity	$k_b = 0.81$ W/(mK)
Grout thermal diffusivity	$\alpha_b = 2.1 \times 10^{-7}$ m <sup>2</sup> /s
Fluid thermal conductivity	$k_f = 0.48$ W/(mK)
Fluid thermal capacity	$(\rho c_p)_f = 4.02 \times 10^6$ J/(m <sup>3</sup> K)
U-tube pipe thermal conductivity	$k_p = 0.42$ W/(mK)
Undisturbed ground temperature	$T^0 = 12.5$ °C
Total mass flow rate	$\dot{m} = 6$ kg/s
Number of segments	$n_s = 12$

The borefield was divided into equivalent boreholes that shared similar borehole wall temperatures and heat extraction rates using the methodology proposed by Prieto and Cimmino [153]. Figure 6.8 shows the borefield studied, in this case a rectangular configuration where each consecutive borehole was 6 m equidistant both horizontally and vertically, and the equivalent boreholes were identified. Equivalent boreholes denoted by the numbers *I*, *II*, *III* each represent 12, 8 and 4 GHEs, respectively. The FEA model was composed of 123,828 6-node prismatic elements with 65,934 nodes in a ground domain, 300 m per side and an axial length equal to 140 m.

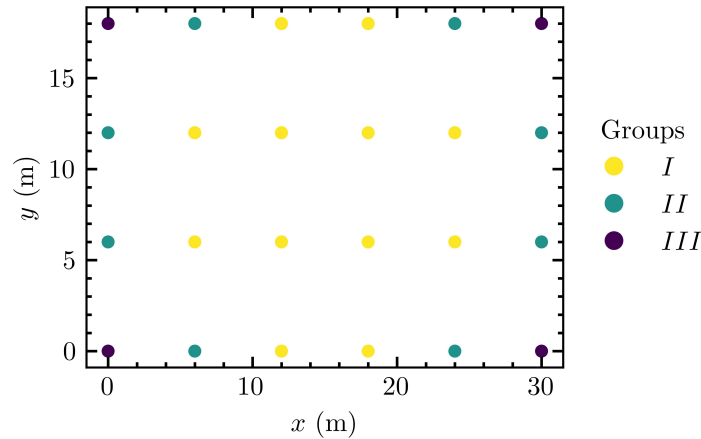


Figure 6.8 Equivalent boreholes for a field of 24 GHEs.

### Simulation of a 10-Year period

Figure 6.9 shows the complete simulation for the first 10 years of heat extraction and heat rejection with the ground ( $\dot{Q}$ ), including inlet and outlet ( $T_{in}$  and  $T_{out}$ ) temperature and the average borehole wall temperature for each equivalent borehole ( $\bar{T}_{b,I}$ ,  $\bar{T}_{b,II}$ ,  $\bar{T}_{b,III}$ ) calculated with the proposed method. Figure 6.9a shows the ground loads ( $\dot{Q} > 0$  corresponds to heat extraction with the ground, negative otherwise) for the 10-year period, generated using the synthetic ground load profile of Bernier et al. [65]. The maximum heat extraction and rejection were equal to 93,502 and  $-76,704$  W, respectively. The average net heat transfer for all 10 years was equal to 3761 W, which means an imbalance towards heat extraction. The impact of this imbalance is shown in Figure 6.9b,c, exhibiting decreasing behavior in both fluid temperatures and borehole wall temperature at the end of the simulation. The maximum and minimum inlet fluid temperatures were 19.98 and 0.95 °C, respectively, and the maximum and minimum outlet fluid temperatures were 17.29 and 4.25 °C, respectively. At the end of the simulation, the fluid had a temperature of 9.17 °C for both  $T_{in}$  and  $T_{out}$ , since there was no heat exchange at this time. This represents a difference between the temperature at the beginning of the simulation and the end of the simulation equal to 3.33 °C. For the average borehole wall temperature for each equivalent borehole, the maximum and minimum temperatures in the 10-year period were, respectively, 14.82 and 7.28 °C for equivalent borehole *I*; 14.86 and 7.37 °C for equivalent borehole *II*; and 14.89 and 7.45 °C for equivalent borehole *III*. At the end of the simulation, the equivalent boreholes (*I*, *II*, *III*) presented average borehole wall temperatures equal to 9.36, 9.44 and 9.52 °C, respectively. Although the variation in the borehole wall temperature between the equivalent boreholes was small, it existed and shows the need to simulate in detail a field composed of several GHEs for larger periods of time. It is also worth mentioning that if the ground loads maintain their imbalance for a longer time, the average borehole wall and fluid temperatures will tend to decrease until they reach steady-state.

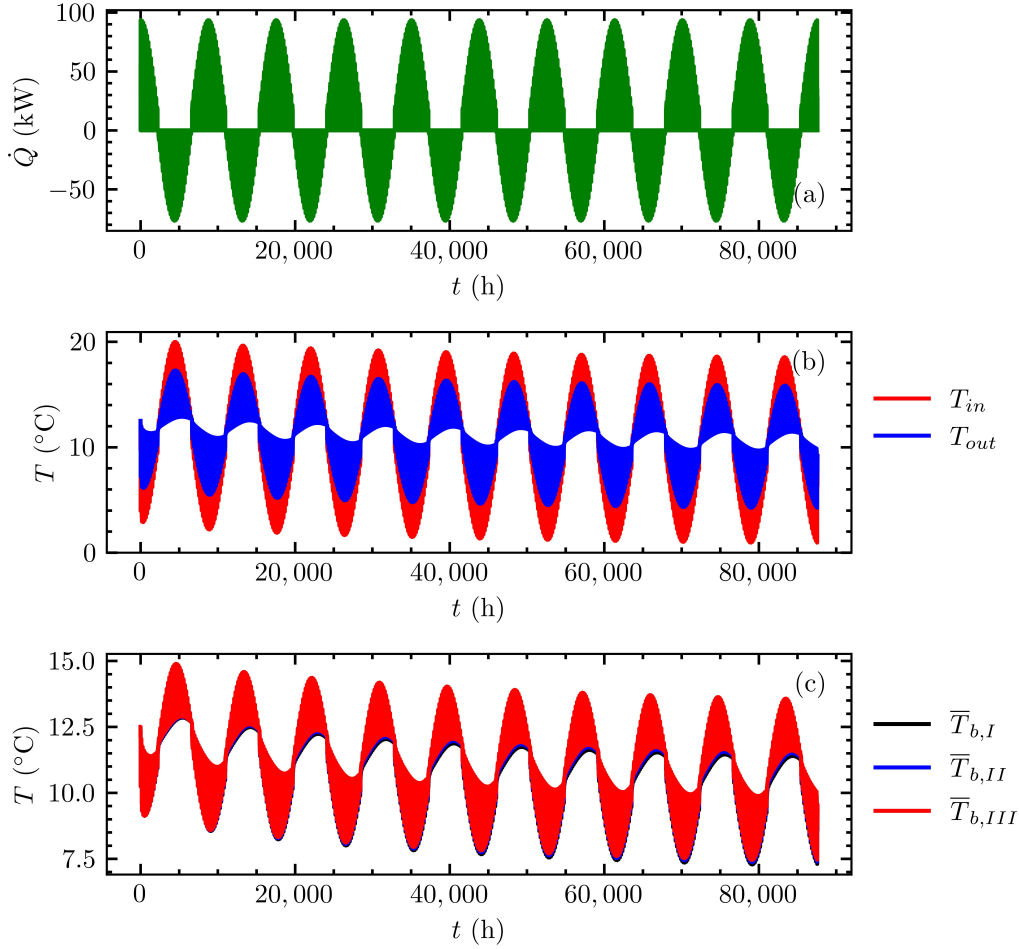


Figure 6.9 Multi-annual simulation over 10 years with the proposed method: (a) ground loads, (b) inlet and outlet fluid temperatures and (c) average borehole wall temperature at each equivalent borehole.

Figure 6.10 compares the inlet and outlet fluid temperatures evaluated with the proposed model and the FEA model. The difference between predicted inlet fluid temperatures is denoted  $\Delta T_{in}$ , and the difference between predicted outlet fluid temperatures is denoted  $\Delta T_{out}$ . The results corresponding to the time steps of the minimum and maximum differences, and at the end of simulation, are presented in Table 6.3. Lastly, the RMSEs for the inlet and outlet fluid temperatures were 0.13 and 0.14 °C over the 10th simulation year, respectively. Therefore, the inlet and outlet temperatures show good agreement when compared with the FEA model.

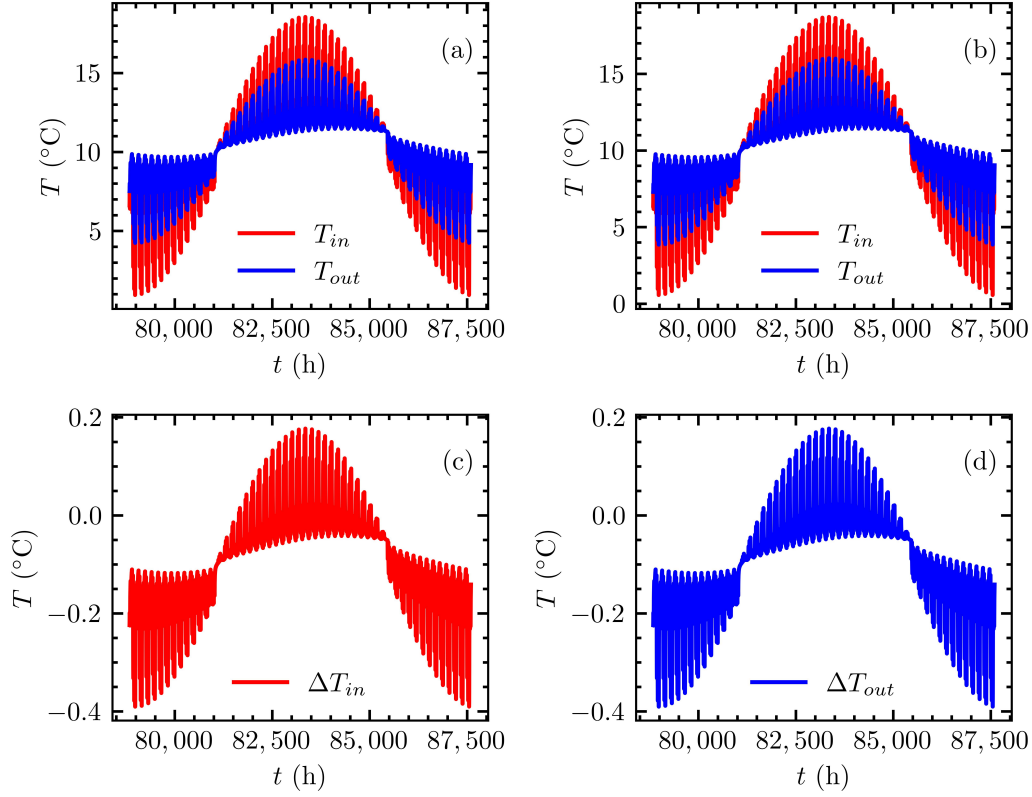


Figure 6.10 Comparison of predicted inlet and outlet fluid temperatures during the 10th year: (a) proposed method, (b) FEA model, (c) error of the inlet temperature and (d) error of the outlet temperature.

Table 6.3 Errors of fluid temperatures during the 10th year.

	$T_{in} (^{\circ}\text{C})$		$T_{out} (^{\circ}\text{C})$		$\Delta T_{in} (^{\circ}\text{C})$	$\Delta T_{out} (^{\circ}\text{C})$
	FEA	Meth.	FEA	Meth.		
Minimum error	0.57	0.95	3.86	4.25	-0.39	-0.39
Maximum error	18.71	18.54	16.02	15.84	0.18	0.18
End of simulation	9.03	9.17	9.03	9.17	-0.14	-0.14

The behavior between the soil and the GHE can be studied through the behavior of the borehole wall temperature. For this purpose, according to the groups identified in Figure 6.8, the average borehole wall temperature for each of the equivalent boreholes was calculated in the FEA model to compare with the proposed methodology. Figure 6.11 shows the average borehole wall temperature for each of the equivalent boreholes for the proposed method and the FEA model, and the error between each of them for the 10th simulation year. For Figure 6.11a–c, the average borehole wall temperature for each equivalent borehole was estimated by means of the proposed method; for Figure 6.11d–f, by the FEA model; and

Figure 6.11g–i shows errors between FEA and the proposed model, for the 10th year. The results corresponding to the time steps of the minimum and maximum differences and at the end of simulation are presented in Table 6.4. The largest error (in magnitude) was reached when the minimum temperature was reached. The RMSEs between FEA and proposed method were 0.10, 0.09 and 0.10 °C, for each equivalent borehole, *I*, *II* and *III*, respectively. The errors show that the proposed model is able to predict with reasonable accuracy the thermal response between GHE and the soil.

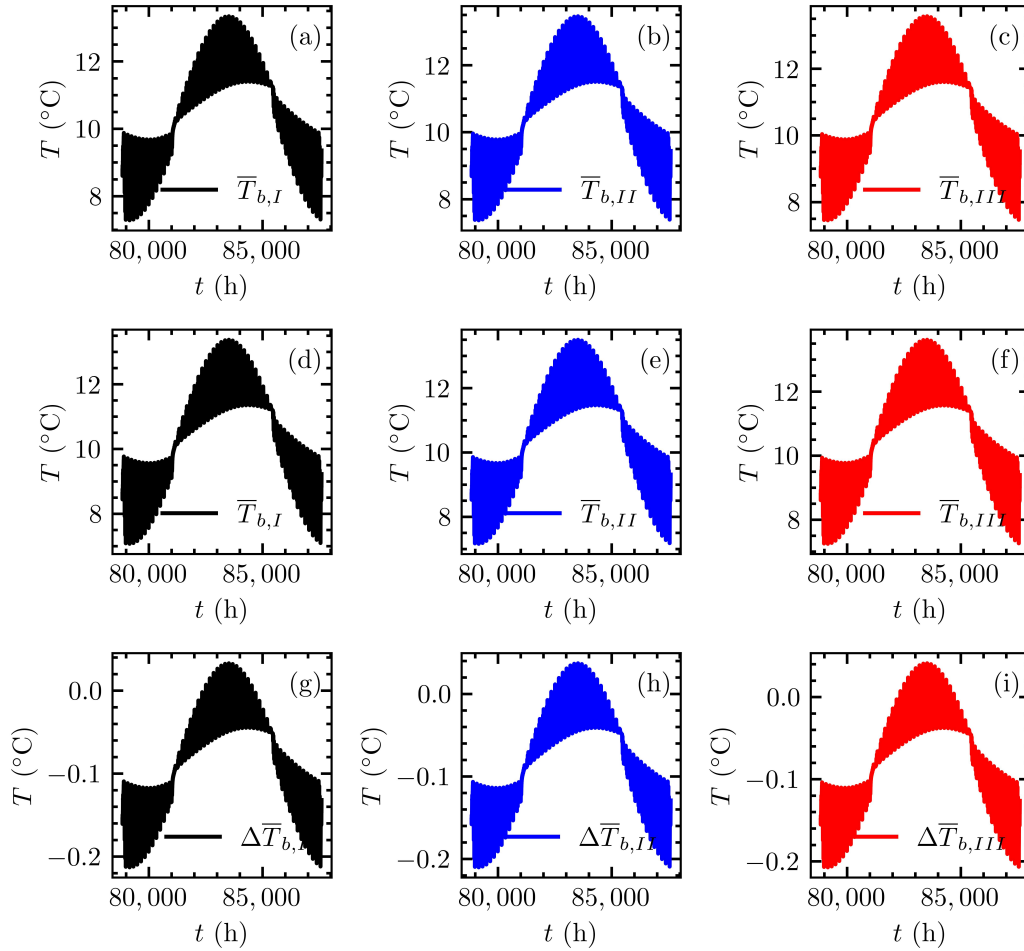


Figure 6.11 Comparison of predicted borehole wall temperatures for each equivalent group (*I*, *II*, *III*) during the 10th year: (a–c) proposed method, (d–f) FEA model and (g–i) error between models.

Table 6.4 Errors on borehole wall temperatures during the 10th year.

	$\bar{T}_{b,I}(\text{°C})$		$\bar{T}_{b,II}(\text{°C})$		$\bar{T}_{b,III}(\text{°C})$		$\Delta\bar{T}_{b,I}(\text{°C})$	$\Delta\bar{T}_{b,II}(\text{°C})$	$\Delta\bar{T}_{b,III}(\text{°C})$
	FEA	Meth.	FEA	Meth.	FEA	Meth.			
Minimum error	7.07	7.28	7.16	7.37	7.45	7.66	−0.21	−0.21	−0.21
Maximum error	13.37	13.34	13.50	13.46	13.61	13.57	0.03	0.04	0.04
End of simulation	9.22	9.36	9.31	9.44	9.39	9.52	−0.14	−0.13	−0.13

The calculation time for this simulation was 310 s: 210 s dedicated to the initialization procedures (i.e., integrals, eigenvalues, coefficients, etc.) and 100 s to the solution of the systems of equations and iterations for the period of 10 years with a time step equal to 1 h.

### **Short-term effects after 10 years**

For the validation of the proposed method with respect to the short-term effects, an additional period of 7 days was simulated following the 10 years of simulation. The time step during this period was set to 1 min. The FEA model was initialized using the final results of the 10-year simulation as initial conditions.

Figure 6.12 shows the inlet and outlet fluid temperatures and the borehole wall temperatures for each of the equivalent boreholes for the FEA model and the proposed method, and a comparison of the results. Figure 6.12a,b shows the temperatures obtained using the proposed method, and Figure 6.12c,d shows the same temperatures obtained with the FEA model. Figure 6.12e,f shows the differences between the FEA and proposed method. Table 6.5 presents the inlet and outlet fluid temperatures at the time of the maximum and minimum errors and at the end of the simulation, and the differences between the FEA and the proposed model. The RMSEs between the two models were 0.23 and 0.24 °C for the inlet and outlet fluid temperatures, respectively. This shows that the proposed method is able to accurately estimate the fluid temperatures when the short-term effects are considered. Table 6.6 compares the average borehole wall temperatures at each equivalent borehole at the times of the maximum and minimum errors and at the end of the simulation, and the differences between the FEA and the proposed model. The RMSE for each equivalent borehole, *I*, *II* and *III*, was 0.16, 0.16 and 0.15 °C, respectively. As previously noted, these results show good agreement when compared with the FEA model.



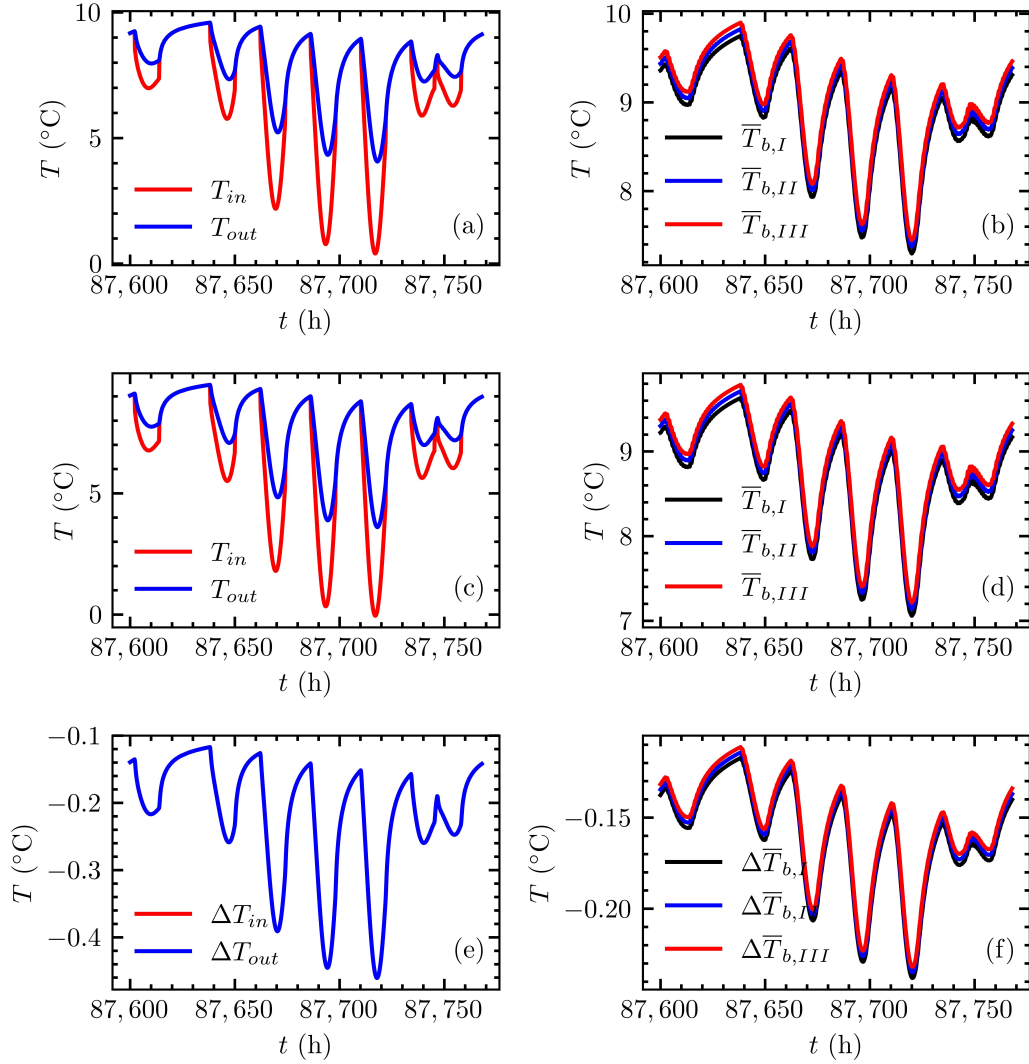


Figure 6.12 Comparison of predicted inlet and outlet fluid temperatures and borehole wall temperatures for each equivalent group (*I*, *II*, *III*) during the 7-day period: (a,b) proposed method, (c,d) FEA model, (e) errors of the inlet and outlet fluid temperatures, and (f) error of the borehole wall temperatures.

Table 6.5 Errors of fluid temperatures during the 7-day period.

	$T_{in}(^{\circ}\text{C})$		$T_{out}(^{\circ}\text{C})$		$\Delta T_{in}(^{\circ}\text{C})$	$\Delta T_{out}(^{\circ}\text{C})$
	FEA	Meth.	FEA	Meth.		
Minimum error	-0.05	0.4	3.6	4.06	-0.46	-0.46
Maximum error	9.47	9.59	9.47	9.59	-0.2	-0.2
End of simulation	8.98	9.12	8.98	9.12	-0.14	-0.14

Table 6.6 Errors of borehole wall temperatures during the 7-day period.

	$\bar{T}_{b,I} (^{\circ}\text{C})$		$\bar{T}_{b,II} (^{\circ}\text{C})$		$\bar{T}_{b,III} (^{\circ}\text{C})$		$\Delta\bar{T}_{b,I} (^{\circ}\text{C})$	$\Delta\bar{T}_{b,II} (^{\circ}\text{C})$	$\Delta\bar{T}_{b,III} (^{\circ}\text{C})$
	FEA	Meth.	FEA	Meth.	FEA	Meth.			
Minimum error	7.06	7.30	7.14	7.37	7.22	7.44	−0.24	−0.24	−0.23
Maximum error	9.63	9.75	9.71	9.83	9.79	9.90	−0.12	−0.11	−0.11
End of simulation	9.16	9.31	9.25	9.39	9.33	9.46	−0.14	−0.14	−0.13

Figure 6.13 shows the fluid temperature profiles and the borehole wall temperature profiles for each of the equivalent boreholes along their lengths estimated with the proposed method and the FEA for the time step where the largest difference (in magnitude) between the two methods was obtained, which in this case corresponded to 7029 min.

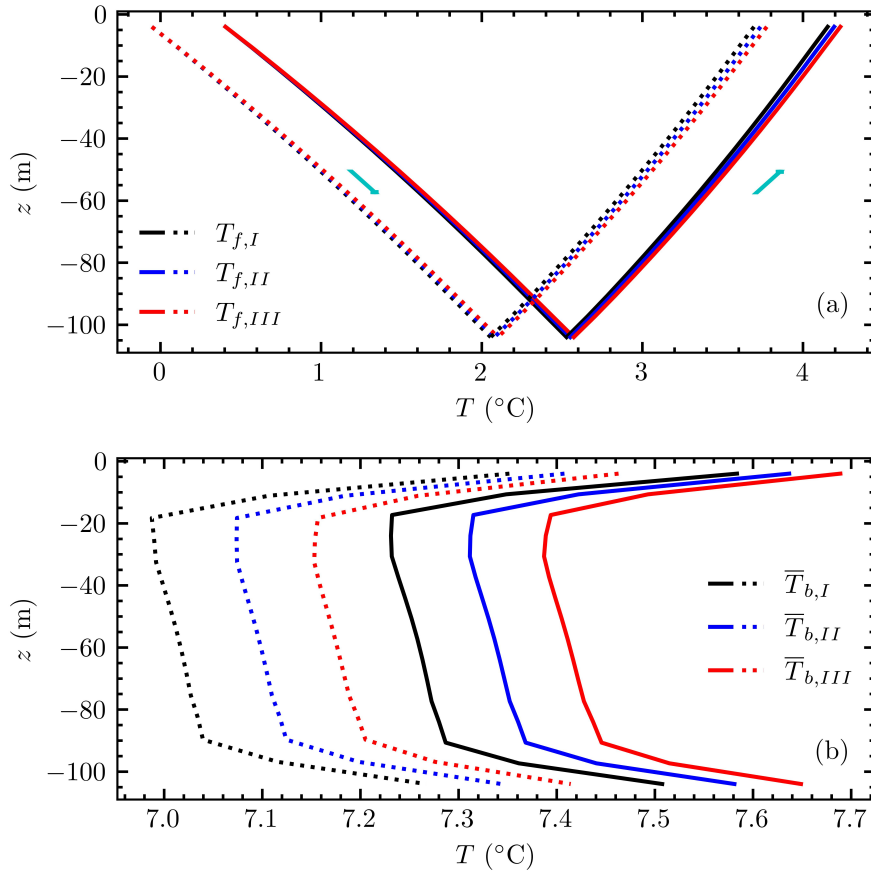


Figure 6.13 Fluid and borehole wall temperature profiles for each equivalent borehole at 7029 min: (a) fluid temperature profiles for the FEA (dotted line) and the proposed method (solid line) for each equivalent borehole, and (b) equivalent borehole wall temperature profiles for the FEA method (dotted line) and the proposed method (continuous line).

The arrows indicate the fluid flow direction for each pipe. The inlet temperatures for each equivalent borehole for the FEA and proposed method were equal to  $-0.05$  and  $0.4$   $^{\circ}\text{C}$ ,

respectively. This amounts to the error previously computed as  $-0.46$  °C between FEA and the proposed method. The outlet temperatures for the proposed method were equal to  $4.15$  °C for *I*,  $4.19$  °C for *II* and  $4.23$  °C for *III*. On the other hand, for the FEA the temperatures were equal to  $3.69$  °C for *I*,  $3.73$  °C for *II* and  $3.76$  °C for *III*.

Figure 6.13b shows the equivalent borehole wall temperature profiles along the lengths of the GHEs for the FEA and proposed model. According to results in Table 6.6, the difference between FEA and proposed method for each equivalent borehole was preserved, and were similar to the differences in the average temperature, being  $-0.24$ ,  $-0.24$  and  $-0.23$  °C for boreholes *I*, *II* and *III*, respectively. A small difference was observed at all equivalent boreholes, top and bottom, equal to  $-0.22$  °C on both parts.

## 6.5 Conclusions

This paper presented a novel approach to the study of heat transfer in a field of thermally interacting GHEs where the heat capacity effects of the fluid, grout and soil are included. In the proposed method, the heat transfer inside the GHE is studied by the transient multipole expansion and coupled with the outside of the GHE by penalizing the interior solution with the equivalent borehole method to include the interactions between the GHEs. The advection inside the pipes is modeled by the energy balance along the pipes and discretized using a finite difference scheme. The method drastically reduces the dimensions of the system of equations due to the use of the equivalent borehole method to limit the number of modeled boreholes.

The main contributions of this paper are listed below:

- The method is able to be used in efficient short-term simulations by extending the transient multipole expansion [143] with an efficient coefficient updating scheme to compute fluid and GHE temperatures.
- It is no longer necessary to separate the solutions for short- and long-term effects as done by some researchers [18, 144, 145], since the heat extraction rates are calculated by the extension of the transient multipole expansion; therefore, the transition between time scales is done naturally by the approaching exact solution. Additionally, no condition is assumed at the borehole wall.
- Calculation times show that it is possible to perform computationally efficient simulations, even when both short- to long-term effects are included. The majority of this calculation time is due to the initialization (210 s on every simulation). The initializa-

tion time for the multipole method is independent of the time step and the number of boreholes. The initialization time for the equivalent borehole method is only weakly dependent on the number of boreholes and the number of time steps. The simulations for Beier's experiment, the 10-year borefield simulation and the 7-day borefield simulation were done in 4 s, 100 s and 16 s, respectively.

The method was first validated against experimental data provided by Beier et al. [155] for a single GHE and against an FEA simulation of the same experiment. The maximum errors for the inlet fluid temperature, outlet fluid temperature and average borehole wall temperature were 0.556, 0.519 and 0.253 °C, respectively, when compared to the experimental data; and 0.317, 0.317 and 0.270 °C, respectively, when compared to the FEA method. The validation showed that the proposed model compares well with the FEA method, and that both methods compare favorably with the experiment. Differences between the proposed method and the FEA method were expected, since the two methods use different models for the interiors of the GHEs. A 10-year simulation of a field of 24 GHEs was then presented to evaluate the long-term accuracy of the proposed method when compared to the FEA method. A 10 year period was simulated with a 1 h time step, followed by a 7-day period with a time step of 1 min to evaluate the short-term accuracy of the proposed method in the context of long-term simulations. For the 10-year period, the last year presented maximum and minimum differences with the FEA method of 0.18 and  $-0.39^{\circ}\text{C}$ , respectively, for both the inlet and outlet fluid temperatures. For the 7-day period, the maximum and minimum differences with the FEA method were  $-0.24$  and  $-0.46^{\circ}\text{C}$ , respectively, for both the inlet and outlet fluid temperatures.

The method is not restricted to applications where the GHEs are connected in parallel, but could also be extended to consider series connections between the boreholes by modifying the model in Section 6.3.3. The method could also be extended to include stratified solutions for anisotropic soils, adapting, for example, the solution by Abdelaziz et al. [74]. Additionally, by specific modifications of the FLS solution, the method could include effects such as groundwater flow by making use of proposed solutions such as the moving infinite line source (MILS) by Diao et al. [88], the moving finite line source (MFLS) by Molina-Giraldo et al. [95] or the stratified MFLS by Luo et al. [104]. This will, however, require future work to adapt the equivalent borehole method to consider groundwater flow during the clustering process.

## 6.6 Appendix A: Load aggregation

The temporal superposition process described in Equation (6.22), repeated here, is instead solved using a load aggregation algorithm:

$$\Delta \bar{T}_{b,\mathcal{I},u}^n = \frac{1}{2\pi k_s} \sum_{\mathcal{J}=1}^{\mathcal{G}} \sum_{v=1}^{n_s} \sum_{p=1}^n Q_{\mathcal{J},v}^p \left( \bar{h}_{\mathcal{I}\mathcal{J},uv}(t^n - t^{p-1}) - \bar{h}_{\mathcal{I}\mathcal{J},uv}(t^n - t^p) \right) \quad (6.36)$$

The load aggregation algorithm presented by Claesson and Javed [158] is used. The load history is discretized in time using geometrically expanding cells:

$$\Delta \tau^k = \Delta t \cdot 2^{\lfloor (k-1)/n_c \rfloor} \quad (6.37a)$$

$$\tau^k = \sum_{p=1}^k \Delta \tau^p \quad (6.37b)$$

where  $\Delta t$  is the width of the first aggregation cell (equal to the simulation time step),  $n_c$  is the number of cells per aggregation level, and  $\lfloor \cdot \rfloor$  is the floor operator. Cells are generated until last value  $\tau^k$  is larger than the maximum simulation time.

Each aggregated load contributes to the average borehole wall temperature for each segment as follows:

$$\Delta \bar{T}_{b,\mathcal{I},u}^n = \frac{1}{2\pi k_s} \sum_{\mathcal{J}=1}^{\mathcal{G}} \sum_{v=1}^{n_s} \sum_{p=1}^{n_c} \overline{Q_{\mathcal{J},v}^{p,n}} \left( \bar{h}_{\mathcal{I}\mathcal{J},uv}(\tau^p) - \bar{h}_{\mathcal{I}\mathcal{J},uv}(\tau^{p-1}) \right) \quad (6.38)$$

where  $\overline{Q_{\mathcal{J},v}^{p,n}}$  are the aggregated loads in each cell  $p$  at a time  $t^n$ .

For  $p \geq 2$ , aggregated loads at a time  $t^n$  are calculated according to the aggregated loads on the previous time step  $t^{n-1}$ :

$$\overline{Q_{\mathcal{J},v}^{p,n}} = \frac{1}{2^{\lfloor (p-1)/n_c \rfloor}} \overline{Q_{\mathcal{J},v}^{p-1,n-1}} + \frac{2^{\lfloor (p-1)/n_c \rfloor} - 1}{2^{\lfloor (p-1)/n_c \rfloor}} \overline{Q_{\mathcal{J},v}^{p,n-1}} \quad (6.39)$$

The first aggregated load ( $p = 1$ ) has its value equal to the average load since the last time step. Here, loads are constant during a time step:

$$\overline{Q_{\mathcal{J},v}^{1,n}} = Q_{\mathcal{J},v}^n \quad (6.40)$$

## 6.7 Appendix B: Additional expressions for the transient multipole method

In addition to the expressions presented in Prieto and Cimmino [143], the proposed method requires the evaluation of the average temperatures at the pipe walls ( $\overline{T_{1,\mathcal{I}}}\big|_{r_q}$ ) and the average temperature at the borehole wall ( $\overline{T_{1,\mathcal{I}}}\big|_{r_b}$ ), along with their derivatives (e.g.,  $\frac{\partial \overline{T_{1,\mathcal{I}}}}{\partial \rho}\big|_{r_b} = \frac{1}{2\pi} \int_0^{2\pi} \frac{\partial T_{1,\mathcal{I}}}{\partial \rho}\big|_{r_b} d\phi$ ). Their evaluation necessitates expressions for averages and derivatives of the eigenfunctions ( $X_1$ ) for the homogeneous problem, and the average temperatures ( $T_{1,ss}$ ) and derivatives for the steady-state non-homogeneous problem.

For the homogeneous problem, the average and derivatives of the eigenfunction  $X_1$  at the pipe boundary ( $\partial\Omega_l$ ) are given by:

$$\begin{aligned} \overline{X_{1,\mathcal{I}}} &= \frac{1}{2\pi} \int_0^{2\pi} X_{1,\mathcal{I}} d\phi = \sum_{m=-M}^M \gamma_{m,\mathcal{I}}^0 J_m(\lambda_{1,\mathcal{I}} l_{0l}) e^{im\theta_{0l}} J_0(\lambda_{1,\mathcal{I}} r_l) \\ &\quad + \gamma_0^l H_0^{(1)}(\lambda_{1,\mathcal{I}} r_l) \\ &\quad + \sum_{j=1, j \neq l}^N \sum_{m=-M}^M \gamma_{m,\mathcal{I}}^j g_{m,\mathcal{I}} \end{aligned} \quad (6.41a)$$

$$\begin{aligned} \frac{\partial \overline{X_{1,\mathcal{I}}}}{\partial \rho}\bigg|_{r_l} &= \lambda_{1,\mathcal{I}} \sum_{m=-M}^M \gamma_{m,\mathcal{I}}^0 J_m(\lambda_{1,\mathcal{I}} l_{0l}) e^{im\theta_{0l}} J'_0(\lambda_{1,\mathcal{I}} r_l) \\ &\quad + \lambda_{1,\mathcal{I}} \gamma_0^l H_0'^{(1)}(\lambda_{1,\mathcal{I}} r_l) \\ &\quad + \lambda_{1,\mathcal{I}} \sum_{j=1, j \neq l}^N \sum_{m=-M}^M \gamma_{m,\mathcal{I}}^j g'_{m,\mathcal{I}} \end{aligned} \quad (6.41b)$$

where

$$g_{m,\mathcal{I}} = \begin{cases} J_m(\lambda_{1,\mathcal{I}} l_{jl}) e^{im\theta_{jl}} H_0^{(1)}(\lambda_{1,\mathcal{I}} r_l) & \text{if } l_{jl} < r_l \\ H_m^{(1)}(\lambda_{1,\mathcal{I}} l_{jl}) e^{im\theta_{jl}} J_0(\lambda_{1,\mathcal{I}} r_l) & \text{if } l_{jl} > r_l \end{cases} \quad (6.42a)$$

$$g'_{m,\mathcal{I}} = \begin{cases} J_m(\lambda_{1,\mathcal{I}} l_{jl}) e^{im\theta_{jl}} H_0'^{(1)}(\lambda_{1,\mathcal{I}} r_l) & \text{if } l_{jl} < r_l \\ H_m^{(1)}(\lambda_{1,\mathcal{I}} l_{jl}) e^{im\theta_{jl}} J'_0(\lambda_{1,\mathcal{I}} r_l) & \text{if } l_{jl} > r_l \end{cases} \quad (6.42b)$$

At the borehole wall boundary ( $\partial\Omega_b$ ):

$$\begin{aligned}\overline{X_{1,\mathcal{I}}} &= \gamma_{0,\mathcal{I}}^0 J_0(\lambda_{1,\mathcal{I}} r_b) \\ &+ \sum_{j=1}^N \sum_{m=-M}^M \gamma_{m,\mathcal{I}}^j J_m(\lambda_{1,\mathcal{I}} l_{j0}) e^{im\theta_{j0}} H_0^{(1)}(\lambda_{1,\mathcal{I}} r_b)\end{aligned}\quad (6.43a)$$

$$\begin{aligned}\left. \frac{\partial \overline{X_{1,\mathcal{I}}}}{\partial \rho} \right|_{r_b} &= \lambda_{1,\mathcal{I}} \gamma_{0,\mathcal{I}}^0 J_0'(\lambda_{1,\mathcal{I}} r_b) \\ &+ \lambda_{1,\mathcal{I}} \sum_{j=1}^N \sum_{m=-M}^M \gamma_{m,\mathcal{I}}^j J_m(\lambda_{1,\mathcal{I}} l_{j0}) e^{im\theta_{j0}} H_0'^{(1)}(\lambda_{1,\mathcal{I}} r_b)\end{aligned}\quad (6.43b)$$

For the steady-state non-homogeneous problem, the average and derivatives of the multipole expansion at the pipe boundary ( $\partial\Omega_l$ ) are given by:

$$\overline{T_{1ss,\mathcal{I}}} = \alpha_{0,\mathcal{I}} + \gamma_{0,\mathcal{I}}^l \ln r_l + \sum_{j=1, j \neq l}^N (\gamma_{0,\mathcal{I}}^j g_{j,\mathcal{I}}) \quad (6.44a)$$

$$\left. \frac{\partial \overline{T_{1ss,\mathcal{I}}}}{\partial \rho} \right|_{r_l} = \gamma_{0,\mathcal{I}}^l \frac{1}{r_l} + \sum_{j=1, j \neq l}^N (\gamma_{0,\mathcal{I}}^j g'_{j,\mathcal{I}}) \quad (6.44b)$$

where

$$g_{j,\mathcal{I}} = \begin{cases} \ln(l_{jl}) & \text{if } l_{jl} > r_l \\ \ln(r_l) & \text{if } l_{jl} < r_l \end{cases} \quad (6.45a)$$

$$g'_{j,\mathcal{I}} = \begin{cases} 0 & \text{if } l_{jl} > r_l \\ \frac{1}{r_l} & \text{if } l_{jl} < r_l \end{cases} \quad (6.45b)$$

$$(6.45c)$$

At the borehole wall boundary ( $\partial\Omega_b$ ):

$$\overline{T_{1ss,\mathcal{I}}} = \alpha_{0,\mathcal{I}} + \sum_{j=1}^N \left\{ \gamma_{0,\mathcal{I}}^j (\ln r_b) \right\} \quad (6.46a)$$

$$\left. \frac{\partial \overline{T_{1ss,\mathcal{I}}}}{\partial \rho} \right|_{r_b} = \sum_{j=1}^N \gamma_{0,\mathcal{I}}^j / r_b \quad (6.46b)$$

## 6.8 Funding

This study is funded by the Natural Sciences and Engineering Research Council of Canada (NSERC) [grant number: RGPIN-2018-04471].



## CHAPTER 7 ARTICLE 4: TRANSIENT HEAT TRANSFER IN GROUND HEAT EXCHANGERS UNDER GROUNDWATER FLOW

**Authors:** Carlos Prieto and Massimo Cimmino

**Article presented at the conference:** *International Ground Source Heat Pump Association (IGSHPA) Research Track*, December 2022, Las Vegas, NV, USA

**Date of publication:** 6 December 2022

### 7.1 Abstract

An analytical solution for the transient heat transfer under groundwater flow for ground heat exchangers (GHEs) is presented. The method is an extension of the transient multipole expansion that describes the transient heat transfer as a pure conduction phenomenon inside and around a GHE including arbitrarily positioned pipes in the grout, coupling an irrotational and incompressible potential field in the ground with constant far-field velocity. The method does not rely on the supposition that groundwater flows through the GHE but instead moves around it. The method is validated against a finite element analysis model comparing the borehole wall temperature for two cases considering different single U-tube pipes position. It is shown that the thermal resistances inside the GHE do not respect the general symmetry condition ( $R_{ij} \neq R_{ji}$  and  $R_{ii} \neq R_{jj}$ ) as opposed to the pure conduction problem.

### 7.2 Introduction

One of the main components of ground-coupled heat pump (GCHP) systems are ground heat exchangers (GHEs) which allow heat transfer between the building and the ground. In many applications the heat transfer between the GHE and the ground can be treated as pure heat conduction due to diffusion in the ground. However, there are cases where the impact of groundwater flow on the heat transfer process is significant. When groundwater is present, the heat transfer process is given by three effects: conduction in the ground, conduction in the groundwater and advection by groundwater. Current analytical models consider that the fluid within the ground moves unidirectionally through the GHE and not around it. This allows the classical heat conduction models such as infinite/finite line sources (ILS/FLS) [62, 67] and cylindrical heat source (CHS) [20] to be extended to their analogs when groundwater is present resulting in the moving infinite/finite line sources (MILS/MFLS) [88, 95] and moving cylindrical heat source (MCHS) [103]. These models have been used to study the response

between the ground and the periphery of the GHE due to the presence of groundwater, finding that when the groundwater velocity increases, the average borehole wall temperature decreases and thus the average temperature of the circulating fluid decreases (in cooling mode) [87, 96, 102];. However, how diffusion-advection of groundwater flow moving around GHE affects the heat transfer between the circulating fluid in the pipes and the borehole wall due to grout diffusion has not been studied, as well as whether the position of the pipes plays an important role in the overall heat transfer.

This paper presents a new analytical solution for the heat transfer problem that relates the groundwater flowing around the GHE by extending the transient multipole expansion for pure conduction presented by Prieto and Cimmino [143] in which any number of pipes could be placed inside the GHE. The groundwater model is reduced from diffusion-advection to a diffusion-reaction model using a special change of variable and coefficient simplification for the reaction term. The average borehole wall temperature for two different pipe positions of a single U-tube is calculated and compared with a finite element analysis (FEA) model to validate the present solution. Thermal resistances are calculated to understand how the pipes position impacts the overall thermal response of the GHE.

### 7.3 Mathematical Model

Figure 7.1 shows a top view of a GHE containing two pipes  $(\partial\Omega_i, \partial\Omega_j)$  arbitrarily positioned  $(O_i, O_j)$  within the grout  $(\Omega_1)$  and bounded by the borehole wall  $(\partial\Omega_b)$  with respect to the ground  $(\Omega_2)$ . The heat-carrier fluid inside the pipes has a constant temperature  $(T_{f_i})$  at each pipe  $i$ . The geometrical parameters of the GHE are the borehole wall radius  $(r_b)$  and the outer pipe radius  $(r_i)$  at each pipe  $i$ . The thermal properties of the grout and the ground are considered isotropic, constant, and homogeneous.  $k_b, k_s$  are the thermal conductivities of grout and ground, and  $\alpha_b, \alpha_s$  are the thermal diffusivities of the grout and ground, respectively. The ground has a constant porosity  $(\epsilon)$  that allows groundwater to pass through with constant volumetric heat capacity  $(\rho c_p)_f$  and thermal conductivity  $(k_f)$  through the whole ground domain. The ground is considered as a semi-infinite domain and extends to  $r_e \rightarrow \infty$ .



field with constant far-field velocity is then:

$$\vec{u} = u_\infty \left(1 - \frac{r_b^2}{\rho^2}\right) \cos \phi \widehat{e}_\rho - u_\infty \left(1 + \frac{r_b^2}{\rho^2}\right) \sin \phi \widehat{e}_\phi = u_\rho \widehat{e}_\rho + u_\phi \widehat{e}_\phi \quad (7.3)$$

where  $\widehat{e}_\rho$  and  $\widehat{e}_\phi$  are unitary vectors in the radial and tangential directions, respectively. The potential field is then  $\psi = u_\infty \left(1 + \frac{r_b^2}{\rho^2}\right) \rho \cos \phi$ .

The boundary and initial conditions of the advection-diffusion equation (Equation (7.1)) are given by:

$$-\beta_k r_k \left. \frac{\partial T_1}{\partial \rho} \right|_{r_k} + T_1|_{r_k} = T_{f_k} \text{ on } \partial\Omega_k \quad (7.4a)$$

$$T_1|_{r_b} = T_2|_{r_b} \text{ on } \partial\Omega_b \quad (7.4b)$$

$$-k_b \left. \frac{\partial T_1}{\partial \rho} \right|_{r_b} = -k_{s,eff} \left. \frac{\partial T_2}{\partial \rho} \right|_{r_b} + [(\rho c_p)_f u_r T_2]|_{r_b} \text{ on } \partial\Omega_b \quad (7.4c)$$

$$T_2|_{r_e \rightarrow \infty} = T^0 \text{ on } \partial\Omega_e \quad (7.4d)$$

$$T_i(\rho, \phi, 0) = T^0 \text{ in } \Omega_1 \cup \Omega_2 \quad (7.4e)$$

Equation (7.4a) corresponds to a Robin boundary condition for each pipe  $k$  with constant fluid temperature  $T_{f_k}$ , where  $\beta_k = 2\pi k_b R_k$  is the dimensionless fluid-to-outer wall pipe thermal resistance and  $R_k$  the fluid-to-outer wall pipe thermal resistance. Equations (7.4b) and (7.4c) describe the continuity conditions for temperature and heat flux, respectively. Here, it is important to mention that Equation (7.4c) is different from the ones encountered in the literature since the dissipation term,  $[(\rho c_p)_f u_r T_2]|_{r_b}$ , is included. In this case, this term is equal to zero since the radial velocity at the borehole wall is 0 due to non-slip condition. Equations (7.4d) and (7.4e) are the far-field temperature and initial temperature, which are both equal to the undisturbed ground temperature  $T^0$ .

### 7.3.2 Groundwater transient multipole expansion

The resolution of the problem defined by Equations (7.1) and (7.4) is based on the methodology proposed in Prieto and Cimmino [143], which separates the heat transfer model as the sum of two subproblems, in this case: a) transient advection-diffusion equation with homogeneous boundary conditions ( $T_{i,h}$ ), and b) steady-state advection-diffusion equation with non-homogenous boundary conditions ( $T_{i,ss}$ ). The following change of variable is introduced to relate the potential field  $\psi$  with the temperature field:

$$T_{i,h} = \Gamma_{i,h} e^{\frac{1}{2\alpha_{s,eff}} \left( \frac{(\rho c_p)_f}{(\rho c_p)_{s,eff}} \right) H(\rho - r_b) \psi} = \Gamma_{i,h} e^{f(\rho, \phi)} \quad (7.5a)$$

$$T_{i,ss} - T^0 = \Gamma_{i,ss} e^{\frac{1}{2\alpha_{s,eff}} \left( \frac{(\rho c_p)_f}{(\rho c_p)_{s,eff}} \right) H(\rho - r_b) \psi} = \Gamma_{i,ss} e^{f(\rho, \phi)} \quad (7.5b)$$

The mathematical model for  $T_{i,h}$  is reduced to a diffusion-reaction model and defined as:

$$\frac{\partial \Gamma_{i,h}}{\partial t} + H(\rho - r_b) \left( \frac{(\rho c_p)_f}{(\rho c_p)_{s,eff}} \right)^2 \left( \frac{u_\rho^2 + u_\phi^2}{4\alpha_i} \right) \Gamma_{i,h} = \alpha_i \nabla^2 \Gamma_{i,h} \quad (7.6a)$$

$$-\beta_k r_k \frac{\partial \Gamma_{1,h}}{\partial \rho} \Big|_{r_k} + \Gamma_{1,h} |_{r_k} = 0 \text{ on } \partial \Omega_k \quad (7.6b)$$

$$\Gamma_{1,h} |_{r_b} = \Gamma_{2,h} |_{r_b} e^{f(r_b, \theta)} \text{ on } \partial \Omega_b \quad (7.6c)$$

$$-k_b \frac{\partial \Gamma_{1,h}}{\partial \rho} \Big|_{r_b} = -k_{s,eff} \frac{\partial \Gamma_{2,h}}{\partial \rho} \Big|_{r_b} e^{f(r_b, \theta)} \text{ on } \partial \Omega_b \quad (7.6d)$$

$$\Gamma_{2,h} |_{r_e \rightarrow \infty} = 0 \text{ on } \partial \Omega_e \quad (7.6e)$$

$$\Gamma_{i,h}(\rho, \phi, 0) = (T^0 - T_{i,ss}) / e^{f(\rho, \phi)} \text{ in } \Omega_1 \cup \Omega_2 \quad (7.6f)$$

For  $T_{i,ss}$ , the problem is described as:

$$H(\rho - r_b) \left( \frac{(\rho c_p)_f}{(\rho c_p)_{s,eff}} \right)^2 \left( \frac{u_\rho^2 + u_\phi^2}{4\alpha_i} \right) \Gamma_{i,ss} = \alpha_i \nabla^2 \Gamma_{i,ss} \quad (7.7a)$$

$$-\beta_k r_k \frac{\partial \Gamma_{1,ss}}{\partial \rho} \Big|_{r_k} + \Gamma_{1,ss} |_{r_k} = T_{fk} - T^0 \text{ on } \partial \Omega_k \quad (7.7b)$$

$$\Gamma_{1,ss} |_{r_b} = \Gamma_{2,ss} |_{r_b} e^{f(r_b, \phi)} \text{ on } \partial \Omega_b \quad (7.7c)$$

$$-k_b \frac{\partial \Gamma_{1,ss}}{\partial \rho} \Big|_{r_b} = -k_{s,eff} \frac{\partial \Gamma_{2,ss}}{\partial \rho} \Big|_{r_b} e^{f(r_b, \phi)} \text{ on } \partial \Omega_b \quad (7.7d)$$

$$\Gamma_{2,ss} |_{r_e \rightarrow \infty} = 0 \text{ on } \partial \Omega_e \quad (7.7e)$$

An approximation of the reaction coefficient  $u_\rho^2 + u_\phi^2 = u_\infty^2 \left( 1 - \frac{2r_b^2}{\rho^2} \cos 2\phi + \frac{r_b^4}{\rho^4} \right) \approx K_{gw} u_\infty^2$  is proposed to simplify the model presented in Equations (7.6a) and (7.7a). This approximation is valid since  $u_r^2 + u_\theta^2$  has a maximum value of  $4u_\infty^2$  for  $\rho = r_b$ ,  $\phi = (2n + 1)\pi$  for  $n \in \mathbb{Z}$  and a minimum value of 0 for  $\rho = r_b$ ,  $\phi = n\pi$ . Moreover, when  $\rho$  is sufficiently large when compared with  $r_b$ , the value is  $u_\infty^2$ . It was found that  $K_{gw} = 1.6$  produces a good approximation.

Equation (7.6a) has a similar structure to those expressed in Prieto and Cimmino [143].

Thus, assuming that  $\Gamma_{i,h}$  is spatiotemporally separable as  $\Gamma_{i,h} = X_i(\rho, \phi) \tau(t)$  results in a Sturm-Liouville problem with  $\tau(t) = \exp\left(-(\lambda_i^j)^2 \alpha_i t\right)$  for unique  $j$  eigenvalues for each domain  $i$  denoted as  $\lambda_i^j$ . The continuity condition requires that  $\alpha_1 (\lambda_1^j)^2 = \alpha_2 (\lambda_2^j)^2$  must hold for all time  $t$ . Therefore, the problem  $X_i(\rho, \phi)$ , defined as the Helmholtz equation for the interior of the GHE (i.e.  $X_1$ ), has the same formulation as that of the transient multipole expansion for a point  $\mathbf{x}$  with coordinates related to a particular pipe center  $O_k$  given by  $\mathbf{x}_k = (\rho_k, \phi_k)$  and for the GHE center  $\mathbf{x}_0 = (\rho_0, \phi_0)$ :

$$X_1(\mathbf{x}; \lambda_1^j) = \sum_{l=-M}^M \gamma_l^0 J_l(\lambda_1^j \rho_0) e^{il\phi_0} + \sum_{k=1}^N \sum_{l=-M}^M \gamma_{l,j}^k H_l^{(1)}(\lambda_1^j \rho_k) e^{il\phi_k} \quad (7.8)$$

For the ground domain, the expansion for  $X_2$  is slightly different:

$$X_2(\mathbf{x}; \lambda_2^j) = \sum_{l=-M}^M \delta_l^0 H_l^{(1)}(\sigma_j \rho_0) e^{il\phi_0} \quad (7.9)$$

where  $\sigma_j^2 = (\lambda_2^j)^2 - u_\infty^2 \left(\frac{K_{qw}}{4\alpha_2^2}\right) \left(\frac{(\rho c_p)_f}{(\rho c_p)_{s,eff}}\right)^2$ , and  $J$  and  $H^{(1)}$  are the first kind Bessel and Hankel functions, respectively. The calculation of the eigenvalues is done by means of singular value decomposition (SVD), as done by Prieto and Cimmino [143]. The coefficients  $\gamma^0, \gamma^k, \delta^0$  are the coefficients that match the boundaries and calculated for each eigenvalue.

The full solution for  $T_{i,h}$  is given by a Fourier-Bessel expansion:

$$T_{i,h}(x, t) = \sum_{j=1}^{\infty} C_j X_i(x; \lambda_i^j) e^{-(\lambda_i^j)^2 \alpha_i t + f(\rho, \phi)} \quad (7.10)$$

where  $C_j$  are in this case:

$$C_j = \frac{\frac{k_b}{\alpha_b} \int_{\Omega_1} (T^0 - T_{2,ss}) \bar{X}_1 d\Omega_1 + \frac{k_{s,eff}}{\alpha_{s,eff}} \int_{\Omega_2} (T^0 - T_{2,ss}) \bar{X}_2 e^{2f(r_b, \phi) - f(\rho, \phi)} d\Omega_2}{\frac{k_b}{\alpha_b} \int_{\Omega_1} X_1 \bar{X}_1 d\Omega_1 + \frac{k_{s,eff}}{\alpha_{s,eff}} \int_{\Omega_2} X_2 \bar{X}_2 e^{2f(r_b, \phi)} d\Omega_2} \quad (7.11)$$

The coefficients expressed in Equation (7.11) are obtained by means of the quasi-orthogonal conditions of the Sturm-Liouville problem and using Green's second identity.

Similarly, for Equation (7.7a), the same procedure is done. For the grout, the same multipole

expansion presented in Prieto and Cimmino [143] is used:

$$\begin{aligned} \Gamma_{1,ss} = & \alpha_0 + \sum_{m=1}^h \left[ \alpha_m \left( \frac{\rho_0}{r_{max}} \right) \cos(m\phi_0) + \beta_m \left( \frac{\rho_0}{r_{max}} \right) \sin(m\phi_0) \right] \\ & + \sum_{k=1}^N \left\{ \gamma_0^k \ln \rho_k + \sum_{m=1}^h \left[ \gamma_m^k \left( \frac{\rho_k}{r_{min}} \right) \cos(m\phi_k) + \delta_m^k \left( \frac{\rho_k}{r_{min}} \right) \sin(m\phi_k) \right] \right\} \end{aligned} \quad (7.12)$$

For the ground, the multipole expansion is given by:

$$\Gamma_{2,ss} = \sum_{l=-h}^h \delta_l^0 K_l \left( u_\infty \left( \frac{\sqrt{K_{gw}}}{2\alpha_2} \right) \left( \frac{(\rho c_p)_f}{(\rho c_p)_{s,eff}} \right) \rho_0 \right) e^{il\phi_0} \quad (7.13)$$

where  $K$  is the modified Bessel function of the second kind of order  $l$  and  $\alpha, \beta, \gamma, \delta$  are the coefficients that match the boundaries which are different from the homogenous problem.

## 7.4 Results

The average borehole wall temperature ( $T_b$ ) is evaluated using the present method and FEA for 4 different far field velocities:  $u_\infty = 0, 10^{-6}, 10^{-5}, 10^{-4}$  m/s. Two cases are studied, with the same thermal properties and geometrical parameters shown in Table 1 but with different positioning of the pipes: (I) the pipes are positioned at  $O_1(-0.05, 0)$ ,  $O_2(0.05, 0)$ , and (II)  $O_1(0, 0.05)$ ,  $O_2(0, -0.05)$ . The FEA model for both cases is composed of 5504 nodes and 9906 triangular elements (second order Lagrange elements) with  $r_e = 55$  m. The parameters for the multipole expansion are set to  $M = 14$  and  $h = 30$ , doubling those shown in Prieto and Cimmino [143] due to the exponential term in the continuity conditions (Equations (7.6c)-(7.6d) and (7.7c)-(7.7d)), and the first 100 eigenvalues are used.

Table 7.1 GHE Parameters

Parameter	Value
Grout thermal conductivity	$k_b = 0.81 \text{ W/(mK)}$
Grout thermal diffusivity	$\alpha_b = 2.13 \times 10^{-7} \text{ m}^2/\text{s}$
Ground thermal conductivity	$k_s = 2.4 \text{ W/(mK)}$
Ground thermal diffusivity	$\alpha_s = 1.2 \times 10^{-6} \text{ m}^2/\text{s}$
Groundwater thermal conductivity	$k_f = 0.48 \text{ W/(mK)}$
Groundwater thermal capacity	$(\rho c_p)_f = 4.2 \times 10^6 \text{ J/(m}^3\text{K)}$
Borehole radius	$r_b = 0.075 \text{ m}$
U-tube pipe outer radius	$r_k = 0.021 \text{ m}$
Dimensionless fluid-to-outer pipe thermal resistance	$\beta_k = 0.480281$
Undisturbed ground temperature	$T^0 = 10 \text{ }^\circ\text{C}$
Porosity	$\epsilon = 0.2$
Shank spacing	$e = 0.05 \text{ m}$

Figure 7.2 shows the average borehole wall temperature calculated by the present method (dotted line) and the FEA method (solid line) for cases I and II for a period of 60000 s with a time-step equal to 60s considering the four different far-field velocities with fluid temperatures equal to  $T_{f_1} = T_{f_2} = 20 \text{ }^\circ\text{C}$  for both cases. Figure 2 also shows temperature contours for the final simulation time with  $u_\infty = 10^{-5} \text{ m/s}$ . As expected, when the far-field velocity increases the average borehole wall temperature decreases and reaches the quasi-steady-state condition earlier. The maximum absolute differences between the proposed method and the FEA appear at approximately 180 h (10740 s) with values of 0.105, 0.115, 0.117, 0.061  $^\circ\text{C}$  for case I and 0.090, 0.103, 0.106, 0.024  $^\circ\text{C}$  for Case II, for each far-field velocity  $u_\infty = 0, 10^{-6}, 10^{-5}, 10^{-4} \text{ m/s}$ , respectively. At the final simulation time, the maximum difference between the proposed method and the FEA is 0.010  $^\circ\text{C}$  for case I with  $u_\infty = 10^{-6} \text{ m/s}$ . The main reason for this discrepancy is the simplification in Equations (7.6a) and (7.7a) for the reaction coefficient. The relatively small errors show that the coefficient  $K_{gw}$  can be used to successfully simplify the problem without significant loss of accuracy. Figure 2 also shows that the borehole wall temperatures are different in cases I and II for the same far-field velocity when  $u_\infty \geq 10^{-5} \text{ m/s}$ . This implies that, under groundwater flow, the orientation of the U-tube influences the internal thermal resistances.



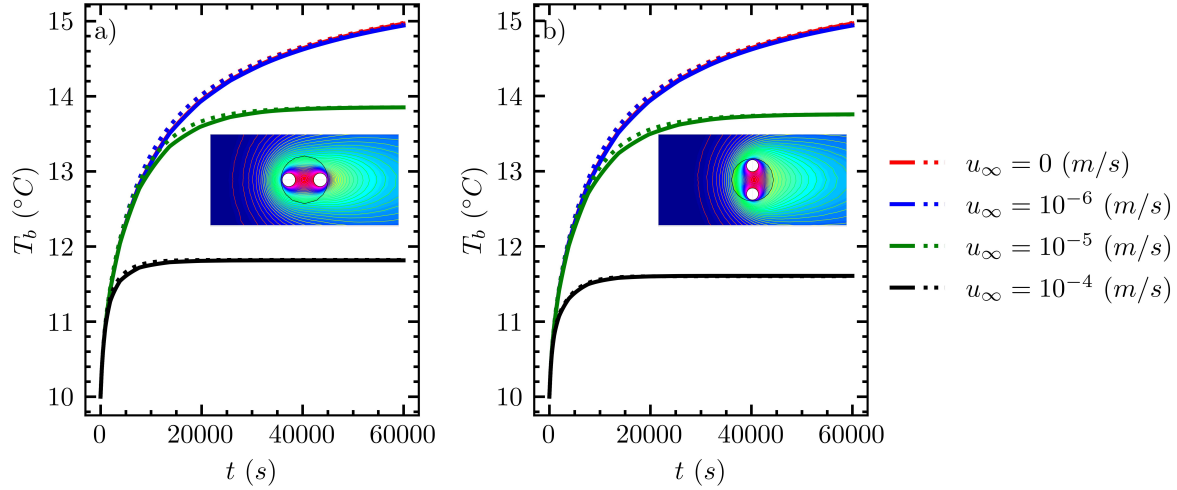


Figure 7.2 Average borehole wall temperature comparison between FEA (continuous line) and present method (discontinuous line) for 4 different far-field velocities: a) Case I and b) Case II

The internal thermal resistances are defined by:

$$T_{f1} - T_b = R_{11}q_1 + R_{12}q_2 \quad (7.14a)$$

$$T_{f2} - T_b = R_{21}q_1 + R_{22}q_2 \quad (7.14b)$$

where  $q_k = \frac{1}{R_k} (T_{fk} - \overline{T_1|_{r_k}})$  is the heat flow at each pipe  $k$ , with  $\overline{T_1|_{r_k}}$  the average outer-wall pipe temperature. Internal thermal resistances are generally symmetrical ( $R_{11} = R_{22}$  and  $R_{12} = R_{21}$ ) in the absence of groundwater flow when symmetrically positioned pipes are considered. To estimate the thermal resistances, two pairs of arbitrary constant fluid temperatures for both pipes are used to solve the system of equations defined by Equations (7.14). Figures 7.3 and 7.4 show the thermal resistances defined in Equation (7.14) for the two cases, with Figures 7.3a and 7.4a corresponding to  $u_\infty = 0 \text{ m/s}$ . The internal thermal resistances are symmetrical for this velocity. The thermal resistances calculated with the multipole method developed by Claesson and Hellström [18] for the quasi-steady-state condition (conduction problem) are  $R_{11} = R_{22} = 0.29 \text{ mK/W}$  and  $R_{12} = R_{21} = -0.029 \text{ mK/W}$  for both cases. Comparing these resistances with the final simulation time shown in Figure 7.3a and Figure 7.3a, the thermal resistances are  $R_{11} = R_{22} = 0.285 \text{ mK/W}$  and  $R_{12} = R_{21} = -0.027 \text{ mK/W}$ . As expected, thermal resistances are symmetrical and are in good agreement with the classical multipole method. There are small differences between the multipole method and the transient multipole expansion since the transient multipole has not reached steady state. When  $t \rightarrow \infty$ , the thermal resistances approach those calculated by Claesson and Hellström [18].

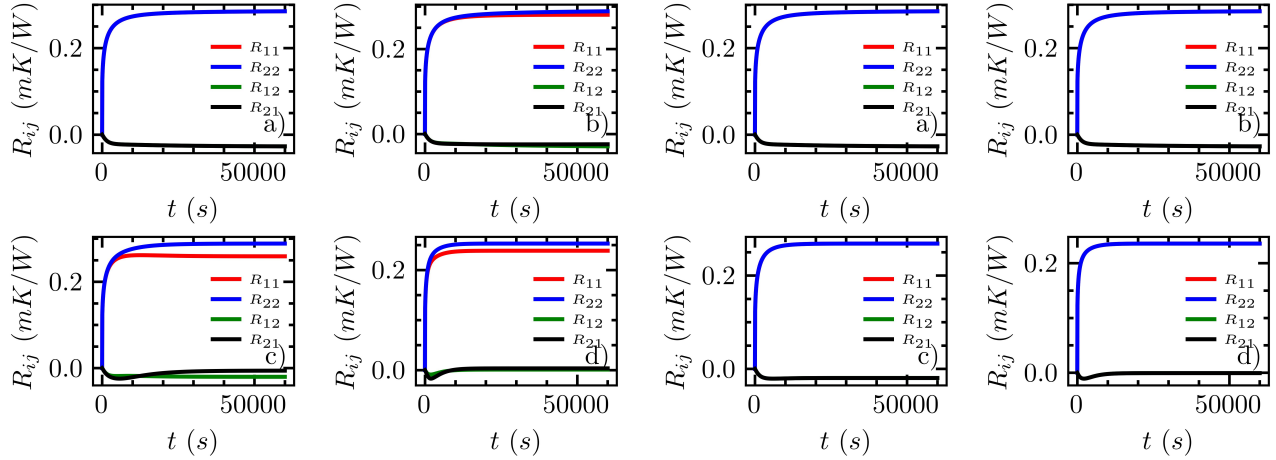


Figure 7.3 Internal thermal resistances for case I with different far-field velocities: a)  $u_\infty = 0$  m/s, b)  $u_\infty = 10^{-6}$  m/s, c)  $u_\infty = 10^{-5}$  m/s and d)  $u_\infty = 10^{-4}$  m/s

Figure 7.4 Internal thermal resistances for case II with different far-field velocities: a)  $u_\infty = 0$  m/s, b)  $u_\infty = 10^{-6}$  m/s, c)  $u_\infty = 10^{-5}$  m/s and d)  $u_\infty = 10^{-4}$  m/s

As shown on Figures 7.3b-d for case I, the thermal resistances decrease when the far-field velocity increases, and the symmetry tends to break down at higher far-field velocities. This is not the case on Figures 7.4b-d for case II where the symmetry holds at all far-field velocities. At the final time, the values of the thermal resistances are  $R_{11} = 0.281, 0.259, 0.239$ ,  $R_{22} = 0.289, 0.289, 0.253$ ,  $R_{12} = -0.029, 0.020, 0.0$ ,  $R_{21} = -0.024, -0.006, 0.003$  for case I, and  $R_{11} = R_{22} = 0.285, 0.267, 0.234$ ,  $R_{12} = R_{21} = -0.027, -0.02, -0.001$  for case II, respectively, for each far-field velocity  $u_\infty = 10^{-6}, 10^{-5}, 10^{-4}$  m/s.

On Figures 7.3c-d and 7.4c-d, it is observed that the resistances  $R_{11}$  and  $R_{22}$  are not equal for case I, however they are equal for case II. This interesting result shows that even though the pipes are symmetrically distributed within the GHE, the symmetry condition does not hold in general. The fact that case II does present symmetry is because the far-field velocity is perpendicular to the spacing between the pipes. This allows using Green's identities to show that for this case the symmetry condition holds. It is also interesting to observe the behavior of thermal resistances  $R_{12}$  and  $R_{21}$  for both cases I and II. Figures 7.3d and 7.4d show that these resistances tend to 0 as the velocity increases. In both cases, this behaviour on thermal resistances is explained in that the heat transfer is due to heat exchange between each pipe and the borehole wall rather than the pipes transferring heat to each other, therefore the groundwater is dissipating heat from the pipes.

## 7.5 Conclusions

A new analytical method for the study of conduction-advection heat transfer inside and around of a GHE was presented. The method allows including a potential field in the ground flowing around the GHE, in this case incompressible and irrotational. No simplification inside the GHE is made, allowing to place different pipe positions. Also, when posing the complete mathematical model, a new boundary condition is considered in Equation 4.3 which takes into account the energy dissipation by means of the groundwater advection.

As a first validation, the method was compared with a high-fidelity FEA simulation, which showed that the present method possesses good agreement despite making an approximation in the reduction of the diffusion-reaction problem by introducing a  $K_{gw}$  coefficient. With this new analytical method, it was shown that the position of the pipes slightly changes the temperature around the GHE. The observation of the temperature around the borehole wall showed that the thermal resistances coming from the linear conduction problem inside the GHE are not symmetric ( $R_{ii} \neq R_{jj}$  and  $R_{ij} \neq R_{ji}$ ). It was found that when the groundwater velocity is sufficiently large, the heat transfer problem is one-dimensional, meaning that to calculate the heat flux of each pipe it is sufficient to know the temperature of each pipe and the average borehole temperature as  $R_{ij} \rightarrow 0$  for  $i \neq j$ .

With these results, the use of methods such as thermal resistance capacitance (TRC) methods should be revisited when including groundwater flow, as the delta-circuit is not always valid. Extending the method from 2D to 3D including thermal interactions between boreholes and time-dependent fluid temperatures could be done using a segmented MFLS solution [101] and a modified equivalent borehole method [153] with a coefficient updating scheme as done in Prieto and Cimmino [143, 159].

## 7.6 Acknowledgment

This study is funded by the Natural Sciences and Engineering Research Council of Canada (NSERC) [grant number: RGPIN-2018-04471].

## CHAPTER 8 GENERAL DISCUSSION

This thesis presented a set of analytical and semi-analytical models that allow the study of the transient heat conduction phenomenon and the effects of groundwater flow. These solutions consider short- and long-term effects by including transient multipole expansion in the interactions and axial effects in a field of thermally interacting GHEs, considering the advection in the pipes within each GHE. The transient multipole expansion was extended to account for the impact that the groundwater has as it moves around the GHE.

Models for the interior of the borehole enable the calculation of heat transfer rates as a function of fluid temperatures inside the borehole (and vice-versa). Computationally efficient steady-state methods, such as the steady-state multipole method, were already available. However, steady-state methods are only valid on long time steps of a few hours or more. It is possible to formulate accurate transient models for the interior of the borehole using numerical methods (such as FEM, FDM or FVM). However, these methods require more significant computational effort, thus limiting their viability in GHE simulations. The two most popular approaches are equivalent pipe methods and TRC methods. Since they are usually constructed from steady-state thermal resistances, they lead to accurate results in long time steps. The thermal capacity of the borehole materials is allocated in an annular region (in the case of equivalent pipe methods) or at arbitrarily positioned nodes (in the case of TRC methods), and thus available models only approximate the short time step response of the GHE. Chapter 4 presents an exact solution to the transient heat conduction on a cross-section of a GHE, thus solving the issue of current approximate short-term solutions. This chapter obtained the analytical solution called transient multipole expansion, which considers an arbitrary distribution of  $N$  pipes within the GHE, thus overcoming the drawbacks mentioned above regarding models that approximate the interior of a GHE. The complete transient heat transfer problem allows a superposition of particular solutions in their homogeneous and non-homogeneous parts, which allows the study of the short-term effects within the GHE. The eigenvalues associated with the Sturm-Liouville problem of the homogeneous part were validated with those found in the literature and the solution for the steady state. This chapter also presented a way to update the coefficients from the Sturm-Liouville problem for the inclusion of time-dependent fluid temperature and extended via the Duhamel's theorem (see Appendix A), meaning that it is possible to estimate the temperatures increments given heat loads. The transient multipole expansion was validated by comparing it against an FEA method for two cases, one pipe positioned at the center of the GHE and two symmetrically positioned in the grout.

To extend the analytical solution presented in Chapter 4, it was necessary to develop a new method that would include axial effects and GHE interaction. Models that account for axial effects are constructed by coupling suitable analytical solutions (e.g.  $g$ -functions) or numerical models for the exterior of the GHE to a model of the borehole interior. However, when studying large fields of thermally interacting GHEs, the calculation of the thermal response becomes computationally burdensome. For this purpose, Chapter 5 develops a novel approach that allows the inclusion of such effects by grouping boreholes having similar borehole wall temperature and heat extraction rates, called equivalent boreholes. The method was based on a hierarchical clustering algorithm; it is possible to cluster completely considering linkage related to the maximum temperature dissimilarity between two boreholes. With a cut-off criterion in the dendrogram, it is possible to find the minimum number of clusters by proceeding to increase by one precision group to increase its precision. The method was validated for several cases, from typical configurations (i.e. Rectangular, L, U, box-shaped) to arbitrarily positioned pipes with or without an internal constraint. The method resulted in a substantial improvement in  $g$ -function computation, allowing one to compute the  $g$ -function of a field of 1024 randomly positioned boreholes in a matter of seconds. This was not possible with the known methods for personal computers, thus allowing the new method to be used not only in design but also in the control and performance of GCHP installations. The complete validation was done using current state-of-the-art methods available in the literature, showing that the equivalent borehole method can accurately predict the thermal response in fields of geothermal boreholes. Furthermore, the equivalent borehole method is fully implemented in the current `pygfunction` (v2.2) library [160], in which the computational time was also further reduced: the  $g$ -function estimation is performed in 0.245 seconds over 30 time steps for a thermally interacting field of 400 randomly positioned boreholes.

Cimmino [77] has shown that the distribution of fluid temperatures and heat transfer rates along the GHE affect the long-term response, so the interior model needs to be considered when initializing the exterior model. Since the thermal capacity of the borehole modifies how fluid temperatures and heat transfer rates are distributed, short-time step effects may change the thermal response for an extended period. Thus, based on the methods of Chapters 4 and 5, it was possible to extend the transient multipole method from 2D to 3D. Chapter 6 penalizes the transient multipole expansion to include thermal interactions and axial temperature distributions in geothermal fields without a boundary condition at the borehole wall. The coupling was done by a uniform discretization of the GHE into segments, following the suggestion of Cimmino and Bernier [73], the use of equivalent boreholes and the inclusion of the advection phenomenon in the pipes for the fluid temperature estimation employing a Finite Difference scheme. Compared to existing methods, no temporal separation of the so-

lution outside and inside the GHE is required since an approaching exact analytical solution performs the coupling. To validate this extension, data found in the literature were used to verify the accuracy of the short-term effects [155] as well as to compare them with an FEA model based on existing methodologies with particular modifications [83,84]. We also proceeded to validate the response of the thermal interactions between the boreholes as well as the axial temperature distribution for a multi-annual simulation over 10 years following a period of 7-days for a field of 24 boreholes located in a rectangular array. This validation was done using an FEA model in two stages; the first 10 years was done using a time step of 1 h while the following 7-day period used a time step of 1 min. Because of this, it was possible to include both short- to long-term effects. This extension was accurate given a maximum absolute difference of 0.5 °C between FEA and the proposed method for the fluid temperatures in the 7 days.

Groundwater advection has been shown to impact the ground temperature response around GHEs. The available works in the literature focused on heat transfer in the ground and, for the most part, used already available thermal resistance methods to model heat transfer inside the borehole. As it has been shown, the formulation of thermal resistance networks relies on the solution of the heat conduction equation inside and outside the GHE. Groundwater flow modifies the temperature field around the GHE and thus impacts the borehole thermal resistance and the long- and short-time step responses of GHEs. Discussed analytical models consider a line source as a representation of GHE, such as the moving line source model. They cannot describe the thermal behaviour near-field of GHE by considering that a centric line in the borehole emanates heat which is different from a real configuration of the borehole. When this assumption is considered, the borehole wall temperature differs from a model that considers a real configuration inside GHE. As opposed to existing methods in the literature, the groundwater movement is around the GHE and does not pass through. This allows the use of an incompressible and irrotational model for groundwater flow. The transient multipole method can be modified to include such an effect, and shown in Chapter 7. The same methodology of superposition of solutions presented in Chapter 4 was used, employing a particular variable change that allows transforming the diffusion-advection model into a diffusion-reaction model. This diffusion-reaction model is separable in space and time, resulting in a Sturm-Liouville problem. In addition, a reaction term approximation was proposed to simplify the problem mathematically. This simplification showed that the method could accurately estimate the temperature profile inside and outside the GHE. This methodology showed that the position of the pipes inside the GHE plays a crucial role. Two cases were simulated with different velocities and pipe positions. It was shown that at higher velocities, the location of the pipes changes the thermal response inside the GHE. In addition,

although the pipes may be symmetrically positioned, the reciprocal thermal resistances from the heat transfer problem are not the same, as opposed to the pure conduction phenomenon. This means that TRC methods should be revisited when including groundwater flow. For mathematical completeness, the proof of Fourier-Bessel coefficients is done in Appendix B, and extra formulas are shown in Appendix C.

## CHAPTER 9 CONCLUSION AND RECOMMENDATIONS FOR FUTURE WORK

This thesis presented different contributions that allow the simulation of short- to long-term effects when multiple pipes are considered within the GHE and the effects of thermal interaction between various GHEs are present. In addition, the effect of groundwater flow moving around the GHE was modelled and assessed. As such, the contributions can be listed as follows:

- An exact approaching solution to study the transient heat transfer at the interior and exterior of a GHE containing multiple pipes in the grout.
- An equivalent borehole method to study the thermal interactions and axial effects between multiple boreholes positioned in the soil.
- A full-time-scale semi-analytical solution that enables the calculation of the fluid temperatures inside the pipes of multiple parallel-connected GHEs.
- An analytical solution to simulate the thermal response within the GHE when groundwater flow is moving around it.

With these contributions, the thermal modelling of GHEs can be done in a computationally efficient and approaching exact way. Therefore, this thesis fills the gap in the scientific literature regarding the analytical solution for studying in full the short- to long-effects of multiple boreholes. Also, the last takeaway is that TRC methods should be revisited when the groundwater is considered since the thermal response on the inside is different from the classical point of view (i.e. pure conduction).

### 9.1 Thesis limitations and future research

One of the main limitations of the present thesis is that the mathematical models are only used for grouted GHEs. If one wishes to use the current methodology to analyze water-filled GHE, simple modifications in the heat transfer problem's analytical solutions are insufficient. Although the mathematical model for the conduction heat transfer phenomenon for any number of pipes inside the GHE was solved analytically, proposing an exact solution, its computational implementation has interesting limitations. One of them is estimating and extracting eigenvalues utilizing singular value decomposition (SVD), which requires running



a broad spectrum of eigenvalues to estimate the real values. This leads to excessive computational time and requires most of the computational time for a typical simulation. In addition, the computation of the integrals needs computational effort and high expertise to stabilize the far-field boundary conditions. Finally, calculating the coefficients that match the boundaries for the steady-state problem produces an ill-posed problem that needs to be regularized by preconditioning.

When grouping boreholes into equivalent boreholes, it has been found that the number of groups generally varies between 3 to 5 for a large spectrum of random and regular arrangements. This can be considered a limitation since a hierarchical clustering algorithm does the clustering. This leads to the fact that although the boreholes have similar behaviour, the selection metric (i.e. complete linkage) does not consider whether the variations are small or large between two boreholes. Therefore, this method tends to overestimate the thermal response, as seen in this thesis. Although the method can analyze large arrays of geothermal fields containing thousands of boreholes, its validation is not straightforward since the techniques found in the literature are computationally demanding and makes it difficult to find reference results. For instance, the Beijing airport is said to have about 10 000 boreholes installed, and it is not possible to know if the method developed here can accurately predict the thermal response of this example.

Since the extension of the 2D to 3D method is based on both the transient multipole and equivalent borehole methods, it is evident that the same limitations are inherited. The main limitation of the present method lies in two parts: a) the calculation of the Fourier-Bessel coefficients at each time step and b) the direct coupling of the penalized solution with the advection model in the pipes. In the coefficient updating scheme, the time step plays an important role because if it is too small or too large, the solution tends to produce incorrect results. This is due to the construction of the Sturm-Liouville problem and its regularity in superimposing the solutions. However, it was found that the method works well for time steps of 1 min and 1 h. Similarly, the coupling between the discretized advection model and the complete solution using the penalty requires an iterative process that can be computationally unstable if the time step is not chosen appropriately. Although the advection model is implicit (i.e. always convergent) and requires the solution of a system of equations at each time step, this iterative method increases the computational consumption.

Finally, the extension of the transient multipole method to include groundwater moving around the GHE has limitations besides the ones inherited from the transient multipole method. The first is the assumption of groundwater movement as a potential flow, and its simplification that allows using a particular variable change that simplifies the problem for

an analytical solution. However, groundwater movement is based on more accurate models such as Darcy-Brinkman-Forchheim, thus making the transient multipole method not easily adaptable. Another limitation is the use of a term approximation in the diffusion-reaction model. Although the approximation term showed an excellent approximation for estimating average borehole wall temperature, its overall effect is unknown and should be studied further.

There are several things that this research opens up as a next project that can be studied in the future and are listed below:

- New computational techniques for eigenvalue extraction and integral computation should be adopted to improve the computational performance of the transient multipole method implementation.
- Extend the ideas of the equivalent borehole method when groundwater flow is included. This can be done by adopting ideas found in the literature, such as MILS, MFLS, or MCHS methods. Also, explore the impact of the selection metric on the overall clustering process.
- The semi-analytical method for 3D transient heat transfer could increase its capability by including both geothermal gradient effects and solutions in which the thermal properties change along the length of the borehole. Also, improve the iterative process for fluid temperature estimation by proposing a "one-shot" style model that allows explicitly building the system of equations to solve it in a single attempt rather than iterating over initial conditions.
- The groundwater transient multipole method can increase its capabilities by extending it to 3D following a methodology similar to that proposed in the semi-analytical solution for the 3D transient heat transfer. For this, it is necessary to initially extend the ideas of the equivalent borehole to include groundwater flow. Subsequently, it is required to adopt a new coefficient updating scheme for the groundwater flow case for estimating the time-dependent fluid temperatures. In addition, the short- and long-term groundwater effects could be studied in their entirety. Also, the effects of soil thermal properties, groundwater velocity, and axial effects could be studied.

## REFERENCES

- [1] S. A. Alkaff, S. C. Sim, and M. N. Ervina Efzan, “A review of underground building towards thermal energy efficiency and sustainable development,” *Renewable and Sustainable Energy Reviews*, vol. 60, pp. 692–713, 2016. [Online]. Available: <http://dx.doi.org/10.1016/j.rser.2015.12.085>
- [2] J. Lizana *et al.*, “Advanced low-carbon energy measures based on thermal energy storage in buildings: A review,” *Renewable and Sustainable Energy Reviews*, vol. 82, pp. 3705–3749, 2018. [Online]. Available: <http://dx.doi.org/10.1016/j.rser.2017.10.093>
- [3] J. Mohtasham, “Review article-renewable energies,” *Energy Procedia*, vol. 74, pp. 1289–1297, 2015. [Online]. Available: <http://www.sciencedirect.com/science/article/pii/S1876610215015428>
- [4] M. Soltani *et al.*, “A comprehensive review of geothermal energy evolution and development,” *International Journal of Green Energy*, vol. 16, no. 13, pp. 971–1009, 2019. [Online]. Available: <http://dx.doi.org/10.1080/15435075.2019.1650047>
- [5] S. Karytsas and H. Theodoropoulou, “Public awareness and willingness to adopt ground source heat pumps for domestic heating and cooling,” *Renewable and Sustainable Energy Reviews*, vol. 34, pp. 49–57, 2014. [Online]. Available: <http://dx.doi.org/10.1016/j.rser.2014.02.008>
- [6] J. Francisco Pinto and G. Carrilho da Graca, “Comparison between geothermal district heating and deep energy refurbishment of residential building districts,” *Sustainable Cities and Society*, vol. 38, pp. 309–324, 2018. [Online]. Available: <http://dx.doi.org/10.1016/j.scs.2018.01.008>
- [7] A. Zaradic, “Direct use geothermal projects state of the nation in canada 2018,” in *Transactions - Geothermal Resources Council*, vol. 42. Geothermal Resources Council, 2018, Conference Proceedings, pp. 1500–1514.
- [8] S. Gehlin, “Thermal response test: method development and evaluation,” PhD Thesis, Luleå University of Technology, 2002.
- [9] A. Bejan, *Convection Heat Transfer*, 4th ed. John Wiley & Sons, Inc., Hoboken., 2013, pp. 1–29. [Online]. Available: <https://onlinelibrary.wiley.com/doi/abs/10.1002/9781118671627.ch1>

- [10] M. Li and A. C. Lai, “Review of analytical models for heat transfer by vertical ground heat exchangers (GHEs): A perspective of time and space scales,” *Applied Energy*, vol. 151, pp. 178–191, 2015.
- [11] A. S. Shirazi and M. Bernier, “Thermal capacity effects in borehole ground heat exchangers,” *Energy and Buildings*, vol. 67, pp. 352–364, 2013. [Online]. Available: <http://www.sciencedirect.com/science/article/pii/S0378778813005203>
- [12] A. Chiasson, S. Rees, and J. Spitler, “A preliminary assessment of the effects of groundwater flow on closed-loop ground source heat pump systems,” *ASHRAE Transactions*, vol. 106, 2000.
- [13] S. H. Lines, M. A. Llano-Serna, and D. J. Williams, “Analysis of groundwater advection and ground-heat exchanger spacing on intermittent ground-source heat pump operation,” in *International Symposium on Energy Geotechnics*. Springer, 2018, Conference Proceedings, pp. 19–26.
- [14] J. E. Bose *et al.*, *Design/data manual for closed-loop ground-coupled heat pump systems*. Atlanta, GA: American Society of Heating, Refrigerating, and Air-Conditioning Engineers, 1985.
- [15] Y. Gu and D. L. O’Neal, “Development of an equivalent diameter expression for vertical U-tubes used in ground-coupled heat pumps,” in *ASHRAE Transactions*, vol. 104. ASHRAE, 1998, Conference Proceedings, pp. 347–355.
- [16] J. Claesson and A. Dunand, *Heat Extraction from the Ground by Horizontal Pipes: A Mathematical Analysis*, ser. Document (Statens råd för byggnadsforskning (Sweden)). Swedish Council for Building Research, 1983. [Online]. Available: <https://books.google.ca/books?id=Br1QAAAAYAAJ>
- [17] J. Bennet, J. Claesson, and G. Hellstrom, “Multipole method to compute the conductive heat flow to and between pipes in a composite cylinder.” University of Lund, Department of Building and Mathematical Physics., Report, 1987.
- [18] J. Claesson and G. Hellstrom, “Multipole method to calculate borehole thermal resistances in a borehole heat exchanger,” *HVAC and R Research*, vol. 17, no. 6, pp. 895–911, 2011. [Online]. Available: <http://dx.doi.org/10.1080/10789669.2011.609927>
- [19] P. Hu *et al.*, “Performance study of a ground heat exchanger based on the multipole theory heat transfer model,” *Energy and Buildings*, vol. 65, pp. 231–241, 2013. [Online]. Available: <http://www.sciencedirect.com/science/article/pii/S0378778813003381>

- [20] H. S. Carslaw and J. C. Jaeger, *Conduction of heat in solids*, 2nd ed. Oxford: Clarendon Press, 1959.
- [21] H. Zeng, N. Diao, and Z. Fang, “Heat transfer analysis of boreholes in vertical ground heat exchangers,” *International Journal of Heat and Mass Transfer*, vol. 46, no. 23, pp. 4467–4481, 2003. [Online]. Available: [http://dx.doi.org/10.1016/S0017-9310\(03\)00270-9](http://dx.doi.org/10.1016/S0017-9310(03)00270-9)
- [22] G. Hellström, “Ground heat storage: thermal analyses of duct storage system,” PhD Thesis, University of Lund, 1991.
- [23] P. Eslami-nejad and M. Bernier, “Heat transfer in double U-tube boreholes with two independent circuits,” *Journal of Heat Transfer*, vol. 133, no. 8, 2011. [Online]. Available: <https://doi.org/10.1115/1.4003747>
- [24] P. Belzile, L. Lamarche, and D. R. Rousse, “Semi-analytical model for geothermal borefields with independent inlet conditions,” *Geothermics*, vol. 60, pp. 144–155, 2016. [Online]. Available: <http://www.sciencedirect.com/science/article/pii/S0375650515001637>
- [25] M. Cimmino, “Fluid and borehole wall temperature profiles in vertical geothermal boreholes with multiple U-tubes,” *Renewable Energy*, vol. 96, pp. 137–147, 2016. [Online]. Available: <http://www.sciencedirect.com/science/article/pii/S096014811630369X>
- [26] Y. Gu and D. L. O’Neal, “Analytical solution to transient heat conduction in a composite region with a cylindrical heat source,” *Journal of Solar Energy Engineering, Transactions of the ASME*, vol. 117, no. 3, pp. 242–248, 1995.
- [27] J. A. Shonder and J. V. Beck, “Determining effective soil formation thermal properties from field data using a parameter estimation technique,” *ASHRAE Transactions*, vol. 105, p. PART 1/, 1999.
- [28] T. Young, “Development, verification, and design analysis of the borehole fluid thermal mass model for approximating short term borehole thermal response,” MSc Thesis, Oklahoma State University, 2004.
- [29] X. Xu and J. Spitler, “Modeling of vertical ground loop heat exchangers with variable convective resistance and thermal mass of the fluid,” in *10th International Conference on Thermal Energy Storage-EcoStock*, 2006, Conference Proceedings.

- [30] L. Lamarche and B. Beauchamp, “New solutions for the short-time analysis of geothermal vertical boreholes,” *International Journal of Heat and Mass Transfer*, vol. 50, no. 7-8, pp. 1408–1419, 2007. [Online]. Available: <http://dx.doi.org/10.1016/j.ijheatmasstransfer.2006.09.007>
- [31] G. Bandyopadhyay, W. Gosnold, and M. Mann, “Analytical and semi-analytical solutions for short-time transient response of ground heat exchangers,” *Energy and Buildings*, vol. 40, no. 10, pp. 1816–1824, 2008. [Online]. Available: <http://dx.doi.org/10.1016/j.enbuild.2008.04.005>
- [32] H. Stehfest, “Algorithm 368: Numerical inversion of laplace transforms [D5],” *Commun. ACM*, vol. 13, no. 1, p. 47–49, 1970. [Online]. Available: <https://doi.org/10.1145/361953.361969>
- [33] S. Javed and J. Claesson, “New analytical and numerical solutions for the short-term analysis of vertical ground heat exchangers,” in *ASHRAE Transactions*, vol. 117. Amer. Soc. Heating, Ref. Air-Conditioning Eng. Inc., 2011, Conference Proceedings, pp. 3–12.
- [34] R. A. Beier, “Transient heat transfer in a U-tube borehole heat exchanger,” *Applied Thermal Engineering*, vol. 62, no. 1, pp. 256–266, 2014. [Online]. Available: <http://www.sciencedirect.com/science/article/pii/S1359431113006480>
- [35] G. Monteyne, S. Javed, and G. Vandersteen, “Heat transfer in a borehole heat exchanger: Frequency domain modeling,” *International Journal of Heat and Mass Transfer*, vol. 69, pp. 129–139, 2014. [Online]. Available: <http://www.sciencedirect.com/science/article/pii/S0017931013008752>
- [36] L. Lamarche, “Short-time analysis of vertical boreholes, new analytic solutions and choice of equivalent radius,” *International Journal of Heat and Mass Transfer*, vol. 91, pp. 800–807, 2015. [Online]. Available: <http://dx.doi.org/10.1016/j.ijheatmasstransfer.2015.07.135>
- [37] N. Kuzmic, Y. L. E. Law, and S. B. Dworkin, “Numerical heat transfer comparison study of hybrid and non-hybrid ground source heat pump systems,” *Applied Energy*, vol. 165, pp. 919–929, 2016. [Online]. Available: <http://dx.doi.org/10.1016/j.apenergy.2015.12.122>
- [38] Y. Brussieux and M. Bernier, “Universal short time  $g^*$ -functions: generation and application,” *Science and Technology for the Built Environment*, vol. 25, no. 8, pp. 993–1006, 2019. [Online]. Available: <http://dx.doi.org/10.1080/23744731.2019.1648132>

- [39] X. Yu *et al.*, “Development of an efficient numerical model and analysis of heat transfer performance for borehole heat exchanger,” *Renewable Energy*, vol. 152, pp. 189–197, 2020. [Online]. Available: <http://www.sciencedirect.com/science/article/pii/S0960148120300495>
- [40] C. Naldi and E. Zanchini, “A one-material cylindrical model to determine short- and long-term fluid-to-ground response factors of single U-tube borehole heat exchangers,” *Geothermics*, vol. 86, p. 101811, 2020. [Online]. Available: <http://www.sciencedirect.com/science/article/pii/S037565051930210X>
- [41] M. De Carli *et al.*, “A computational capacity resistance model (CaRM) for vertical ground-coupled heat exchangers,” *Renewable Energy*, vol. 35, no. 7, pp. 1537–1550, 2010. [Online]. Available: <http://dx.doi.org/10.1016/j.renene.2009.11.034>
- [42] A. Zarrella, M. Scarpa, and M. De Carli, “Short time step analysis of vertical ground-coupled heat exchangers: The approach of CaRM,” *Renewable Energy*, vol. 36, no. 9, pp. 2357–2367, 2011. [Online]. Available: <http://dx.doi.org/10.1016/j.renene.2011.01.032>
- [43] D. Bauer *et al.*, “Thermal resistance and capacity models for borehole heat exchangers,” *International Journal of Energy Research*, vol. 35, no. 4, pp. 312–320, 2011. [Online]. Available: <http://dx.doi.org/10.1002/er.1689>
- [44] D. Bauer, W. Heidemann, and H. J. G. Diersch, “Transient 3D analysis of borehole heat exchanger modeling,” *Geothermics*, vol. 40, no. 4, pp. 250–260, 2011. [Online]. Available: <http://www.sciencedirect.com/science/article/pii/S0375650511000460>
- [45] P. Pasquier and D. Marcotte, “Short-term simulation of ground heat exchanger with an improved TRCM,” *Renewable Energy*, vol. 46, pp. 92–99, 2012. [Online]. Available: <http://dx.doi.org/10.1016/j.renene.2012.03.014>
- [46] P. Pasquier and D. Marcotte, “Joint use of quasi-3D response model and spectral method to simulate borehole heat exchanger,” *Geothermics*, vol. 51, pp. 281–299, 2014. [Online]. Available: <http://dx.doi.org/10.1016/j.geothermics.2014.02.001>
- [47] A. Minaei and M. Maerefat, “A new analytical model for short-term borehole heat exchanger based on thermal resistance capacity model,” *Energy and Buildings*, vol. 146, pp. 233–242, 2017. [Online]. Available: <http://dx.doi.org/10.1016/j.enbuild.2017.04.064>
- [48] A. Minaei and M. Maerefat, “Thermal resistance capacity model for short-term borehole heat exchanger simulation with non-stiff ordinary differential

- equations,” *Geothermics*, vol. 70, pp. 260–270, 2017. [Online]. Available: <http://dx.doi.org/10.1016/j.geothermics.2017.06.011>
- [49] H. A. Wetter M, “TRNSYS Type 451: Vertical borehole heat exchanger EWS model, version 3.1-model description and implementing into TRNSYS.” Transsolar GmbH, Report, 1997.
- [50] T. Oppelt, I. Riehl, and U. Gross, “Modelling of the borehole filling of double U-pipe heat exchangers,” *Geothermics*, vol. 39, no. 3, pp. 270–276, 2010. [Online]. Available: <http://dx.doi.org/10.1016/j.geothermics.2010.06.001>
- [51] F. Ruiz-Calvo *et al.*, “Coupling short-term (B2G model) and long-term (g-function) models for ground source heat exchanger simulation in TRNSYS. Application in a real installation,” *Applied Thermal Engineering*, vol. 102, pp. 720–732, 2016. [Online]. Available: <http://dx.doi.org/10.1016/j.applthermaleng.2016.03.127>
- [52] C. Yavuzturk and J. D. Spitler, “Short time step response factor model for vertical ground loop heat exchangers,” in *ASHRAE Transactions*, vol. 105. ASHRAE, 1999, Conference Proceedings, p. PART 2/.
- [53] M. Li and A. C. K. Lai, “Analytical model for short-time responses of ground heat exchangers with u-shaped tubes: Model development and validation,” *Applied Energy*, vol. 104, pp. 510–516, 2013. [Online]. Available: <http://dx.doi.org/10.1016/j.apenergy.2012.10.057>
- [54] J. Jaeger, “Heat conduction in composite circular cylinders,” *The London, Edinburgh, and Dublin Philosophical Magazine and Journal of Science*, vol. 32, no. 213, pp. 324–335, 1941. [Online]. Available: <https://doi.org/10.1080/14786444108521306>
- [55] M. Li and A. C. K. Lai, “New temperature response functions (G functions) for pile and borehole ground heat exchangers based on composite-medium line-source theory,” *Energy*, vol. 38, no. 1, pp. 255–263, 2012. [Online]. Available: <http://dx.doi.org/10.1016/j.energy.2011.12.004>
- [56] Y. Yang and M. Li, “Short-time performance of composite-medium line-source model for predicting responses of ground heat exchangers with single u-shaped tube,” *International Journal of Thermal Sciences*, vol. 82, pp. 130–137, 2014. [Online]. Available: <http://www.sciencedirect.com/science/article/pii/S1290072914000805>
- [57] N. Bnilam and R. Al-Khoury, “A spectral model for heat transfer with friction heat gain in geothermal borehole heat exchangers,” *Applied Mathematical*



- Modelling*, vol. 40, no. 15-16, pp. 7410–7421, 2016. [Online]. Available: <https://dx.doi.org/10.1016/j.apm.2016.02.031>
- [58] J. Woloszyn and A. Gola, “Experimental verification and programming development of a new MDF borehole heat exchanger numerical model,” *Geothermics*, vol. 59, pp. 67–76, 2016. [Online]. Available: <http://dx.doi.org/10.1016/j.geothermics.2015.10.006>
- [59] J. Woloszyn and A. Golas, “Modelling of a borehole heat exchanger using a finite element with multiple degrees of freedom,” *Geothermics*, vol. 47, pp. 13–26, 2013. [Online]. Available: <http://dx.doi.org/10.1016/j.geothermics.2013.01.002>
- [60] J. M. Rivero and M. Hermanns, “Enhanced multipole method for the transient thermal response of slender geothermal boreholes,” *International Journal of Thermal Sciences*, vol. 164, p. 106531, 2021. [Online]. Available: <https://dx.doi.org/10.1016/j.ijthermalsci.2020.106531>
- [61] W. Thomson, *Mathematical and Physical Papers*, ser. Cambridge Library Collection - Physical Sciences. Cambridge: Cambridge University Press, 2011, vol. 1. [Online]. Available: <https://www.cambridge.org/core/books/mathematical-and-physical-papers/667F15735E71C8D36ED6BA064CB5CE11>
- [62] L. R. Ingersoll, O. J. Zobel, and A. C. Ingersoll, “Heat conduction with engineering and geological applications,” *Heat Conduction with Engineering and Geological Applications*, p. 278, 1948.
- [63] L. R. Ingersoll, O. J. Zobel, and A. C. Ingersoll, *Heat conduction : with engineering, geological and other applications*, rev. ed. Madison: University of Wisconsin, 1954.
- [64] J. Deerman, “Simulation of vertical U-tube ground-coupled heat pump systems using the cylindrical heat source solution,” *ASHRAE transactions*, vol. 97, no. 1, pp. 287–295, 1991.
- [65] M. A. Bernier *et al.*, “A multiple load aggregation algorithm for annual hourly simulations of GCHP systems,” *HVAC&R Research*, vol. 10, no. 4, pp. 471–487, 2004. [Online]. Available: <https://www.tandfonline.com/doi/abs/10.1080/10789669.2004.10391115>
- [66] S. Kavanaugh, “Design method for commercial ground-coupled heat pumps,” *ASHRAE Transactions*, vol. 101, pp. 1088–1094, 1995.

- [67] P. Eskilson, “Thermal analysis of heat extraction boreholes,” PhD Thesis, University of Lund, 1987.
- [68] H. Y. Zeng, N. R. Diao, and Z. H. Fang, “A finite line-source model for boreholes in geothermal heat exchangers,” *Heat Transfer—Asian Research*, vol. 31, no. 7, pp. 558–567, 2002. [Online]. Available: <https://onlinelibrary.wiley.com/doi/abs/10.1002/htj.10057>
- [69] L. Lamarche and B. Beauchamp, “A new contribution to the finite line-source model for geothermal boreholes,” *Energy and Buildings*, vol. 39, no. 2, pp. 188–198, 2007. [Online]. Available: <http://www.sciencedirect.com/science/article/pii/S0378778806001824>
- [70] T. V. Bandos *et al.*, “Finite line-source model for borehole heat exchangers: effect of vertical temperature variations,” *Geothermics*, vol. 38, no. 2, pp. 263–270, 2009. [Online]. Available: <http://www.sciencedirect.com/science/article/pii/S0375650509000054>
- [71] J. Claesson and S. Javed, “An analytical method to calculate borehole fluid temperatures for time-scales from minutes to decades,” in *ASHRAE Transactions*, vol. 117. Amer. Soc. Heating, Ref. Air-Conditioning Eng. Inc., 2011, Conference Proceedings, pp. 279–288.
- [72] M. Cimmino, M. Bernier, and F. Adams, “A contribution towards the determination of g-functions using the finite line source,” *Applied Thermal Engineering*, vol. 51, no. 1, pp. 401–412, 2013. [Online]. Available: <http://www.sciencedirect.com/science/article/pii/S135943111200573X>
- [73] M. Cimmino and M. Bernier, “A semi-analytical method to generate g-functions for geothermal bore fields,” *International Journal of Heat and Mass Transfer*, vol. 70, pp. 641–650, 2014. [Online]. Available: <https://dx.doi.org/10.1016/j.ijheatmasstransfer.2013.11.037>
- [74] S. L. Abdelaziz *et al.*, “Multilayer finite line source model for vertical heat exchangers,” *Geothermics*, vol. 51, pp. 406–416, 2014.
- [75] A. Lazzarotto, “A methodology for the calculation of response functions for geothermal fields with arbitrarily oriented boreholes – part 1,” *Renewable Energy*, vol. 86, pp. 1380–1393, 2016.

- [76] L. Lamarche, “Analytical g-function for inclined boreholes in ground-source heat pump systems,” *Geothermics*, vol. 40, no. 4, pp. 241–249, 2011. [Online]. Available: <http://www.sciencedirect.com/science/article/pii/S0375650511000459>
- [77] M. Cimmino, “The effects of borehole thermal resistances and fluid flow rate on the g-functions of geothermal bore fields,” *International Journal of Heat and Mass Transfer*, vol. 91, pp. 1119–1127, 2015.
- [78] L. Zhang, Q. Zhang, and G. Huang, “A transient quasi-3D entire time scale line source model for the fluid and ground temperature prediction of vertical ground heat exchangers (GHEs),” *Applied Energy*, vol. 170, pp. 65–75, 2016. [Online]. Available: <http://www.sciencedirect.com/science/article/pii/S0306261916302550>
- [79] X. Zhang *et al.*, “Improvement on an analytical finite line source model considering complex initial and boundary conditions: Part 1, model development and validation,” *Energy and Buildings*, vol. 198, pp. 1–10, 2019.
- [80] G. Hellstrom, “Comparison between theoretical models and field experiments for ground heat systems,” in *Document - Swedish Council for Building Research*. Swedish Council for Building Research, 1983, Conference Proceedings, pp. 102–115.
- [81] J. Claesson and G. Hellstrom, “Model studies of duct storage systems,” vol. 1. Springer Verlag, 1981, Conference Proceedings, pp. 762–778.
- [82] D. Pahud and G. Hellström, “The new duct ground heat model for TRNSYS,” in *In Proceedings of Eurotherm Seminar No. 49, A.A. van Steenhoven and W.G.J. van Helden*, 1996, Conference Proceedings.
- [83] H. Diersch *et al.*, “Finite element modeling of borehole heat exchanger systems. part 1. fundamentals,” *Computers and Geosciences*, vol. 37, no. 8, pp. 1122–1135, 2011. [Online]. Available: <http://dx.doi.org/10.1016/j.cageo.2010.08.003>
- [84] H. J. G. Diersch *et al.*, “Finite element modeling of borehole heat exchanger systems. part 2. numerical simulation,” *Computers and Geosciences*, vol. 37, no. 8, pp. 1136–1147, 2011. [Online]. Available: <http://dx.doi.org/10.1016/j.cageo.2010.08.002>
- [85] P. Monzó *et al.*, “A novel numerical approach for imposing a temperature boundary condition at the borehole wall in borehole fields,” *Geothermics*, vol. 56, pp. 35–44, 2015. [Online]. Available: <http://www.sciencedirect.com/science/article/pii/S0375650515000346>

- [86] J. Claesson and G. Hellström, “Analytical studies of the influence of regional groundwater flow on the performance of borehole heat exchangers,” in *Proc. of the 8th International Conference on Thermal energy storage, Terrastock*, vol. 28, 2000, Conference Proceedings.
- [87] M. G. Sutton, D. W. Nutter, and R. J. Couvillion, “A ground resistance for vertical bore heat exchangers with groundwater flow,” *Journal of Energy Resources Technology*, vol. 125, no. 3, pp. 183–189, 2003. [Online]. Available: <https://doi.org/10.1115/1.1591203>
- [88] N. Diao, Q. Li, and Z. Fang, “Heat transfer in ground heat exchangers with groundwater advection,” *International Journal of Thermal Sciences*, vol. 43, no. 12, pp. 1203–1211, 2004. [Online]. Available: <http://www.sciencedirect.com/science/article/pii/S1290072904001139>
- [89] A. Chiasson and A. O’Connell, “New analytical solution for sizing vertical borehole ground heat exchangers in environments with significant groundwater flow: Parameter estimation from thermal response test data,” *HVAC&R Research*, vol. 17, no. 6, pp. 1000–1011, 2011. [Online]. Available: <https://www.tandfonline.com/doi/abs/10.1080/10789669.2011.609926>
- [90] R. Al-Khoury, P. G. Bonnier, and R. B. J. Brinkgreve, “Efficient finite element formulation for geothermal heating systems. part i: Steady state,” *International Journal for Numerical Methods in Engineering*, vol. 63, no. 7, pp. 988–1013, 2005. [Online]. Available: <http://dx.doi.org/10.1002/nme.1313>
- [91] R. Al-Khoury and P. G. Bonnier, “Efficient finite element formulation for geothermal heating systems. part ii: Transient,” *International Journal for Numerical Methods in Engineering*, vol. 67, no. 5, pp. 725–745, 2006. [Online]. Available: <http://dx.doi.org/10.1002/nme.1662>
- [92] R. Fan *et al.*, “A study on the performance of a geothermal heat exchanger under coupled heat conduction and groundwater advection,” *Energy*, vol. 32, no. 11, pp. 2199–2209, 2007. [Online]. Available: <https://dx.doi.org/10.1016/j.energy.2007.05.001>
- [93] M. Nabi and R. Al-Khoury, “An efficient finite volume model for shallow geothermal systems. part i: Model formulation,” *Computers and Geosciences*, vol. 49, pp. 290–296, 2012. [Online]. Available: <http://dx.doi.org/10.1016/j.cageo.2012.03.019>

- [94] M. Nabi and R. Al-Khoury, “An efficient finite volume model for shallow geothermal systems-part ii: Verification, validation and grid convergence,” *Computers and Geosciences*, vol. 49, pp. 297–307, 2012. [Online]. Available: <http://dx.doi.org/10.1016/j.cageo.2012.03.023>
- [95] N. Molina-Giraldo *et al.*, “A moving finite line source model to simulate borehole heat exchangers with groundwater advection,” *International Journal of Thermal Sciences*, vol. 50, no. 12, pp. 2506–2513, 2011. [Online]. Available: <http://www.sciencedirect.com/science/article/pii/S129007291100192X>
- [96] V. Wagner *et al.*, “Analytical approach to groundwater-influenced thermal response tests of grouted borehole heat exchangers,” *Geothermics*, vol. 46, pp. 22–31, 2013. [Online]. Available: <https://dx.doi.org/10.1016/j.geothermics.2012.10.005>
- [97] M. Tye-Gingras and L. Gosselin, “Generic ground response functions for ground exchangers in the presence of groundwater flow,” *Renewable Energy*, vol. 72, pp. 354–366, 2014. [Online]. Available: <http://www.sciencedirect.com/science/article/pii/S0960148114004121>
- [98] J. A. Rivera, P. Blum, and P. Bayer, “Analytical simulation of groundwater flow and land surface effects on thermal plumes of borehole heat exchangers,” *Applied Energy*, vol. 146, pp. 421–433, 2015. [Online]. Available: <https://dx.doi.org/10.1016/j.apenergy.2015.02.035>
- [99] L. H. Dai *et al.*, “Analysis on the transient heat transfer process inside and outside the borehole for a vertical u-tube ground heat exchanger under short-term heat storage,” *Renewable Energy*, vol. 87, pp. 1121–1129, 2016. [Online]. Available: <http://www.sciencedirect.com/science/article/pii/S0960148115302342>
- [100] S. Erol and B. François, “Multilayer analytical model for vertical ground heat exchanger with groundwater flow,” *Geothermics*, vol. 71, pp. 294–305, 2018. [Online]. Available: <http://www.sciencedirect.com/science/article/pii/S0375650517301293>
- [101] M. Cimmino and B. R. Baliga, “A hybrid numerical-semi-analytical method for computer simulations of groundwater flow and heat transfer in geothermal borehole fields,” *International Journal of Thermal Sciences*, vol. 142, pp. 366–378, 2019. [Online]. Available: <https://dx.doi.org/10.1016/j.ijthermalsci.2019.04.012>
- [102] S. Cai *et al.*, “An analytical full-scale model to predict thermal response in boreholes with groundwater advection,” *Applied Thermal Engineering*, vol. 168, p.

- 114828, 2020. [Online]. Available: <http://www.sciencedirect.com/science/article/pii/S1359431119312402>
- [103] R. Al-Khoury *et al.*, “A spectral model for a moving cylindrical heat source in a conductive-convective domain,” *International Journal of Heat and Mass Transfer*, vol. 163, p. 120517, 2020.
- [104] Y. Luo, N. Cheng, and G. Xu, “Analytical modeling and thermal analysis of deep coaxial borehole heat exchanger with stratified-seepage-segmented finite line source method (S3-FLS),” *Energy and Buildings*, vol. 257, p. 111795, 2022.
- [105] J. Claesson and J. Bennet, “Multipole method to compute the conductive heat flows to and between pipes in a cylinder.” University of Lund, Department of Building and Mathematical Physics., Report, 1987.
- [106] H. Salt, “Transient conduction in a two-dimensional composite slab—I. theoretical development of temperature modes,” *International Journal of Heat and Mass Transfer*, vol. 26, no. 11, pp. 1611–1616, 1983. [Online]. Available: <https://www.sciencedirect.com/science/article/pii/S0017931083800805>
- [107] M. D. Mikhailov and M. N. Özisik, “Transient conduction in a three-dimensional composite slab,” *International Journal of Heat and Mass Transfer*, vol. 29, pp. 340–342, 1986.
- [108] A. Haji-Sheikh and J. Beck, “Temperature solution in multi-dimensional multi-layer bodies,” *International Journal of Heat and Mass Transfer*, vol. 45, no. 9, pp. 1865–1877, 2002.
- [109] M. F. Abdul Azeez and A. F. Vakakis, “Axisymmetric transient solutions of the heat diffusion problem in layered composite media,” *International Journal of Heat and Mass Transfer*, vol. 43, no. 20, pp. 3883–3895, 2000.
- [110] N. D. Milpaevi and M. Raynaud, “Analytical solution of transient heat conduction in a two-layer anisotropic cylindrical slab excited superficially by a short laser pulse,” *International Journal of Heat and Mass Transfer*, vol. 47, pp. 1627–1641, 2004.
- [111] V. P. Nguyen *et al.*, “Meshless methods: A review and computer implementation aspects,” *Mathematics and Computers in Simulation*, vol. 79, no. 3, pp. 763–813, 2008. [Online]. Available: <https://www.sciencedirect.com/science/article/pii/S0378475408000062>

- [112] T. E., “Ein gegenstück zum ritzschen verfahren,” in *Proceedings of the 2nd International Congress of Applied Mechanics*, 1926, Conference Proceedings, pp. 131–137.
- [113] E. Kita and N. Kamiya, “Trefftz method: an overview,” *Advances in Engineering Software*, vol. 24, no. 1-3, pp. 3–12, 1995. [Online]. Available: [https://dx.doi.org/10.1016/0965-9978\(95\)00067-4](https://dx.doi.org/10.1016/0965-9978(95)00067-4)
- [114] F. Závíska, “Über die beugung elektromagnetischer wellen an parallelen, unendlich langen kreiszylindern,” *Annalen der Physik*, vol. 345, no. 5, pp. 1023–1056, 1913.
- [115] X. Wu and A. Kishk, “Hybrid of method of moments and cylindrical eigenfunction expansion to study substrate integrated waveguide circuits,” *IEEE Transactions on Microwave Theory and Techniques*, vol. 56, no. 10, pp. 2270–2276, 2008.
- [116] J. T. Chen *et al.*, “Boundary element analysis for the helmholtz eigenvalue problems with a multiply connected domain,” *Proceedings of the Royal Society of London. Series A: Mathematical, Physical and Engineering Sciences*, vol. 457, no. 2014, pp. 2521–2546, 2001. [Online]. Available: <https://royalsocietypublishing.org/doi/abs/10.1098/rspa.2001.0806>
- [117] J. T. Chen, L. W. Liu, and S. W. Chyuan, “Acoustic eigenanalysis for multiply-connected problems using dual BEM,” *Communications in Numerical Methods in Engineering*, vol. 20, no. 6, pp. 419–440, 2004. [Online]. Available: <http://msvlab.hre.ntou.edu.tw/paper/cnme/cnme2004.pdf>
- [118] C. M. Linton and D. V. Evans, “The interaction of waves with arrays of vertical circular cylinders,” *Journal of Fluid Mechanics*, vol. 215, no. -1, p. 549, 1990.
- [119] P. A. Martin, “Multiple scattering interaction of time-harmonic wave with N obstacles,” *The Journal of the Acoustical Society of America*, vol. 121, no. 5, pp. 2473–2474, 2006.
- [120] C. W. Tittle, “Boundary value problems in composite media: Quasi-orthogonal functions,” *Journal of Applied Physics*, vol. 36, no. 4, pp. 1486–1488, 1965.
- [121] J. Chen, I. Chen, and Y. Lee, “Eigensolutions of multiply connected membranes using the method of fundamental solutions,” *Engineering Analysis with Boundary Elements*, vol. 29, no. 2, pp. 166–174, 2005.
- [122] J. Chen *et al.*, “Eigensolutions of the Helmholtz equation for a multiply connected domain with circular boundaries using the multipole Trefftz method,” *Engineering Analysis with Boundary Elements*, vol. 34, no. 5, pp. 463–470, 2010.

- [123] J. H. Graf, “Ueber die addition und subtraction der argumente bei bessel’schen functionen nebst einer anwendung,” *Mathematische Annalen*, vol. 43, no. 1, pp. 136–144, 1893.
- [124] M. Abramowitz, *Handbook of Mathematical Functions, With Formulas, Graphs, and Mathematical Tables*. Dover Publications, Inc., 1974.
- [125] C.-S. Liu, “A highly accurate collocation Trefftz method for solving the Laplace equation in the doubly connected domains,” *Numerical Methods for Partial Differential Equations*, vol. 24, no. 1, pp. 179–192, 2008. [Online]. Available: <https://onlinelibrary.wiley.com/doi/pdf/10.1002/num.20257>
- [126] M. D. Bird and C. R. Steele, “A solution procedure for laplace’s equation on multiply connected circular domains,” *Journal of Applied Mechanics*, vol. 59, no. 2, pp. 398–404, 06 1992. [Online]. Available: <https://doi.org/10.1115/1.2899533>
- [127] S. Van Der Walt, S. C. Colbert, and G. Varoquaux, “The NumPy array: A structure for efficient numerical computation,” *Computing in Science & Engineering*, vol. 13, no. 2, pp. 22–30, 2011. [Online]. Available: <https://dx.doi.org/10.1109/MCSE.2011.37>
- [128] P. Virtanen *et al.*, “Scipy 1.0: fundamental algorithms for scientific computing in python,” *Nature Methods*, vol. 17, no. 3, pp. 261–272, 2020. [Online]. Available: <https://dx.doi.org/10.1038/s41592-019-0686-2>
- [129] D. Crowdy, “Quadrature domains and fluid dynamics,” ser. Quadrature Domains and Their Applications. Birkhäuser Basel, 2005, Conference Proceedings, pp. 113–129.
- [130] ASHRAE, *Chapter 35 : Geothermal Energy*. HVAC Applications, 2019.
- [131] J. D. Spitler and S. E. Gehlin, “Thermal response testing for ground source heat pump systems—an historical review,” *Renewable and Sustainable Energy Reviews*, vol. 50, pp. 1125–1137, 2015.
- [132] M. Ahmadfard and M. Bernier, “A review of vertical ground heat exchanger sizing tools including an inter-model comparison,” *Renewable and Sustainable Energy Reviews*, vol. 110, pp. 247–265, 2019.
- [133] I. Cupeiro Figueroa, M. Cimmino, and L. Helsen, “A methodology for long-term model predictive control of hybrid geothermal systems: The shadow-cost formulation,” *Energies*, vol. 13, no. 23, p. 6203, 2020.



- [134] M. S. Mitchell and J. D. Spitler, “Characterization, testing, and optimization of load aggregation methods for ground heat exchanger response-factor models,” *Science and Technology for the Built Environment*, vol. 25, no. 8, pp. 1036–1051, 2019.
- [135] A. Lazzarotto, “A network-based methodology for the simulation of borehole heat storage systems,” *Renewable Energy*, vol. 62, pp. 265–275, 2014. [Online]. Available: <https://www.sciencedirect.com/science/article/pii/S0960148113003650>
- [136] L. Lamarche, “Mixed arrangement of multiple input-output borehole systems,” *Applied Thermal Engineering*, vol. 124, pp. 466–476, 2017. [Online]. Available: <https://www.sciencedirect.com/science/article/pii/S1359431117307500>
- [137] M. Cimmino, “A finite line source simulation model for geothermal systems with series- and parallel-connected boreholes and independent fluid loops,” *Journal of Building Performance Simulation*, vol. 11, no. 4, pp. 414–432, 2018.
- [138] M. Cimmino, “Fast calculation of the g-functions of geothermal borehole fields using similarities in the evaluation of the finite line source solution,” *Journal of Building Performance Simulation*, vol. 11, no. 6, pp. 655–668, 2018. [Online]. Available: [https://publications.polymtl.ca/3000/1/2018\\_Cimmino\\_Fast\\_calculation\\_g-functions\\_geothermal\\_borehole.pdf](https://publications.polymtl.ca/3000/1/2018_Cimmino_Fast_calculation_g-functions_geothermal_borehole.pdf)
- [139] B. Dusseault, P. Pasquier, and D. Marcotte, “A block matrix formulation for efficient g-function construction,” *Renewable Energy*, vol. 121, pp. 249–260, 2018. [Online]. Available: <https://www.sciencedirect.com/science/article/pii/S096014811731296X>
- [140] A. Nguyen and P. Pasquier, “A successive flux estimation method for rapid g-function construction of small to large-scale ground heat exchanger,” *Renewable Energy*, vol. 165, pp. 359–368, 2021.
- [141] L. Lamarche, “g-function generation using a piecewise-linear profile applied to ground heat exchangers,” *International Journal of Heat and Mass Transfer*, vol. 115, pp. 354–360, 2017.
- [142] M. Ahmadfard and M. Bernier, “Modifications to ASHRAE’s sizing method for vertical ground heat exchangers,” *Science and Technology for the Built Environment*, vol. 24, no. 7, pp. 803–817, 2018. [Online]. Available: <http://dx.doi.org/10.1080/23744731.2018.1423816>

- [143] C. Prieto and M. Cimmino, “Transient multipole expansion for heat transfer in ground heat exchangers,” *Science and Technology for the Built Environment*, vol. 27, no. 3, pp. 253–270, 2021. [Online]. Available: <https://doi.org/10.1080/23744731.2020.1845072>
- [144] A. Laferrière *et al.*, “Development and validation of a full-time-scale semi-analytical model for the short- and long-term simulation of vertical geothermal bore fields,” *Geothermics*, vol. 86, p. 101788, 2020. [Online]. Available: <https://dx.doi.org/10.1016/j.geothermics.2019.101788>
- [145] M. Li *et al.*, “Full-scale temperature response function (G-function) for heat transfer by borehole ground heat exchangers (GHEs) from sub-hour to decades,” *Applied Energy*, vol. 136, pp. 197–205, 2014. [Online]. Available: <https://dx.doi.org/10.1016/j.apenergy.2014.09.013>
- [146] M. Cimmino, “*pygfunction* : an open-source toolbox for the evaluation of thermal response factors for geothermal borehole fields.” Proceedings of eSim 2018, 2018, pp. 492–501.
- [147] S. Zhou, Z. Xu, and F. Liu, “Method for determining the optimal number of clusters based on agglomerative hierarchical clustering,” *IEEE Transactions on Neural Networks and Learning Systems*, vol. 28, no. 12, pp. 3007–3017, 2017. [Online]. Available: <https://dx.doi.org/10.1109/tnnls.2016.2608001>
- [148] C. Patil and I. Baidari, “Estimating the optimal number of clusters k in a dataset using data depth,” *Data Science and Engineering*, vol. 4, no. 2, pp. 132–140, 2019. [Online]. Available: <https://dx.doi.org/10.1007/s41019-019-0091-y>
- [149] Y. Jung *et al.*, “A decision criterion for the optimal number of clusters in hierarchical clustering,” *Journal of Global Optimization*, vol. 25, no. 1, pp. 91–111, 2003.
- [150] M. Cimmino, “Semi-analytical method for g-function calculation of bore fields with series- and parallel-connected boreholes,” *Science and Technology for the Built Environment*, vol. 25, no. 8, pp. 1007–1022, 2019. [Online]. Available: <https://doi.org/10.1080/23744731.2019.1622937>
- [151] J. W. Lund and T. L. Boyd, “Direct utilization of geothermal energy 2015 worldwide review,” *Geothermics*, vol. 60, pp. 66–93, 2016. [Online]. Available: <https://dx.doi.org/10.1016/j.geothermics.2015.11.004>

- [152] S. J. Self, B. V. Reddy, and M. A. Rosen, “Geothermal heat pump systems: Status review and comparison with other heating options,” *Applied Energy*, vol. 101, pp. 341–348, 2013.
- [153] C. Prieto and M. Cimmino, “Thermal interactions in large irregular fields of geothermal boreholes: the method of equivalent boreholes,” *Journal of Building Performance Simulation*, vol. 14, no. 4, pp. 446–460, 2021. [Online]. Available: <https://dx.doi.org/10.1080/19401493.2021.1968953>
- [154] O. Alaie, R. Maddahian, and G. Heidarinejad, “Investigation of thermal interaction between shallow boreholes in a GSHE using the FLS-STRCM model,” *Renewable Energy*, vol. 175, pp. 1137–1150, 2021. [Online]. Available: <https://dx.doi.org/10.1016/j.renene.2021.05.073>
- [155] R. A. Beier, M. D. Smith, and J. D. Spitler, “Reference data sets for vertical borehole ground heat exchanger models and thermal response test analysis,” *Geothermics*, vol. 40, no. 1, pp. 79–85, 2011. [Online]. Available: <http://www.sciencedirect.com/science/article/pii/S0375650511000022>
- [156] DHI-WASY, *FEFLOW Finite Element Subsurface Flow and Transport Simulation System—White Papers: Volume 5*, Berlin, GE, 2010.
- [157] P. Eskilson and J. Claesson, “Simulation model for thermally interacting heat extraction boreholes,” *Numerical Heat Transfer*, vol. 13, no. 2, pp. 149–165, 1988. [Online]. Available: <https://doi.org/10.1080/10407788808913609>
- [158] J. Claesson and S. Javed, “A load-aggregation method to calculate extraction temperatures of borehole heat exchangers,” *ASHRAE Transactions*, vol. 118, pp. 530–539, 01 2012.
- [159] C. Prieto and M. Cimmino, “Semi-analytical method for 3D transient heat transfer in thermally interacting fields of ground heat exchangers,” *Thermo*, vol. 2, no. 3, pp. 171–199, 2022.
- [160] M. Cimmino and J. C. Cook, “pygfunction 2.2 : New features and improvements in accuracy and computational efficiency,” in *Proc. of the IGSHPA Research Track*, vol. 1, 2022, Conference Proceedings.

## APPENDIX A TIME-DEPENDENT FLUID TEMPERATURES BY MEANS OF DUHAMEL'S THEOREM

This appendix shows an extension of Chapter 4, specifically Section 4.3.3 where the estimation of the temperature profile of the GHE and its periphery considering time-dependent fluid temperatures is shown. The complete transient heat transfer problem for the inside and outside of the GHE is repeated here:

$$\frac{1}{\alpha_i} \frac{\partial T_i}{\partial t} = \nabla^2 T_i \text{ in } \Omega_i, i = 1, 2 \quad (\text{A.1a})$$

$$- \beta_k R_k \frac{\partial T_1}{\partial \rho_k} \Big|_{R_k} + T_1 = T_{f_k}(t) \text{ on } \partial\Omega_k, k = 1, \dots, N \quad (\text{A.1b})$$

$$-k_b \frac{\partial T_1}{\partial \rho_0} \Big|_{R_0} = -k_s \frac{\partial T_2}{\partial \rho_0} \Big|_{R_0} \text{ on } \partial\Omega_0 \quad (\text{A.1c})$$

$$T_1|_{R_0} = T_2|_{R_0} \text{ on } \partial\Omega_0 \quad (\text{A.1d})$$

$$T_2(R_e, \phi, t)|_{R_e \rightarrow \infty} = 0 \text{ on } \partial\Omega_e \quad (\text{A.1e})$$

$$T_i(\rho, \phi, 0) = T^0 \text{ in } \Omega_i, i = 1, 2 \quad (\text{A.1f})$$

Separating the problem into  $N$ -subproblems using the linearity of Equation (A.1) and subtracting  $T^0$  from the full problem:

$$T_i = T^0 + \sum_{j=1}^N T'_{ij} \quad (\text{A.2})$$

Then, the new transient heat transfer problem for subproblem  $j$  at domain  $i$  is given by:

$$\frac{1}{\alpha_i} \frac{\partial T'_{ij}}{\partial t} = \nabla^2 T'_{ij} \text{ in } \Omega_i, i = 1, 2 \quad (\text{A.3a})$$

$$- \beta_k R_k \frac{\partial T'_{1j}}{\partial \rho_k} \Big|_{R_k} + T'_{1j} = \delta_k^j T'_{f_k}(t) \text{ on } \partial\Omega_k, k = 1, \dots, N \quad (\text{A.3b})$$

$$-k_b \frac{\partial T'_{1j}}{\partial \rho_0} \Big|_{R_0} = -k_s \frac{\partial T'_{2j}}{\partial \rho_0} \Big|_{R_0} \text{ on } \partial\Omega_0 \quad (\text{A.3c})$$

$$T'_{1j}|_{R_0} = T'_{2j}|_{R_0} \text{ on } \partial\Omega_0 \quad (\text{A.3d})$$

$$T'_{2j}(R_e, \phi, t)|_{R_e \rightarrow \infty} = 0 \text{ on } \partial\Omega_e \quad (\text{A.3e})$$

$$T'_{ij}(\rho, \phi, 0) = 0 \text{ in } \Omega_i, i = 1, 2 \quad (\text{A.3f})$$

where,  $T'_{f_k}(t) = T_{f_k}(t) - T^0$  and  $\delta_k^j$  is the Kronecker delta which is equal to 1 if  $j = k$  and 0 otherwise.

Since the fluid temperature in Equation (A.3b) is time-dependent, it is possible to construct the solution employing the Duhamel's theorem. In this case, the Duhamel's theorem states that:

$$T'_{ij} = \int_0^t T'_{f_j} \frac{\partial H_{ij}}{\partial t}(\rho, \phi, t - \tau) d\tau = - \int_0^t T'_{f_j} \frac{\partial H_{ij}}{\partial \tau}(\rho, \phi, t - \tau) d\tau \quad (\text{A.4})$$

where  $H_{ij}$  is the solution of Equation (A.3) with  $T'_{f_k}(t) = 1$ .

Solving for  $H_{ij}$  for each subproblem  $j$  follows the same structure of the transient multipole expansion shown in Section 4.3.1 and 4.3.2. Interestingly, when splitting the problem  $H_{ij}$  into the homogeneous transient problem and non-homogeneous steady-state problem, the transient problem is solved just once and the steady-state problem  $N$  times at the initialization.

The integral in Equation (A.4) could be considered as Riemann-Stieltjes for a discontinuous function  $T'_{f_j}$ . Let's consider  $n$  discontinuities for the fluid temperature  $T_{f_j}$  and step-wise variations for each pipe at each time step  $n$ , i.e. over  $\tau^{(n-1)} < t \leq \tau^n$  (where  $\tau^n = \tau^{(n-1)} + \Delta t$ ):

$$- \int_0^t T'_{f_j} \frac{\partial H_{ij}}{\partial \tau}(\rho, \phi, t - \tau) d\tau = - \left[ \int_0^{\tau^1} + \int_{\tau^1}^{\tau^2} + \cdots + \int_{\tau^{(n-1)}}^t \right] \left( T'_{f_j} \frac{\partial H_{ij}}{\partial \tau}(\rho, \phi, t - \tau) d\tau \right) \quad (\text{A.5})$$

Integrating by parts:

$$\begin{aligned} - \int_0^t T'_{f_j} \frac{\partial H_{ij}}{\partial \tau} d\tau &= -T'_{f_j} H_{ij} \Big|_0^{\tau^1} + \int_0^{\tau^1} H_{ij} \frac{\partial T'_{f_j}}{\partial \tau} d\tau \\ &\quad - T'_{f_j} H_{ij} \Big|_{\tau^1}^{\tau^2} + \int_{\tau^1}^{\tau^2} H_{ij} \frac{\partial T'_{f_j}}{\partial \tau} d\tau \\ &\quad \vdots \\ &\quad - T'_{f_j} H_{ij} \Big|_{\tau^{(n-1)}}^t + \int_{\tau^{(n-1)}}^t H_{ij} \frac{\partial T'_{f_j}}{\partial \tau} d\tau \end{aligned} \quad (\text{A.6})$$

Now, expanding the evaluation of the functions and compacting the integrals yields:

$$\begin{aligned} - \int_0^{t_f} T'_{f_j} \frac{\partial H_{ij}}{\partial \tau} dt &= H_{ij}(\rho, \phi, t) T'_{f_j}(0) + H_{ij}(\rho, \phi, t - \tau^1) [T'_{f_j}(\tau^1)^+ - T'_{f_j}(\tau^1)^-] \\ &\quad + H_{ij}(\rho, \phi, t - \tau^2) [T'_{f_j}(\tau^2)^+ - T'_{f_j}(\tau^2)^-] + \cdots + \int_0^{\tau^n} H_{ij} \frac{\partial T'_{f_j}}{\partial \tau} d\tau \\ &= \sum_{z=0}^{n-1} H_{ij}(\rho, \phi, t - \tau^z) [T'_{f_j}(\tau^z)^+ - T'_{f_j}(\tau^z)^-] \end{aligned}$$

(A.7)

where  $\tau^z = z\Delta t$ , and the  $+$ ,  $-$  mean the discontinuous function is approaching from the right and left, respectively, at the time the function is evaluated. The integral in Equation (A.7) is 0 since the step-wise variations make derivative 0 in this case for all the small changes.

The complete solution Equation (A.1) is then:

$$T_i = T^0 + \sum_{j=1}^N \sum_{z=0}^{n-1} H_{ij}(\rho, \phi, t - \tau^z) \left[ T'_{f_j}(\tau^z)^+ - T'_{f_j}(\tau^z)^- \right] \quad (\text{A.8})$$

Equation (A.8) could be used in combination with a load aggregation algorithm such as presented in Claesson and Javed [158] for the estimation of the fluid temperatures.

## APPENDIX B QUASI-ORTHOGONAL CONDITION FOR THE GROUNDWATER TRANSIENT MULTIPOLE EXPANSION

The homogeneous problem for  $T_{i,h}$  for the groundwater transient multipole expansion expressed in Chapter 7, specifically Section 7.3.2, is repeated here (replacing):

$$\frac{\partial \Gamma_{i,h}}{\partial t} + H(\rho - r_b) \left( \frac{(\rho c_p)_f}{(\rho c_p)_{s,eff}} \right)^2 \left( \frac{u_\rho^2 + u_\phi^2}{4\alpha_i} \right) \Gamma_{i,h} = \alpha_i \nabla^2 \Gamma_{i,h} \quad (\text{B.1a})$$

$$-\beta_k r_k \frac{\partial \Gamma_{1,h}}{\partial \rho} \Big|_{r_k} + \Gamma_{1,h} \Big|_{r_k} = 0 \text{ on } \partial \Omega_k \quad (\text{B.1b})$$

$$\Gamma_{1,h} \Big|_{r_b} = \Gamma_{2,h} \Big|_{r_b} e^{f(r_b, \theta)} \text{ on } \partial \Omega_b \quad (\text{B.1c})$$

$$-k_b \frac{\partial \Gamma_{1,h}}{\partial \rho} \Big|_{r_b} = -k_{s,eff} \frac{\partial \Gamma_{2,h}}{\partial \rho} \Big|_{r_b} e^{f(r_b, \theta)} \text{ on } \partial \Omega_b \quad (\text{B.1d})$$

$$\Gamma_{2,h} \Big|_{r_e \rightarrow \infty} = 0 \text{ on } \partial \Omega_e \quad (\text{B.1e})$$

$$\Gamma_{i,h}(\rho, \phi, 0) = (T^0 - T_{i,ss})/e^{f(\rho, \phi)} \text{ in } \Omega_1 \cup \Omega_2 \quad (\text{B.1f})$$

Assuming that  $\Gamma_{i,h}$  is spatiotemporally separable as  $\Gamma_{i,h} = X_i(\rho, \phi) \tau(t)$  results in a Sturm-Liouville problem with  $\tau(t) = \exp\left(-(\lambda_i^j)^2 \alpha_i t\right)$  for unique  $j$  eigenvalues for each domain  $i$  denoted as  $\lambda_i^j$ . The continuity condition requires that  $\alpha_1 (\lambda_1^j)^2 = \alpha_2 (\lambda_2^j)^2$  must hold for all time  $t$ . Therefore, Equation (B.1a) is transformed as follows:

$$\nabla^2 X_i^j + [(\lambda_i^j)^2 - u_{eff}^2] X_i^j = 0 \quad (\text{B.2})$$

where  $u_{eff}^2 = K_{gw} \frac{u_\infty^2}{4\alpha_i} \left( \frac{(\rho c_p)_f}{(\rho c_p)_{s,eff}} \right)^2 H(\rho - r_b)$  and for notation simplicity  $X_i^j = X_i(\rho, \phi; \lambda_i^j)$ .

To prove the quasi-orthogonal condition expressed in Equation (7.11), suppose there exist two eigenvalues  $j$  and  $n$  for Equation (B.2). Both equations associated with eigenvalues  $j$  and  $n$  are multiplied by  $\bar{X}_i^n k_i e^{2f(\rho, \phi)}$  and  $\bar{X}_i^j k_i e^{2f(\rho, \phi)}$ , respectively. Then, subtracting and integrating the whole domain  $\Omega_1 \cup \Omega_2$ , the multiplied equations yields:

$$\int_{\Omega_1 \cup \Omega_2} k_i \left( \bar{X}_i^n \nabla^2 X_i^j - \bar{X}_i^j \nabla^2 X_i^n \right) e^{2f(\rho, \phi)} d\Omega = - [(\lambda_i^j)^2 - (\lambda_i^n)^2] \int_{\Omega_1 \cup \Omega_2} k_i X_i^j \bar{X}_i^n e^{2f(\rho, \phi)} d\Omega \quad (\text{B.3})$$

Equation (B.3) could be partitioned for both domains  $\Omega_1$  and  $\Omega_2$ . Applying Green's second

identity to the LHS for the first domain  $\Omega_1$  gives:

$$\begin{aligned} k_b \int_{\Omega_1} \left( \bar{X}_1^n \nabla^2 X_1^j - \bar{X}_1^j \nabla^2 X_1^n \right) d\Omega = & k_b \sum_{l=1}^N \int_{\partial\Omega_l} \left( \bar{X}_1^n \frac{\partial X_1^j}{\partial \rho} \Big|_{r_l} - \bar{X}_1^j \frac{\partial X_1^n}{\partial \rho} \Big|_{r_l} \right) dS \\ & + k_b \int_{\partial\Omega_b^-} \left( \bar{X}_1^n \frac{\partial X_1^j}{\partial \rho} \Big|_{r_b} - \bar{X}_1^j \frac{\partial X_1^n}{\partial \rho} \Big|_{r_b} \right) dS \end{aligned} \quad (\text{B.4})$$

Now for the second domain  $\Omega_2$ :

$$\begin{aligned} k_{s,eff} \int_{\Omega_2} \left( \bar{X}_2^n \nabla^2 X_2^j - \bar{X}_2^j \nabla^2 X_2^n \right) d\Omega = & k_{s,eff} \int_{\partial\Omega_b^+} \left( \bar{X}_2^n \frac{\partial X_2^j}{\partial \rho} \Big|_{r_b} - \bar{X}_2^j \frac{\partial X_2^n}{\partial \rho} \Big|_{r_b} \right) e^{2f(r_b, \phi)} dS \\ & + k_{s,eff} \int_{\partial\Omega_e} \left( \bar{X}_2^n \frac{\partial X_2^j}{\partial \rho} \Big|_{r_e} - \bar{X}_2^j \frac{\partial X_2^n}{\partial \rho} \Big|_{r_e} \right) e^{2f(r_e, \phi)} dS \end{aligned} \quad (\text{B.5})$$

The terms in RHS in Equation (B.4) correspond to the evaluation at the  $N$  pipe boundaries and the contribution of the borehole wall through the domain  $\Omega_1$ . Similarly, in Equation (B.5), the RHS terms correspond to the contribution of the borehole wall and the far-field boundary, respectively. In Equation (B.4), the contribution by the  $N$  pipes is 0 since the homogeneous Robin boundary condition expressed in Equation (B.1b) guarantees that the difference vanishes in the domain  $\Omega_1$ . On the other hand, the far-field contribution in Equation (B.5) is 0 since the far-field boundary condition given by Equation (B.1e) is 0. Therefore, Equation (B.3) is then:

$$\begin{aligned} k_b \int_{\partial\Omega_b^-} \left( \bar{X}_1^n \frac{\partial X_1^j}{\partial \rho} \Big|_{r_b} - \bar{X}_1^j \frac{\partial X_1^n}{\partial \rho} \Big|_{r_b} \right) dS + & k_{s,eff} \int_{\partial\Omega_b^+} \left( \bar{X}_2^n \frac{\partial X_2^j}{\partial \rho} \Big|_{r_b} - \bar{X}_2^j \frac{\partial X_2^n}{\partial \rho} \Big|_{r_b} \right) e^{2f(r_b, \phi)} dS = \\ & - \left[ (\lambda_i^j)^2 - (\lambda_i^n)^2 \right] \int_{\Omega_1 \cup \Omega_2} k_i X_i^j \bar{X}_i^n e^{2f(\rho, \phi)} d\Omega \end{aligned} \quad (\text{B.6})$$

Now, using the continuity condition given by Equations (B.1c) and (B.1d) and noting that normal vectors at  $\partial\Omega_b$  are in the opposite direction when approaching from domain  $\Omega_1$  with respect  $\Omega_2$ , the LHS in Equation (B.6) is then 0. Therefore, the only way that RHS in Equation (B.6) holds is that the eigenvalue must be  $\lambda_i^j = \lambda_i^n$  for all  $j = n$  (i.e. RHS integral is 0 for all  $j \neq n$ ). Thus, the Fourier-Bessel coefficients based on the quasi-orthogonal condition are written as follows using the continuity condition  $\alpha_1 (\lambda_1^j)^2 = \alpha_2 (\lambda_2^j)^2$  in the



RHS of Equation B.6:

$$C_j = \frac{\frac{k_b}{\alpha_b} \int_{\Omega_1} (T^0 - T_{2,ss}) \bar{X}_1 d\Omega_1 + \frac{k_{s,eff}}{\alpha_{s,eff}} \int_{\Omega_2} (T^0 - T_{2,ss}) \bar{X}_2 e^{2f(r_b, \phi) - f(\rho, \phi)} d\Omega_2}{\frac{k_b}{\alpha_b} \int_{\Omega_1} X_1 \bar{X}_1 d\Omega_1 + \frac{k_{s,eff}}{\alpha_{s,eff}} \int_{\Omega_2} X_2 \bar{X}_2 e^{2f(r_b, \phi)} d\Omega_2} \quad (\text{B.7})$$

## APPENDIX C    ADDITIONAL FORMULAS FOR THE GROUNDWATER TRANSIENT MULTIPOLE EXPANSION

In addition to the formulas presented in Chapter 4 and in Chapter 6 (section 6.7) for the transient multipole expansion for pure conduction that correspond to the same mathematical structure for the groundwater flow phenomena, the solution for the non-homogeneous steady-state problem is slightly different and must be explicit presented.

The groundwater multipole expansion for the ground is repeated here:

$$\Gamma_{2,ss} = \sum_{l=-h}^h \delta_l^0 K_l \left( u_\infty \left( \frac{\sqrt{K_{gw}}}{2\alpha_2} \right) \left( \frac{(\rho c_p)_f}{(\rho c_p)_{s,eff}} \right) \rho_0 \right) e^{il\phi_0} \quad (C.1)$$

At the borehole wall boundary ( $\partial\Omega_b$ ):

$$\begin{aligned} \Gamma_{2,ss}|_{r_b} &= \sum_{l=-h}^h \delta_l^0 K_l \left( u_\infty \left( \frac{\sqrt{K_{gw}}}{2\alpha_2} \right) \left( \frac{(\rho c_p)_f}{(\rho c_p)_{s,eff}} \right) r_b \right) e^{il\phi_0} \\ \frac{\partial \Gamma_{2,ss}}{\partial \rho} \Big|_{r_b} &= u_\infty \left( \frac{\sqrt{K_{gw}}}{2\alpha_2} \right) \left( \frac{(\rho c_p)_f}{(\rho c_p)_{s,eff}} \right) \sum_{l=-h}^h \delta_l^0 K'_l \left( u_\infty \left( \frac{\sqrt{K_{gw}}}{2\alpha_2} \right) \left( \frac{(\rho c_p)_f}{(\rho c_p)_{s,eff}} \right) r_b \right) e^{il\phi_0} \\ \overline{\Gamma_{2,ss}}|_{r_b} &= \delta_l^0 K_0 \left( u_\infty \left( \frac{\sqrt{K_{gw}}}{2\alpha_2} \right) \left( \frac{(\rho c_p)_f}{(\rho c_p)_{s,eff}} \right) r_b \right) \\ \frac{\partial \overline{\Gamma_{2,ss}}}{\partial \rho} \Big|_{r_b} &= u_\infty \left( \frac{\sqrt{K_{gw}}}{2\alpha_2} \right) \left( \frac{(\rho c_p)_f}{(\rho c_p)_{s,eff}} \right) \delta_l^0 K'_0 \left( u_\infty \left( \frac{\sqrt{K_{gw}}}{2\alpha_2} \right) \left( \frac{(\rho c_p)_f}{(\rho c_p)_{s,eff}} \right) r_b \right) \end{aligned} \quad (C.2)$$

where  $\frac{\partial \overline{\Gamma_{2,ss}}}{\partial \rho} \Big|_{r_b} = \frac{1}{2\pi} \int_0^{2\pi} \frac{\partial \Gamma_{2,ss}}{\partial \rho} \Big|_{r_b} d\phi$  and  $\overline{\Gamma_{2,ss}}|_{r_b} = \frac{1}{2\pi} \int_0^{2\pi} \Gamma_{2,ss}|_{r_b} d\phi$ .